



HAL
open science

New Results on Stochastic Geometry Modeling of Cellular Networks: Modeling, Analysis and Experimental Validation

Wei Lu

► **To cite this version:**

Wei Lu. New Results on Stochastic Geometry Modeling of Cellular Networks: Modeling, Analysis and Experimental Validation. Electronics. Université Paris Saclay (COMUE), 2015. English. NNT : 2015SACLS253 . tel-01418769

HAL Id: tel-01418769

<https://theses.hal.science/tel-01418769>

Submitted on 17 Dec 2016

HAL is a multi-disciplinary open access archive for the deposit and dissemination of scientific research documents, whether they are published or not. The documents may come from teaching and research institutions in France or abroad, or from public or private research centers.

L'archive ouverte pluridisciplinaire **HAL**, est destinée au dépôt et à la diffusion de documents scientifiques de niveau recherche, publiés ou non, émanant des établissements d'enseignement et de recherche français ou étrangers, des laboratoires publics ou privés.

NNT: 2015SACLS253

THESE DE DOCTORAT
DE
L'UNIVERSITE PARIS-SACLAY
PREPAREE A
L'UNIVERSITE PARIS-SUD

ÉCOLE DOCTORALE N° 580

Sciences et technologies de l'information et de la communication

Spécialité de doctorat: Réseaux, Information et Communications

Par

M. Wei Lu

New Results on Stochastic Geometry Modeling of Cellular
Networks: Modeling, Analysis and Experimental Validation

Thèse présentée et soutenue à Gif sur Yvette, le 16 décembre 2015:

Composition du Jury:

- M. Pierre Duhamel, Directeur de recherche, L2S, CNRS, France, Président du Jury
- M. François Baccelli, Directeur de recherche, INRIA, France, Rapporteur
- M. Robert Schober, Professeur, Universität Erlangen-Nürnberg, Allemagne, Rapporteur
- M. Laurent Decreusefond, Professeur, Télécom ParisTech, France, Examineur
- M. Ali Ghayeb, Professeur, Texas A&M University at Qatar, Qatar, Examineur
- M. Anthony Busson, Professeur, Université Lyon 1, France, Directeur de thèse
- M. Marco Di Renzo, Chargé de recherche, L2S, CNRS, France, Co-directeur de thèse

Titre: Nouveaux Résultats sur la Modélisation des Réseaux Cellulaires basée sur la Géométrie Stochastique: Analyse des Performances et Validation Expérimentale

Mots clés: réseaux cellulaire, relais, géométrie stochastique

Résumé: : L'hétérogénéité et l'irrégularité croissante des déploiements des réseaux sans fil de nouvelles générations soulèvent des défis importants dans l'évaluation de performances de ces réseaux. Les modèles classiques s'appuyant sur des modèles hexagonaux pour décrire les emplacements géographiques des nœuds de transmission sont difficilement adaptables à ces réseaux. Dans ce contexte, il a été proposé un nouveau paradigme de modélisation des réseaux sans fil qui s'appuie sur les processus ponctuels de Poisson (PPP), et de manière générale sur la géométrie stochastique. L'analyse, au travers de ces outils mathématiques, présente une complexité indépendante de la taille du réseau, et permet d'estimer avec précision des quantités pratiques liées aux performances des réseaux cellulaires. Cette thèse a porté sur la faisabilité mathématique de l'approche fondée sur les PPP en proposant de nouvelles méthodes mathématiques d'approximations justes incorporant des modèles de propagation du canal radio.

Dans un premier temps, un nouveau cadre mathématique, considéré comme une approche Equivalent-in-Distribution (EiD), a été proposée pour le calcul exact de la probabilité d'erreur dans les réseaux cellulaires. L'approche proposée, s'appuyant donc sur la géométrie aléatoire et des modèles spatiaux, montre une complexité faible en terme d'évaluation numérique et est applicable à un grand nombre de configurations MIMO pour lesquelles nous considérons différentes techniques de modulation et techniques de récupération du signal.

Dans un deuxième temps, nous étudions les performances des réseaux cellulaires en présence de relais, où trois processus ponctuels de Poisson modélisent respectivement les nœuds relais, les stations de base, et les terminaux mobiles. Pour ce modèle, nous avons considéré des critères souples d'association. Le cadre mathématique proposé et les résultats associés ont montré que les performances dépendent fortement des exposants des fonctions d'atténuation sur les deux premiers sauts sans fil. Nous montrons aussi qu'une mauvaise configuration du réseau peut amener à des gains négligeables de l'utilisation de cette technique.

Enfin, nous considérons la modélisation des réseaux cellulaires au travers d'un PPP et d'un modèle unifié d'atténuation de signal généralisée qui prend en compte deux types de liaisons physiques : line-of-sight (LOS) et non-line-of-sight (NLOS). Un modèle

de complexité réduite décrivant les propriétés de la liaison radio a aussi été proposée et permet de prendre en compte dans nos calculs un grand nombre de modèle radio proposés dans la littérature. Les résultats montrent, entre autres, qu'une densité optimale pour le déploiement des BS existe lorsque les liens LOS/NLOS sont classés en fonction de leur charge. Nous comparons nos résultats, s'appuyant donc sur un PPP pour modéliser la position des stations de bases et notre modèle de canal radio, avec des simulations de Monte Carlo décrivant des déploiements réels de stations de bases et un modèle de type blocages de construction empiriques. Une bonne correspondance est observée.

Titre: New Results on Stochastic Geometry Modeling of Cellular Networks: Modeling, Analysis and Experimental Validation

Key words: cellular networks, relays, stochastic geometry

Abstract: The increasing heterogeneity and irregular deployment of the emerging wireless networks give enormous challenges to the conventional hexagonal model for abstracting the geographical locations of wireless transmission nodes. Against this backdrop, a new network paradigm by modeling the wireless nodes as a Poisson Point Process (PPP), leveraging on the mathematical tools of stochastic geometry for tractable mathematical analysis, has been proposed with the capability of fairly accurately estimating the performance of practical cellular networks. This dissertation investigated the mathematical tractability of the PPP-based approach by proposing new mathematical methodologies, fair approximations incorporating practical channel propagation models.

First, a new mathematical framework, which is referred to as an Equivalent-in-Distribution (EiD)-based approach, has been proposed for computing exact error probability of cellular networks based on random spatial networks. The proposed approach is easy to compute and is shown to be applicable to a bunch of multi-input-multi-output (MIMO) setups where the modulation techniques and signal recovery techniques are explicitly considered.

Second, the performance of relay-aided cooperative cellular networks, where the relay nodes, the base stations, and the mobile terminals are modeled according to three independent PPPs, has been analyzed by assuming flexible cell association criteria. It is shown from the mathematical framework that the performance highly depends on the path-loss exponents of one-hop and two-hop links, and the relays provide negligible gains on the performance if the system is not adequately designed.

Third, the PPP modeling of cellular networks with unified signal attenuation model is generalized by taking into account the effect of line-of-sight (LOS) and non-line-of-sight (NLOS) channel propagation. A tractable yet accurate link state model has been proposed to estimate other models available in the literature. It is shown that an optimal density for the base stations (BSs) deployment exists when the LOS/NLOS links are classified in saturate load cellular networks. In addition, the Monte Carlo simulation results of the real BSs deployments with empirical building blockages are compared with those with PPP distributed BSs with the proposed link state approximation at the end of this dissertation as supplementary material. In general, a good matching is observed.

Acknowledgements

First of all, I would like to extend my sincerest thanks and appreciations to my supervisor Dr. Marco Di Renzo and Dr. Anthony Busson for their kind guidance and continual inspiration during my studying. Working with them in the past three years is an exciting and valuable experience. Specifically, Marco's close guidance, his mathematical rigor and perfection in my work has helped me mature as a researcher. In addition to my advisor, my would like to thank my committee members Prof. Pierre Duhamel, Prof. François Baccelli, Prof. Robert Schober, Prof. Laurent Decreusefond, and Prof. Ali Ghrayeb for their constructive comments on my thesis.

A special thank is also extended to my colleague and my friend, Peng Guan, for his encouraging and patience to listen to my ideas and help me in every possible ways. I also want to thank the secretaries in the Laboratory of Signal and System, Maryvonne Giron and Delphine Maucherat for providing comfortable research environment and taking care of the administrative matters.

Most importantly, I would like to thank my parents, Xuzong Lu and Aixin Hou for their unconditional love and support throughout my life. Last but not least, I also want to thank my loving girlfriend, Wei Jiang, who is always there for me, patient and supportive.

The work in this dissertation is supported in part by the European Commission under the auspices of the FP7-PEOPLE MITN-CROSSFIRE project (grant 317126).

Contents

Acknowledgements	i
Contents	ii
Abbreviations	v
Notations and Symbols	vi
1 Introduction	1
1.1 Background	1
1.2 Publications	3
1.3 Contributions and Recognitions	5
1.4 Organization of the dissertation	8
2 The Equivalent-in-Distribution based approach for error performance evaluation	10
2.1 Introduction	10
2.2 System Model	12
2.3 The framework for SISO transmission over Nakagami- m fading	16
2.4 Extension to MIMO Cellular Networks	25
2.4.1 Single-Input-Multiple-Output (SIMO) Transmission over Rayleigh Fading	27
2.4.2 Orthogonal Space-Time Block Coding (OSTBC) Transmission over Rayleigh Fading	27
2.4.3 Zero-Forcing (ZF) MIMO Receiver over Rayleigh Fading	30
2.4.4 Zero-Forcing MIMO Precoding over Rayleigh Fading	31
2.5 Insights from the Mathematical Framework	33
2.6 Numerical and Simulation Results	35
2.7 Conclusion	38
Appendix 2.A Useful Notable Integrals	40
Appendix 2.B Proofs of Propositions and Lemmas	42
Appendix 2.C Proofs of Theorems and Corollaries	46
Appendix 2.D Proof of Proposition 2.3	49
3 Stochastic Geometry Analysis of Relay-aided Cellular Networks	50
3.1 Introduction	50
3.2 System Model	53
3.2.1 Network Deployment Modeling	53

3.2.2	Channel Modeling	54
3.2.3	Cell Association and Relaying Protocol	55
3.2.4	Load Modeling	59
3.3	Problem Formulation and Useful Lemmas	62
3.3.1	Problem Formulation	64
3.3.2	Useful Lemmas	68
3.4	System-Level Performance Evaluation	68
3.4.1	Coverage Probability	70
3.4.2	Average Rate	75
3.4.3	Performance Trends, Design Insight and System-Level Optimization	76
3.5	Numerical and Simulation Results	82
3.6	Conclusion	90
Appendix 3.A	Lemma 3.1, Lemma 3.2 and Lemma 3.3	91
Appendix 3.B	Proofs of Proposition 3.1	93
4	Stochastic Geometry Modeling and Analysis of Cellular Networks over Multi-State Channel Model	102
4.1	Introduction	102
4.2	System Model	104
4.2.1	Base Stations Modeling	104
4.2.2	Link States Modeling	105
4.2.3	Channel Modeling	106
4.2.3.1	Path-Loss Modeling	106
4.2.3.2	Fast Fading	107
4.2.4	Radiation Pattern Modeling	107
4.2.5	Cell Association Criterion	108
4.2.6	Problem Formulation	109
4.3	Tractable Modeling on Link States and Radiation Patterns	111
4.3.1	Multi-ball Link State Approximation	111
4.3.2	Path-loss Intensity Matching	112
4.3.3	Multi-Lobe Radiation Pattern Approximation	114
4.3.4	Radiation Pattern Matching	115
4.4	The Coverage Probability of Cellular Networks	115
4.4.1	Preliminaries	115
4.4.2	Characteristic function of the aggregate interference	117
4.4.3	Prony approximation on the CDF of Gamma distribution	119
4.4.4	Coverage Probability for Smallest path-loss Association	120
4.4.5	Coverage Probability for Highest Received Power Association	121
4.4.6	Fast Fourier Transform Based Efficient Computation	122
4.4.7	Generalization	124
4.5	Performance Trends and Design Insights	125
4.6	Numerical and Simulation Results	127
4.7	Conclusion	131
Appendix 4.A	Useful Notable integrals	132
Appendix 4.B	Proof of Propositions in Section 4.4.2	133
5	Conclusion and Future Work	136

5.1	Summary	136
5.2	Future work	137
A	Simulation and Experimental Validation of the PPP Abstraction with Multi-State Channel Model	140
A.1	Introduction	140
A.2	System Model	141
A.2.1	Base Stations Modeling	141
A.2.2	Buildings Modeling	143
A.2.3	Blockages Modeling	143
A.2.3.1	Empirical-Based Model	143
A.2.3.2	Multi-Ball Approximation	144
A.2.3.3	1-State Model	144
A.2.4	Channel Modeling	144
A.2.5	Cell Association Modeling	145
A.2.6	Problem Statement	146
A.3	Numerical Results: Experimental Validation	146
Simulation Setup		146
Multi-Ball Approximation of the Blockages		147
PPP-Based Modeling of the BSs		149
Achievable Performance: Impact of Blockages		150
A.4	Conclusion	150
	Bibliography	152

Abbreviations

3GPP	3rd Generation Partnership Project
APEP	Average Pairwise Error Probability
ASEP	Average Symbol Error Probability
BS	Base Station
CCDF	Complementary Cumulative Density Function
CDF	Cumulative Density Function
CF	Characteristic Function
CSI	Channel State Information
EiD	Equivalent-in-Distribution
FFT	Fast Fourier Transform
LOS	Line-Of-Sight
LTE	Long-Term Evolution
LTE-A	Long-Term Evolution Advanced
MGF	Moment Generating Function
MIMO	Multiple-Input-Multiple-Output
MT	Mobile Terminal
NLOS	Non-Line-Of-Sight
PDF	Probability Density Function
PPP	Poisson Point Process
RN	Relay Node
RV	Random Variable
SINR	Signal to Interference plus Noise Ratio
SISO	Single-Input-Single-Output
SIMO	Single-Input-Multiple-Output
ZF	Zero Forcing

Notations and Symbols

e	the Euler's number
j	$= \sqrt{-1}$ the imaginary unit
\emptyset	the empty set
\cup	the union of sets
\cap	the intersection of sets
$X \stackrel{d}{=} Y$	the RVs X and Y are equivalent in distribution
$x \propto y$	the x is directly proportional to y
\mathbb{C}	the field of complex numbers
\mathbb{R}	the field of real numbers
$(\cdot)_q$	the Pochhammer symbol with non-negative integer q
$(\cdot)!$	the factorial operator
$\binom{\cdot}{\cdot}$	the binomial coefficient
x^*	the conjugate operators of a complex number x
$ x $	the modulus operator of a complex number x
$\arg\{x\}$	phase operator of a complex number x
$\ \mathbf{x}\ $	the norm of vector \mathbf{x}
$\ \mathbf{X}\ $	the Frobenius norm of matrix \mathbf{X}
\mathbf{X}^H	the Hermitian of matrix \mathbf{X}
$\delta(\cdot)$	the Dirac delta function
$\mathbf{1}(\cdot)$	the indicator function
$\mathbf{1}_{[a,b]}(\cdot)$	the generalized indicator function $\mathbf{1}_{[a,b]}(r) = 1$ if $r \in [a, b)$, $\mathbf{1}_{[a,b]}(r) = 0$ if $r \notin [a, b)$
$\mathcal{H}(\cdot)$	the Heaviside step function
$\overline{\mathcal{H}}(\cdot)$	$= 1 - \mathcal{H}(\cdot)$, the complimentary Heaviside step function
$\llbracket \cdot \rrbracket$	the round operator

$\mathbb{E}\{\cdot\}$	the expectation operator
$\mathbb{E}_X\{\cdot\}$	the expectation with respect to X
$\mathbb{E}_{(\cdot)\setminus X}\{\cdot\}$	the expectation with respect to all random variables except X
$\text{Re}\{\cdot\}$	real part operator
$\text{Im}\{\cdot\}$	imaginary part operator
$\text{Pr}\{\cdot\}$	the probability
$\max\{\cdot, \cdot\}$	the maximum function
$\min\{\cdot, \cdot\}$	the minimum function
$\text{card}\{\mathbb{S}\}$	the cardinality of the set \mathbb{S}
$\Gamma(\cdot)$	the Gamma function [1, Eq. (6.1.1)]
$\Gamma(\cdot, \cdot)$	the upper-incomplete Gamma function [1, Eq. (6.5.3)]
$\gamma(\cdot, \cdot)$	the lower-incomplete Gamma function [1, Eq. (6.5.2)]
${}_pF_q(\cdot; \cdot; \cdot)$	hypergeometric function [2, Ch. IV]
$J_\nu(\cdot)$	Bessel function of the first kind [1, Eq. (9.1.10)]
$G_{p,q}^{m,n} \left(\begin{matrix} (\cdot) \\ (\cdot) \end{matrix} \middle \begin{matrix} (\mathbf{a}_p) \\ (\mathbf{b}_q) \end{matrix} \right)$	Meijer G-function [3, Sec. 2.24]
$\mathcal{U}(a, b)$	a uniform distribution in (a, b)
$\mathcal{N}(\mu, \sigma^2)$	a real Gaussian distribution with mean μ and variance σ^2
$\mathcal{CN}(\mu, \sigma^2)$	a complex Gaussian distribution with mean μ and variance σ^2
$\mathcal{G}(m, \Omega)$	Gamma distribution with fading parameter m and mean square value Ω [4, Eq. (2.21)].
χ_d^2	Chi-Square distribution with d degrees of freedom [5, Eq. (54)].
$\mathcal{F}(d_1, d_2)$	F-distribution [5, Eq. (61)] with parameters d_1 and d_2
$\mathcal{M}_X(s)$	the MGF of a real RV X , $\mathcal{M}_X(s) = \mathbb{E}\{\exp(-sX)\}$
$\text{CF}_X(\omega)$	the CF of a real RV X , $\text{CF}_X(\omega) = \mathbb{E}\{\exp(j\omega X)\}$
$\text{CF}_{\mathbf{X}}(\boldsymbol{\omega})$	the CF of a complex RV \mathbf{X} , $\boldsymbol{\omega} = (\omega_1, \omega_2)$ $\text{CF}_{\mathbf{X}}(\boldsymbol{\omega}) = \mathbb{E}\{\exp(j(\omega_1 \text{Re}\{\mathbf{X}\} + \omega_2 \text{Im}\{\mathbf{X}\}))\}$
$\mathbf{F}_{f(x_n)}[k]$	the k -th output of the FFT of the discrete finite input $f(x_n)$

Chapter 1

Introduction

1.1 Background

Accurate yet tractable modeling of cellular networks and its performance evaluation have been a longstanding open research problem in the communication society. The most frequently considered base station (BS) geometry model is the hexagonal model [6], where the BSs are placed ideally in a regular infinite hexagonal lattice. This model, however, is considered to be too idealized even for modeling a carefully planned macro cellular system since the real sites are usually deviated from its theoretical positions due to the unavailability of candidate sites in their theoretical positions in reality. Moreover, due to the increasing heterogeneity and densification of the emerging cellular networks, where the small cell BSs are randomly overlaid within the macro cell, the accuracy of the traditional hexagonal grid modeling, which has been used for decades, is questionable. Another limitation of the conventional hexagonal model is its mathematical intractability. Explicit derivation of the performance of hexagonal wireless networks by taking into account the effect of other-cell interference is intractable, thus, expensive and time consuming system level simulation is needed for performance evaluation. To this end, the bi-dimensional point process abstraction modeling [7], which leverages tools from stochastic geometry for tractable characterization and performance analysis, is increasingly attracting the attention of the research community.

Among all the point processes available in the literature, the homogeneous Poisson Point Process (PPP) is the most popular one thanks to its tractability in the performance

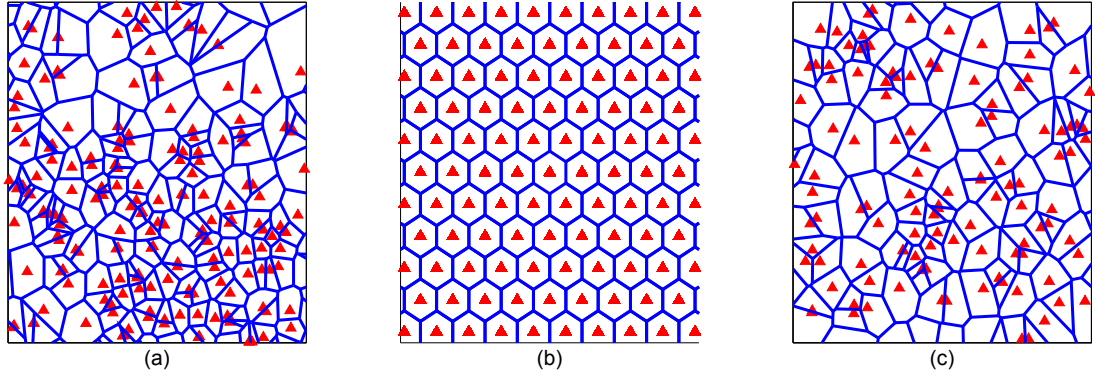


FIGURE 1.1: BS deployments and the voronoi cell, the triangle denotes the locations of BSs, the solid line is the voronoi boundary: (a) Actual BS locations in London, (b) hexagonal model, (c) PPP distributed BSs.

analysis and system optimization. The definition of the bi-dimensional PPP in the Euclidean plane \mathbb{R}^2 is as follows [8, Ch. 2]:

Definition 1.1. The point process $\Phi \in \mathbb{R}^2$ is a PPP with intensity λ if 1) for every bounded closed set $B \subset \mathbb{R}^2$, the counting measure of the point process on B , $\Phi(B)$, follows a Poisson distribution with mean $\lambda[B]$, where $[\cdot]$ is the Lebesgue measure in two dimensions and λ is the expected number of points per unit area, and 2) $\Phi(B_1), \Phi(B_2), \dots, \Phi(B_k)$ are independent if B_1, B_2, \dots, B_k are disjoint.

An illustration of the PPP distributed BSs, the hexagonal modeled BSs and the real BS locations in an urban area in London, UK is available in 1.1, where the database of the BSs locations is available from [9]. From the definition, the PPP-based abstraction model indicates that the wireless nodes are distributed independently of each other and no repulsion between nodes are considered. Obviously, it is an idealized model that neglects the spatial correlation among the BSs. Its accuracy in modeling realistic cellular networks in urban area is, however, surprisingly good compared to the hexagonal lattice. More specifically, the authors in [10] compare the the PPP model with the grid model and the real BS locations in a Long-Term Evolution (LTE) cellular network. They have shown that the PPP approach provides a lower bound of the coverage probability of realistic site deployment, whereas the grid counterpart provides an upper bound. In [11], similar comparisons have been done by considering the real BS deployments in urban areas in several metropolitans where the BS locations are from the public database. They have concluded that the PPP model is more accurate than the hexagonal grid model for modeling BSs in urban areas. Furthermore, the authors in [12] show that precise

success probabilities of all motion-invariant point process can be obtained by shifting the success probability curve of the PPP with the same density, which further stimulate the motivation of studying the PPP distributed wireless networks. Inspired by its accuracy and flexibility, the performance analysis, system design and optimization by using the PPP-based approach have been one of the major interests in the communications society, *e.g.*, in [10, 13–27], and the references therein.

In my doctoral research, emphasis has been put on the mathematical tractability of the PPP abstraction model regarding i) the end-to-end performance analysis of emerging cellular networks by taking into account the impact of network interference, ii) the design of interference-aware transceivers that exploit the statistical knowledge of network interference for performance improvement, iii) modeling, analyzing and optimization of relay-aided cooperative cellular networks where the relay nodes are randomly distributed, iv) system-level analysis and optimization of cellular networks with simultaneous wireless information and power transfer, and v) the performance evaluation of cellular networks by explicitly taking into account the effect of line-of-sight(LOS) and non-line-of-sight(NLOS) channel propagations. So far, six journal papers and nine conference papers have been published/submitted incorporating the findings in the depicted research interests. The full publication list and brief summaries of each journal paper are given in the next section.

1.2 Publications

Journal Publications

[R1] Marco Di Renzo and Wei Lu, “The Equivalent-in-Distribution (EiD)-based Approach: On the Analysis of Cellular Networks Using Stochastic Geometry”, *IEEE Communications Letters*, Vol. 18, No. 5, pp. 761-764, May, 2014.

[R2] Marco Di Renzo and Wei Lu, “End-to-End Error Probability and Diversity Analysis of AF-based Dual-Hop Cooperative Relaying in a Poisson Field of Interferers at the Destination”, *IEEE Transactions on Wireless Communications*, Vol. 14, No. 1, pp.15-32, Jan 2015.

[R3] Marco Di Renzo and Wei Lu, “On the Diversity Order of Selection Combining Dual-Branch Dual-Hop AF Relaying in a Poisson Field of Interferers at the Destination”, *IEEE Transactions on Vehicular Technology*, Vol. 64, No. 4, pp.1620-1628, April 2015.

[R4] Marco Di Renzo and Wei Lu, “Stochastic Geometry Modeling and Performance Evaluation of MIMO Cellular Networks by Using the Equivalent-in-Distribution (EiD)-Based Approach”, *IEEE Transactions on Communications*, Vol. 63, No. 3, pp.977-996, March 2015.

[R5] Wei Lu and Marco Di Renzo, “Stochastic Geometry Modeling and System-Level Analysis/Optimization of Relay-Aided Downlink Cellular Networks”, *IEEE Transactions on Communications*, Vol. 63, No. 11, pp.4063-4085, November 2015.

[R6] Wei Lu and Marco Di Renzo, “System-Level Analysis/Optimization of Cellular Networks with Simultaneous Wireless Information and Power Transfer: Stochastic Geometry Modeling”, submitted to *IEEE Transactions on Vehicular Technology*.

Conference Publications

[R7] Wei Lu and Marco Di Renzo, “Performance Analysis of Spatial Modulation MIMO in a Poisson Field of Interferers”, International Conference on Computing, Networking and Communications (ICNC), Hawaii, USA, February 3-6, 2014. Best Paper Nominated.

[R8] Wei Lu, Marco Di Renzo and Anthony Busson, “Stochastic Geometry Modeling and Analysis of the Error Probability of Two-tier Cellular Networks”, EUCNC, Bologna, Italy, June 23-26, 2014.

[R9] Wei Lu, Marco Di Renzo, “Performance evaluation of relay-aided cellular networks by using stochastic geometry”, IEEE CAMAD, Athens, Greece, Dec 1-3, 2014. Best Paper Award.

[R10] Wei Lu and Marco Di Renzo, “Interference-Aware Dual-Hop Cooperative Relaying in a Poisson Field of Interferers”, IEEE GLOBECOM, Austin, USA, Dec 8-12, 2014.

[R11] Wei Lu and Marco Di Renzo, “Stochastic Geometry Analysis of Multi-User MIMO Cellular Networks Using Zero-Forcing Precoding”, IEEE ICC, London, UK, June 8-12, 2015.

[R12] Wei Lu and Marco Di Renzo, “Accurate Stochastic Geometry Modeling and Analysis of mmWave Cellular Networks”, IEEE ICUWB, Montreal, Canada, Oct 4-7, 2015.

[R13] Wei Lu and Marco Di Renzo, “Stochastic Geometry Modeling of mmWave Cellular Networks: Analysis and Experimental Validation”, IEEE M&N, Coimbra, Portugal, Oct 12-13, 2015.

[R14] Wei Lu and Marco Di Renzo, “Stochastic Geometry Modeling of Cellular Networks: Analysis, Simulation and Experimental Validation”, ACM MSWiM, Cancun, Mexico, Nov 2-6, 2015.

[R15] Wei Lu and Marco Di Renzo, “On Stochastic Geometry Analysis and Optimization of Wireless-Powered Cellular Networks”, IEEE GLOBECOM, San Diego, USA, Dec 6-10, 2015.

1.3 Contributions and Recognitions

The main findings of the published/submitted journal papers are summarized as follows:

In [R1], the Equivalent-in-Distribution (EiD)-based approach to the analysis of cellular networks is introduced. It is based upon finding EiD representations of the aggregate other-cell interference of cellular networks, which lead to tractable and exact mathematical formulations of the Average Symbol Error Probability (ASEP) for arbitrary bi-dimensional modulations. As a byproduct, a new lemma is introduced, which provides a single-integral expression of the ASEP in terms of the Complementary Cumulative Distribution Function (CCDF) of the Signal-to-Interference-plus-Noise-Ratio (SINR).

In [R2], the mathematical frameworks to the analysis of amplify-and-forward dual-hop cooperative relaying protocols are provided in the presence of Nakagami- m fading, additive noise at the relay, as well as additive noise and symmetric alpha-stable interference at the destination. Quasi-static and fast-varying interference scenarios are investigated, which arise, *e.g.*, when either the same or different interferers are active during the broadcast and relaying phases, respectively. A maximal ratio combining demodulator is studied, by assuming that the aggregate interference is either unknown (interference-oblivious) or can be estimated (interference-aware) at the destination. Closed-form

expressions of the end-to-end moment generating function are provided and the achievable diversity order is studied for different setups. The diversity order is shown to depend on the path-loss exponent of the interfering network. Under the assumption that the transmit-powers of cooperative and interfering networks are independent, it is proved that the interference-aware maximal ratio diversity combiner is capable of achieving second-order diversity only asymptotically, as the amplitude path-loss exponent tends to one.

In [R3], the diversity order of Selection Combining (SC) receiver and that of the Maximal Ratio Combining (MRC) receiver are investigated in the presence of randomly distributed interferers at the destination. More specifically, an amplify-and-forward dual-branch dual-hop cooperative relaying protocol in the presence of Nakagami- m fading, additive noise at the relay, as well as additive noise and symmetric alpha-stable interference at the destination is investigated. By contrasting the diversity order of SC against the diversity of MRC studied in [R2], it is shown that both combining schemes provide the same diversity order if the distribution of the aggregate interference is unknown to the destination (interference-oblivious design). They may achieve a different diversity order, on the other hand, if the aggregate interference can be estimated at the destination (interference-aware design). Also, it is shown that the achievable diversity order depends on the aggregate interference in the broadcast and relaying phases being spatially correlated or independent.

In [R4], the EiD-based approach in [R1] to the analysis of Single-Input-Single-Output (SISO) cellular networks for transmission over Rayleigh fading channels has been generalized to compute the error probability of the PPP distributed cellular networks incorporating a set of multiple-input-multiple-output (MIMO) structures, the modulation techniques and signal recovery techniques. The rationale of proposed approach relies on finding a series of conditional compound Gaussian representation of the aggregate interference from the demodulator. Then, the well-developed technologies for the error probability analysis for end-to-end communication over additive-white-Gaussian-noise (AWGN) channels can be applied if the non-Gaussian random variables are conditioned. Finally, the exact error probability in the presence of non-Gaussian distributed interference can be obtained by removing the conditions. This approach is shown to be applicable to SISO networks with Nakagami- m fading, single-input-multiple-output (SIMO)

networks with Rayleigh fading, and MIMO cellular networks over Rayleigh fading, including spatial-multiplexing, orthogonal space-time block coding (OSTBC), zero-forcing (ZF) reception and zero-forcing precoding. The performance trends with respect to the MIMO setups are observed from an asymptotic analysis of the error probability.

In [R5], the performance of the relay-aided cellular networks is investigated where the relay nodes, the BSs and the mobile terminals (MTs) are assumed to be distributed according to two independent PPPs. A flexible cell association criterion and relay-aided transmission protocol based on the biased average received power are considered. The mathematical intractability, when dealing with the spatial correlation between the active relays and serving BSs for cooperative transmission, has been solved through reasonable approximations based on the geometry structure. It is shown, from the mathematical frameworks, that the coverage and rate of the system highly depends on the path-loss exponents of the one- and two-hop links, and a system level optimization is proposed by modifying the biasing factors for the one- and two-hop transmission which maximizes the coverage or the rate.

In [R6], a new mathematical approach for the analysis and optimization of cellular networks with simultaneous wireless information and power transfer is introduced. The proposed methodology leverages stochastic geometry for system-level analysis of cellular networks, by modeling base stations locations as points of a spatial Poisson point process. The trade-offs emerging from simultaneous wireless information and power transfer transmission are characterized through the concept of “feasibility regions” and are quantified through the joint cumulative distribution function of average harvested energy and average rate, which is formulated in terms of easy-to-compute two-fold integrals. To gain insight on the achievable performance, in addition, an upper-bound is proposed, and its accuracy is discussed. The system model encompasses a realistic channel model that accounts for line-of-sight and non-line-of-sight links, different cell association criteria, practical receivers based on time switching and power splitting, directional beamforming. The analysis shows that optimal values for the time switching and power splitting ratios exist, as well as that directional beamforming and network densification are capable of enhancing the achievable performance. More specifically: i) high directional antennas lead cellular networks to operate in the noise-limited regime, which is proved to provide optimal performance, and ii) because of the existence of line-of-sight and non-line-of-sight links, an optimal deployment density for the base stations

is proved to exist for typical system setups.

While in pursuing a doctoral degree, I also got the following recognitions.

- Exemplary Reviewer of IEEE Transactions on Communications in 2014
- Exemplary Reviewer of IEEE Communications Letters in 2014
- 2014 IEEE CAMAD Best Paper Award
- 2014 IEEE ICNC Single Best Paper Award Nomination

1.4 Organization of the dissertation

In order to save the space and to report the latest research findings, the present dissertation is structured based on the research findings published in [R4], [R5], which are reported in Chapter 2–3, while other research achievements in [R1], [R2], [R3] and [R6] are, on the other hand, not presented in this dissertation. In addition, the most recent research on the mathematical tractability of the PPP model in the presence of LOS/NLOS channel states is also included and reported in Chapter 4.

In specific, the researching findings in Chapter 2–4 tackles the often cited questions on stochastic geometry modeling about its mathematical flexibility of i) the symbol level error probability analysis by explicitly taking into account the modulator and the demodulator, ii) modeling the relaying cellular networks where the positions of the transmitting nodes, i.e., relays and BSs, might be spatially correlated due to the cell association, and iii) modeling realistic but more complicated channel propagation to shed light on the system design and optimization of practical cellular networks. In addition to investigating the flexibility of stochastic geometry on modeling various network architectures, Chapter 2–4 also tried to address the common concerns on the complexity of the mathematical frameworks obtained by using stochastic geometry on modeling relatively complicated network architectures. Several approximations have been proposed to this end to simplify the frameworks while keeping a good accuracy. All the mathematical frameworks proposed in this dissertation have been tested and can be efficiently evaluated by the commercial mathematical computation program, *e.g.*, Mathematica 10.

The outline of the present dissertation are summarized as follows.

In Chapter 2, the EiD-based approach is introduced for the error probability evaluation of MIMO cellular networks, which corresponds to the main contributions in [R4] as depicted previously. In Chapter 3, a tractable mathematical framework for the analysis and optimization of two-hop relay-aided cellular networks is introduced, which corresponds to the main contributions in [R5].

In Chapter 2 and 3, a fundamental assumption on the nature of signal attenuation is that the received signal/power (including the interference) decays like $r^{-\beta}$ over distance r , where $\beta > 2$ is referred to as the power path-loss exponent. Although in ubiquitous use in literatures of stochastic geometry, this path loss model is quite idealized. In Chapter 4, more practical two-state path-loss models are assumed, where the effect of LOS and NLOS propagations have been explicitly taken into account, for network modeling and performance analysis. Different link state models, consisting of the probabilities of links being in LOS or in NLOS, are compared. Furthermore, a more tractable model has been proposed, which is referred to as multi-ball state model and is shown to be capable of accurately approximating other state models with an acceptable complexity. The proposed framework also accounts for the antenna radiation pattern as well as the multi-tier heterogeneous networks. It is shown that the performance trends of the PPP distributed cellular networks with two-state channel model are different from their counterparts with the single-state model.

In Chapter 2–4, the emphasis has been put on the mathematical tractability of the PPP-based approach. Finally, in Appendix A, the accuracy of the PPP abstraction model is studied through comparing the coverage probabilities of PPP distributed single-tier cellular networks against those of real BSs deployment from two telecom operators in London, UK. The effect of LOS and NLOS channel propagation is also considered in the comparison by considering both the empirical blockage caused by the buildings and the multi-ball state model, which shows the flexibility and accuracy of the proposed approximation on modeling empirical blockage models. Since only Monte Carlo simulation results are shown in this Chapter, it is included in the dissertation as appendix. The results are also published in [R14].

Chapter 2

The Equivalent-in-Distribution based approach for error performance evaluation

2.1 Introduction

One of the main advantage of the PPP abstraction to model the cellular network is its mathematical tractability in the performance analysis [10]. Two main performance metrics have been studied to date, *i.e.*, the outage probability and the average rate [10, 21, 24]. Less attention has been given, on the other hand, to the computation of the ASEP, which is, however, a relevant figure of merit to wireless systems analysis and design. In fact, it is directly related to the bit, packet, block and frame error probabilities, which are important performance metrics to the design of cellular networks [28]. Indeed, mathematical frameworks relying on the PPP-based abstraction are available to the computation of the ASEP of ad hoc networks [19, 20]. They are not applicable, however, to cellular networks, as the aggregate interference of decentralized (ad hoc) and centralized (cellular) networks has a different distribution.

Moreover, from [25, Table I], in particular, it is apparent that most mathematical frameworks available to date in the field of stochastic geometry are applicable to the analysis of SISO cellular networks. A few exceptions to this status quo, however, exist. In [27], coverage probability and area spectral efficiency of MIMO cellular networks are studied

with the aid of tools from stochastic geometry and stochastic ordering. Various downlink MIMO transmission schemes are studied and compared, including space division multiple access, single user beamforming and the baseline SISO setup. In [25], the error probability of spatial multiplexing MIMO transmission is investigated with the aid of stochastic geometry and the Gil-Pelaez theorem. In [29], the energy efficiency potential of MIMO cellular networks that use maximal ratio transmission is studied. In [30], the physical-layer security potential of regularized channel inversion precoding applied to MIMO cellular networks is investigated.

Against these backgrounds, in this chapter, a new mathematical approach to the computation of the ASEP of downlink MIMO cellular networks is introduced. Its rationale relies upon finding EiD representations of the aggregate other-cell interference, which is formulated as a linear combination of conditionally Gaussian random variables (RVs). With the aid of this mathematical formulation, the error probability is computed by first conditioning upon the non-Gaussian RVs and by then removing the conditioning. The usefulness of this approach lies in the possibility of obtaining *exact* mathematical expressions in the presence of non-Gaussian distributed interference. The new mathematical framework is based on the computation of the moment generating function (MGF) of the equivalent power gain of the intended link, which makes the EiD-based approach applicable to a number of MIMO arrangements for transmission over Rayleigh fading channels. Also, we show that the proposed approach is also applicable to SISO cellular networks for transmission over Nakagami- m fading channels. Compared to [27], our approach is different since it does not exploit stochastic ordering. Compared to [25], our approach: i) is not based on the Gil-Pelaez inversion theorem; ii) is applicable to many MIMO schemes; and iii) provides, in many cases, exact integral expressions of the error probability, while [25] does not, as it is based on the computation of pairwise error probabilities. In the presence of other-cell interference and noise, the error probability is formulated in terms of a two-fold integral. The framework is shown to reduce to the computation of a single integral in interference-limited cellular networks. Also, a simple closed-form expression is introduced, which provides meaningful insights on the impact of various system parameters that determine the achievable performance of MIMO cellular networks.

The remainder of the present chapter is organized as follows. In Section 2.2, the system

TABLE 2.1: Recurrent parameters and symbols.

Symbol	Meaning
Ψ	PPP of BSs
N_t	number of antennas at each BS
N_r	number of antennas at the MT
N_s	number of time-slots of a data transmission frame
N_u	number of intended MTs for MIMO cellular networks using zero-forcing precoding
τ	index of the time-slot
$\boldsymbol{\eta}$	vector of modulated information symbols
M	number of information symbols transmitted in N_s time slots
\mathbf{M}	number of candidate modulated symbols
μ_χ	modulated symbols
$\mathbf{s}(\tau)$	the set of space-time encoded symbols emitted by the BS in τ -th time slot
E	BSs transmi-energy per transmission
b	amplitude path-loss exponent

model is introduced. In Section 2.3, the mathematical framework for the SISO transmission over Nakagami- m is first introduced. In Section 2.4, the framework has been extended to be applicable to various MIMO transmission schemes. In Section 2.5, the framework is further investigated and it is shown to provide relevant insight in to the design of MIMO cellular networks. In Section 2.6, numerical illustrations are provided to substantiate the proposed approach with the aid of Monte Carlo simulations. Finally, Section 2.7 concludes this chapter.

Notation: The following notations are used in this chapter. $\mathbf{x} \in \mathbb{S}^{K \times 1}$ denotes a $K \times 1$ column-vector with entries belonging to the set \mathbb{S} . The k th entry is denoted by $\mathbf{x}^{(k)}$. $\mathbf{X} \in \mathbb{S}^{K \times L}$ denotes a $K \times L$ matrix with entries belonging to the set \mathbb{S} . The (k, l) th entry is denoted by $\mathbf{X}^{(k, l)}$. $\tilde{\mathbf{X}}$ denotes the hypothesis of \mathbf{X} , $\bar{\mathbf{X}}$ denotes the post-processed matrix \mathbf{X} at the MT. Let a generic function $f(x)$ with complex random variable x , the writing $f(x) = f(|x|)$ indicates that the function $f(x)$ is independent from the phase of x . The recurrent parameters and symbols are summarized in Table 2.1.

2.2 System Model

To illustrate the EiD based approach, in this chapter, we consider a bi-dimensional downlink cellular network deployment as shown in Figure 2.1, where a typical multi-antenna Mobile Terminal (MT) is located at the origin and the multi-antenna BSs are modeled as points of a homogeneous PPP (Ψ) of density λ . The number of antennas at

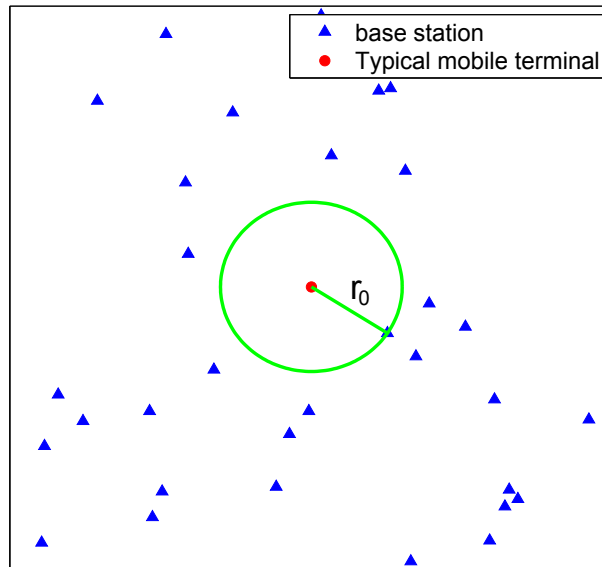


FIGURE 2.1: An example of the PPP distributed cellular networks. The MT located at the origin is served by the closest BS, all the interfering nodes are distributed outside the circular area centered at the origin with radius r_0 .

each BS and at the MT is denoted by N_t and N_r , respectively. Based on the properties of homogeneous PPPs, there is no loss of generality in assuming the MT to be located at the origin [7]. The distance from the i th BS to the MT is denoted by r_i for $i \in \Psi$. The MT is assumed to be tagged to the nearest BS, *i.e.*, a shortest distance cell association criterion is considered. The serving BS is denoted by BS_0 and its distance from the MT is denoted by r_0 , which is a RV with Probability Density Function (PDF) equal to $f_{r_0}(\xi) = 2\pi\lambda\xi \exp(-\pi\lambda\xi^2)$ [10]. According to the properties of homogeneous PPPs [7, Theorem 1.4.5], the set of interfering BSs $i \in \Psi^{(\setminus 0)} = \Psi \setminus \{BS_0\}$ is still a homogeneous PPP outside the ball centered at the origin and of radius r_0 . By definition of shortest distance cell association, $r_i > r_0$ for $i \in \Psi^{(\setminus 0)}$. Full frequency reuse is assumed, *i.e.*, all interfering BSs transmit in the same frequency band as BS_0 . Upon completion of the cell association, the interfering BSs transmit packets with equal probabilities $0 \leq p \leq 1$, which represent independent activity factors. This model finds application to the analysis of, *e.g.*, slotted-ALOHA cellular networks [31] and it is particularly suited in the context of PPP-based abstraction modeling, since, due to the independent thinning property of PPPs [7, Proposition 1.3.5], the set of interfering BSs is still a PPP of density $p\lambda$.

In the depicted downlink MIMO cellular network model, data transmission occurs in frames of N_s time-slots each. The signal received at the MT in the τ th time-slot can be formulated as follows ($\tau = 1, 2, \dots, N_s$):

$$\mathbf{y}(\tau) = \underbrace{\sqrt{E/N_t r_0^{-b}} \mathbf{H}_0 \mathbf{s}_0(\tau)}_{\mathbf{x}(\tau)} + \underbrace{\sqrt{E/N_t} \sum_{i \in \Psi^{(0)}} r_i^{-b} \mathbf{H}_i \mathbf{s}_i(\tau)}_{\mathbf{i}_{\text{agg}}(\tau; r_0)} + \mathbf{n}(\tau) \quad (2.1)$$

where $\mathbf{y}(\cdot) \in \mathbb{C}^{N_r \times 1}$; $\mathbf{x}(\cdot) \in \mathbb{C}^{N_r \times 1}$ is the intended signal from BS₀; $\mathbf{i}_{\text{agg}}(\cdot, \cdot) \in \mathbb{C}^{N_r \times 1}$ is the aggregate other-cell interference; and $\mathbf{n}(\cdot) \in \mathbb{C}^{N_r \times 1}$ is the Additive White Gaussian Noise (AWGN). More specifically: i) E is the BSs transmit-energy per transmission, which is equally split among the N_t antennas; ii) $\mathbf{s}_0^{(t)}(\tau) = \Theta^{(\tau, t)}(\boldsymbol{\eta}_0; \mathcal{S}_{\mathcal{I}}^{(0)}) \in \mathbb{C}$, for $t = 1, 2, \dots, N_t$ and $\tau = 1, 2, \dots, N_s$, is the vector of space-time encoded symbols emitted by BS₀, where $\Theta(\cdot; \cdot)$ is the $N_s \times N_t$ space-time encoding matrix, $\boldsymbol{\eta}_0$ is the vector of modulated information symbols and $\mathcal{S}_{\mathcal{I}}^{(0)}$ is the *side information* available at BS₀. In particular, M independent information symbols are transmitted in N_s time-slots, *i.e.*, $\boldsymbol{\eta}_0$ is a $M \times 1$ column-vector and $\boldsymbol{\eta}_0^{(m)} \in \mathbb{M}$ for $m = 1, 2, \dots, M$ with \mathbb{M} denoting the set of modulated symbols. The generic $M = \text{card}\{\mathbb{M}\}$ symbols of \mathbb{M} are denoted by $\mu_\chi \in \mathbb{C}$ for $\chi = 1, 2, \dots, M$. A zero-mean and an average unit-energy constraints are assumed, *i.e.*, $(1/M) \sum_{\chi=1}^M \mu_\chi = 0$ and $(1/M) \sum_{\chi=1}^M |\mu_\chi|^2 = 1$, respectively. For example, they can be the M symbols of either a Phase Shift Keying (PSK) or a Quadrature Amplitude Modulation (QAM) constellation diagram. The rate provided by (2.1) is $\mathcal{R} = (M/N_s) \log_2(M)$ bits per channel use (bpcu); iii) $\mathbf{H}_0 \in \mathbb{C}^{N_r \times N_t}$ is the channel matrix of the BS₀-to-MT link, where $\mathbf{H}_0^{(r, t)} = \left| \mathbf{H}_0^{(r, t)} \right| \exp \left\{ j \arg \left\{ \mathbf{H}_0^{(r, t)} \right\} \right\} \in \mathbb{C}$ and $\arg \left\{ \mathbf{H}_0^{(r, t)} \right\} \sim \mathcal{U}(0, 2\pi)$ for $t = 1, 2, \dots, N_t$ and $r = 1, 2, \dots, N_r$. Quasi-static fading is assumed in (2.1), which implies that \mathbf{H}_0 is constant in the N_s times-slots of a frame, *i.e.*, $\mathbf{H}_0(\tau) = \mathbf{H}_0$ for $\tau = 1, 2, \dots, N_s$, while it changes independently from one frame to another. The channel envelope $\left| \mathbf{H}_0^{(r, t)} \right|$ is assumed to follow a Rayleigh distribution [4, Sec. 2.2.1.1]. The only exception is the SISO setup in Section 2.3, where $\left| \mathbf{H}_0^{(r, t)} \right|$ follows a Nakagami- m distribution with fading parameter m [4, Sec. 2.2.1.4]; iv) $b > 1$ is the amplitude path-loss exponent; v) $\mathbf{n}^{(r)}(\tau) \sim \mathcal{CN}(0, \mathcal{N}_0)$ are independent and identically distributed (i.i.d.) RVs for $r = 1, 2, \dots, N_r$, $\tau = 1, 2, \dots, N_s$. Similar notation and assumptions are adopted for the interfering channels of $\mathbf{i}_{\text{agg}}(\cdot; \cdot)$. As for the other-cell interference model, (2.1) assumes the so-called isotropic scenario [20, Sec. II-B], where the N_r antennas at the MT are omnidirectional and are subject to the interference

generated by all interfering BSs. Moreover, the aggregate other-cell interference depends on r_0 , since the interfering BSs must lie outside the ball of radius r_0 and centered at the origin. This originates from the shortest distance cell association criterion. The transmit- and receive-antennas are assumed to be co-located, hence the transmission distances r_0 and r_i for $i \in \Psi^{(\setminus 0)}$ are independent of the antennas inter-distances. Similar to the intended link, locations and channels of all interfering BSs are assumed not to change in the N_s times-slots of a frame. All channels are i.i.d. with mean square value $\mathbb{E} \left\{ \left| \mathbf{H}_0^{(r,t)} \right|^2 \right\} = \mathbb{E} \left\{ \left| \mathbf{H}_i^{(r,t)} \right|^2 \right\} = \Omega$ for $t = 1, 2, \dots, N_t$, $r = 1, 2, \dots, N_r$, $i \in \Psi^{(\setminus 0)}$. The signal model in (2.1) is sufficiently general to account for a large number of MIMO schemes, which are studied in Section 2.4.

Remark 2.1. In the system model of interest, an uncoded transmission is assumed, while the channel coding, which is one of the essential components of digital communications chain, has been neglected in this report. Actually, the EiD-based approach can be extended to the case in the presence of channel coding with a long codewords by making some assumptions on the dynamics of the channels and of the interferers. For example, for mathematical tractability, a block-fading channel, a fast-fading channel or a quasi-static fading channel can be assumed for the duration of a codeword. As for the interfering nodes, the dynamics of the locations of the interferers need to be taken into account as well. One of the reasonable assumption might be to assume that the locations of the interferers are static for the duration of a codeword, but the associated channel gains may change according to the three depicted possibilities. In this case, the other-cell aggregate interference seen at the typical MT during a codeword will be partially correlated across the symbols of the codeword because of the full correlation of the spatial locations and of the possible correlation of the channel dynamics. How to deal with this partially correlated interference is still an open research question in stochastic geometry modeling and analysis. Thus, the system in the presence of channel coding has been postponed to future research. \square

Also, the following preliminaries are introduced.

Preliminary 2.1. Let a complex RV X . It is said to be spherically symmetric (or circularly symmetric or rotationally invariant) if its PDF, denoted by $f_X(\cdot)$, depends only on $|X|$, i.e., $f_X(x) = f_X(|x|)$ [19, 32]. \square

Remark 2.2. Let $X = X^{(\text{re})} + jX^{(\text{im})}$ be a complex spherically symmetric RV, where $X^{(\text{re})}$ and $X^{(\text{im})}$ denote the real and imaginary part of X , respectively. Then, the following properties hold [19, 32]: i) $X \stackrel{d}{=} X \exp\{j\phi\}$, where $\phi \in [0, 2\pi)$ is an arbitrary constant, ii) the characteristic function of a random variable X is $\text{CF}_X(\boldsymbol{\omega}) = \text{CF}_X(|\boldsymbol{\omega}|)$, iii) $\text{CF}_{X^{(\text{re})}}(|\boldsymbol{\omega}|) = \text{CF}_{X^{(\text{im})}}(|\boldsymbol{\omega}|) = \text{CF}_X(|\boldsymbol{\omega}|)$, iv) $\text{CF}_X(|\boldsymbol{\omega}|) = \mathbb{E}_{X^{(\text{re})}}\{\cos(|\boldsymbol{\omega}| X^{(\text{re})})\} = \mathbb{E}_{X^{(\text{im})}}\{\cos(|\boldsymbol{\omega}| X^{(\text{im})})\}$, and v) a linear combination of spherically symmetric RVs is still a spherically symmetric RV. \square

Preliminary 2.2. Let a complex RV X . The RV $X^{(\text{GCG})}$ is said to be a *Generalized Compound Gaussian (GCG) representation* of X if the following equality in distribution holds:

$$X \stackrel{d}{=} X^{(\text{GCG})} = \sum_{q=1}^{+\infty} \sqrt{\mathbf{B}_q} \mathbf{G}_q \quad (2.2)$$

and: i) $\{\mathbf{B}_q\}_{q=1}^{+\infty}$ are independent real RVs with $\mathcal{M}_{\mathbf{B}_q}(s) = \exp\{-s^q\}$, ii) $\{\mathbf{G}_q\}_{q=1}^{+\infty}$ are independent complex Gaussian RVs with distribution $\mathbf{G}_q \sim \mathcal{CN}(0, \sigma_{\mathbf{G}_q}^2)$, iii) $\{\mathbf{B}_q\}_{q=1}^{+\infty}$ and $\{\mathbf{G}_q\}_{q=1}^{+\infty}$ are independent RVs. \square

2.3 The framework for SISO transmission over Nakagami- m fading

In this section, the mathematical framework for studying the average symbol error probability of SISO cellular network over Nakagami- m fading is presented by invoking the EiD-based approach. Also, the framework is formulated by introducing some general notations and results to make it extendable to the MIMO arrangements in the next section.

Let a SISO transmission scheme and a Nakagami- m fading channel model [33, Sec. 2]. Thus, we have $N_t = N_r = N_s = 1$, $M = 1$. Moreover, to make our framework more digestible, the received signal at the MT in (2.1) is re-written by:

$$y = \sqrt{E} r_0^{-b} h_0 \eta_0 + \sqrt{E} \sum_{i \in \Psi(\setminus 0)} r_i^{-b} h_i \eta_i + n \quad (2.3)$$

where $y = \bar{\mathbf{y}}(1)$, $\eta_0 = \boldsymbol{\eta}_0^{(1)} = \mathbf{s}_0^{(1)}(1)$, $\eta_i = \boldsymbol{\eta}_i^{(1)} = \mathbf{s}_i^{(1)}(1)$ for $i \in \Psi^{(\setminus 0)}$, $h_0 = \mathbf{H}_0^{(1,1)}$, $h_i = \mathbf{H}_i^{(1,1)}$ for $i \in \Psi^{(\setminus 0)}$. The channel fading for each link is assumed to be independent and identically distributed and follows Nakagami- m distribution, i.e., $h_0, h_i \sim \mathcal{G}(m, \Omega)$.

The detector at the MT is assumed to have full channel state information (CSI), i.e., the side information at the MT is $\mathcal{S}_{\mathcal{I}} = \sqrt{E}r_0^{-b}\bar{\mathcal{S}}_{\mathcal{I}}$, $\bar{\mathcal{S}}_{\mathcal{I}} = h_0$. Let $\tilde{\eta}_0$ be the hypothesis of η_0 and $\Delta_0 = \eta_0 - \tilde{\eta}_0$, thus, the decision matrix of the demodulator at the receiver for SISO transmission can be formulated as:

$$\begin{aligned} \Lambda(\Delta_0) &= |y - \mathcal{S}_{\mathcal{I}}\tilde{\eta}_0|^2 \\ &= \left| \sqrt{E}r_0^{-b}h_0\Delta_0 + \sum_{i \in \Psi^{(\setminus 0)}} \sqrt{E}r_i^{-b}h_i\eta_i + n \right|^2 \\ &\propto Er_0^{-2b}|h_0|^2|\Delta_0|^2 + 2\text{Re} \left\{ \sqrt{E}r_0^{-b}(h_0\Delta_0)^*n \right\} \\ &\quad + 2\text{Re} \left\{ \sqrt{E}r_0^{-b}(h_0\Delta_0)^* \left(\sum_{i \in \Psi^{(\setminus 0)}} \sqrt{E}r_i^{-b}h_i\eta_i \right) \right\} \end{aligned} \quad (2.4)$$

where \propto indicates that the terms independent from Δ_0 are neglected since they do not affect the decision on the hypothesis. The demodulated symbol from the received signal y is the hypothesis $\tilde{\eta}_0 \in \mathbb{M}$ which minimizes $\Lambda(\Delta_0)$.

The physical interpretation of each addend in (2.4) is as follows: 1) $Er_0^{-2b}|h_0|^2|\Delta_0|^2$ is the output in the decision metric related to the useful signal of the serving BS; 2) $\sqrt{E}r_0^{-b}(h_0\Delta_0)^*n$ is the output in the decision metric related to the additive Gaussian noise at the receiver; 3) $\sqrt{E}r_0^{-b}(h_0\Delta_0)^* \left(\sum_{i \in \Psi^{(\setminus 0)}} \sqrt{E}r_i^{-b}h_i\eta_i \right)$ is the output in the decision metric related to the aggregate other-cell interference. In order to make the framework presented for SISO cellular networks easily extendable to MIMO setups and to ease the presentation in the next section, we introduce the following notations:

$$\left\{ \begin{array}{l} \mathcal{D}_1(\bar{\mathcal{S}}_{\mathcal{I}}, \boldsymbol{\Delta}_0(\boldsymbol{\tau})) = \mathcal{D}_1(h_0, \Delta_0) = |h_0|^2|\Delta_0|^2 \\ \mathcal{D}_2(\bar{\mathcal{S}}_{\mathcal{I}}, \boldsymbol{\Delta}_0(\boldsymbol{\tau}), \mathbf{n}(\boldsymbol{\tau})) = \mathcal{D}_2(h_0, \Delta_0, n) = (h_0\Delta_0)^*n \\ \mathcal{D}_3(\bar{\mathcal{S}}_{\mathcal{I}}, \boldsymbol{\Delta}_0(\boldsymbol{\tau}), \mathbf{i}_{\text{agg}}(\boldsymbol{\tau}; r_0)) = \mathcal{D}_3(h_0, \Delta_0, \mathbf{i}_{\text{agg}}(1; r_0)) \\ \quad = (h_0\Delta_0)^* \sum_{i \in \Psi^{(\setminus 0)}} \sqrt{E}r_i^{-b}h_i\eta_i \end{array} \right. \quad (2.5)$$

and

$$\mathcal{D}_0(\bar{\mathcal{S}}_{\mathcal{I}}, \mathbf{\Delta}_0(\boldsymbol{\tau})) \stackrel{(a)}{=} \frac{\mathcal{N}_0 \mathcal{D}_1^2(\bar{\mathcal{S}}_{\mathcal{I}}, \mathbf{\Delta}_0(\boldsymbol{\tau}))}{\mathbb{E}_{\mathbf{n}(\boldsymbol{\tau})} \left\{ \left| \mathcal{D}_2(\bar{\mathcal{S}}_{\mathcal{I}}, \mathbf{\Delta}_0(\boldsymbol{\tau}), \mathbf{n}(\boldsymbol{\tau})) \right|^2 \right\}} \stackrel{(b)}{=} |h_0|^2 |\Delta_0|^2 \quad (2.6)$$

where $\mathcal{D}_0(\cdot, \cdot)$ in (2.6) is introduced to ease the presentation of the SINR later discussed in the present section and its extension in the next section. Specifically, (a) is the general definition, (b) is for SISO networks.

With the aid of the new notations in (2.5), the decision matrix in (2.4) can be expressed by a more general manner as follows:

$$\begin{aligned} \Lambda(\mathbf{\Delta}_0(\boldsymbol{\tau})) &= \sum_{\tau=1}^{N_s} \|\bar{\mathbf{y}}(\tau) - \tilde{\mathbf{y}}(\tau)\|^2 \\ &\propto (E/N_t) r_0^{-2b} \mathcal{D}_1(\bar{\mathcal{S}}_{\mathcal{I}}, \mathbf{\Delta}_0(\boldsymbol{\tau})) \\ &\quad + 2\sqrt{E/N_t} r_0^{-b} \operatorname{Re} \left\{ \mathcal{D}_2(\bar{\mathcal{S}}_{\mathcal{I}}, \mathbf{\Delta}_0(\boldsymbol{\tau}), \mathbf{n}(\boldsymbol{\tau})) \right\} \\ &\quad + 2\sqrt{E/N_t} r_0^{-b} \operatorname{Re} \left\{ \mathcal{D}_3(\bar{\mathcal{S}}_{\mathcal{I}}, \mathbf{\Delta}_0(\boldsymbol{\tau}), \mathbf{i}_{\text{agg}}(\boldsymbol{\tau}; r_0)) \right\} \end{aligned} \quad (2.7)$$

where $\bar{\mathbf{y}}(\boldsymbol{\tau}) = \bar{\psi}(\mathcal{S}_{\mathcal{I}}, \mathbf{y}(\boldsymbol{\tau})) \in \mathbb{C}^{N \times 1}$ is the post-processed received signal, $\tilde{\mathbf{y}}(\boldsymbol{\tau}) = \tilde{\psi}(\mathcal{S}_{\mathcal{I}}, \tilde{\mathbf{s}}_0(\boldsymbol{\tau})) \in \mathbb{C}^{N \times 1}$ is the hypothesis of the post-processed received signal at the receiver, $\bar{\psi}(\cdot)$ and $\tilde{\psi}(\cdot)$ are demodulator- and modulator-dependent functions, respectively, N is the vectors size that depends on the transmission scheme being considered. As for the SISO network with Nakagami- m fading channels, no post-processing is assumed. Moreover, let $\mathcal{Z}_{0,i} = (h_0 \Delta_0)^* h_i \eta_i$ for $i \in \Psi^{(\wedge 0)}$ be *i.i.d.* spherically symmetric complex RVs, thanks to the uniformly distributed phase of channel fading and according to *Preliminary 2.1*, and its raw integer moments, is given in the following lemma.

Lemma 2.1. *Let a complex RV $\mathcal{Z}_{0,i} = (h_0 \Delta_0)^* h_i \eta_i$, where $|h_i|^2 \sim \mathcal{G}(m, \Omega)$, $\arg\{h_i\} \sim \mathcal{U}(0, 2\pi)$, while η_i , h_0 and Δ_0 are complex random numbers. Let $\mathcal{Z}_{0,i}^{(\text{re})} = \operatorname{Re}\{\mathcal{Z}_{0,i}\}$. The raw integer moments of any even order of $\mathcal{Z}_{0,i}^{(\text{re})}$ with respect to h_i and η_i are as follows:*

$$\begin{aligned} \mathbb{E} \left\{ \left(\mathcal{Z}_{0,i}^{(\text{re})} \right)^{2q} \right\} &= \mathbb{E}_{\eta_i} \left\{ \mathbb{E}_{h_i} \left\{ \left(\mathcal{Z}_{0,i}^{(\text{re})} \right)^{2q} \right\} \right\} \\ &= \left(|h_0|^2 |\Delta_0|^2 \right)^q \left(\frac{\Gamma(m+q)}{m^q \Gamma(m)} \frac{\Gamma(q+1/2)}{\sqrt{\pi} \Gamma(q+1)} \Omega^q \right) \mathbb{E}_{\eta_i} \left\{ |\eta_i|^{2q} \right\} \end{aligned} \quad (2.8)$$

Proof: See *Appendix 2.B*. □

Remark 2.3. As for the MIMO setups which will be introduced in Section 2.4, there exists a similar $\mathcal{Z}_{0,i}$ as in Lemma 2.1 depending on the channel gains, $\mathbf{H}_i^{(r,t)}$, and on the information symbols, $\mathbf{s}_i(\cdot)$, of the interfering BSs, as well as on the information symbols, $\mathbf{U}_0(\cdot)$, of the serving BS. Since $\mathbf{H}_i^{(r,t)}$ are complex Gaussian RVs, their phase is uniformly distributed and, thus, from Preliminary 2.1, they are spherically symmetric RVs. Since $\mathcal{Z}_{0,i}$ is the linear combination of $\mathbf{H}_i^{(r,t)}$, according to Remark 2.2, it is spherically symmetric as well.

The raw integer moments of a generic $\mathcal{Z}_{0,i}$, when Rayleigh fading channels are assumed, is given in the following lemma.

Lemma 2.2. *Let $\mathcal{Z}_{0,i}$ be a complex RV defined as follows:*

$$\mathcal{Z}_{0,i} = \sum_{r=1}^{N_r} \sum_{t=1}^{N_t} \sum_{\tau=1}^{N_s} \mathbf{H}_i^{(r,t)} \mathbf{s}_i^{(t)}(\tau) \mathbf{U}_0^{(r)}(\tau) \quad (2.9)$$

where $\mathbf{H}_i^{(r,t)}$ are i.i.d. complex Gaussian RVs, i.e., $\mathbf{H}_i^{(r,t)} \sim \mathcal{CN}(0, \Omega)$ for $r = 1, 2, \dots, N_r$, $t = 1, 2, \dots, N_t$, $\mathbf{s}_i(\tau)$ and $\mathbf{U}_0(\tau)$ are $N_t \times 1$ and $N_r \times 1$ complex random vectors, respectively, for $\tau = 1, 2, \dots, N_s$. Let $\mathcal{Z}_{0,i}^{(\text{re})} = \text{Re}\{\mathcal{Z}_{0,i}\}$. The raw integer moments of any even order of $\mathcal{Z}_{0,i}^{(\text{re})}$ with respect to \mathbf{H}_i and $\mathbf{s}_i(\tau)$ are:

$$\begin{aligned} & \mathbb{E} \left\{ \left(\mathcal{Z}_{0,i}^{(\text{re})} \right)^{2q} \right\} \\ &= \mathbb{E}_{\mathbf{s}_i(\tau)} \left\{ \mathbb{E}_{\mathbf{H}_i} \left\{ \left(\mathcal{Z}_{0,i}^{(\text{re})} \right)^{2q} \right\} \right\} \\ &= \frac{\sqrt{\pi}}{\Gamma(1/2 - k)} (-1)^q \Omega^q \mathbb{E}_{\mathbf{s}_i(\tau)} \left\{ \left(\sum_{r=1}^{N_r} \sum_{t=1}^{N_t} \left| \sum_{\tau=1}^{N_s} \mathbf{s}_i^{(t)}(\tau) \mathbf{U}_0^{(r)}(\tau) \right|^2 \right)^q \right\} \end{aligned} \quad (2.10)$$

Proof: See Appendix 2.B. □

As discussed at the beginning of this chapter, the rationale of the EiD-based approach relies upon finding a conditional Gaussian representation of the non-Gaussian distributed interference, which is an enabling technique to reuse the framework developed for AWGN channel for the error probability analysis. In particular, the EiD representation of the interference related term, $\mathcal{D}_3(\cdot, \cdot, \cdot)$, is given in the following proposition.

Proposition 2.1. *Let Ψ and $\Psi^{(\setminus 0)}$ be the PPPs of density λ of available and interfering BSs, respectively. Let p be the activity factors of the BSs. Let $b > 1$ be the amplitude*

path-loss exponent and $r_i > r_0$ for $i \in \Psi^{(\setminus 0)}$ be the distances from the interfering BSs to the MT. Let $Z_{0,i}$ be i.i.d. spherically symmetric complex RVs for $i \in \Psi^{(\setminus 0)}$ and let $Z_{0,i}^{(\text{re})} = \text{Re}\{Z_{0,i}\}$ have zero mean and finite raw integer moments of any even order. Let $\mathcal{D}_3(\cdot, \cdot, \cdot)$ has the following form:

$$\mathcal{D}_3(\bar{\mathcal{S}}_{\mathcal{I}}, \mathbf{\Delta}_0(\boldsymbol{\tau}), \mathbf{i}_{\text{agg}}(\boldsymbol{\tau}; r_0)) = \sum_{i \in \Psi^{(\setminus 0)}} \sqrt{E/N_t} r_i^{-b} Z_{0,i} \quad (2.11)$$

The GCG representation of $\mathcal{D}_3(\cdot, \cdot, \cdot)$ can be formulated as:

$$\begin{aligned} \mathcal{D}_3(\bar{\mathcal{S}}_{\mathcal{I}}, \mathbf{\Delta}_0(\boldsymbol{\tau}), \mathbf{i}_{\text{agg}}(\boldsymbol{\tau}; r_0)) &\stackrel{d}{=} \mathcal{D}_3^{(\text{GCG})}(\bar{\mathcal{S}}_{\mathcal{I}}, \mathbf{\Delta}_0(\boldsymbol{\tau}), \mathbf{i}_{\text{agg}}(\boldsymbol{\tau}; r_0)) \\ &= \sqrt{E/N_t} \sum_{q=1}^{+\infty} \left(r_0^{(-b+1/q)} (p\lambda\pi)^{1/(2q)} \sqrt{\mathbf{B}_q} \mathbf{G}_q \right) \end{aligned} \quad (2.12)$$

where $\mathcal{M}_{\mathbf{B}_q}(s) = \exp\{-s^q\}$ and $\mathbf{G}_q \sim \mathcal{CN}\left(0, \sigma_{\mathbf{G}_q}^2(\bar{\mathcal{S}}_{\mathcal{I}}, \mathbf{\Delta}_0(\boldsymbol{\tau}))\right)$ with:

$$\sigma_{\mathbf{G}_q}^2(\bar{\mathcal{S}}_{\mathcal{I}}, \mathbf{\Delta}_0(\boldsymbol{\tau})) = \left((-1)^q \frac{(-1/b)_q}{(1/2)_q (1-1/b)_q} \frac{1}{q!} \mathbb{E} \left\{ \left(Z_{0,i}^{(\text{re})} \right)^{2q} \right\} \right)^{1/q} \quad (2.13)$$

Proof: The proof following by comparing the CFs of $\mathcal{D}_3(\cdot, \cdot, \cdot)$ and $\mathcal{D}_3^{(\text{GCG})}(\cdot, \cdot, \cdot)$, where the detail is available in Appendix 2.B. \square

Remark 2.4. Proposition 2.1 holds for all the wireless network setups where the PPP distributed interfering nodes are outside the disc with radius r_0 and the interference related term $\mathcal{D}_3(\cdot, \cdot, \cdot)$ can be formulated as in (2.11). \square

By capitalizing on the GCG representation of $\mathcal{D}_3(\cdot, \cdot, \cdot)$, and by conditioning upon all the non-Gaussian RVs, the output of the decision matrix is equivalent as those in the AWGN channels. Thus, the SINR of the output of the decision matrix in (2.7), conditioned on $\left(r_0, \bar{\mathcal{S}}_{\mathcal{I}}, \mathbf{\Delta}_0(\boldsymbol{\tau}), \{\mathbf{B}_q\}_{q=1}^{+\infty}\right)$, can be defined and formulated by the same manner as in the

AWGN channels:

$$\begin{aligned}
& \text{SINR} \left(r_0, \bar{\mathcal{S}}_{\mathcal{I}}, \mathbf{\Delta}_0(\tau), \{B_q\}_{q=1}^{+\infty} \right) \\
&= \frac{E}{N_t} r_0^{-2b} \frac{|\mathcal{D}_1(\bar{\mathcal{S}}_{\mathcal{I}}, \mathbf{\Delta}_0(\tau))|^2}{2\mathbb{E}_{\mathbf{n}(\tau)} \left\{ |\mathcal{D}_2(\bar{\mathcal{S}}_{\mathcal{I}}, \mathbf{\Delta}_0(\tau), \mathbf{n}(\tau))|^2 \right\} + 2\mathbb{E}_{\{G_q\}} \left| \mathcal{D}_3^{(\text{GCG})}(\bar{\mathcal{S}}_{\mathcal{I}}, \mathbf{\Delta}_0(\tau), \mathbf{i}_{\text{agg}}(\tau; r_0)) \right|^2} \\
&\stackrel{(a)}{=} \frac{E}{N_t} r_0^{-2b} \frac{\mathcal{D}_0(\bar{\mathcal{S}}_{\mathcal{I}}, \mathbf{\Delta}_0(\tau))/2}{\mathcal{N}_0 + \frac{E}{N_t} r_0^{-2b} \sum_{q=1}^{+\infty} \left((p\lambda\pi r_0^2)^{1/q} B_q \bar{\sigma}_{G_q}^2 \right)}
\end{aligned} \tag{2.14}$$

where (a) follows by introducing the notation $\bar{\sigma}_{G_q}^2$ which is defined to satisfy the following constraint:

$$\bar{\sigma}_{G_q}^2 \stackrel{(b)}{=} \sigma_{G_q}^2(\bar{\mathcal{S}}_{\mathcal{I}}, \mathbf{\Delta}_0(\tau)) \frac{\mathcal{D}_0(\bar{\mathcal{S}}_{\mathcal{I}}, \mathbf{\Delta}_0(\tau))}{\mathcal{D}_1^2(\bar{\mathcal{S}}_{\mathcal{I}}, \mathbf{\Delta}_0(\tau))} \stackrel{(c)}{=} \frac{\sigma_{G_q}^2(\bar{\mathcal{S}}_{\mathcal{I}}, \mathbf{\Delta}_0(\tau))}{|h_0|^2 |\Delta_0|^2} \tag{2.15}$$

(b) is the general definition, while (c) is the special case for the SISO networks. From the SINR defined in (2.14), the symbol error probability for arbitrary bi-dimensional modulation scheme, conditioned on r_0 and $\{B_q\}_{q=1}^{+\infty}$, can be computed with the aid of the moment generating function (MGF)-based approach, which is well-known for AWGN channels [4] and is presented by the following lemma to make the report self-contained.

Lemma 2.3. *Let a bi-dimensional modulation scheme with equi-probable symbols, which is identified by the quadruplets of parameters $(\alpha_1, \beta_1, \gamma_1, \delta_1)$ and $(\alpha_2, \beta_2, \gamma_2, \delta_2)$ [20, Table III]. Let a demodulator with perfect knowledge of side information, $\mathcal{S}_{\mathcal{I}}$, be formulated as:*

$$\hat{\boldsymbol{\eta}}_0 = \arg \min_{\hat{\boldsymbol{\eta}}_0 \in \mathbb{M}} \{ \Lambda(\mathbf{\Delta}_0(\tau)) \} \tag{2.16}$$

Let $\mathcal{D}_0(\bar{\mathcal{S}}_{\mathcal{I}}, \mathbf{\Delta}_0(\tau))$ defined in (2.6) which can be decomposed by $\mathcal{D}_0(\bar{\mathcal{S}}_{\mathcal{I}}, \mathbf{\Delta}_0(\tau)) = \bar{\mathcal{D}}_0(\bar{\mathcal{S}}_{\mathcal{I}}) \tilde{\mathcal{D}}_0(\mathbf{\Delta}_0(\tau))$ with $\mathbb{E}_{\mathbf{\Delta}_0(\tau)} \left\{ \tilde{\mathcal{D}}_0(\mathbf{\Delta}_0(\tau)) \right\} = 2$. The ASEP of (2.16), i.e., $\text{ASEP} = \Pr \{ \hat{\boldsymbol{\eta}}_0 \neq \boldsymbol{\eta}_0 \}$ can be formulated as follows,

$$\begin{aligned}
\text{ASEP} = \mathbb{E}_{r_0} \left\{ \mathbb{E}_{\{B_q\}_{q=1}^{+\infty}} \left\{ \delta_1 \text{P}_E \left(r_0, \{B_q\}_{q=1}^{+\infty}; \alpha_1, \beta_1, \gamma_1 \right) \right. \right. \\
\left. \left. - \delta_2 \text{P}_E \left(r_0, \{B_q\}_{q=1}^{+\infty}; \alpha_2, \beta_2, \gamma_2 \right) \right\} \right\}
\end{aligned} \tag{2.17}$$

where:

$$P_E \left(r_0, \{\mathbf{B}_q\}_{q=1}^{+\infty}; \alpha, \beta, \gamma \right) = \frac{1}{\pi} \int_0^\alpha \mathcal{M}_{\bar{\mathcal{D}}_0} \left(\frac{\beta \sin^2(\gamma)}{2 \sin^2(\omega)} \overline{\text{SINR}} \left(r_0, \{\mathbf{B}_q\}_{q=1}^{+\infty} \right) \right) d\omega \quad (2.18)$$

with $\mathcal{M}_{\bar{\mathcal{D}}_0}(s) = \mathbb{E}_{\bar{\mathcal{S}}_{\mathcal{I}}} \left\{ \exp \left\{ -s \bar{\mathcal{D}}_0(\bar{\mathcal{S}}_{\mathcal{I}}) \right\} \right\}$ and $\overline{\text{SINR}}(\cdot, \cdot)$ is defined as follows:

$$\overline{\text{SINR}} \left(r_0, \{\mathbf{B}_q\}_{q=1}^{+\infty} \right) = \frac{E}{N_t} r_0^{-2b} \left(\mathcal{N}_0 + \frac{E}{N_t} \sum_{q=1}^{+\infty} \left(r_0^{(-2b+2/q)} (p\lambda\pi)^{1/q} \mathbf{B}_q \bar{\sigma}_{\mathbf{G}_q}^2 \right) \right)^{-1} \quad (2.19)$$

Proof: See Appendix 2.B. □

As for the SISO transmission over Nakagami- m fading, $\mathcal{M}_{\bar{\mathcal{D}}_0}(s) = \mathbb{E}_{h_0} \left\{ \exp \left(-s|h_0|^2 \right) \right\} = (1 + s\Omega/m)^{-m}$.

Remark 2.5. The mathematical formulation of the ASEP in (2.17) is possible thanks to the EiD-based representation of the aggregate other-cell interference, *i.e.*, $\mathcal{D}_3(\cdot, \cdot, \cdot)$. In fact, by conditioning upon r_0 , and $\{\mathbf{B}_q\}_{q=1}^{+\infty}$, the decision metric of the demodulator in (2.7) boils down to that of an equivalent demodulator in AWGN. As a consequence, the widely adopted mathematical formulation of the ASEP of bi-dimensional modulations can be used [20, Table III]. As a first step, in fact, only the randomness of the AWGN and of the complex Gaussian RVs $\{\mathbf{G}_q\}_{q=1}^{+\infty}$ is taken into account. As shown in (2.17), the conditioning with respect to r_0 , and $\{\mathbf{B}_q\}_{q=1}^{+\infty}$ is removed subsequently. This constitutes the main flexibility and usefulness of the EiD-based approach. □

Remark 2.6. The constraint $\mathbb{E}_{\Delta_0(\tau)} \left\{ \tilde{\mathcal{D}}_0(\Delta_0(\tau)) \right\} = 2$ represents a normalization factor that can be understood by direct inspection of (2.6) and of Section 2.4. From (2.6), in particular, for SISO networks, $\tilde{\mathcal{D}}_0(\Delta_0(\tau)) = |\Delta_0|^2$, which implies $\mathbb{E}_{\Delta_0(\tau)} \left\{ \tilde{\mathcal{D}}_0(\Delta_0(\tau)) \right\} = 2$ as a result of the zero-mean and average unit-energy constraints assumed for the constellation diagram. □

Lemma 2.3 gives the well-know framework to compute the ASEP in AWGN channels, while the procedure to remove these conditions related to the shortest distance r_0 , and to the RVs $\{\mathbf{B}_q\}_{q=1}^{+\infty}$ introduced by the EiD approach has been proposed in the following theorem.

Theorem 2.1. Let $\mathcal{M}_{\bar{\mathcal{D}}_0}(s) = (1 + s\Omega_0)^{-m_0}$, where m_0 and Ω_0 are parameters depending on $\mathcal{D}_0(\bar{\mathcal{S}}_{\mathcal{I}}, \Delta_0(\tau))$. Let $f_{r_0}(\xi) = 2\pi\lambda\xi \exp \left\{ -\pi\lambda\xi^2 \right\}$ and $\mathcal{M}_{\mathbf{B}_q}(s) = \exp \left\{ -s^q \right\}$ for

every integer q . Let the $\overline{\text{SINR}}(\cdot, \cdot)$ defined in (2.19). The unconditional MGF can be formulated by

$$\begin{aligned} \mathcal{M}_{\text{SINR}}(s) &= \mathbb{E}_{r_0} \left\{ \mathbb{E}_{\{\mathbf{B}_q\}_{q=1}^{+\infty}} \left\{ \mathcal{M}_{\bar{\mathcal{D}}_0} \left(s \overline{\text{SINR}} \left(r_0, \{\mathbf{B}_q\}_{q=1}^{+\infty} \right) \right) \right\} \right\} \\ &= 1 - m_0 \Omega_0 (E/N_t) \pi \lambda s \\ &\quad \times \int_0^{+\infty} \int_0^{+\infty} \left\{ {}_1F_1(m_0 + 1; 2; -\Omega_0 (E/N_t) sy) \right. \\ &\quad \left. \times \exp \left\{ -\mathcal{N}_0 x^b y \right\} \exp \left\{ -\pi \lambda \tilde{\mathcal{Q}}((E/N_t) y) x \right\} \right\} dx dy \end{aligned} \quad (2.20)$$

where $\tilde{\mathcal{Q}}(\xi) = p\mathcal{Q}(\xi) + 1$, and $\mathcal{Q}(\xi) = \sum_{q=1}^{+\infty} \left(\xi \bar{\sigma}_{\mathbf{G}_q}^2 \right)^q$.

Proof: See Appendix 2.C. □

Corollary 2.1. Let the $\text{SINR}(\cdot, \cdot)$ in (2.19) with $E/\mathcal{N}_0 \rightarrow +\infty$, i.e., an interference-limited regime is considered. Then, $\mathcal{M}_{\text{SINR}}(\cdot)$ in (2.20) simplifies as follows:

$$\begin{aligned} \mathcal{M}_{\text{SINR}}(s)|_{E/\mathcal{N}_0 \rightarrow +\infty} &= \mathcal{M}_{\text{SINR}}^{(\infty)}(s) \\ &= 1 - m_0 \Omega_0 s \int_0^{+\infty} \frac{{}_1F_1(m_0 + 1; 2; -\Omega_0 sz)}{\tilde{\mathcal{Q}}(z)} dz \end{aligned} \quad (2.21)$$

Proof: See Appendix 2.C. □

Remark 2.7. The MGF of $\bar{\mathcal{D}}_0(\bar{\mathcal{S}}_{\mathcal{I}})$, $\mathcal{M}_{\bar{\mathcal{D}}_0}(s) = (1 + s\Omega_0)^{-m_0}$, holds if $\bar{\mathcal{D}}_0(\bar{\mathcal{S}}_{\mathcal{I}})$ follows the Gamma distribution with fading parameter m_0 and mean square value Ω_0 . For example, for SISO transmission over Nakagami- m fading, $m_0 = m$, $\Omega_0 = \Omega/m$.

With the aid of the unconditional MGF of the SINR in *Theorem 2.1*, the error probability integral introduced in *Lemma 2.3* can be computed as in the following theorem.

Theorem 2.2. Let $\mathcal{M}_{\bar{\mathcal{D}}_0}(s) = (1 + s\Omega_0)^{-m_0}$, $f_{r_0}(\xi) = 2\pi\lambda\xi \exp\{-\pi\lambda\xi^2\}$, $\mathcal{M}_{\mathbf{B}_q}(s) = \exp\{-s^q\}$ for every integer q . Let the $\overline{\text{SINR}}(\cdot, \cdot)$ in (2.19) and the error probability integral in *Lemma 2.3* be expressed as follows:

$$\mathcal{I}(\alpha, \beta, \gamma) = \mathbb{E}_{r_0, \{\mathbf{B}_q\}_{q=1}^{+\infty}} \left\{ \frac{1}{\pi} \int_0^\alpha \mathcal{M}_{\bar{\mathcal{D}}_0} \left(\frac{\beta \sin^2(\gamma)}{2 \sin^2(\omega)} \overline{\text{SINR}} \left(r_0, \{\mathbf{B}_q\}_{q=1}^{+\infty} \right) \right) d\omega \right\} \quad (2.22)$$

Then, the following identity holds

$$\begin{aligned} \mathcal{I}(\alpha, \beta, \gamma) &= \frac{\alpha}{\pi} - m_0 \lambda \int_0^{+\infty} \int_0^{+\infty} \left\{ \exp \left\{ - \left(\frac{E}{\mathcal{N}_0 N_t} \right)^{-1} \frac{z}{\kappa \Omega_0} x^b \right\} \right. \\ &\quad \left. \times \exp \left\{ -\pi \lambda x \tilde{\mathcal{Q}} \left(\frac{z}{\kappa \Omega_0} \right) \right\} \mathcal{T}(z; m_0, \alpha) \right\} dx dz \end{aligned} \quad (2.23)$$

where $\kappa = \beta \sin^2(\gamma)/2$, $\tilde{\mathcal{Q}}(\xi) = p\mathcal{Q}(\xi) + 1$, $\mathcal{Q}(\xi) = \sum_{q=1}^{+\infty} \left(\xi \bar{\sigma}_{\mathbb{G}_q}^2 \right)^q$ and $\mathcal{T}(\cdot; \cdot, \cdot)$ is defined in (2.38) of Appendix 2.A.

Proof: See Appendix 2.C. □

Corollary 2.2. Let the error probability integral in (2.23) with $E/\mathcal{N}_0 \rightarrow +\infty$, i.e., an interference-limited regime is considered. Then, the following identity holds:

$$\begin{aligned} \mathcal{I}(\alpha, \beta, \gamma)|_{E/\mathcal{N}_0 \rightarrow +\infty} &= \mathcal{I}^{(\infty)}(\alpha, \beta, \gamma) \\ &= \frac{\alpha}{\pi} - \frac{m_0}{\pi} \int_0^{+\infty} \frac{\mathcal{T}(z; m_0, \alpha)}{\tilde{\mathcal{Q}}(z/(\kappa \Omega_0))} dz \end{aligned} \quad (2.24)$$

Proof: See Appendix 2.C. □

Finally, the function $\tilde{\mathcal{Q}}(\xi)$ (or $\mathcal{Q}(\xi)$) consisting of an infinity series, can be represented with the aid of the hypergeometric functions. In specific, as for the SISO networks, $\mathcal{Q}(\xi)$ is computed as in the following lemma.

Lemma 2.4. Let $\sigma_{\mathbb{G}_q}^2(\cdot, \cdot)$ in (2.13) with $\mathbb{E} \left\{ \left(\mathcal{Z}_{0,i}^{(\text{re})} \right)^{2q} \right\}$ formulated as in (2.8). Let $\bar{\sigma}_{\mathbb{G}_q}^2$ satisfy the equality in (2.15) with $\mathcal{D}_1^2(\bar{\mathcal{S}}_{\mathcal{I}}, \mathbf{\Delta}_0(\boldsymbol{\tau})) / \mathcal{D}_0(\bar{\mathcal{S}}_{\mathcal{I}}, \mathbf{\Delta}_0(\boldsymbol{\tau})) = |h_0|^2 |\Delta_0|^2$. Let $\mathcal{Q}(X) = \sum_{q=1}^{+\infty} \left(X \bar{\sigma}_{\mathbb{G}_q}^2 \right)^q$. For every $X > 0$, the following identity holds:

$$\mathcal{Q}(X) = \mathbb{E}_{s_i} \left\{ {}_2F_2 \left(-\frac{1}{b}, m; 1 - \frac{1}{b}; 1; -|s_i|^2 \frac{\Omega}{m} X \right) \right\} - 1 \quad (2.25)$$

Proof: See Appendix 2.B. □

The extension of Lemma 2.4 to MIMO arrangements over Rayleigh fading, which will be described in detail in the next section, is given by the following lemma.

Lemma 2.5. Let $\sigma_{\mathbb{G}_q}^2(\cdot, \cdot)$ in (2.13) with $\mathbb{E} \left\{ \left(\mathcal{Z}_{0,i}^{(\text{re})} \right)^{2q} \right\}$ formulated as in (2.10). Let a function $\phi(\cdot)$ such that:

$$\sum_{r=1}^{N_r} \sum_{t=1}^{N_t} \left| \sum_{\tau=1}^{N_s} \mathbf{s}_i^{(t)}(\tau) \mathbf{U}_0^{(r)}(\tau) \right|^2 = \phi(\mathbf{s}_i(\boldsymbol{\tau})) \sum_{r=1}^{N_r} \sum_{\tau=1}^{N_s} \left| \mathbf{U}_0^{(r)}(\tau) \right|^2 \quad (2.26)$$

Let $\bar{\sigma}_{\mathbb{G}_q}^2$ satisfy the equality in (2.15) with $\frac{\mathcal{D}_1^2(\bar{\mathcal{S}}_{\mathcal{I}}, \mathbf{\Delta}_0(\tau))}{\mathcal{D}_0(\bar{\mathcal{S}}_{\mathcal{I}}, \mathbf{\Delta}_0(\tau))} = \sum_{r=1}^{N_r} \sum_{\tau=1}^{N_s} \left| \mathbf{U}_0^{(r)}(\tau) \right|^2$. Let $\mathcal{Q}(X) = \sum_{q=1}^{+\infty} \left(X \bar{\sigma}_{\mathbb{G}_q}^2 \right)^q$. For every $X > 0$, the following identity holds:

$$\mathcal{Q}(X) = \mathbb{E}_{\mathbf{s}_i(\boldsymbol{\tau})} \left\{ {}_1F_1 \left(-\frac{1}{b}; 1 - \frac{1}{b}; -\phi(\mathbf{s}_i(\boldsymbol{\tau})) \Omega X \right) \right\} - 1 \quad (2.27)$$

Proof: See Appendix 2.B. □

Remark 2.8. Lemma 2.5 indicates that the conditional variance of the GCG representation in (2.12) can be expressed by a hypergeometric function even though it consists of an infinity series. If $N_s = 1$, the equality in (2.26) is always satisfied with $\phi(\mathbf{s}_i(1)) = \sum_{t=1}^{N_t} \left| \mathbf{s}_i^{(t)}(1) \right|^2$, i.e., $\sum_{r=1}^{N_r} \sum_{t=1}^{N_t} \left| \mathbf{s}_i^{(t)}(1) \mathbf{U}_0^{(r)}(1) \right|^2 = \left(\sum_{t=1}^{N_t} \left| \mathbf{s}_i^{(t)}(1) \right|^2 \right) \left(\sum_{r=1}^{N_r} \left| \mathbf{U}_0^{(r)}(1) \right|^2 \right)$. □

2.4 Extension to MIMO Cellular Networks

In this section, the depicted simple framework for SISO cellular networks over Nakagami- m fading has been extended to studying various MIMO arrangements, and it is proved that their error probability performance can be formulated as in *Theorem 2.2* and in *Corollary 2.2* for interference-limited cellular networks. By direct inspection of *Theorem 2.2* and *Corollary 2.2*, it is apparent that the error probability integrals in (2.23) and (2.24) depend only on three parameters, i.e., m_0 , Ω_0 and $\mathcal{Q}(\cdot)$. In the following subsections, such a triplet of parameters is computed for relevant MIMO schemes. It is worth mentioning that for some MIMO setups the proposed mathematical framework provides only approximated expressions of the error probability, as explained in the sequel.

A summary of the triplet $(m_0, \Omega_0, \mathcal{Q}(\cdot))$ is provided in Table 2.2 for all MIMO schemes analyzed in the present chapter. Also, Table 2.2 highlights when the framework is exact

TABLE 2.2: Summary of parameters for the computation of (2.23) in *Theorem 2.2* and of (2.24) in *Corollary 2.2* for various MIMO setups. As for the MIMO setup of Section 2.4.2, the framework is exact for [34, Eq. (32), Eq. (40)] and an approximation for [34, Eq. (37), Eq. (38), Eq. (39)]. Also, $\bar{p} = 2$ for [34, Eq. (37), Eq. (38)] and $\bar{p} = 1$ for [34, Eq. (32), Eq. (39), Eq. (40)].

MIMO Setup	m_0	Ω_0	$\mathcal{Q}(\xi)$	E/A
SISO (Nakagami- m)	m	Ω/m	$\mathbb{E}_{\eta_0} \{ \mathcal{F}(m, \eta_0 ^2 \xi) \}$	E
SIMO	N_r	Ω	$\mathbb{E}_{\eta_0} \{ \mathcal{F}(1, \eta_0 ^2 \xi) \}$	E
OSTBC	$N_r N_t$	$\bar{p}\Omega$	$\mathbb{E}_{\eta_0} \{ \mathcal{F}(1, \ \eta_0\ ^2 \xi) \}$	E/A
ZF Reception	$N_r - N_t + 1$	Ω	$\mathbb{E}_{\eta_0} \{ \mathcal{F}(1, \ \eta_0\ ^2 \xi) \}$	E
ZF Precoding	$N_t - N_u + 1$	Ω/N_u	$\mathcal{F}(1, \xi)$	A

or approximated. In particular, the following short-hand notations are used in Table 2.2, i) $\tilde{\mathcal{Q}}(\xi) = p\mathcal{Q}(\xi) + 1$; ii) $\mathcal{F}(m, z) = {}_2F_2(m, -\frac{1}{b}; 1 - \frac{1}{b}, 1; -\Omega z/m) - 1$, which reduces to $\mathcal{F}(1, z) = {}_1F_1(-\frac{1}{b}, 1 - \frac{1}{b}, -\Omega z) - 1$ when $m = 1$; iii) the short hand notation $\eta_0 \in \mathbb{M}$, $\boldsymbol{\eta}_0 \in \mathbb{M}^{M \times 1}$, $M = \text{card}\{\mathbb{M}\}$, $\mathbb{E}_{\eta_0} \{ \vartheta(|\eta_0|^2) \} = (1/M) \sum_{\chi=1}^M \vartheta(|\mu_\chi|^2)$, $\mathbb{E}_{\boldsymbol{\eta}_0} \{ \vartheta(\|\boldsymbol{\eta}_0\|^2) \} = (1/M^M) \sum_{\chi_1=1}^M \sum_{\chi_2=1}^M \cdots \sum_{\chi_M=1}^M \vartheta(\sum_{k=1}^M |\mu_{\chi_k}|^2)$, where $\vartheta(\cdot)$ is a generic function; iv) E = Exact, A = Approximation.

For all analyzed MIMO transmission schemes, the following procedure similar as the one depicted in Section 2.3 is applied:

1. From the signal model in (2.1) and the demodulator in (2.7), the functions $\mathcal{D}_1(\cdot, \cdot)$, $\mathcal{D}_2(\cdot, \cdot, \cdot)$ and $\mathcal{D}_3(\cdot, \cdot, \cdot)$ are computed.
2. The function $\mathcal{D}_0(\cdot, \cdot)$ is computed such that the constraints in (2.6) and (2.15) are both satisfied. The difference between *exact* and *approximated* results may emerge at this step: if all constraints are satisfied with equality, the mathematical formulation is exact. Otherwise, it is an approximation.
3. By letting $\mathcal{M}_{\bar{\mathcal{D}}_0}(s)$ for the single-stream demodulator in *Lemma 2.3*, the parameters m_0 and Ω_0 are computed from $\mathcal{D}_0(\cdot, \cdot)$ such that $\mathcal{M}_{\bar{\mathcal{D}}_0}(s) = (1 + s\Omega_0)^{-m_0}$ holds.
4. From $\mathcal{D}_3(\cdot, \cdot, \cdot)$ and (2.11), the RV $\mathcal{Z}_{0,i}$ is identified. It is proved that $\mathcal{Z}_{0,i}$ can be formulated as shown in *Lemma 2.2*. Thus, the function $\mathcal{Q}(\cdot)$ is obtained either

from (2.27). The difference between *exact* and *approximated* results may emerge at this step: if the equality in (2.26) is satisfied, the mathematical formulation is exact. Otherwise, it is an approximation.

2.4.1 Single-Input-Multiple-Output (SIMO) Transmission over Rayleigh Fading

Let a SIMO transmission scheme and a Rayleigh fading channel model [33, Sec. 2]. Thus, $N_t = N_s = 1$, $M = 1$, $\mathbf{s}_0^{(1)}(1) = \boldsymbol{\eta}_0^{(1)}$, $\mathbf{s}_i^{(1)}(1) = \boldsymbol{\eta}_i^{(1)}$ for $i \in \Psi^{(\setminus 0)}$, $|\mathbf{H}_0^{(r,1)}|^2 \sim \mathcal{G}(1, \Omega)$ and $|\mathbf{H}_i^{(r,1)}|^2 \sim \mathcal{G}(1, \Omega)$ for $r = 1, 2, \dots, N_r$ and $i \in \Psi^{(\setminus 0)}$. Let the interference-oblivious demodulator in (2.16) with side information $\bar{\mathcal{S}}_{\mathcal{I}} = \mathbf{H}_0^{(r,1)}$ for $r = 1, 2, \dots, N_r$, $\bar{\mathbf{y}}(1) = \bar{\psi}(\bar{\mathcal{S}}_{\mathcal{I}}, \mathbf{y}(1)) = \mathbf{y}(1)$, *i.e.*, perfect CSI is assumed at the demodulator. Then, the hypothesis of the useful signal would be $\tilde{\mathbf{y}}^{(r)}(1) = \tilde{\psi}(\bar{\mathcal{S}}_{\mathcal{I}}, \tilde{\mathbf{s}}_0(1)) = \sqrt{E}r_0^{-b} \mathbf{H}_0^{(r,1)} \tilde{\boldsymbol{\eta}}_0^{(1)}$ for $r = 1, 2, \dots, N_r$ and $N = N_r$.

By inserting (2.1) in (2.7), we obtain $\boldsymbol{\Delta}_0^{(1)}(1) = \tilde{\boldsymbol{\eta}}_0^{(1)} - \boldsymbol{\eta}_0^{(1)}$ and

$$\left\{ \begin{array}{l} \mathcal{D}_1(\bar{\mathcal{S}}_{\mathcal{I}}, \boldsymbol{\Delta}_0(\boldsymbol{\tau})) = \left| \boldsymbol{\Delta}_0^{(1)}(1) \right|^2 \sum_{r=1}^{N_r} \left| \mathbf{H}_0^{(r,1)} \right|^2 \\ \mathcal{D}_2(\bar{\mathcal{S}}_{\mathcal{I}}, \boldsymbol{\Delta}_0(\boldsymbol{\tau}), \mathbf{n}(\boldsymbol{\tau})) = \left(\boldsymbol{\Delta}_0^{(1)}(1) \right)^* \sum_{r=1}^{N_r} \left(\mathbf{H}_0^{(r,1)} \right)^* \mathbf{n}^{(r)}(1) \\ \mathcal{D}_3(\bar{\mathcal{S}}_{\mathcal{I}}, \boldsymbol{\Delta}_0(\boldsymbol{\tau}), \mathbf{i}_{\text{agg}}(\boldsymbol{\tau}; r_0)) = \sum_{i \in \Psi^{(\setminus 0)}} \sqrt{E/N_t r_i^{-b}} \sum_{r=1}^{N_r} \mathbf{H}_i^{(r,1)} \mathbf{s}_i^{(1)}(1) \mathbf{U}_0^{(r)}(1) \end{array} \right. \quad (2.28)$$

where $\mathbf{U}_0^{(r)}(1) = \left(\mathbf{H}_0^{(r,1)} \boldsymbol{\Delta}_0^{(1)}(1) \right)^*$.

Therefore, from $\mathcal{D}_3(\cdot, \cdot, \cdot)$, the *i.i.d.* spherically symmetric complex RVs in Lemma 2.2 is defined by $\mathcal{Z}_{0,i} = \sum_{r=1}^{N_r} \mathbf{H}_i^{(r,1)} \mathbf{s}_i^{(1)}(1) \mathbf{U}_0^{(r)}(1)$. From (2.6) and (2.15), $\mathcal{D}_{0,1}(\bar{\mathcal{S}}_{\mathcal{I}}, \boldsymbol{\Delta}_0(\boldsymbol{\tau})) = \left| \boldsymbol{\Delta}_0^{(1)}(1) \right|^2 \sum_{r=1}^{N_r} \left| \mathbf{H}_0^{(r,1)} \right|^2$. Thus, $\bar{\mathcal{D}}_0(\bar{\mathcal{S}}_{\mathcal{I}}) = \sum_{r=1}^{N_r} \left| \mathbf{H}_0^{(r,1)} \right|^2 \sim \mathcal{G}(N_r, N_r \Omega)$ and $(m_0, \Omega_0) = (N_r, \Omega)$ [4, Eq. (2.22)]. Since $\mathcal{Z}_{0,i}$ is formulated as in Lemma 2.2 with $N_t = N_s = 1$, from Remark 2.8 we conclude that $\mathcal{Q}(\cdot)$ follows from (2.27) with $\phi(\mathbf{s}_i(1)) = \left| \mathbf{s}_i^{(1)}(1) \right|^2$.

2.4.2 Orthogonal Space-Time Block Coding (OSTBC) Transmission over Rayleigh Fading

Let an OSTBC MIMO transmission scheme and a Rayleigh fading channel model [33, Sec. 2]. Based on [34, Sec. V-E], generalized complex orthogonal designs of size

N_t are considered. Thus, $M/N_s \leq 1$ and the $N_s \times N_t$ space-time encoding matrix $\Theta(\boldsymbol{\eta}_0; \mathcal{S}_{\mathcal{I}}^{(0)}) = \Theta(\boldsymbol{\eta}_0)$ satisfies the property $\Theta^H(\boldsymbol{\eta}_0) \Theta(\boldsymbol{\eta}_0) = \mathbf{D}_{\Theta}(\boldsymbol{\eta}_0)$, where $\mathbf{D}_{\Theta}^{(t_1, t_2)}(\boldsymbol{\eta}_0) = \sum_{m=1}^M \mathbf{p}_t^{(m)} \left| \boldsymbol{\eta}_0^{(m)} \right|^2$ for $t_1 = t_2 = t = 1, 2, \dots, N_t$, $\mathbf{D}_{\Theta}^{(t_1, t_2)}(\boldsymbol{\eta}_0) = 0$ for $t_1 \neq t_2 = 1, 2, \dots, N_t$ and $\mathbf{p}_t^{(m)}$ are strictly positive numbers for $t = 1, 2, \dots, N_t$ and $m = 1, 2, \dots, M$. For example, $\bar{p} = \mathbf{p}_t^{(m)}$ for $t = 1, 2, \dots, N_t$ and $m = 1, 2, \dots, M$ with $\bar{p} = 2$ and $\bar{p} = 1$ if the OSTBC encoding matrices of different sizes in [34, Eq. (37), Eq. (38)] and in [34, Eq. (32), Eq. (39), Eq. (40)] are considered, respectively.

As for the channels, $\left| \mathbf{H}_0^{(r,t)} \right|^2 \sim \mathcal{G}(1, \Omega)$ and $\left| \mathbf{H}_i^{(r,t)} \right|^2 \sim \mathcal{G}(1, \Omega)$ for $t = 1, 2, \dots, N_t$, $r = 1, 2, \dots, N_r$ and $i \in \Psi^{(\setminus 0)}$. Let the interference-oblivious demodulator in (2.16) with $\bar{\mathcal{S}}_{\mathcal{I}} = \mathbf{H}_0$, $\bar{\mathbf{y}}(\boldsymbol{\tau}) = \bar{\psi}(\mathcal{S}_{\mathcal{I}}, \mathbf{y}(\boldsymbol{\tau})) = \mathbf{y}(\boldsymbol{\tau})$, $\tilde{\mathbf{y}}(\boldsymbol{\tau}) = \tilde{\psi}(\mathcal{S}_{\mathcal{I}}, \tilde{\mathbf{s}}_0(\boldsymbol{\tau})) = \sqrt{E/N_t} r_0^{-b} \Theta(\tilde{\boldsymbol{\eta}}_0)$ and $N = N_r$. By inserting (2.1) in (2.7), the multi-stream demodulator can be re-written in terms of the single-stream demodulator by exploiting the properties of $\Theta(\cdot)$ as follows:

$$\Lambda(\boldsymbol{\Delta}_0(\boldsymbol{\tau})) = \sum_{m=1}^M \Lambda_m(\boldsymbol{\Delta}_0(\boldsymbol{\tau})) \quad (2.29)$$

where $\Lambda_m(\boldsymbol{\Delta}_0(\boldsymbol{\tau}))$ has the same structure as (2.7) except that it depends on the m th information symbol, *i.e.*, $\mathcal{D}_{\chi}(\cdot) \mapsto \mathcal{D}_{\chi, m}(\cdot)$ for $\chi = \{0, 1, 2, 3, \text{IAI}\}$.

In particular, the received signals at the MT from the intended link are orthogonal according to the property of the encoding matrix. This might not be true, on the other hand, for the interfering links since the matrices of the interfering links are designed for their intended users. Let $\boldsymbol{\Delta}_i(\cdot)$ for $i \in \Psi$ be formulated as follows ($\tau = 1, 2, \dots, N_s$):

$$\begin{aligned} \boldsymbol{\Delta}_i^{(t)}(\boldsymbol{\tau}) &= \Theta^{(\tau, t)}(\tilde{\boldsymbol{\eta}}_0) - \Theta^{(\tau, t)}(\boldsymbol{\eta}_0) \\ &= \sum_{m=1}^M \boldsymbol{\alpha}^{(t)}(\boldsymbol{\tau}) \left(\tilde{\boldsymbol{\eta}}_i^{(m)} - \boldsymbol{\eta}_i^{(m)} \right) + \sum_{m=1}^M \boldsymbol{\beta}^{(t)}(\boldsymbol{\tau}) \left(\tilde{\boldsymbol{\eta}}_i^{(m)} - \boldsymbol{\eta}_i^{(m)} \right)^* \end{aligned} \quad (2.29)$$

where $\boldsymbol{\alpha}(\cdot)$ and $\boldsymbol{\beta}(\cdot)$ are $N_t \times 1$ complex vectors for $\tau = 1, 2, \dots, N_s$, which depend on the space-time encoding matrix $\Theta(\cdot)$. Then, with the aid of the property [34, Def. 5.5.1] as follows (it holds for $i \in \Psi$):

$$\sum_{r=1}^{N_r} \sum_{\tau=1}^{N_s} \left| \sum_{t=1}^{N_t} \mathbf{H}_i^{(r,t)} \boldsymbol{\Delta}_i^{(t)}(\boldsymbol{\tau}) \right|^2 = \sum_{r=1}^{N_r} \sum_{t=1}^{N_t} \left| \mathbf{H}_i^{(r,t)} \right|^2 \left(\sum_{m=1}^M \mathbf{p}_t^{(m)} \left| \tilde{\boldsymbol{\eta}}_i^{(m)} - \boldsymbol{\eta}_i^{(m)} \right|^2 \right) \quad (2.30)$$

we obtain, for $m = 1, 2, \dots, M$, the following identities hold:

$$\begin{cases} \mathcal{D}_{1,m}(\bar{\mathcal{S}}_{\mathcal{I}}, \mathbf{\Delta}_0(\tau)) = \left| \tilde{\boldsymbol{\eta}}_0^{(m)} - \boldsymbol{\eta}_0^{(m)} \right|^2 \sum_{r=1}^{N_r} \sum_{t=1}^{N_t} \mathbf{p}_t^{(m)} \left| \mathbf{H}_0^{(r,t)} \right|^2 \\ \mathcal{D}_{2,m}(\bar{\mathcal{S}}_{\mathcal{I}}, \mathbf{\Delta}_0(\tau), \mathbf{n}(\tau)) = \sum_{r=1}^{N_r} \sum_{\tau=1}^{N_s} \left(\mathbf{n}^{(r)}(\tau) \right)^* \\ \times \left(\sum_{t=1}^{N_t} \mathbf{H}_0^{(r,t)} \left(\boldsymbol{\alpha}^{(t)}(\tau) \left(\tilde{\boldsymbol{\eta}}_0^{(m)} - \boldsymbol{\eta}_0^{(m)} \right) + \boldsymbol{\beta}^{(t)}(\tau) \left(\tilde{\boldsymbol{\eta}}_0^{(m)} - \boldsymbol{\eta}_0^{(m)} \right)^* \right) \right) \end{cases} \quad (2.31)$$

and $\mathcal{D}_{3,m}(\cdot, \cdot, \cdot)$ can be formulated as shown in (2.11) with the definitions as follows,

$$\begin{cases} \mathcal{Z}_{0,i} = \sum_{r=1}^{N_r} \sum_{\tau=1}^{N_s} \left[\left(\sum_{u=1}^{N_t} \mathbf{H}_i^{(r,u)} \mathbf{s}_i^{(u)}(\tau) \right) \mathbf{U}_0^{(r)} \right] = \sum_{r=1}^{N_r} \sum_{u=1}^{N_t} \sum_{\tau=1}^{N_s} \mathbf{H}_i^{(r,u)} \mathbf{s}_i^{(u)}(\tau) \mathbf{U}_0^{(r)}(\tau) \\ \mathbf{U}_0^{(r)} = \sum_{t=1}^{N_t} \mathbf{H}_0^{(r,t)} \left(\boldsymbol{\alpha}^{(t)}(\tau) \left(\tilde{\boldsymbol{\eta}}_0^{(m)} - \boldsymbol{\eta}_0^{(m)} \right) + \boldsymbol{\beta}^{(t)}(\tau) \left(\tilde{\boldsymbol{\eta}}_0^{(m)} - \boldsymbol{\eta}_0^{(m)} \right)^* \right) \end{cases} \quad (2.32)$$

It is apparent that $\mathcal{Z}_{0,i}$ in (2.32) is formulated as shown in (2.9) of Lemma 2.2. To proceed with the analysis, it is important to understand whether the equality in (2.26) is satisfied for arbitrary generalized complex orthogonal designs. This issue is addressed in Definition 2.1, Proposition 2.2 and Remark 2.9.

Definition 2.1. Let a generalized complex orthogonal design Θ , according to [34, Sec. V-E]. Let $\mathcal{Z}_{0,i}$ in (2.32). Θ is said to be *interference-orthogonal* if the equality in (2.26) is satisfied for $\phi(\mathbf{s}_i(\tau)) = \sum_{m=1}^M \left| \boldsymbol{\eta}_i^{(m)} \right|^2$. \square

Proposition 2.2. The generalized complex orthogonal designs in [34, Eq. (32), Eq. (40)] are interference-orthogonal, while those in [34, Eqs. (37)–(39)] are not interference-orthogonal.

Proof: The proof follows by direct inspection of the generalized complex orthogonal designs and by checking whether the identity $\sum_{t=1}^{N_t} \left| \sum_{\tau=1}^{N_s} (\Theta^{(\tau,t)}(\boldsymbol{\eta}_0))^* \mathbf{v}^{(\tau)} \right|^2 = \left(\sum_{\tau=1}^{N_s} |\mathbf{v}^{(\tau)}|^2 \right) \times \left(\sum_{m=1}^M \left| \boldsymbol{\eta}_0^{(m)} \right|^2 \right)$ is satisfied for an arbitrary complex vector \mathbf{v} . The equality holds for the codes in [34, Eq. (32), Eq. (40)]. \square

Remark 2.9. The reason why some generalized complex orthogonal designs are not interference-orthogonal is due to the quasi-static assumption for the other-cell interference. This implies, in fact, that the terms $\mathbf{i}^{(r)}(\tau) = \sum_{u=1}^{N_t} \mathbf{H}_i^{(r,u)} \mathbf{s}_i^{(u)}(\tau)$ in (2.32)

are not independent for $r = 1, 2, \dots, N_r$, since they originate from interfering BSs belonging to the same PPP. Comparing $\mathcal{D}_{2,m}(\cdot, \cdot, \cdot)$ in (2.31) with $\mathcal{Z}_{0,i}$ in (2.32), we note that this does not occur for $\mathcal{D}_{2,m}(\cdot, \cdot, \cdot)$, since the noise terms $\mathbf{n}^{(r)}(\tau)$ are independent for $r = 1, 2, \dots, N_r$, $\tau = 1, 2, \dots, N_s$. The generalized complex orthogonal designs in [34] are designed based on the independence property of the AWGN. Hence, some code constructions may not satisfy the interference-orthogonal property that originates from the partial correlation of the interference across the receive-antennas and the time-slots. \square

The proposed mathematical approach is applicable to interference-orthogonal generalized complex orthogonal designs. It can be applied to generalized complex orthogonal designs that are not interference-orthogonal, *by assuming* that the equality in (2.26) holds true. In this latter case, the framework is no longer exact, but it is an approximation. In Section 2.6, it is shown that it is accurate enough for typical MIMO setups though.

If Θ is interference-orthogonal, the equalities in (2.6) and (2.15) are satisfied and we are able to obtain $\mathcal{D}_{0,m}(\bar{\mathcal{S}}_{\mathcal{I}}, \mathbf{\Delta}_0(\boldsymbol{\tau})) = \left| \tilde{\boldsymbol{\eta}}_0^{(m)} - \boldsymbol{\eta}_0^{(m)} \right|^2 \sum_{r=1}^{N_r} \sum_{t=1}^{N_t} \mathbf{p}_t^{(m)} \left| \mathbf{H}_0^{(r,t)} \right|^2$ and $\bar{\mathcal{D}}_{0,m}(\bar{\mathcal{S}}_{\mathcal{I}}) = \sum_{r=1}^{N_r} \sum_{t=1}^{N_t} \mathbf{p}_t^{(m)} \left| \mathbf{H}_0^{(r,t)} \right|^2$. Since, for typical OSTBCs [34], $\bar{p} = \mathbf{p}_t^{(m)}$ for $t = 1, 2, \dots, N_t$ and $m = 1, 2, \dots, M$, then $\bar{\mathcal{D}}_{0,m}(\bar{\mathcal{S}}_{\mathcal{I}}) \sim \mathcal{G}(N_r N_t, N_r N_t \Omega \bar{p})$. This implies $(m_0, \Omega_0) = (N_r N_t, \bar{p} \Omega)$ [4, Eq. (2.22)]. Since $\mathcal{Z}_{0,i}$ is formulated as in Lemma 2.2 with $N_s = 1$, from Remark 2.8 we conclude that $\mathcal{Q}(\cdot)$ follows from (2.27) with $\phi(\mathbf{s}_i(\boldsymbol{\tau})) = \sum_{m=1}^M \left| \boldsymbol{\eta}_i^{(m)} \right|^2$.

2.4.3 Zero-Forcing (ZF) MIMO Receiver over Rayleigh Fading

Let a MIMO transmission scheme with ZF-based reception and a Rayleigh fading channel model [33, Sec. 2]. Thus, $N_r \geq N_t$, $N_s = 1$, $M = N_t$, $\mathbf{s}_0(1) = \boldsymbol{\eta}_0$, $\mathbf{s}_i(1) = \boldsymbol{\eta}_i$ for $i \in \Psi^{(\setminus 0)}$, $\left| \mathbf{H}_0^{(r,t)} \right|^2 \sim \mathcal{G}(1, \Omega)$ and $\left| \mathbf{H}_i^{(r,t)} \right|^2 \sim \mathcal{G}(1, \Omega)$ for $t = 1, 2, \dots, N_t$, $r = 1, 2, \dots, N_r$ and $i \in \Psi^{(\setminus 0)}$. Let the demodulator in (2.7) with $\bar{\mathcal{S}}_{\mathcal{I}} = \mathbf{H}_0$, $\bar{\mathbf{y}}(1) = \bar{\psi}(\mathcal{S}_{\mathcal{I}}, \mathbf{y}(1)) = (\mathbf{H}_0^H \mathbf{H}_0)^{-1} \mathbf{H}_0^H \mathbf{y}(1)$, $\tilde{\mathbf{y}}(1) = \tilde{\psi}(\mathcal{S}_{\mathcal{I}}, \tilde{\mathbf{s}}_0(1)) = \sqrt{E/N_t r_0^{-b}} \tilde{\mathbf{s}}_0(1)$ and $N = M = N_t$.

Accordingly, the multi-stream demodulator can be re-written in the single-stream formulation similar as (2.29). Let $\mathbf{W}_0 = (\mathbf{H}_0^H \mathbf{H}_0)^{-1} \mathbf{H}_0^H$ denote the $(M = N_t) \times N_r$ ZF

decoding matrix at the receiver, $\mathbf{\Delta}_0(1) = \tilde{\boldsymbol{\eta}}_0 - \boldsymbol{\eta}_0$, then the following identities hold:

$$\begin{cases} \mathcal{D}_{1,m}(\bar{\mathcal{S}}_{\mathcal{I}}, \mathbf{\Delta}_0(\boldsymbol{\tau})) = \left| \mathbf{\Delta}_0^{(m)}(1) \right|^2 \\ \mathcal{D}_{2,m}(\bar{\mathcal{S}}_{\mathcal{I}}, \mathbf{\Delta}_0(\boldsymbol{\tau}), \mathbf{n}(\boldsymbol{\tau})) = \left(\mathbf{\Delta}_0^{(m)}(1) \right)^* \sum_{r=1}^{N_r} \mathbf{W}_0^{(m,r)} \mathbf{n}^{(r)}(1) \end{cases} \quad (2.33)$$

and $\mathcal{D}_{3,m}(\cdot, \cdot, \cdot)$ as shown in (2.11) with

$$\begin{cases} \mathcal{Z}_{0,i} = \sum_{r=1}^{N_r} \sum_{t=1}^{N_t} \mathbf{H}_i^{(r,t)} \mathbf{s}_i^{(t)}(1) \mathbf{U}_0^{(r)}(1) \\ \mathbf{U}_0^{(r)}(1) = \left(\mathbf{\Delta}_0^{(m)}(1) \right)^* \mathbf{W}_0^{(m,r)} \end{cases} \quad (2.34)$$

From (2.6) and (2.15), we obtain that

$$\begin{aligned} \mathcal{D}_{0,m}(\bar{\mathcal{S}}_{\mathcal{I}}, \mathbf{\Delta}_0(\boldsymbol{\tau})) &= \left| \mathbf{\Delta}_0^{(m)}(1) \right|^2 \left(\sum_{r=1}^{N_r} \left| \mathbf{W}_0^{(m,r)} \right|^2 \right)^{-1} \\ &\stackrel{(a)}{=} \left| \mathbf{\Delta}_0^{(m)}(1) \right|^2 \left(\tilde{\mathbf{W}}_0^{(m,m)} \right)^{-1} \end{aligned} \quad (2.35)$$

where $\tilde{\mathbf{W}}_0 = (\mathbf{H}_0^H \mathbf{H}_0)^{-1}$ and (a) follows from direct inspection of \mathbf{W}_0 . Thus, $\mathcal{D}_{0,m}(\bar{\mathcal{S}}_{\mathcal{I}}) = \left(\tilde{\mathbf{W}}_0^{(m,m)} \right)^{-1} \stackrel{(b)}{\sim} \mathcal{G}(N_r - N_t + 1, (N_r - N_t + 1)\Omega)$, where (b) follows from [35, Sec. III] and [36, Corollary 3.2.6, Theorem 3.2.10]. This implies $(m_0, \Omega_0) = (N_r - N_t + 1, \Omega)$ [4, Eq. (2.22)]. Since $\mathcal{Z}_{0,i}$ is formulated as in Lemma 2.2 with $N_s = 1$, from Remark 2.8 we conclude that $\mathcal{Q}(\cdot)$ follows from (2.27) with $\phi(\mathbf{s}_i(1)) = \sum_{t=1}^{N_t} \left| \mathbf{s}_i^{(t)}(1) \right|^2$.

2.4.4 Zero-Forcing MIMO Precoding over Rayleigh Fading

Let a MIMO transmission scheme with ZF-based precoding and a Rayleigh fading channel model [33, Sec. 3]. Let N_u single-antenna MTs be served by intended and interfering BSs in the same channel use within their respective cells. The signal model in (2.1) is still applicable with minor changes. With a slight abuse of notation, let \mathbf{H}_0 denote the $N_u \times N_t$ downlink channel matrix of the links from BS₀ to its N_u intended MTs. Likewise, let denote by \mathbf{H}_i for $i \in \Psi^{(\setminus 0)}$ the $N_u \times N_t$ downlink channel matrices of the interfering BSs towards the same N_u MTs as BS₀. Also, let $\hat{\mathbf{H}}_i$ for $i \in \Psi^{(\setminus 0)}$ denote the $N_u \times N_t$ downlink channel matrix of the links from the i th interfering BS (BS _{i}) towards its intended N_u single-antenna MTs. In general, $\hat{\mathbf{H}}_i \neq \mathbf{H}_i$. Then, (2.1) still holds by replacing N_r with N_u and by letting $N_t \geq N_u$, $N_r = N_s = 1$, $M = N_u$, $\left| \mathbf{H}_0^{(u,t)} \right|^2 \sim \mathcal{G}(1, \Omega)$ and $\left| \mathbf{H}_i^{(u,t)} \right|^2 \sim \mathcal{G}(1, \Omega)$ for $t = 1, 2, \dots, N_t$, $u = 1, 2, \dots, N_u$ and $i \in \Psi^{(\setminus 0)}$.

Let $\underline{\mathbf{V}}_0$ denote the $N_t \times N_u$ precoding matrix used at BS_0 , which is defined as $\underline{\mathbf{V}}_0 = \mathbf{V}_0 / \|\mathbf{V}_0 \boldsymbol{\eta}_0\|$ with $\mathbf{V}_0 = \mathbf{H}_0^H (\mathbf{H}_0 \mathbf{H}_0^H)^{-1}$. Likewise, let $\hat{\underline{\mathbf{V}}}_i$ denote the precoding matrix used at BS_i , which is $\hat{\underline{\mathbf{V}}}_i = \hat{\mathbf{V}}_i / \|\hat{\mathbf{V}}_i \boldsymbol{\eta}_i\|$ with $\hat{\mathbf{V}}_i = \hat{\mathbf{H}}_i^H (\hat{\mathbf{H}}_i \hat{\mathbf{H}}_i^H)^{-1}$ for $i \in \Psi^{(\wedge 0)}$. Based on these precoding matrices, which assume that the side information available at BS_0 and BS_i is $\mathcal{S}_{\mathcal{I}}^{(0)} = \underline{\mathbf{V}}_0$ and $\mathcal{S}_{\mathcal{I}}^{(i)} = \hat{\underline{\mathbf{V}}}_i$, respectively, the transmitted vectors are $\mathbf{s}_0(1) = \Theta(\boldsymbol{\eta}_0; \mathcal{S}_{\mathcal{I}}^{(0)}) = \underline{\mathbf{V}}_0 \boldsymbol{\eta}_0$ and $\mathbf{s}_i(1) = \Theta(\boldsymbol{\eta}_i; \mathcal{S}_{\mathcal{I}}^{(i)}) = \hat{\underline{\mathbf{V}}}_i \boldsymbol{\eta}_i$ for $i \in \Psi^{(\wedge 0)}$.

Let the interference-oblivious demodulator in (2.7) with $\mathcal{S}_{\mathcal{I}} = \|\mathbf{V}_0 \boldsymbol{\eta}_0\|$, as well as $\bar{\mathbf{y}}(1) = \bar{\psi}(\mathcal{S}_{\mathcal{I}}, \mathbf{y}(1)) = \mathbf{y}(1)$, $\tilde{\mathbf{y}}(1) = \tilde{\psi}(\mathcal{S}_{\mathcal{I}}, \tilde{\mathbf{s}}_0(1)) = \sqrt{E/N_t r_0^{-b}} (\tilde{\boldsymbol{\eta}}_0(1) / \|\mathbf{V}_0 \boldsymbol{\eta}_0\|)$ and $N = M = N_u$. Accordingly, the multi-stream demodulator in (2.7) can be re-written in the single-stream formulation similar to (2.29) for each intended user $u = m = 1, 2, \dots, N_u$. In particular, we have $\boldsymbol{\Delta}_0(1) = \tilde{\boldsymbol{\eta}}_0 - \boldsymbol{\eta}_0$, and the following identities hold:

$$\begin{cases} \mathcal{D}_{1,m}(\bar{\mathcal{S}}_{\mathcal{I}}, \boldsymbol{\Delta}_0(\boldsymbol{\tau})) = \left| \boldsymbol{\Delta}_0^{(m)}(1) \right|^2 \|\mathbf{V}_0 \boldsymbol{\eta}_0\|^{-2} \\ \mathcal{D}_{2,m}(\bar{\mathcal{S}}_{\mathcal{I}}, \boldsymbol{\Delta}_0(\boldsymbol{\tau}), \mathbf{n}(\boldsymbol{\tau})) = \left(\boldsymbol{\Delta}_0^{(m)}(1) \right)^* \|\mathbf{V}_0 \boldsymbol{\eta}_0\|^{-1} \mathbf{n}^{(1)}(1) \end{cases} \quad (2.36)$$

and $\mathcal{D}_{3,m}(\cdot, \cdot, \cdot)$ as shown in (2.11) with $\mathcal{Z}_{0,i} = \sum_{t=1}^{N_t} \mathbf{H}_i^{(m,t)} \underline{\mathbf{s}}_i^{(t)}(1) \mathbf{U}_0^{(m)}(1)$, where $\underline{\mathbf{s}}_i(1) = \left\| \hat{\mathbf{V}}_i \boldsymbol{\eta}_i \right\|^{-1} \mathbf{s}_i(1)$ and $\mathbf{U}_0^{(m)}(1) = \left(\boldsymbol{\Delta}_0^{(m)}(1) \right)^* \|\mathbf{V}_0 \boldsymbol{\eta}_0\|^{-1}$. From (2.6) and (2.15), we obtain $\mathcal{D}_{0,m}(\bar{\mathcal{S}}_{\mathcal{I}}, \boldsymbol{\Delta}_0(\boldsymbol{\tau})) = \left| \boldsymbol{\Delta}_0^{(m)}(1) \right|^2 \|\mathbf{V}_0 \boldsymbol{\eta}_0\|^{-2}$ and $\mathcal{D}_{0,m}(\bar{\mathcal{S}}_{\mathcal{I}}) = \|\mathbf{V}_0 \boldsymbol{\eta}_0\|^{-2}$. Since $\mathcal{Z}_{0,i}$ is formulated as in Lemma 2.2 with $N_s = N_r = 1$, from Remark 2.8 we conclude that $\mathcal{Q}(\cdot)$ follows from (2.27) with $\phi(\underline{\mathbf{s}}_i(1)) = \sum_{t=1}^{N_t} \left| \underline{\mathbf{s}}_i^{(t)}(1) \right|^2 = \left\| \hat{\mathbf{V}}_i \boldsymbol{\eta}_i \right\|^{-2} \sum_{t=1}^{N_t} \left| \mathbf{s}_i^{(t)}(1) \right|^2 = 1$, since $\mathbf{s}_i(1) = \hat{\mathbf{V}}_i \boldsymbol{\eta}_i$ for $i \in \Psi^{(\wedge 0)}$.

So far, the analysis for ZF precoding is exact and no approximations have been used. To complete the analysis, the distribution of $\mathcal{D}_{0,m}(\bar{\mathcal{S}}_{\mathcal{I}}) = \|\mathbf{V}_0 \boldsymbol{\eta}_0\|^{-2} = (\boldsymbol{\eta}_0^* \mathbf{V}_0^H \mathbf{V}_0 \boldsymbol{\eta}_0)^{-1}$ needs to be computed. To the best of our knowledge, however, it is unknown for discrete modulation schemes. To get a tractable yet accurate mathematical framework, we exploit two approximations for the computation of the distribution of $\mathcal{D}_{0,m}(\cdot)$. First of all, we assume that $\boldsymbol{\eta}_0$ follows a unit-energy complex Gaussian distribution, *i.e.*, $\boldsymbol{\eta}_0^{(m)} \sim \mathcal{CN}(0, 1)$ for $m = 1, 2, \dots, M = N_u$. From [5, Eq. (103), Eq. (105)], we obtain $\boldsymbol{\eta}_0^* \mathbf{V}_0^H \mathbf{V}_0 \boldsymbol{\eta}_0 \sim N_u (N_t - N_u + 1)^{-1} \mathcal{F}(2N_u, 2(N_t - N_u + 1))$, which implies the following, $\mathcal{D}_{0,m}(\bar{\mathcal{S}}_{\mathcal{I}}) \sim ((N_t - N_u + 1)/N_u) \mathcal{F}(2(N_t - N_u + 1), 2N_u)$. Second of all, we approximate this resulting scaled F-distribution with a scaled Chi-Square distribution, *i.e.*, $\mathcal{D}_{0,m}(\bar{\mathcal{S}}_{\mathcal{I}}) \sim (2N_u)^{-1} \chi_{2(N_t - N_u + 1)}^2$, which is known to be accurate for $N_u \gg 1$ and, in turn, can be re-written in terms of a Gamma distribution, *i.e.*, we

have the distribution $\mathcal{D}_{0,m}(\bar{\mathcal{S}}_{\mathcal{I}}) \sim \mathcal{G}(N_t - N_u + 1, N_u^{-1}(N_t - N_u + 1)\Omega)$. This implies $(m_0, \Omega_0) = (N_t - N_u + 1, \Omega/N_u)$ [4, Eq. (2.22)]. In Section 2.6, these approximations are shown to be accurate enough for typical MIMO setups.

2.5 Insights from the Mathematical Framework

In this section, we elaborate further on the analysis of the proposed mathematical framework in an attempt of shedding lights on the impact of system parameters and MIMO transmission scheme on the achievable performance. In particular, we focus our attention on the interference-limited regime, since this is the most interesting case study for cellular networks and it is more mathematically tractable as well. Thus, our departing point is (2.24). Furthermore, we focus our attention on constant-envelope modulations, *e.g.*, multi-level PSK, as they lead to a simplified mathematical analysis and experiences confirm that similar conclusions can be drawn for other modulations. In this case, the expectations in Table 2.2 can be computed in closed-form, since $|\boldsymbol{\eta}_0^{(m)}| = 1$ for $m = 1, 2, \dots, M$.

Under these assumptions and from (2.24), the ASEP of PSK modulation can be formulated as follows:

$$\begin{aligned} \text{ASEP}_{\text{PSK}} &= \mathcal{I}^{(\infty)}(\alpha, \beta, \gamma) \\ &= \frac{\alpha}{\pi} - \frac{m_0}{\pi} \int_0^{+\infty} \frac{\mathcal{T}(z; m_0, \alpha)}{p_1 F_1(-1/b; 1-1/b; -(\kappa_{\text{MIMO}}/\kappa_{\text{MOD}})z) - p + 1} dz \end{aligned} \quad (2.33)$$

where i) $(\alpha, \beta, \gamma) = (\pi - \pi/M, 2, \pi/M)$, ii) $\kappa_{\text{MOD}} = (1/2)\beta \sin^2(\gamma) = \sin^2(\pi/M)$, iii) $(m_0, \kappa_{\text{MIMO}}) = (N_r, 1)$ for SIMO, iv) $(m_0, \kappa_{\text{MIMO}}) = (N_r N_t, M/\bar{p})$ for OSTBCs, v) $(m_0, \kappa_{\text{MIMO}}) = (N_r - N_t + 1, M = N_t)$ for ZF reception, and finally, vi) $(m_0, \kappa_{\text{MIMO}}) = (N_t - N_u + 1, M = N_u)$ for ZF precoding.

Proposition 2.3. *Let ASEP_{PSK} in (2.33). The following approximation holds:*

$$\text{ASEP}_{\text{PSK}} \approx \mathcal{K}_{\text{PSK}}^{(0)} - \frac{\mathcal{K}_{\text{PSK}}^{(0)}}{\sqrt{\pi}\Gamma(\mathcal{K}_{\text{PSK}}^{(1)})} G_{4,3}^{2,3} \left(\mathcal{K}_{\text{PSK}}^{(2)} \left| \begin{array}{cccc} 1/2 & 0 & 0 & 1 \\ 0 & \mathcal{K}_{\text{PSK}}^{(1)} & 0 & \end{array} \right. \right) \quad (2.34)$$

where $\mathcal{K}_{\text{PSK}}^{(0)} = 1/2$ if $M = 2$ and $\mathcal{K}_{\text{PSK}}^{(0)} = 1$ if $M \geq 4$, $\mathcal{K}_{\text{PSK}}^{(1)} = m_0$ and $\mathcal{K}_{\text{PSK}}^{(2)} = p(b-1)^{-1} \sin^{-2}(\pi/M) \kappa_{\text{MIMO}}$.

Proof: See Appendix 2.D. □

In spite of being an approximation, (2.34) is surprisingly simple and insightful. In particular, it depends on two main parameters, *i.e.*, $\mathcal{K}_{\text{PSK}}^{(1)}$ and $\mathcal{K}_{\text{PSK}}^{(2)}$. By direct inspection of the Meijer G-function in (2.34), it follows that ASEP_{PSK} monotonically decreases as $\mathcal{K}_{\text{PSK}}^{(1)}$ increases and that it monotonically increases as $\mathcal{K}_{\text{PSK}}^{(2)}$ increases. From (2.34), the following performance trends can be inferred:

- The ASEP gets worse as either p or M increase. Also, it gets better as b increases. These trends are in agreement with previously reported results for specific MIMO transmission schemes [25].
- Let M be fixed and independent of other MIMO parameters. The ASEP gets worse as κ_{MIMO} increases. This implies that the error performance gets worse as M , *i.e.*, the number of simultaneously transmitted information symbols, increases for OSTBCs, ZF reception ($N_t = M$) and ZF precoding ($N_u = M$).
- Let the rate $\mathcal{R} = (M/N_s) \log_2(M)$ be fixed and M be computed from it, *i.e.*, $M = 2^{\mathcal{R}(M/N_s)^{-1}}$. Thus, $\bar{\mathcal{K}}_{\text{PSK}}^{(2)} = \sin^{-2}(\pi/M) \kappa_{\text{MIMO}} \propto 2^{2\mathcal{R}(M/N_s)^{-1}} M$. Accordingly, the error performance is expected to get better as M increases (*e.g.*, $M = N_t$ for ZF reception and $M = N_u$ for ZF precoding).
- The ASEP gets better as m_0 increases. Thus, the error performance gets better with the “degrees of freedom” of MIMO transmission. For example, this occurs if: i) N_r increases for SIMO, ii) $N_r N_t$ increases for OSTBCs, iii) $N_r - N_t$ increases for ZF reception, and iv) $N_t - N_u$ increases for ZF precoding.
- The first three case studies assume that $\mathcal{K}_{\text{PSK}}^{(1)}$ is fixed, while the fourth that $\mathcal{K}_{\text{PSK}}^{(2)}$ is fixed. For some MIMO setups, however, $\mathcal{K}_{\text{PSK}}^{(1)}$ and $\mathcal{K}_{\text{PSK}}^{(2)}$ may not be chosen independently of each other. Because of the opposite behavior of (2.34) as a function of $\mathcal{K}_{\text{PSK}}^{(1)}$ and $\mathcal{K}_{\text{PSK}}^{(2)}$, some non-trivial trends may emerge.

These considerations are reasonable, somehow expected and in agreement with intuition. They confirm the validity of our mathematical approach for performance evaluation of cellular networks. At the same time, (2.34) provides a simple mathematical formulation that allows us to *quantify* the impact of important system parameters. In particular,

(2.34) accounts for a large number of MIMO transmission schemes via the parameter κ_{MIMO} . These trends are substantiated in Section 2.6 with the aid of Monte Carlo simulations.

2.6 Numerical and Simulation Results

In this section, numerical examples are shown to substantiate the accuracy of the mathematical frameworks and to confirm the performance trends highlighted in Section 2.5. The frameworks are compared against Monte Carlo simulations, which are obtained by using the similar procedure described in [21, Sec. V], [25, Sec. VI]. To increase the readability, the methodology used for the evaluation of ASEP is described as follows:

Step 1: A finite circular area of radius R_A around the origin, i.e., where the probe mobile terminal is located, is considered as the simulated area. The radius is chosen to be sufficiently large to minimize the truncation error committed in simulating the infinite bi-dimensional plane. In practice, the radius is chosen such that at least 1000 BSs are simulated.

Step 2: In the finite circular region of area, the number of BSs are generated as a RV following the Poisson distribution with density λ and area πR_A^2 , and the BSs are distributed following a uniform distribution over the simulated area.

Step 4: The closest BS is chosen as the serving BS of the MT, while all other active BSs are interfering nodes to the useful link.

Step 5: Independent channel gains are generated for each link from the BS to the MT, the precoding matrices are generated at each BS accordingly.

Step 6: Given the received signal from all the active BSs in N_s time-slots, the MT decodes M intended information symbols by the demodulator in (2.16).

Step 7: Finally, by repeating Step 1–Step 7 for $N_{\text{mc}} = 10^6$ times, the ASEP is computed by the number of incorrect estimations of the transmitted symbols divided by MN_{mc} .

The accuracy of the PPP-based abstraction with unified path-loss model for modeling the error performance of cellular networks is investigated in [25, Sec. VI], by comparing

it with grid-based abstraction models. Hence, similar curves are not reported in this section. The simulation setup is summarized in the caption of each figure, where markers show Monte Carlo simulations, solid lines the framework from (2.23) and dashed lines the framework from (2.24). As for the implementation of the mathematical frameworks for QAM with $M \geq 4$, the parameters as follows are used: $\alpha_1 = \pi/2$, $\beta_1 = 3/(M-1)$, $\gamma_1 = \pi/2$, $\delta_1 = 4(\sqrt{M}-1)/\sqrt{M}$ and $\alpha_2 = \pi/4$, $\beta_2 = 6/(M-1)$, $\gamma_2 = \pi/4$, $\delta_2 = 4(\sqrt{M}-1)^2/M$. If $M = 2$, the quadruplet $(\alpha, \beta, \gamma, \delta) = (\pi/2, 2, \pi/2, 1)$ is used.

Selected numerical examples are illustrated in Figs 2.2–2.6, where the ASEP is depicted as a function of E/\mathcal{N}_0 , which is a reference signal-to-noise-ratio that is computed at a fixed reference distance of one meter from the transmitter. These figures confirm the accuracy of the proposed mathematical frameworks. Furthermore, the performance trends highlighted in Section 2.5 as a function of the MIMO setups are confirmed. The approximations proposed in Section 2.4.2 (see Fig. 2.4(b)) and in Section 2.4.4 (see Fig. 2.5(b)) are confirmed to be sufficiently accurate in the considered setup. Similar accuracies are obtained for different parameters. Some figures deserve special comments.

In agreement with [25], Fig. 2.2 confirms that the impact of the fading severity is negligible in the presence of other-cell interference. The path-loss exponent has a different impact in noise- and interference-limited regimes. In particular, a bigger path-loss is beneficial in interference-limited cellular networks, since the other-cell interference is reduced. Figure 2.3(b) shows a similar behavior in the presence of receive-diversity. Figure 2.3(a) confirms that receive-diversity is still beneficial, but the gain in the presence of other-cell interference is reduced compared to the noise-limited scenario. The limited receive diversity gain in the interference-limited network is due to the partial correlation of the interference seen at each receive antenna. Specifically, in the noise-limited scenario, the receive diversity originates from the independence of the channel gains as well as the independence of the additive Gaussian noise of each link. When the system is interference-limited, the positions of the interfering nodes are the same for all the co-located receive antennas, which indicates that the aggregate interference is partially correlated, which reduces the diversity.

Figure 2.4 shows that the performance gain offered by transmit-diversity compared to receive-diversity in noise-limited networks is not observable in the presence of other-cell

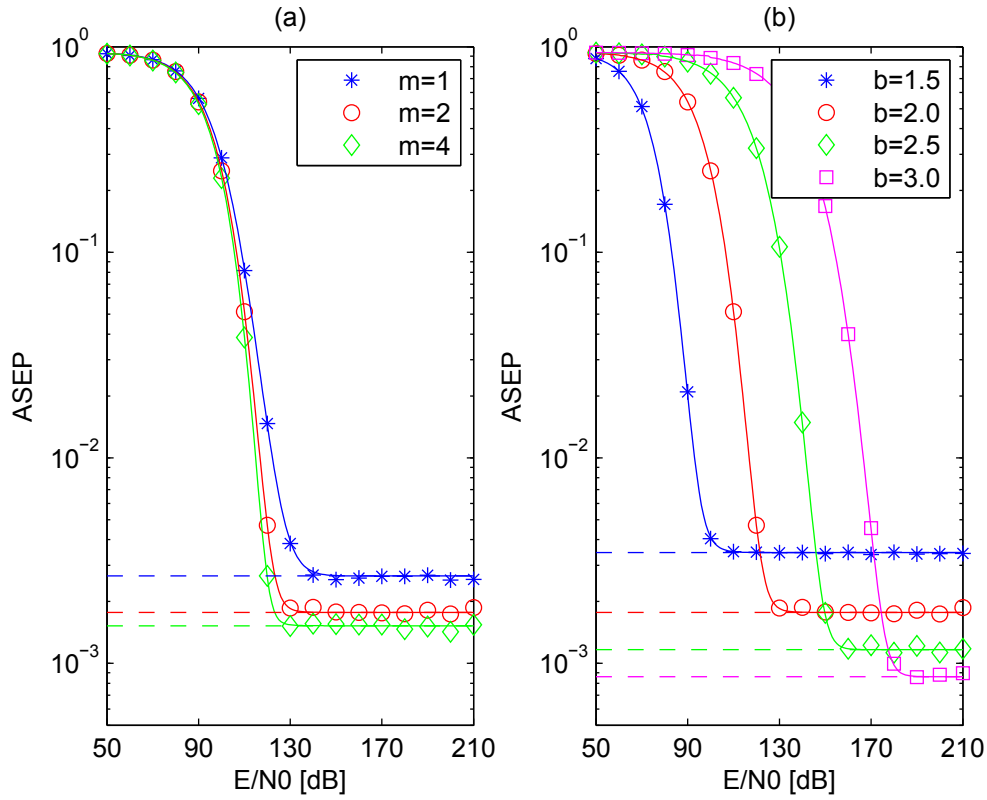


FIGURE 2.2: ASEP of SISO transmission over Nakagami- m fading ($\Omega = 1$). Setup: (a) $\lambda = 10^{-5}$, $p = 10^{-3}$, $M = 16$, and $b = 2$; (b) $\lambda = 10^{-5}$, $p = 10^{-3}$, $M = 16$, and $m = 2$.

interference. In fact, the ASEP of Fig. 2.3(a) and Fig. 2.4(a) is almost the same. This result can be understood by direct inspection of (2.34). $\mathcal{K}_{\text{PSK}}^{(1)}$ is larger for OSTBC than for SIMO, which would lead to a better ASEP for OSTBC. κ_{MIMO} , however, is larger for OSTBC than for SIMO, which would lead to a worse ASEP for OSTBC. This trade-off leads to the almost no gain of transmit-diversity in the considered setup.

Figure 2.5 compares ZF reception and ZF precoding under similar operating conditions, and under the assumption that M is independent of N_t and N_u , respectively. As discussed in Section 2.5, the figure confirms that the ASEP gets worse by increasing N_t and N_u . A close inspection of Figs. 2.5(a) and 5(b) reveals that ZF reception and precoding provide almost the same performance in the interference-limited regime. Architectural design and mo/demodulation complexity are, however, quite different between them.

Figure 2.6 provides a sound confirmation of some non-trivial trends highlighted in Section 2.5. Figure 2.6(a) shows that the ASEP may get worse by increasing N_t , while Fig. 2.6(b) shows that the ASEP gets better by increasing N_t . The trend in Fig. 2.6(a) originates from the fact that $\mathcal{K}_{\text{PSK}}^{(1)}$ decreases by increasing N_t and that this effect is not

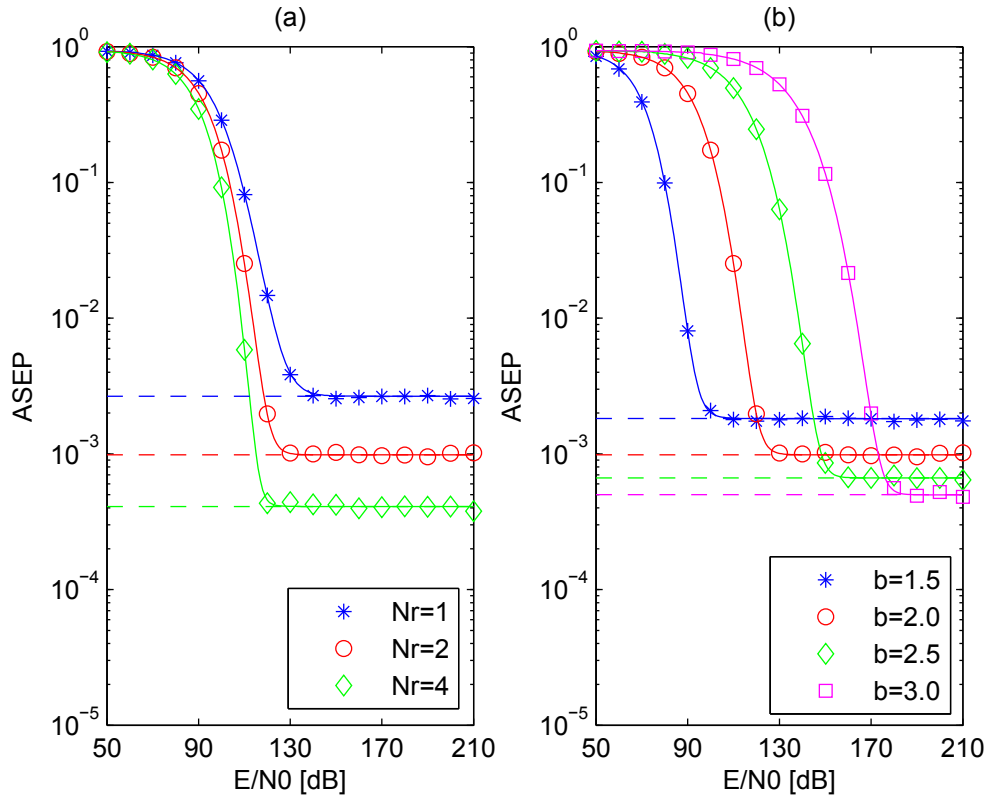


FIGURE 2.3: ASEP of SIMO transmission over Rayleigh fading ($\Omega = 1$). Setup: (a) $\lambda = 10^{-5}$, $p = 10^{-3}$, $M = 16$, and $b = 2$; (b) $\lambda = 10^{-5}$, $p = 10^{-3}$, $M = 16$, and $N_r = 2$.

counterbalanced by the reduction of the modulation order M . On the other hand, the trend in Fig. 2.6(b) follows because $\mathcal{K}_{\text{PSK}}^{(1)}$ is kept fixed by increasing N_r . As a result, reducing the modulation order M is beneficial ($\mathcal{K}_{\text{PSK}}^{(2)}$ decreases).

In conclusion, the proposed mathematical frameworks are sufficiently accurate and insightful to the analysis, design and optimization of MIMO-aided cellular networks.

2.7 Conclusion

In this chapter, a new mathematical methodology for performance evaluation of downlink MIMO cellular networks is introduced. The proposed approach relies on a PPP-based abstraction model for the locations of cellular BSs and it exploits results from stochastic geometry for the computation of the distribution of the other-cell interference. Based on a new exact and closed-form expression of the CF of the other-cell interference, an EiD representation for it is introduced, which is shown to be conveniently formulated in terms of an infinite summation of conditionally Gaussian and independent RVs with

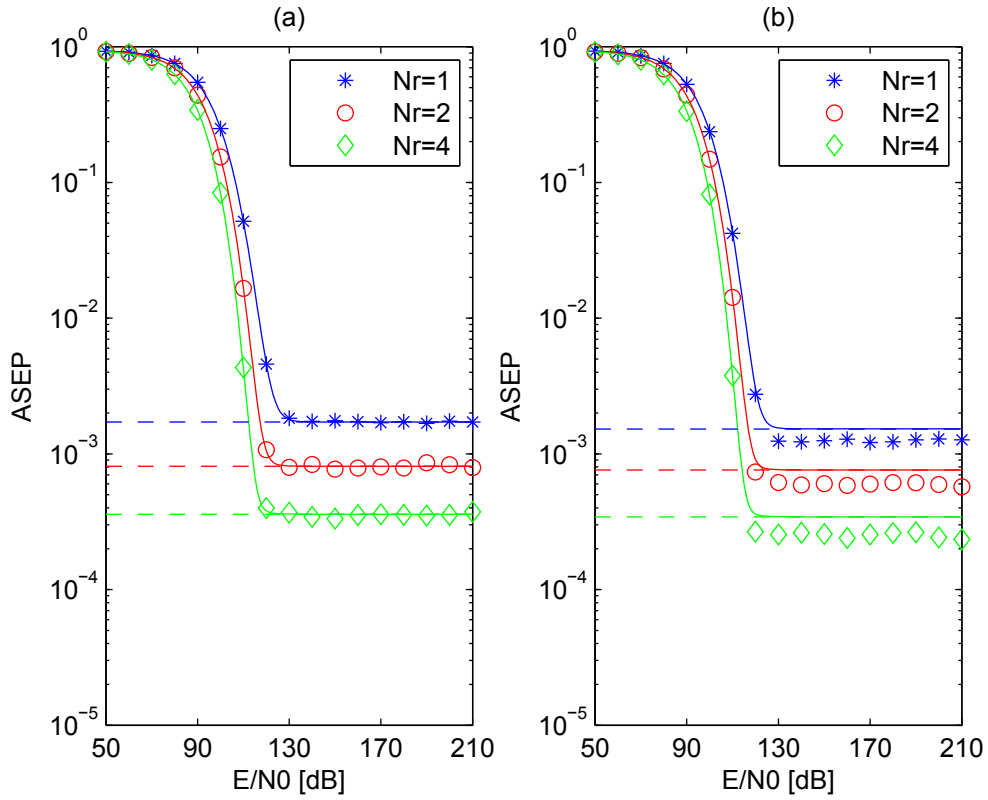


FIGURE 2.4: ASEP of OSTBC transmission over Rayleigh fading ($\Omega = 1$). Setup: (a) H2 code in [34, Eq. (32)] (Alamouti), $\lambda = 10^{-5}$, $p = 10^{-3}$, $M = 16$ ($\mathcal{R} = 4\text{bpcu}$), and $b = 2$; (b) H3 code in [34, Eq. (39)], $\lambda = 10^{-5}$, $p = 10^{-3}$, $M = 16$ ($\mathcal{R} = 3\text{bpcu}$), and $b = 2$.

zero mean and finite variance. By capitalizing on this mathematical formulation, a two-fold integral expression of the error probability for various MIMO transmission schemes is computed. In the interference-limited regime, exact single-integral and closed-form approximated expressions are provided, which are shown to offer insightful information on the impact of system parameters and MIMO setups.

The application of the *EiD*-based approach goes beyond the performance evaluation of downlink MIMO cellular networks. It can, in principle, be applied to all system setups where non-Gaussian distributed RVs possess an *EiD* representation that can be formulated in terms of complex Gaussian RVs with zero mean. For example, the authors have recently extended it for application to heterogeneous cellular networks with an arbitrary number of tiers, different densities, transmit powers and biases for each tier [37]. Other potential generalizations and applications of the *EiD*-based approach include the analysis of heterogeneous cellular networks with channel coding at the physical layer as well as the analysis of relay-aided (heterogeneous) cellular networks [13, 14, 16].

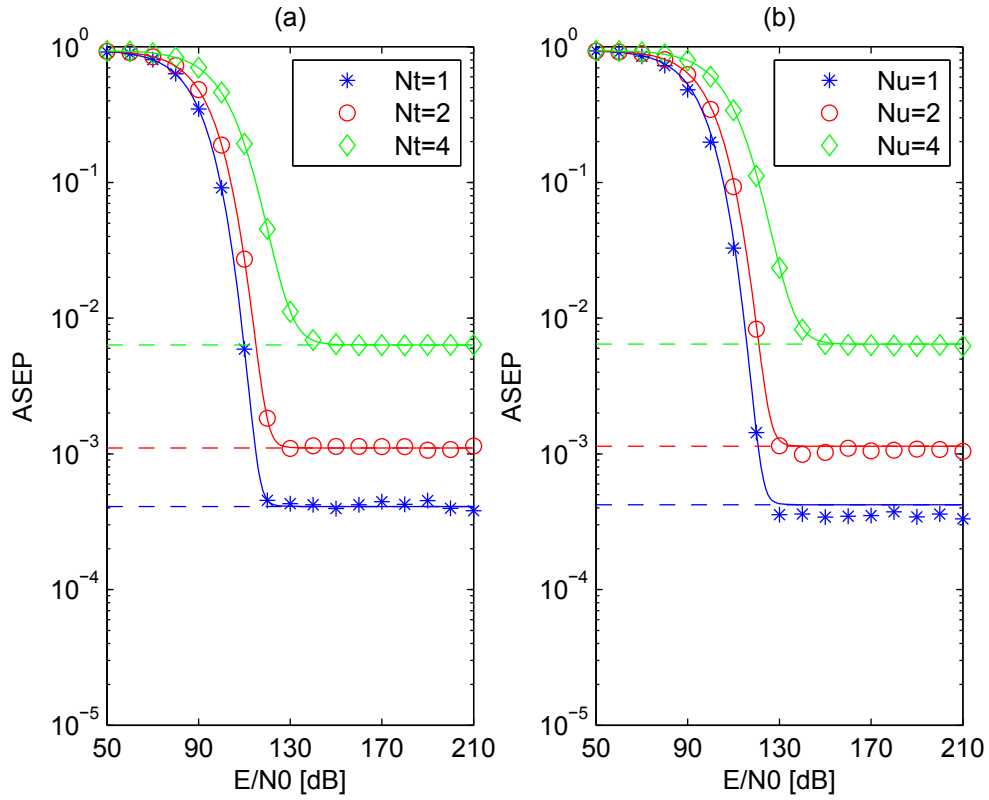


FIGURE 2.5: ASEP of ZF-based MIMO transmission over Rayleigh fading ($\Omega = 1$). Setup: (a) ZF reception, $\lambda = 10^{-5}$, $p = 10^{-3}$, $M = 16$, $b = 2$, and $N_r = 4$; (b) ZF precoding, $\lambda = 10^{-5}$, $p = 10^{-3}$, $M = 16$, $b = 2$, and $N_t = 4$.

Appendix

2.A Useful Notable Integrals

Notable Integral 2.1. Let p be a complex number with $\text{Re}\{p\} > 0$. Let X be a non-negative real number. The following identity holds [38, Eq. (6)]:

$$X^{-p} = \frac{1}{\Gamma(p)} \int_0^{+\infty} z^{p-1} \exp\{-zX\} dz \quad (2.35)$$

Notable Integral 2.2. Let p be a complex number with $\text{Re}\{p\} > 0$. Let X be a non-negative real number. The following identity holds [39, Eq. (4)]:

$$\exp\{-p/X\} = 1 - \sqrt{p} \int_0^{+\infty} z^{-1/2} J_1(2\sqrt{pz}) \exp\{-zX\} dz \quad (2.36)$$

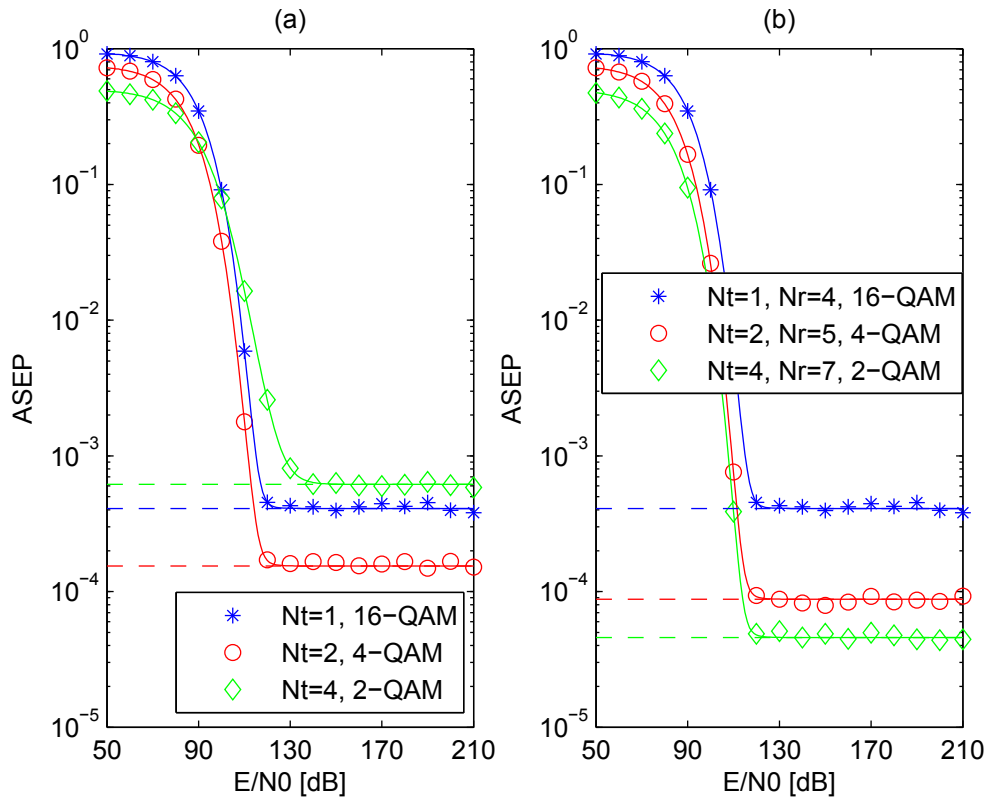


FIGURE 2.6: ASEP of ZF-based MIMO reception over Rayleigh fading ($\Omega = 1$). Setup: (a) $\lambda = 10^{-5}$, $p = 10^{-3}$, $b = 2$, and $N_r = 4$; (b) $\lambda = 10^{-5}$, $p = 10^{-3}$, and $b = 2$.

Notable Integral 2.3. Let m be a real number with $m \geq 1/2$. Let s and X be non-negative real numbers. The following identity holds [20, Eq. (18)]:

$$\begin{aligned}
 & s\Gamma(m+1)X^{1/2} {}_1F_1(m+1; 2; -sX) \\
 &= \int_0^{+\infty} \sqrt{sz} z^{m-1} \exp\{-z\} J_1\left(2\sqrt{szX}\right) dz
 \end{aligned} \tag{2.37}$$

Notable Integral 2.4. Let m be an integer number with $m \geq 1/2$. Let ω be a real number, and X and μ be non-negative real numbers. The following identity holds [40]

and [20, Eq. (22)].

$$\begin{aligned}
& \mathcal{T}(X; m, \mu) \\
&= \int_0^\mu \frac{1}{\sin^2(\omega)} {}_1F_1\left(m+1; 2; -\frac{X}{\sin^2(\omega)}\right) d\omega \\
&= \begin{cases} \sum_{k=0}^{m-1} \frac{(1-m)_k}{k!(2)_k} X^k \left[\frac{\exp\{-X\}}{2} \sum_{n=0}^k \binom{k}{n} X^{-(n+1/2)} \Gamma\left(n+\frac{1}{2}, X \cot^2(\mu)\right) \right], \\ \quad \text{if } 0 \leq \mu \leq \pi/2 \\ \sum_{k=0}^{m-1} \frac{(1-m)_k}{k!(2)_k} X^k \left[\frac{\exp\{-X\}}{2} \sum_{n=0}^k \binom{k}{n} X^{-(n+1/2)} (2\Gamma\left(n+\frac{1}{2}\right) - \Gamma\left(n+\frac{1}{2}, X \cot^2(\mu)\right)) \right], \\ \quad \text{if } \mu > \pi/2 \end{cases}
\end{aligned} \tag{2.38}$$

2.B Proofs of Propositions and Lemmas

Proof of Proposition 2.1. The proof consists of two steps: 1) the CFs of $\mathcal{D}_3(\cdot, \cdot, \cdot)$, *i.e.*, $\text{CF}_{\mathcal{D}_3}(\cdot; \cdot)$, and of $\mathcal{D}_3^{\text{(GCG)}}(\cdot, \cdot, \cdot)$, *i.e.*, $\text{CF}_{\mathcal{D}_3^{\text{(GCG)}}}(\cdot; \cdot)$, conditioned upon r_0 are computed and 2) it is shown that they are the same, thus proving their equivalence in distribution. The CF of $\mathcal{D}_3(\cdot, \cdot, \cdot)$ is computed by using the same steps as in [15, Proposition 1]. To make the report self-contained, the proof in [15, Proposition 1] is repeated here. The difference is that the channel envelopes are assumed to have a generic distribution instead of being Rayleigh distributed. The channel phase is, on the other hand, always uniformly distributed. In particular, the CF conditioned on r_0 can be computed as follows,

$$\begin{aligned}
& \text{CF}_{\mathcal{D}_3}(\boldsymbol{\omega}; r_0) \\
&= \mathbb{E}_{|r_0} \left\{ \exp \left(-j\boldsymbol{\omega} \sum_{i \in \Psi(\setminus 0)} \sqrt{E/N_t} r_i^{-b} \mathcal{Z}_{0,i} \right) \right\} \\
&\stackrel{(a)}{=} \exp \left[-2\pi p \lambda \int_{r_0}^{+\infty} \left(1 - \text{CF}_{\mathcal{Z}_{0,i}} \left(\boldsymbol{\omega} \sqrt{\frac{E}{N_t}} r_i^{-b} \right) \right) dr_i \right] \\
&\stackrel{(b)}{=} \exp \left[-2\pi p \lambda \int_{r_0}^{+\infty} \left(1 - \mathbb{E}_{\mathcal{Z}_{0,i}} \left\{ \cos \left(|\boldsymbol{\omega}| \sqrt{\frac{E}{N_t}} r_i^{-b} \mathcal{Z}_{0,i}^{(\text{re})} \right) \right\} \right) dr_i \right] \\
&\stackrel{(c)}{=} \exp \left\{ -p \lambda \pi r_0^2 \mathbb{E}_{\mathcal{Z}_{0,i}} \left\{ -1 + {}_1F_2 \left(-\frac{1}{b}; \frac{1}{2}, 1 - \frac{1}{b}; -\frac{|\boldsymbol{\omega}|^2 E}{4 N_t} r_0^{-2b} \left(\mathcal{Z}_{0,i}^{(\text{re})} \right)^2 \right) \right\} \right\} \\
&\stackrel{(d)}{=} \exp \left\{ -p \lambda \pi r_0^2 \sum_{q=1}^{+\infty} \frac{(-1/b)_q}{(1/2)_q (1-1/b)_q} \frac{(-1)^q}{q!} \left(\frac{|\boldsymbol{\omega}|^2 E}{4 N_t} r_0^{-2b} \right)^q \mathbb{E} \left\{ \left(\mathcal{Z}_{0,i}^{(\text{re})} \right)^{2q} \right\} \right\}
\end{aligned} \tag{2.39}$$

where (a) follows by applying the Probability Generating Functional (PGFL) theorem of PPPs [7], (b) follows because, as mentioned in *Remark 2.3*, the RVs $\mathcal{Z}_{0,i}$ are spherically symmetric and, thus, property iv) in *Remark 2.2* holds, (c) follows by solving the integral with respect to r_i with the aid of [41, Eq. (3.771.4)] and (d) follows from the series expansion of the generalized hypergeometric function [2, Ch. 5, Eq. (2)].

From (2.39), it follows that $\text{CF}_{\mathcal{D}_3}(\boldsymbol{\omega}; r_0) = \text{CF}_{\mathcal{D}_3}(|\boldsymbol{\omega}|^2; r_0)$, in other words, the CF of $\mathcal{D}_3(\cdot, \cdot, \cdot)$ depends only on the absolute value of $\boldsymbol{\omega}$. It proves, according to *Remark 2.2*, that $\mathcal{D}_3(\cdot, \cdot, \cdot)$ is a spherically symmetric RV. It is worth mentioning that this holds for arbitrary values of $r_0 \geq 0$. Accordingly, the notation $\text{CF}_{\mathcal{D}_3}(|\boldsymbol{\omega}|^2; r_0)$ is used in what follows.

Also, the CF of $\mathcal{D}_3^{(\text{GCG})}(\cdot, \cdot, \cdot)$ is computed as follows:

$$\begin{aligned}
& \text{CF}_{\mathcal{D}_3^{(\text{GCG})}}(\boldsymbol{\omega}; r_0) \\
&= \mathbb{E}_{\{\mathbf{G}_q\}, \{\mathbf{B}_q\}} \left\{ \exp \left\{ -j\boldsymbol{\omega} \sqrt{E/N_t} \sum_{q=1}^{+\infty} \left(r_0^{(-b+1/q)} (p\lambda\pi)^{1/(2q)} \sqrt{\mathbf{B}_q} \mathbf{G}_q \right) \right\} \right\} \\
&\stackrel{(a)}{=} \prod_{q=1}^{+\infty} \mathbb{E}_{\{\mathbf{B}_q\}} \left\{ \exp \left\{ -s \frac{|\boldsymbol{\omega}|^2}{4} \frac{E}{N_t} r_0^{-2b+2/q} (p\lambda\pi)^{1/q} \sigma_{\mathbf{G}_q}^2 (\bar{\mathcal{S}}_I, \boldsymbol{\Delta}_0(\boldsymbol{\tau})) \mathbf{B}_q \right\} \right\} \\
&= \prod_{q=1}^{+\infty} \exp \left\{ - \left(\frac{|\boldsymbol{\omega}|^2}{4} \frac{E}{N_t} r_0^{-2b+2/q} (p\lambda\pi)^{1/q} \right)^q \sigma_{\mathbf{G}_q}^{2q} (\bar{\mathcal{S}}_I, \boldsymbol{\Delta}_0(\boldsymbol{\tau})) \right\}
\end{aligned} \tag{2.40}$$

where (a) is by the independence of $\{\mathbf{G}_q\}_{q=1}^{\infty}$, $\{\mathbf{B}_q\}_{q=1}^{\infty}$ and by the CF of a complex zero mean Gaussian RB. Finally, by inserting (2.13) in (2.40) and by comparing it with (2.39), we found that they are exactly the same. Thus, $\mathcal{D}_3(\cdot, \cdot, \cdot)$ and $\mathcal{D}_3^{(\text{GCG})}(\cdot, \cdot, \cdot)$ are equivalent in distribution.

Proof of Lemma 2.1. By definition, $\mathbb{E}_{h_i} \left\{ \left(\mathcal{Z}_{0,i}^{(\text{re})} \right)^{2q} \right\} \stackrel{(a)}{=} |s_i|^{2q} |h_0|^{2q} |\Delta_0|^{2q} \mathcal{K}_1 \mathcal{K}_2$, with:

$$\begin{cases} \mathcal{K}_1 = \mathbb{E}_{|h_i|^2} \left\{ |h_i|^{2q} \right\} \stackrel{(b)}{=} \frac{\Gamma(m+q)}{\Gamma(m) m^q} \Omega^q \\ \mathcal{K}_2 = \mathbb{E}_{\arg\{h_i\}} \left\{ \cos^{2q}(\arg\{h_i\} + \arg\{s_i + h_0 + \delta_0\}) \right\} \\ \stackrel{(c)}{=} \frac{1}{2\pi} \int_0^{2\pi} \cos^{2q}(x) dx \stackrel{(d)}{=} \frac{\Gamma(q+1/2)}{\Gamma(q+1) \sqrt{\pi}} \end{cases} \tag{2.41}$$

where (a) follows from the statistical independence of $|h_i|^2$ and $\arg\{h_i\}$; (b) follows from [4, Eq. (2.23)]; (c) follows from the fact that $\arg\{h_i\}$ is uniformly distributed in $[0, 2\pi)$

and that the integral is independent of the constant term $\arg \{s_i + h_0 + \delta_0\}$; and (d) follows from [41, Eq. (2.516.2)] and $\Gamma(q + 1/2) = 2^{-q} \sqrt{\pi} (2q - 1)!!$. The proof follows by computing the expectation with respect to s_i .

Proof of Lemma 2.2. Let $\mathcal{Z}_{0,i}$ in (2.9). By definition, the following identity holds

$$\begin{aligned} \mathcal{Z}_{0,i}^{(\text{re})} &= \sum_{r=1}^{N_r} \sum_{t=1}^{N_t} \sum_{\tau=1}^{N_s} \left| \mathbf{H}_i^{(r,t)} \right| \left| \mathbf{s}_i^{(t)}(\tau) \right| \left| \mathbf{U}_0^{(r)}(\tau) \right| \\ &\quad \times \cos \left(\arg \left\{ \mathbf{H}_i^{(r,t)} \right\} + \arg \left\{ \mathbf{s}_i^{(t)}(\tau) \right\} + \arg \left\{ \mathbf{U}_0^{(r)}(\tau) \right\} \right) \\ &\stackrel{(a)}{\sim} \mathcal{N}_{|\mathbf{U}_0(\boldsymbol{\tau}), \mathbf{s}_i(\boldsymbol{\tau})} \left(0, \frac{\Omega}{2} \sum_{r=1}^{N_r} \sum_{t=1}^{N_t} \left| \sum_{\tau=1}^{N_s} \mathbf{s}_i^{(t)}(\tau) \mathbf{U}_0^{(r)}(\tau) \right|^2 \right) \end{aligned} \quad (2.42)$$

where (a) is by $\left| \mathbf{H}_i^{(r,t)} \right| \cos \left(\arg \left\{ \mathbf{H}_i^{(r,t)} \right\} + \arg \left\{ \mathbf{s}_i^{(t)}(\tau) \right\} + \arg \left\{ \mathbf{U}_0^{(r)}(\tau) \right\} \right) \sim \mathcal{N}(0, \Omega/2)$ and that $\mathbf{H}_i^{(r,t)}$ are i.i.d. RVs with zero mean. From (2.42), the raw moments with respect to \mathbf{H}_i are computed with the aid of [42, Eq. (13)]. The proof follows by computing the expectation with respect to $\mathbf{s}_i(\boldsymbol{\tau})$.

Proof of Lemma 2.3. By direct inspection of (2.7) and (2.29), it follows that $\Lambda_m(\cdot)$ is the decision metric of a single-stream demodulator in zero-mean AWGN, by conditioning upon $r_0, \{\mathbf{B}_q\}_{q=1}^{+\infty}, \bar{\mathcal{S}}_{\mathcal{I}}$ [4, Ch. 7]. By conditioning upon $r_0, \{\mathbf{B}_q\}_{q=1}^{+\infty}, \bar{\mathcal{S}}_{\mathcal{I}}$, in fact, the first addend of (2.7) is a constant and the last two addends of (2.7) are Gaussian RVs with zero mean. Accordingly, from [20, Sec. IV-B, Table III], the ASEP can be formulated as follows:

$$\begin{aligned} \text{ASEP}_m &= \mathbb{E}_{r_0, \{\mathbf{B}_q\}_{q=1}^{+\infty}, \bar{\mathcal{S}}_{\mathcal{I}}} \left\{ \frac{\delta_1}{\pi} \int_0^{\alpha_1} \exp \left\{ -\frac{\beta_1 \sin^2(\gamma_1)}{2 \sin^2(\omega)} \Upsilon_m \right\} d\omega \right. \\ &\quad \left. - \frac{\delta_2}{\pi} \int_0^{\alpha_2} \exp \left\{ -\frac{\beta_2 \sin^2(\gamma_2)}{2 \sin^2(\omega)} \Upsilon_m \right\} d\omega \right\} \end{aligned} \quad (2.43)$$

where $\Upsilon_m = \Upsilon_m \left(r_0, \{\mathbf{B}_q\}_{q=1}^{+\infty}, \bar{\mathcal{S}}_{\mathcal{I}} \right)$ is the conditional SINR, which, from (2.7), is defined as $\Upsilon_m \left(r_0, \{\mathbf{B}_q\}_{q=1}^{+\infty}, \bar{\mathcal{S}}_{\mathcal{I}} \right) = \mathbb{E}_{\boldsymbol{\Delta}_0(\boldsymbol{\tau})} \left\{ \Upsilon_m \left(r_0, \{\mathbf{B}_q\}_{q=1}^{+\infty}, \bar{\mathcal{S}}_{\mathcal{I}}, \boldsymbol{\Delta}_0(\boldsymbol{\tau}) \right) \right\}$, which can be

calculated by

$$\begin{aligned}
& \Upsilon_m \left(r_0, \{\mathbf{B}_q\}_{q=1}^{+\infty}, \bar{\mathcal{S}}_{\mathcal{I}}, \mathbf{\Delta}_0(\boldsymbol{\tau}) \right) \\
& \stackrel{(a)}{=} \frac{\left(\frac{E}{N_t}\right)^2 r_0^{-4b} \mathcal{D}_{1,m}^2(\bar{\mathcal{S}}_{\mathcal{I}}, \mathbf{\Delta}_0(\boldsymbol{\tau}))}{4 \left(\frac{E}{N_t}\right) r_0^{-2b} \left(\frac{\sigma_N^2}{2}\right) + 4 \left(\frac{E}{N_t}\right) r_0^{-2b} \left(\frac{\sigma_I^2}{2}\right)} \\
& \stackrel{(b)}{=} \frac{\left(\frac{E}{N_t}\right) r_0^{-2b} \bar{\mathcal{D}}_0(\bar{\mathcal{S}}_{\mathcal{I}}) \tilde{\mathcal{D}}_{0,m}(\mathbf{\Delta}_0(\boldsymbol{\tau}))}{2\mathcal{N}_0 + 2 \left(\frac{E}{N_t}\right) \sum_{q=1}^{+\infty} \left(r_0^{(-2b+2/q)} (p\lambda\pi)^{1/q} \mathbf{B}_q \bar{\sigma}_{\mathbf{G}_q}^2 \right)}
\end{aligned} \tag{2.44}$$

where (a) follows from (2.7) and shorthands $\sigma_N^2 = \mathbb{E}_{\mathbf{n}(\boldsymbol{\tau})} \left\{ \left| \mathcal{D}_{2,m}(\bar{\mathcal{S}}_{\mathcal{I}}, \mathbf{\Delta}_0(\boldsymbol{\tau}), \mathbf{n}(\boldsymbol{\tau})) \right|^2 \right\}$ and $\sigma_I^2 = \mathbb{E}_{\{\mathbf{G}_q\}_{q=1}^{+\infty}} \left\{ \left| \mathcal{D}_{3,m}^{(\text{GCG})}(\bar{\mathcal{S}}_{\mathcal{I}}, \mathbf{\Delta}_0(\boldsymbol{\tau}), \mathbf{i}_{\text{agg}}(\boldsymbol{\tau}; r_0)) \right|^2 \right\}$ and (b) follows from the equalities in (2.6) and (2.15), *i.e.*, $\sigma_N^2 = [\mathcal{D}_{1,m}^2(\bar{\mathcal{S}}_{\mathcal{I}}, \mathbf{\Delta}_0(\boldsymbol{\tau})) / \mathcal{D}_{0,m}(\bar{\mathcal{S}}_{\mathcal{I}}, \mathbf{\Delta}_0(\boldsymbol{\tau}))] \mathcal{N}_0$ for noise-related term and interference-related $\sigma_I^2 = \left[(E/N_t) \sum_{q=1}^{+\infty} \left(r_0^{(-2b+2/q)} (p\lambda\pi)^{1/q} \mathbf{B}_q \bar{\sigma}_{\mathbf{G}_q}^2 \right) \right] \times [\mathcal{D}_{1,m}^2(\bar{\mathcal{S}}_{\mathcal{I}}, \mathbf{\Delta}_0(\boldsymbol{\tau})) / \mathcal{D}_{0,m}(\bar{\mathcal{S}}_{\mathcal{I}}, \mathbf{\Delta}_0(\boldsymbol{\tau}))]$.

Since $\mathbb{E}_{\mathbf{\Delta}_0(\boldsymbol{\tau})} \left\{ \tilde{\mathcal{D}}_{0,m}(\mathbf{\Delta}_0(\boldsymbol{\tau})) \right\} = 2$, the conditional SINR Υ_m simplifies to:

$$\begin{aligned}
\Upsilon_m &= \Upsilon_m \left(r_0, \{\mathbf{B}_q\}_{q=1}^{+\infty}, \bar{\mathcal{S}}_{\mathcal{I}} \right) \\
&= \frac{E}{N_t} r_0^{-2b} \bar{\mathcal{D}}_0(\bar{\mathcal{S}}_{\mathcal{I}}) \left[\mathcal{N}_0 + \frac{E}{N_t} \sum_{q=1}^{+\infty} \left(r_0^{(-2b+2/q)} (p\lambda\pi)^{1/q} \mathbf{B}_q \bar{\sigma}_{\mathbf{G}_q}^2 \right) \right]^{-1}
\end{aligned} \tag{2.45}$$

The proof follows by applying the MGF-based approach [4] to the computation of $\mathbb{E}_{\bar{\mathcal{D}}_0(\bar{\mathcal{S}}_{\mathcal{I}})} \{ \cdot \}$.

Proof of Lemma 2.4. Let us start from the identity $\mathcal{D}_1^2(\bar{\mathcal{S}}_{\mathcal{I}}, \mathbf{\Delta}_0(\boldsymbol{\tau})) / \mathcal{D}_0(\bar{\mathcal{S}}_{\mathcal{I}}, \mathbf{\Delta}_0(\boldsymbol{\tau})) = |h_0|^2 |\Delta_0|^2$. Then the following equalities hold,

$$\begin{aligned}
\mathcal{Q}(X) &= \sum_{q=1}^{+\infty} \left(X \bar{\sigma}_{\mathbf{G}_q}^2 \right)^q \\
&= \sum_{q=0}^{+\infty} \left(X \bar{\sigma}_{\mathbf{G}_q}^2 \right)^q - 1 \\
&\stackrel{(a)}{=} \sum_{q=0}^{+\infty} \frac{(-1/b)_q}{(1/2)_q (1-1/b)_q} \frac{(-1)^q \Gamma(m+q)}{q!} \frac{\Gamma(q+1/2)}{\Gamma(m)} \frac{\Gamma(q+1/2)}{\Gamma(q+1) \sqrt{\pi}} \left(\frac{\Omega}{m} X \right)^q \mathbb{E}_{s_i} \left\{ |s_i|^{2q} \right\} - 1 \\
&\stackrel{(b)}{=} \mathbb{E}_{s_i} \left\{ \sum_{q=0}^{+\infty} \frac{(-1/b)_q}{(1/2)_q (1-1/b)_q} \frac{(-1)^q \Gamma(m+q)}{q!} \frac{\Gamma(q+1/2)}{\Gamma(m)} \frac{\Gamma(q+1/2)}{\Gamma(q+1) \sqrt{\pi}} \left(|s_i|^2 \frac{\Omega}{m} X \right)^q \right\} - 1
\end{aligned} \tag{2.46}$$

where (a) follows from (2.13) and (b) originates from the linearity property of the expectation operator. Equation (2.25) is obtained from the series representation of the generalized hypergeometric function [2, Ch. 5, Eq. (2)] and from the equality $\frac{\Gamma(m+q)\Gamma(q+1/2)}{(1/2)_q\Gamma(m)\Gamma(q+1)\sqrt{\pi}} = \frac{(m)_q}{(1)_q}$ for every q .

Proof of Lemma 2.5. We know that the relation $\mathcal{D}_1^2(\bar{\mathcal{S}}_L, \mathbf{\Delta}_0(\boldsymbol{\tau}))/\mathcal{D}_0(\bar{\mathcal{S}}_L, \mathbf{\Delta}_0(\boldsymbol{\tau})) = \sum_{r=1}^{N_r} \sum_{\tau=1}^{N_s} \left| \mathbf{U}_0^{(r)}(\boldsymbol{\tau}) \right|^2$ holds. Then, the following equalities hold

$$\begin{aligned}
\mathcal{Q}(X) &= \sum_{q=1}^{+\infty} \left(X \bar{\sigma}_{\mathbb{G}_q}^2 \right)^q \\
&= \sum_{q=0}^{+\infty} \left(X \bar{\sigma}_{\mathbb{G}_q}^2 \right)^q - 1 \\
&\stackrel{(a)}{=} \sum_{q=0}^{+\infty} \frac{(-1/b)_q}{(1/2)_q} \frac{1}{(1-1/b)_q} \frac{1}{q!} \frac{\sqrt{\pi}}{\Gamma(1/2-q)} (X\Omega)^q \mathbb{E}_{\mathbf{s}_i(\boldsymbol{\tau})} \{ (\phi(\mathbf{s}_i(\boldsymbol{\tau})))^q \} - 1 \\
&\stackrel{(b)}{=} \mathbb{E}_{\mathbf{s}_i(\boldsymbol{\tau})} \left\{ \sum_{q=0}^{+\infty} \frac{(-1/b)_q}{(1/2)_q} \frac{1}{(1-1/b)_q} \frac{1}{q!} \frac{\sqrt{\pi}}{\Gamma(1/2-q)} (\phi(\mathbf{s}_i(\boldsymbol{\tau})) \Omega X)^q \right\} - 1
\end{aligned} \tag{2.47}$$

where (a) follows from (2.13) and (b) originates from the linearity property of the expectation operator. Equation (2.27) is obtained from the series representation of the generalized hypergeometric function [2, Ch. 5, Eq. (2)] and from the equality $\sqrt{\pi} \left[(1/2)_q \Gamma(1/2-q) \right]^{-1} = (-1)^q$ for every q .

2.C Proofs of Theorems and Corollaries

Proof of Theorem 2.1. Let the MGF of the SINR be defined as $\mathcal{M}_{\text{SINR}}(s; r_0, \{\mathbb{B}_q\}_{q=1}^{+\infty}) = \mathcal{M}_{\bar{\mathcal{D}}_0}(s_{\text{SINR}}(r_0, \{\mathbb{B}_q\}_{q=1}^{+\infty}))$, where the $\text{SINR}(r_0, \{\mathbb{B}_q\}_{q=1}^{+\infty})$ is given in (2.19). Then,

the following equalities hold,

$$\begin{aligned}
& \mathcal{M}_{\text{SINR}} \left(s; r_0, \{\mathbf{B}_q\}_{q=1}^{+\infty} \right) \\
&= \left(1 + s \frac{(E/N_t) \Omega_0 r_0^{-2b}}{\mathcal{N}_0 + (E/N_t) \sum_{q=1}^{+\infty} \left(r_0^{(-2b+2/q)} (p\lambda\pi)^{1/q} \mathbf{B}_q \bar{\sigma}_{\mathbf{G}_q}^2 \right)} \right)^{-m_0} \\
&\stackrel{(a)}{=} \frac{1}{\Gamma(m_0)} \int_0^{+\infty} x^{m_0-1} \exp\{-x\} \\
&\quad \times \exp \left\{ - \frac{\left(\frac{E}{N_t} \right) \Omega_0 s}{\mathcal{N}_0 r_0^{2b} + \left(\frac{E}{N_t} \right) \sum_{q=1}^{+\infty} \left(r_0^{2/q} (p\lambda\pi)^{1/q} \mathbf{B}_q \bar{\sigma}_{\mathbf{G}_q}^2 \right)} x \right\} dx \\
&\stackrel{(b)}{=} 1 - \frac{1}{\Gamma(m_0)} \int_0^{+\infty} x^{m_0-1} \exp\{-x\} \\
&\quad \times \left[\sqrt{\frac{E\Omega_0}{N_t}} s x \int_0^{+\infty} y^{-1/2} J_1 \left(2\sqrt{\frac{E\Omega_0}{N_t}} sxy \right) \exp \left\{ -y \mathcal{A} \left(r_0, \{\mathbf{B}_q\}_{q=1}^{+\infty} \right) \right\} dy \right] dx \\
&\stackrel{(c)}{=} 1 - m_0 \frac{E\Omega_0}{N_t} s \int_0^{+\infty} {}_1F_1 \left(m_0 + 1; 2; -\frac{E\Omega_0}{N_t} sy \right) \\
&\quad \times \exp \left\{ -y \left(\mathcal{N}_0 r_0^{2b} + \frac{E}{N_t} \sum_{q=1}^{+\infty} \left(r_0^{2/q} (p\lambda\pi)^{1/q} \mathbf{B}_q \bar{\sigma}_{\mathbf{G}_q}^2 \right) \right) \right\} dy
\end{aligned} \tag{2.48}$$

where: (a) follows from (2.35), (b) follows from (2.36), $\int_0^{+\infty} x^{m_0-1} \exp\{-x\} dx = \Gamma(m_0)$ and by using the shorthand $\mathcal{A} \left(r_0, \{\mathbf{B}_q\}_{q=1}^{+\infty} \right) = \mathcal{N}_0 r_0^{2b} + (E/N_t) \sum_{q=1}^{+\infty} \left(r_0^{2/q} (p\lambda\pi)^{1/q} \mathbf{B}_q \bar{\sigma}_{\mathbf{G}_q}^2 \right)$, and (c) follows from (2.37).

The next step is the computation of the expectation with respect to the RVs $\{\mathbf{B}_q\}_{q=1}^{+\infty}$, *i.e.*, $\mathcal{M}_{\text{SINR}}(s; r_0) = \mathbb{E}_{\{\mathbf{B}_q\}_{q=1}^{+\infty}} \left\{ \mathcal{M}_{\text{SINR}} \left(s; r_0, \{\mathbf{B}_q\}_{q=1}^{+\infty} \right) \right\}$. From (2.48), the following equalities hold:

$$\begin{aligned}
\mathcal{M}_{\text{SINR}} \left(s; \sigma_{\text{IAI}}^2, r_0 \right) &= 1 - m_0 \frac{E\Omega_0}{N_t} s \\
&\quad \times \int_0^{+\infty} {}_1F_1 \left(m_0 + 1; 2; -\frac{E\Omega_0}{N_t} sy \right) \exp \left\{ -y \mathcal{N}_0 r_0^{2b} \right\} \mathcal{S}(y; r_0) dy
\end{aligned} \tag{2.49}$$

$$\begin{aligned}
\mathcal{S}(y; r_0) &= \mathbb{E}_{\{\mathbf{B}_q\}_{q=1}^{+\infty}} \left\{ \exp \left\{ -y \frac{E}{N_t} \sum_{q=1}^{+\infty} \left(r_0^{2/q} (p\lambda\pi)^{1/q} \mathbf{B}_q \bar{\sigma}_{\mathbf{G}_q}^2 \right) \right\} \right\} \\
&\stackrel{(a)}{=} \prod_{q=1}^{+\infty} \mathbb{E}_{\mathbf{B}_q} \left\{ \exp \left\{ -y \frac{E}{N_t} r_0^{2/q} (p\lambda\pi)^{1/q} \mathbf{B}_q \bar{\sigma}_{\mathbf{G}_q}^2 \right\} \right\} \\
&\stackrel{(b)}{=} \prod_{q=1}^{+\infty} \exp \left\{ - \left(y \frac{E}{N_t} r_0^{2/q} (p\lambda\pi)^{1/q} \bar{\sigma}_{\mathbf{G}_q}^2 \right)^q \right\} \\
&= \exp \left\{ -p\lambda\pi r_0^2 \sum_{q=1}^{+\infty} \left(y \frac{E}{N_t} \bar{\sigma}_{\mathbf{G}_q}^2 \right)^q \right\} \\
&= \exp \left\{ -p\lambda\pi r_0^2 \mathcal{Q} \left(y \frac{E}{N_t} \right) \right\}
\end{aligned} \tag{2.50}$$

where: (a) holds because the RVs $\{\mathbf{B}_q\}_{q=0}^{+\infty}$ are independent for every q and (b) follows from $\mathcal{M}_{\mathbf{B}_q}(s) = \exp\{-s^q\}$. Also, $\mathcal{Q}(\cdot)$ is defined in (2.20). The final step is the computation of the expectation with respect to the RV r_0 , *i.e.*, $\mathcal{M}_{\text{SINR}}(s) = \mathbb{E}_{r_0} \{\mathcal{M}_{\text{SINR}}(s; r_0)\} = \int_0^{+\infty} \mathcal{M}_{\text{SINR}}(s; \xi) f_{r_0}(\xi) d\xi$. With the aid of some changes of variables, the final expression can be formulated as shown in (2.20). This concludes the proof.

Proof of Corollary 2.1. The proof follows from (2.20) by letting $\mathcal{N}_0 = 0$ and by computing the integral with respect to the variable x with the aid of the notable integral $\int_0^{+\infty} \exp\{-\mathcal{K}x\} dx = 1/\mathcal{K}$ for $\mathcal{K} > 0$.

Proof of Theorem 2.2. With the aid of (2.20), $\mathcal{I}(\cdot, \cdot, \cdot)$ in (2.22) can be re-written as follows,

$$\begin{aligned}
&\mathcal{I}(\alpha, \beta, \gamma) \\
&= \frac{1}{\pi} \int_0^\alpha \mathcal{M}_{\text{SINR}} \left(\frac{\beta \sin^2(\gamma)}{2 \sin^2(\omega)} \right) d\omega \\
&\stackrel{(a)}{=} \frac{\alpha}{\pi} - m_0 \lambda \int_0^{+\infty} \int_0^{+\infty} \exp \left\{ - \left(\frac{E}{\mathcal{N}_0 N_t} \right)^{-1} \frac{z}{\kappa \Omega_0} x^b \right\} \exp \left\{ -\pi \lambda \tilde{\mathcal{Q}} \left(\frac{z}{\kappa \Omega_0} \right) x \right\} \\
&\quad \times \left(\frac{z}{\kappa \Omega_0} \right) \left[\int_0^\alpha \frac{1}{\sin^2(\omega)} {}_1F_1 \left(m_0 + 1; 2; -\frac{z}{\sin^2(\omega)} \right) d\omega \right] dx dz
\end{aligned} \tag{2.51}$$

where (a) follows from the change of variable $(E/N_t) \kappa \Omega_0 y = z$ and by exchanging the order of integration. The proof follows by computing the integral in the square brackets with the aid of (2.38).

Proof of Corollary 2.2. The proof follows from (2.23) by letting $\mathcal{N}_0 = 0$ and by computing the integral with respect to the variable x with the aid of the notable integral $\int_0^{+\infty} \exp\{-\mathcal{K}x\} dx = 1/\mathcal{K}$ for $\mathcal{K} > 0$.

2.D Proof of Proposition 2.3

From (2.33), we have the equalities below

$$\begin{aligned}
\text{ASEP}_{\text{PSK}} &\stackrel{(a)}{\approx} \frac{\alpha}{\pi} - \frac{m_0}{\pi} \int_0^{+\infty} \frac{\mathcal{T}(z; m_0, \alpha)}{1 + \bar{k}z} dz \\
&\stackrel{(b)}{=} \frac{\alpha}{\pi} - \frac{m_0}{\pi} \int_0^\alpha \left(\int_0^{+\infty} \frac{{}_1F_1(m_0 + 1; 2; -y)}{1 + \bar{k} \sin^2(\omega) y} dy \right) d\omega \\
&\stackrel{(c)}{=} \frac{\alpha}{\pi} - \frac{1}{\pi\Gamma(m_0)} \int_0^\alpha G_{3,2}^{2,2} \left(\bar{k} \sin^2(\omega) \left| \begin{array}{c} 0 \ 0 \ 1 \\ 0 \ m_0 \end{array} \right. \right) d\omega \\
&\stackrel{(d)}{\approx} \frac{\kappa_0}{2} - \frac{\kappa_0}{\pi\Gamma(m_0)} \int_0^{\pi/2} G_{3,2}^{2,2} \left(\bar{k} \sin^2(\omega) \left| \begin{array}{c} 0 \ 0 \ 1 \\ 0 \ m_0 \end{array} \right. \right) d\omega \\
&\stackrel{(e)}{=} \frac{\kappa_0}{2} - \frac{\kappa_0}{2\pi\Gamma(m_0)} \int_0^1 x^{-1/2} (1-x)^{-1/2} G_{3,2}^{2,2} \left(\bar{k}x \left| \begin{array}{c} 0 \ 0 \ 1 \\ 0 \ m_0 \end{array} \right. \right) d\omega \\
&\stackrel{(f)}{=} \frac{\kappa_0}{2} - \frac{\kappa_0}{2\sqrt{\pi}\Gamma(m_0)} G_{4,3}^{2,3} \left(\bar{k} \left| \begin{array}{c} 1/2 \ 0 \ 0 \ 1 \\ 0 \ m_0 \ 0 \end{array} \right. \right)
\end{aligned} \tag{2.52}$$

where: (a) follows by using the series representation of the generalized hypergeometric function [2, Chapter 5, Eq. (2)], *i.e.*, ${}_1F_1(-1/b; 1-1/b; -(\kappa_{\text{MIMO}}/\kappa_{\text{MOD}})z) \approx 1 + (b-1)^{-1}(\kappa_{\text{MIMO}}/\kappa_{\text{MOD}})z$ and by introducing $\bar{k} = (b-1)^{-1}p(\kappa_{\text{MIMO}}/\kappa_{\text{MOD}})$; (b) follows from (2.38) and some changes of variable; (c) follows by using the Mellin-Barnes integration theorem [3, Eq. (2.24.1.1)]; (d) follows from $\alpha = \pi - \pi/M = \pi/2$ for $M = 2$, from the approximation $\alpha = \pi - \pi/M \approx \pi$ for $M \geq 4$ and from the symmetry of $\sin^2(\cdot)$. In particular, $\kappa_0 = 1$ if $M = 2$ and $\kappa_0 = 2$ if $M \geq 4$; (e) follows from the change of variable $x = \sin^2(\omega)$; (f) follows from [41, Eq. (7.811.2)]. The proof follows by inserting the specific parameters of PSK modulation in (2.52).

Chapter 3

Stochastic Geometry Analysis of Relay-aided Cellular Networks

3.1 Introduction

The deployment of Relay Nodes (RNs), as network infrastructure elements without a dedicated wired backhaul connection, has been considered by the IEEE 802.16j working group [43] and by the Third Generation Partnership Project's Long Term Evolution Advanced (3GPP LTE-A) [44] for enhancing, in a cost-effective manner, coverage and rate of cellular networks. Currently, practical cellular networks employ half-duplex RNs, *i.e.*, the RNs can either receive or transmit data but not at the same time and on the same frequency, for forwarding data packets from the Base Stations (BSs) to the Mobile Terminals (MTs). Several protocols have been proposed in the literature for relay-aided cellular networks, which include Amplify-and-Forward (AF), Decode-and-Forward (DF) and Demodulate-and-Forward (DemF) relaying [45].

The available literature on the mathematical performance evaluation of relay-aided wireless networks is vast, and it encompasses noise-limited [46–49] and interference-limited [50–57] operating scenarios. Further information is available in [13, 14]. Even though the available frameworks provide relevant insight on the performance of relay-aided wireless networks, they are not directly applicable to cellular networks. They, in fact, are applicable either to network deployments where the locations of BSs and RNs are fixed and known a priori (see, *e.g.*, [50–52]) or to ad hoc networks, where the interferers are

randomly located in the whole plane and, thus, the notion of cell is not explicitly taken into account (see, *e.g.*, [13, 14, 54, 58]). Furthermore, the interference generated by the RNs is not considered in the system model, which, on the other hand, is one of the main challenges faced by deploying RNs in cellular networks [44].

In this chapter, we develop a tractable approach to the mathematical performance evaluation and optimization of relay-aided cellular networks, which explicitly accounts for the centralized nature of cellular networks as opposed to their ad hoc counterpart. The motivation and the significance of our work lie in understanding and quantifying the impact of the presence of the RNs in cellular networks. Since the operating principle of cellular networks is different from ad hoc networks, the conclusions and the insights from [14, 50–56] cannot be guaranteed to hold, *a priori*, for relay-aided cellular networks. Notably, a fundamental challenge of relay-aided cellular networks, compared with ad hoc and cellular networks, lies in the cell association criterion, which consists of selecting a pair of serving BS and RN. As a result, new mathematical frameworks to shed light on and to quantify the benefits of deploying the RNs in the presence of other-cell interference and using practical cell association criteria to choose the pair of serving BS and RN are needed. To the best of the authors' knowledge, no mathematical approach of this kind is available in the literature.

To this end, we capitalize on the so-called stochastic geometry abstraction modeling of cellular networks [24], which, since its first inception in [10], has been routinely used for system-level performance evaluation and optimization due to its mathematical tractability and accuracy [59, 60]. This approach has been successfully applied to the modeling and analysis of downlink cellular networks [10, 15], multi-antenna cellular networks [26, 27, 61], heterogeneous cellular networks [21–23, 62], uplink cellular networks [63, 64] and millimeter-wave cellular networks [65, 66], just to cite some relevant examples. Recent developments in this field of research are available in [61]. To the best of the authors' knowledge, stochastic geometry modeling has never been applied to the analysis of relay-aided cellular networks.

In the present chapter, we exploit stochastic geometry for modeling relay-aided downlink cellular networks, as well as we introduce a tractable mathematical framework for computing coverage, rate and for studying the role of the RNs in cellular networks. More specifically, the locations of BSs, RNs and MTs are modeled as points of three

TABLE 3.1: Recurrent parameters and symbols.

Symbol	Meaning
Φ_X	PPP of network elements $X = \{\text{BS}, \text{RN}, \text{MT}\}$
$\Phi_X^{(I)}$	PPP of interfering network elements $X = \{\text{BS}, \text{RN}\}$
λ_X	density of network elements $X = \{\text{BS}, \text{RN}, \text{MT}\}$
N_{RB}	number of resource blocks
$\text{BS}_0, \text{BS}_{\text{R0}}$	serving BSs of one- and two-hop transmission
RN_0	serving RN for two-hop transmission
MT_0	probe MT
$\beta_{X,Y}$	path-loss exponent of the X-to-Y link
$S_{X,Y}$	shadowing of the X-to-Y link
$h_{X,Y}$	fast-fading of the X-to-Y link
P_T	total transmit power
P_X	transmit power of network element X
K_T	power splitting ratio
$\mathcal{B}_{\text{BS}}, \mathcal{B}_{\text{RN}}$	bias coefficients
$\chi_{1\text{hop}}, \chi_{2\text{hop}}$	one-, two-hop transmission probabilities
σ_N^2	thermal noise power
B_W	transmission bandwidth per resource block
$\eta_{\text{cell}} = (\mathcal{B}_{\text{BS}} P_T) / (\mathcal{B}_{\text{RN}} (1 - K_T) P_T)$	it is a shorthand notation

independent and homogeneous Poisson Point Processes (PPPs). A flexible cell association and relay-aided transmission protocol based on the best biased average received power are considered. It is shown that coverage and rate highly depend on the path-loss exponents of one- and two-hop links, as well as that, if the system is not well designed, the presence of RNs may provide negligible performance gains. By capitalizing on the proposed analytical framework, a system-level and interference-aware optimization criterion of the bias coefficients for cell association is proposed, which is shown to enhance the end-to-end coverage probability in the interference-limited regime. In addition, it guarantees that, regardless of the system setup, relay-aided cellular networks are never worse than cellular networks (without using the RNs).

This chapter is organized as follows. In Section 3.2, the system model is introduced. In Section 3.3, the problem is formulated in mathematical terms. In Section 3.4, the frameworks for computing coverage and rate are provided, and relevant insights are discussed. In Section 3.5, the mathematical analysis is validated via Monte Carlo simulations and numerical results are presented. Finally, Section 3.6 concludes this chapter.

Recurrent parameters and symbols are summarized in Table 3.1.

3.2 System Model

3.2.1 Network Deployment Modeling

A downlink relay-aided cellular network is considered. BSs, RNs and MTs are modeled as points of three independent and homogeneous PPPs, which are denoted by Φ_{BS} , Φ_{RN} and Φ_{MT} of density λ_{BS} , λ_{RN} and λ_{MT} , respectively. In addition, BSs, RNs and MTs are assumed to be equipped with a single antenna for both transmission and reception. The analysis of multi-antenna transmitters and receivers is postponed to future research. Both BSs and RNs are assumed to have N_{RB} Resource Blocks (RBs), *e.g.*, carrier frequencies/wavelengths, available for serving the MTs. In general, every BS provides service to multiple MTs. For each tagged MT, every BS picks at random and with probability $1/N_{\text{RB}}$ the RB where to transmit. The RNs transmit on the same RB as the BS they are paired to, according to the association criterion and relaying protocol described in Section 3.2.3. Further details on the load model and N_{RB} are provided in Section 3.2.4. Each RB is split in two time-slots. In the first time-slot, only the BSs are allowed to transmit. In the second time-slot, only the RNs are allowed to transmit. Further information on the relaying protocol is provided in Section 3.2.3. Without loss of generality and in agreement with the Slivnyak theorem [7, vol. 1, Th. 1.4.5], the performance of a typical MT located at the origin of the bi-dimensional plane is studied. This typical MT is denoted by MT_0 . It can be served either via a one- or a two-hop link with the aid of a RN. In the first case, the BS serving MT_0 is denoted by BS_0 . In the second case, the RN serving MT_0 is denoted by RN_0 and the BS serving RN_0 is denoted by $\text{BS}_{\text{R}0}$. In the first time-slot, as a result, interference is generated by all active BSs with the exception of the serving BS, *i.e.*, BS_0 or $\text{BS}_{\text{R}0}$. In the second time-slot, on the other hand, interference is generated by all active RNs with the exception of the serving RN, *i.e.*, RN_0 . Further information on BS association and relaying protocol are provided in Section 3.2.3. Since we are interested in analyzing the performance of a typical MT, MT_0 , the analysis is conducted for an arbitrary RB, where MT_0 receives its intended signal. The sets of interfering BSs and RNs in the RB of interest are denoted by $\Phi_{\text{BS}}^{(I)}$ and $\Phi_{\text{RN}}^{(I)}$, respectively. They are further detailed in Section 3.2.4.

Remark 3.1. Assuming that the RNs are distributed according to a PPP is particularly suitable in the context of the present chapter for two main reasons. The RNs may be idle MTs that are willing to assist the transmission of other active MTs. In this case, the PPP

modeling assumption may be deemed to be appropriate. In other cases, on the other hand, the RNs may be deployed by the network operators and, thus, their locations may not be totally random. In our case study, however, we adopt a PPP-based abstraction model for the locations of the BSs. In this context, a non-random deployment of the RNs may be in contrast with it and may not be convenient for mathematical analysis. Assuming the RNs to be distributed according to a PPP is, on the other hand, an integral part of the PPP-based modeling of cellular networks [67]. In some scenarios, the locations of BSs and RNs may exhibit some level of correlation. This correlation may be modeled by using point processes that are not PPP. These scenarios are, however, beyond the scope of the present report and they are postponed to a future research contribution. It is worth emphasizing, finally, that several other papers available in the literature have used a PPP for modeling the RNs, *e.g.*, [68] and references therein. \square

3.2.2 Channel Modeling

The channel model takes into account path-loss, shadowing and fast-fading, which are described as follows. Throughout the present chapter, the propagation channels related to network elements of the same type are assumed to be independent and identically distributed (i.i.d.). If a generic BS-to-RN link is considered, *e.g.*, from the BS $BS_i \in \Phi_{BS}$ to the RN $RN_k \in \Phi_{RN}$, the channel parameters are identified by using the subscript “BS,RN”. A similar notation holds for the channel parameters related to other network elements.

A. Path-Loss

Let r_{X_i, Y_k} be the distance between two generic network elements X_i and Y_k . Based on the downlink network model of Section 3.2.1, we have $X_i \in \{BS_i, RN_i\}$ and $Y_k \in \{RN_k, MT_k\}$, where BS_i , RN_i and MT_i denote the generic BS, RN and MT of Φ_{BS} , Φ_{RN} and Φ_{MT} , respectively. The path-loss, $l(\cdot)$, of this generic link is defined as $l(r_{X_i, Y_k}) = \kappa_0 r_{X_i, Y_k}^{\beta_{X, Y}}$, where κ_0 denotes the free-space path-loss at a distance of one meter and $\beta_{X, Y} > 2$ denotes the power path-loss exponent. In particular, $\kappa_0 = (4\pi/\nu)^2$, where ν is the transmission wavelength. The considered path-loss is usually known as the “close-in” model [69].

B. Shadowing

In addition to the distance-dependent path-loss, the generic (X_i, Y_k) link is subject to mid-scale fading that is denoted by S_{X_i, Y_k} . S_{X_i, Y_k} is assumed to follow a log-normal distribution [70], whose PDF is $f_{S_{X_i, Y_k}}(\xi) = \frac{10 \log_{10}(e)}{\sqrt{2\pi\sigma_{X,Y}^2} \xi} \exp\left(-\frac{(10 \log_{10}(\xi) - \mu_{X,Y})^2}{(2\sigma_{X,Y}^2)}\right)$ [4], where $\mu_{X,Y}$ and $\sigma_{X,Y}^2$ denote the mean and the variance of the random variable $10 \log_{10}(S_{X_i, Y_k})$. Spatial correlation of shadowing is not considered in this report. It may, however, be taken into account as in [71].

C. Fast-Fading

Besides path-loss and shadowing, the generic (X_i, Y_k) link is subject to a random complex channel gain, which is denoted by h_{X_i, Y_k} . The power gain $|h_{X_i, Y_k}|^2$ is assumed to follow an exponential distribution (*i.e.*, Rayleigh fading is considered) having mean square value equal to $\Omega_{X,Y}$. The probability density function of $|h_{X_i, Y_k}|^2$ is $f_{|h_{X_i, Y_k}|^2}(\xi) = (1/\Omega_{X,Y}) \exp(-\xi/\Omega_{X,Y})$ [4].

3.2.3 Cell Association and Relaying Protocol

The typical MT, MT_0 , can be served either via a one- or a two-hop link. In the first case, MT_0 is served by BS_0 and a single time-slot is used. In the second case, MT_0 is served by RN_0 , which, in turn, is served by BS_{R0} . In this latter case, two subsequent time-slots are used. Thus, a half-duplex relaying cellular network is assumed. The extension to full-duplex scheme is not that straightforward and has been postponed to future research. More details are discussed in Section 3.5. A DF relaying protocol is considered [45]. As a consequence, a typical downlink transmission may occur either in one or in two time-slots. All transmissions in the same RB occur at the same transmission wavelength ν . Let P_T be the total transmit power budget for serving MT_0 . Let P_{BS_0} , P_{RN_0} and $P_{BS_{R0}}$ denote the transmit powers of BS_0 , RN_0 and BS_{R0} . In order to ensure the so-called total power constraint [45], they are defined as $P_{BS_0} = P_T$, $P_{RN_0} = (1 - K_T) P_T$ and $P_{BS_{R0}} = K_T P_T$, where $0 < K_T < 1$ is a power splitting coefficient.

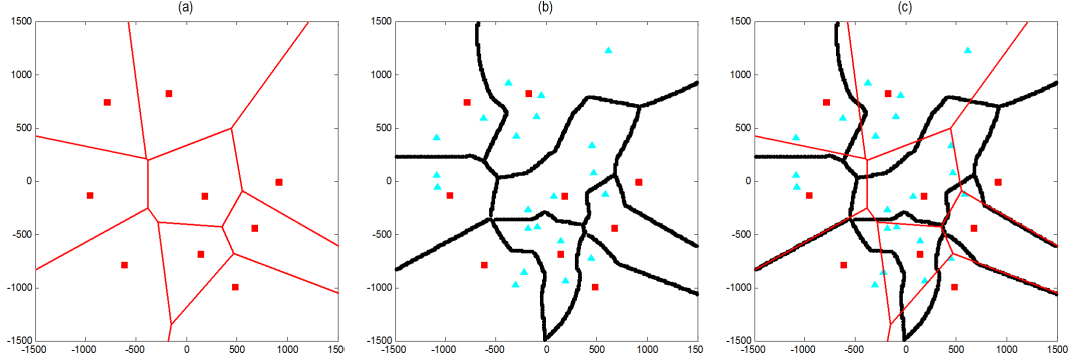


FIGURE 3.1: Coverage regions in the absence of shadowing in an area of 9 square kilometers. Squares and triangles denote BSs and RNs, respectively. (a) Without relays. (b) With relays. (c) Figures (a) and (b) are overlapped to show the difference. Setup: $P_T = 40$ dBm, $K_T = 0.5$ and $\beta_{BS,MT} = \beta_{RN,MT} = 4$.

The triplet BS_0 , RN_0 and BS_{R0} is identified by using the cell association criterion as follows:

$$\begin{aligned} BS_0 &= \arg \min_{BS_i \in \Phi_{BS}} \left\{ \frac{l(r_{BS_i, MT_0})}{P_T S_{BS_i, MT_0}} \right\}; & RN_0 &= \arg \min_{RN_k \in \Phi_{RN}} \left\{ \frac{l(r_{RN_k, MT_0})}{(1 - K_T) P_T S_{RN_k, MT_0}} \right\} \\ BS_{R0} &= \arg \min_{BS_i \in \Phi_{BS}} \left\{ \frac{l(r_{BS_i, RN_0})}{K_T P_T S_{BS_i, RN_0}} \right\} \end{aligned} \quad (3.1)$$

Remark 3.2. Eq. (3.1) ensures that MT_0 receives the highest power from the available BSs and RNs, as well as that the serving RN, RN_0 , receives the highest power from the available BSs. Also, P_T and K_T do not affect the selection of BS_0 , RN_0 and BS_{R0} in (3.1). They, in fact, are independent of the subscripts i and k . Moreover, BS_0 and BS_{R0} might be two different BSs on the plane or they may indicate the same BS which provides the highest power to MT_0 and the highest power to RN_0 among all the BSs. \square

Let the triplet of network elements BS_0 , RN_0 and BS_{R0} from (3.1). The typical MT, MT_0 , is served either via a one- or a two-hop link according to the cell association criterion as follows:

$$\begin{cases} \text{one-hop} : BS_0 \rightarrow MT_0 & \text{if } \frac{l(r_{BS_0, MT_0})}{\mathcal{B}_{BS} P_T S_{BS_0, MT_0}} \leq \frac{l(r_{RN_0, MT_0})}{\mathcal{B}_{RN} (1 - K_T) P_T S_{RN_0, MT_0}} \\ \text{two-hop} : BS_{R0} \rightarrow RN_0 \rightarrow MT_0 & \text{if } \frac{l(r_{BS_0, MT_0})}{\mathcal{B}_{BS} P_T S_{BS_0, MT_0}} > \frac{l(r_{RN_0, MT_0})}{\mathcal{B}_{RN} (1 - K_T) P_T S_{RN_0, MT_0}} \end{cases} \quad (3.2)$$

where \mathcal{B}_{BS} and \mathcal{B}_{RN} are non-negative constants, and BS_0 , RN_0 , BS_{R0} are obtained from (3.1).

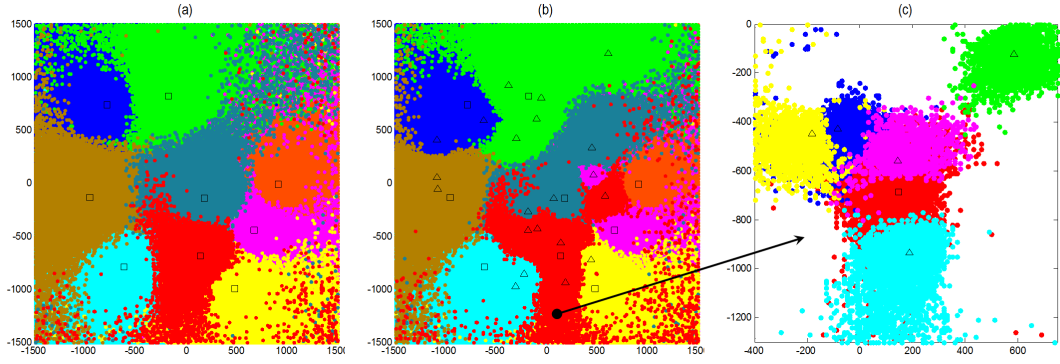


FIGURE 3.2: Coverage regions in the presence of shadowing in an area of 9 square kilometers. Squares and triangles denote BSs and RNs, respectively. Points with the same color are served by the same BS in (a) and (b), and by the same RN in (c). (a) Without relays. (b) With relays. (c) One cell of figure (b) is magnified to highlight the association area of each RN of the cell. Setup: $P_T = 40$ dBm, $K_T = 0.5$, $\beta_{BS,MT} = \beta_{RN,MT} = 4$, $\mu_{BS,MT} = \mu_{RN,MT} = 0$ dB and $\sigma_{BS,MT} = \sigma_{RN,MT} = 4$ dB.

Remark 3.3. The association/transmission criterion in (3.2) resembles the so-called biased cell association often used in multi-tier cellular networks [23], where \mathcal{B}_{BS} and \mathcal{B}_{RN} play the role of bias coefficients. In (3.2), \mathcal{B}_{BS} and \mathcal{B}_{RN} play a similar role by prioritizing either one- or two-hop transmission depending on the system parameters. In Section 3.4.3 and Section 3.5, it is shown that the best choice of \mathcal{B}_{BS} and \mathcal{B}_{RN} depends on the path-loss exponents $\beta_{X,Y}$ for $X \in \{BS, RN\}$ and $Y \in \{RN, MT_0\}$. Throughout the present chapter, without loss of generality, it is assumed that $\mathcal{B}_{RN} = 1$ and $\mathcal{B}_{BS} \geq 0$. If $\mathcal{B}_{BS} = 1$, there is no bias. \square

Remark 3.4. The rationale of introducing the concept of prioritization originates from the fact that the cell association in (3.1) and (3.2) takes only the signal powers into account, while the other-cell interference is neglected. In cellular networks in the absence of RNs, the authors of [72, Lemma 1] have proved that a cell association based only on the signal power is optimal. This is not necessarily true for relay-aided cellular networks. An example confirming this statement is provided in Section 3.4.3, which motivates the related optimization problem in (3.30). As better discussed in Section 3.4.3, in particular, the concept of prioritization can be thought as adding (long-term) interference-awareness in the cell association criterion, eventually leading to better performance. The numerical examples shown in Section 3.5 confirm that without prioritization, *i.e.*, without interference-awareness ($\mathcal{B}_{BS} = \mathcal{B}_{RN} = 1$), worse performance is obtained. \square

Remark 3.5. Thanks to the bias coefficients in (3.2), the relay-aided cellular network

under analysis subsumes the cellular network setup, *i.e.*, when the RNs are not used. By direct inspection of (3.2), in fact, it follows that all transmissions are likely to be one-hop and two-hop if $\mathcal{B}_{\text{BS}} \gg 1$ and $\mathcal{B}_{\text{BS}} \ll 1$, respectively. More specifically: i) if $\mathcal{B}_{\text{BS}} = \infty$, the system model reduces to a cellular network without using the RNs, and ii) if $\mathcal{B}_{\text{BS}} = 0$, all the MTs are served via a two-hop link. In Section 3.5, in particular, these two case studies are analyzed as well, in order to better highlight the impact of using the RNs in cellular networks. \square

Remark 3.6. Let $\mathcal{B}_{\text{BS}} = \mathcal{B}_{\text{RN}} = 1$. The cell association in (3.1), (3.2) can be interpreted as follows. Let MT_0 , the BS and RN providing the highest received power to it are identified, *i.e.*, BS_0 , RN_0 . If the power received from BS_0 is higher than that received from RN_0 , then MT_0 is served by BS_0 . Otherwise, MT_0 is served by RN_0 . In this latter case, RN_0 is served by the BS providing the highest received power to it, *i.e.*, BS_{R_0} . BS_0 and BS_{R_0} are, in general, different, ensuring that the best access point for each hop is selected. \square

The association/transmission criterion in (3.1) and (3.2) takes the presence of RNs into account. It is expected, as a consequence, that the coverage regions of the available BSs are different compared to cellular networks in the absence of RNs. An example of coverage regions computed according to (3.1) and (3.2) is illustrated in Fig. 3.1 and in Fig. 3.2, in the absence and in the presence of RNs. More specifically, Fig. 3.1 shows the conventional voronoi diagram of BSs (in the absence of relaying) in (a) and the boundary of cells consisting of one serving BS and several relay nodes in (b). The relays in each cell bounded by the black solid lines is connected to the only BS in its cell, and the MTs falling in the cell are tagged to either a relaying node or the BS in that cell. The comparison of these two cases is in (c). As for Fig. 3.1, constant shadowing has been assumed for the illustration purpose only, which is equivalent to the absence of shadowing for the cell association point of view. In Fig. 3.2, the positions of the BSs and relays are the same as those in Fig. 3.1, the shadowing for the links between each candidate serving nodes and each pixel (possible location of MT), on the other hand, is assumed to be independently distributed.

3.2.4 Load Modeling

Two operating scenarios are considered: 1) saturated traffic load and 2) light traffic load.

A. Saturated Traffic Load

In this case, the number of MTs is much larger than that of BSs and RNs. This occurs if $\lambda_{\text{MT}} \gg \lambda_{\text{BS}}$ and $\lambda_{\text{MT}} \gg \lambda_{\text{RN}}$. Also, λ_{MT} is assumed to be sufficiently high that all the BSs are active in every RB. Thus, the set of interfering BSs in the RB of interest, $\Phi_{\text{BS}}^{(I)}$, is equal to the set of all available BSs except the serving BS. If MT_0 is served via a one-hop link, the serving BS is BS_0 and $\Phi_{\text{BS}}^{(I)} = \Phi_{\text{BS}} \setminus \text{BS}_0$. If MT_0 is served via a two-hop link, the serving BS is $\text{BS}_{\text{R}0}$ and $\Phi_{\text{BS}}^{(I)} = \Phi_{\text{BS}} \setminus \text{BS}_{\text{R}0}$.

Remark 3.7. Based on the properties of PPPs [7], $\Phi_{\text{BS}}^{(I)}$ is a homogeneous PPP of density $\lambda_{\text{BS}}^{(I)} = \lambda_{\text{BS}}$. Some interfering BSs, however, may serve their respective MTs either via a one- or a two-hop link. These two sets of interfering BSs are denoted by $\Phi_{\text{BS}}^{(I,1\text{hop})}$ and $\Phi_{\text{BS}}^{(I,2\text{hop})}$, respectively, such that $\Phi_{\text{BS}}^{(I)} = \Phi_{\text{BS}}^{(I,1\text{hop})} \cup \Phi_{\text{BS}}^{(I,2\text{hop})}$ and $\Phi_{\text{BS}}^{(I,1\text{hop})} \cap \Phi_{\text{BS}}^{(I,2\text{hop})} = \emptyset$. Since the cell association in (3.1), (3.2) is distance-dependent, the sets $\Phi_{\text{BS}}^{(I,1\text{hop})}$ and $\Phi_{\text{BS}}^{(I,2\text{hop})}$ are not homogeneous PPPs. The locations of the interfering BSs in $\Phi_{\text{BS}}^{(I,1\text{hop})}$ and $\Phi_{\text{BS}}^{(I,2\text{hop})}$ are expected to exhibit, in particular, some level of spatial correlation. Due to the mathematical intractability of taking these spatial correlations into account, we resort to *Approximation 3.1* for system-level evaluation. The accuracy of *Approximation 3.1* is investigated in Section 3.5 with the aid of Monte Carlo simulations. \square

Approximation 3.1. Let $\chi_{1\text{hop}}$ and $\chi_{2\text{hop}}$ be the probabilities that MT_0 is served via a one- and a two-hop link, respectively. $\chi_{1\text{hop}}$ and $\chi_{2\text{hop}}$ are computed in Section 3.3.2. Since all the MTs receive service in our system model, then $\chi_{1\text{hop}} + \chi_{2\text{hop}} = 1$. The sets of interfering BSs, $\Phi_{\text{BS}}^{(I,1\text{hop})}$ and $\Phi_{\text{BS}}^{(I,2\text{hop})}$, in a generic RB are assumed to be two homogeneous and independent PPPs of density $\lambda_{\text{BS}}^{(I,1\text{hop})} = \chi_{1\text{hop}}\lambda_{\text{BS}}^{(I)}$ and $\lambda_{\text{BS}}^{(I,2\text{hop})} = \chi_{2\text{hop}}\lambda_{\text{BS}}^{(I)}$, respectively. The spatial constraints originating from (3.1) and (3.2) are, however, taken into account for system-level performance evaluation, as discussed in Section 3.3.1. \square

Remark 3.8. In the saturated traffic case, all the available BSs are active in a generic RB. With the exception of the serving BS, all the other BSs act as interferers. The number

of active RNs is, however, smaller than the number of available RNs. Let $\Phi_{\text{RN}}^{(I)}$ denote the set of active interfering RNs for the typical MT, MT_0 , in the RB of interest. Based on the relaying protocol of Section 3.2.3, the number of interfering RNs, $\text{card}\{\Phi_{\text{RN}}^{(I)}\}$, must satisfy the condition $\text{card}\{\Phi_{\text{RN}}^{(I)}\} = \text{card}\{\Phi_{\text{BS}}^{(I,2\text{hop})}\}$. This holds because paired BSs and RNs transmit in the same RB. Since a sub-set of available RNs are active in a generic RB and the cell association in (3.1), (3.2) is distance-dependent, $\Phi_{\text{RN}}^{(I)}$ is not a homogeneous PPP. The locations of the interfering RNs are expected to exhibit some level of spatial correlation. Similar to Remark 3.7, for mathematical tractability, we resort to Approximation 3.2 for system-level analysis. Its accuracy is investigated in Section 3.5. \square

Approximation 3.2. The set of interfering RNs, $\Phi_{\text{RN}}^{(I)}$, in a generic RB is assumed to be a homogeneous PPP of density $\lambda_{\text{RN}}^{(I)} = \chi_{2\text{hop}}\lambda_{\text{BS}}^{(I)}$, where $\lambda_{\text{BS}}^{(I)} = \lambda_{\text{BS}}$. Also, the locations of BSs and RNs are assumed to be independent. The constraint $\text{card}\{\Phi_{\text{RN}}^{(I)}\} = \text{card}\{\Phi_{\text{BS}}^{(I,2\text{hop})}\}$ originating from the relaying protocol and the spatial constraints originating from (3.1) and (3.2) are, however, taken into account for system-level performance evaluation, as discussed in Section 3.3.1. Thus, some level of spatial correlation is accounted for. \square

B. Light Traffic Load

In this case, the number of MTs is small. This occurs if $\lambda_{\text{MT}} \ll N_{\text{RB}}\lambda_{\text{BS}}$ and $\lambda_{\text{MT}} \ll N_{\text{RB}}\lambda_{\text{RN}}$. Since the RBs are chosen at random and with equal probability by each BS, the density of interfering BSs in a generic RB is equal to $\lambda_{\text{BS}}^{(I)} = \lambda_{\text{MT}}/N_{\text{RB}}$. As a result, some BSs are inactive in the RB of interest. Similar to the saturated traffic case, the set of interfering BSs in that RB is denoted by $\Phi_{\text{BS}}^{(I)}$, and it can be split in two disjoint sets corresponding to the interfering BSs serving their associated MTs either via a one-, $\Phi_{\text{BS}}^{(I,1\text{hop})}$, or a two-hop, $\Phi_{\text{BS}}^{(I,2\text{hop})}$, link.

Remark 3.9. Since some BSs are inactive in a generic RB and the cell association in (3.1), (3.2) is distance-dependent, the set of interfering BSs in that RB, $\Phi_{\text{BS}}^{(I)}$, is not a homogeneous PPP. The locations of the interfering BSs are expected to exhibit some level of spatial correlation. Similar to Remark 3.7, for mathematical tractability, we use Approximation 3.3 for system-level analysis. Its accuracy is studied in Section 3.5. \square

Approximation 3.3. The sets of interfering BSs, $\Phi_{\text{BS}}^{(I)}$, $\Phi_{\text{BS}}^{(I,1\text{hop})}$ and $\Phi_{\text{BS}}^{(I,2\text{hop})}$ in a generic RB are assumed to be three homogeneous PPPs of density $\lambda_{\text{BS}}^{(I)} = \lambda_{\text{MT}}/N_{\text{RB}}$, $\lambda_{\text{BS}}^{(I,1\text{hop})} = \chi_{1\text{hop}}\lambda_{\text{BS}}^{(I)}$ and $\lambda_{\text{BS}}^{(I,2\text{hop})} = \chi_{2\text{hop}}\lambda_{\text{BS}}^{(I)}$, respectively. Also, $\Phi_{\text{BS}}^{(I,1\text{hop})}$ and $\Phi_{\text{BS}}^{(I,2\text{hop})}$ are assumed to be independent. Similar to *Approximations 3.1, 3.2*, the spatial constraints originating from (3.1) and (3.2) are, however, taken into account for system-level analysis. \square

Remark 3.10. As for the active RNs, comments similar to *Remark 3.8* hold. Hence, $\Phi_{\text{RN}}^{(I)}$ is not a homogeneous PPP. For mathematical tractability, *Approximation 3.4* is used. Its accuracy is studied in Section 3.5. \square

Approximation 3.4. The set of interfering RNs, $\Phi_{\text{RN}}^{(I)}$, in a generic RB is assumed to be a homogeneous PPP of density $\lambda_{\text{RN}}^{(I)} = \chi_{2\text{hop}}\lambda_{\text{BS}}^{(I)}$, where $\lambda_{\text{BS}}^{(I)} = \lambda_{\text{MT}}/N_{\text{RB}}$. Also, the locations of BSs and RNs are assumed to be independent. Similar to *Approximation 3.2*, however, the constraint $\text{card}\{\Phi_{\text{RN}}^{(I)}\} = \text{card}\{\Phi_{\text{BS}}^{(I,2\text{hop})}\}$ and the spatial constraints originating from (3.1) and (3.2) are taken into account in Section 3.3.1. \square

Remark 3.11. In the present report, only saturated and light traffic load models are investigated. The analysis of general load conditions requires, in fact, the knowledge of the distribution of the cells size in the presence of RNs [73]. This distribution is, however, unknown even in the absence of RNs and, usually, it is empirically derived from Monte Carlo simulations [74]. To the best of the authors' knowledge, however, there are no empirical results for the size distribution of Poisson cells in the presence of RNs. As shown in Fig. 3.1 and Fig. 3.2, the shape and size of the cells in the presence and in the absence of RNs look different. In order to study general load conditions, the empirical cells size distribution in the presence of RNs needs to be estimated beforehand. The approach proposed in the present report, fortunately, is directly applicable to relay-aided cellular networks with general load conditions. The methodology introduced in [73] is, in fact, directly applicable to our case study if the distribution of the cells size is known. Due to space limitations, however, the extension to general load conditions is postponed to future research. \square

3.3 Problem Formulation and Useful Lemmas

In this section, we provide a mathematical formulation of the problem at hand. We begin by introducing the definitions of Signal-to-Interference-plus-Noise-Ratio (SINR), which are used for computing the performance metrics of interest. The SINRs are introduced in what follows, by considering one- and two-hop links.

For ease of presentation, some recurrent notation is introduced. The random variable $\mathcal{Z}_{X,Y} = l(r_{X,Y})/S_{X,Y}$ for $X \in \{\text{BS}, \text{RN}\}$ and $Y \in \{\text{RN}, \text{MT}_0\}$ denotes the ratio of path-loss and shadowing for a generic (X, Y) link. $\sigma_N^2 = 10^{\sigma_N^2(\text{dBm})/10}$ denotes the thermal noise power, where $\sigma_N^2(\text{dBm}) = -174 + 10 \log_{10}(\text{B}_W) + \mathcal{F}_{\text{dB}}$, \mathcal{F}_{dB} is the noise figure in dB and B_W is the transmission bandwidth of each RB. $P_{\text{BS}_i}^{(1\text{hop})} = P_{\text{BS}_0} = P_T$ for $\text{BS}_i \in \Phi_{\text{BS}}^{(1,1\text{hop})}$ denotes the transmit power of the BSs that serve their MTs via a one-hop link. $P_{\text{BS}_j}^{(2\text{hop})} = P_{\text{BS}_{\text{R0}}} = K_T P_T$ for $\text{BS}_j \in \Phi_{\text{BS}}^{(1,2\text{hop})}$ denotes the transmit power of the BSs that serve their MTs via a two-hop link. $P_{\text{RN}_k} = P_{\text{RN}_0} = (1 - K_T) P_T$ for $\text{RN}_k \in \Phi_{\text{RN}}^{(1)}$ denotes the transmit power of the RNs. $\eta_{\text{cell}} = (\mathcal{B}_{\text{BS}} P_T) / (\mathcal{B}_{\text{RN}} (1 - K_T) P_T)$ is a shorthand used for simplifying the writing of (3.2).

A. Definition of SINR: One-Hop Link

If the typical MT, MT_0 , is served via a one-hop link, the SINR at MT_0 can be formulated as follows:

$$\text{SINR}_{\text{BS}_0, \text{MT}_0} = \frac{P_{\text{BS}_0} |h_{\text{BS}_0, \text{MT}_0}|^2 \mathcal{Z}_{\text{BS}_0, \text{MT}_0}^{-1}}{\sigma_N^2 + \mathcal{I}_{\text{BS}_0 \rightarrow \text{MT}_0}^{(1\text{hop})}(\mathcal{Z}_{\text{BS}_0, \text{MT}_0}) + \mathcal{I}_{\text{BS}_0 \rightarrow \text{MT}_0}^{(2\text{hop})}(\mathcal{Z}_{\text{BS}_0, \text{MT}_0})} \quad (3.3)$$

where we have introduced the aggregate other-cell interferences as follows:

$$\begin{aligned} \mathcal{I}_{\text{BS}_0 \rightarrow \text{MT}_0}^{(1\text{hop})}(\mathcal{Z}_{\text{BS}_0, \text{MT}_0}) &= \sum_{\text{BS}_i \in \Phi_{\text{BS}}^{(1,1\text{hop})}} P_{\text{BS}_i}^{(1\text{hop})} |h_{\text{BS}_i, \text{MT}_0}|^2 \mathcal{Z}_{\text{BS}_i, \text{MT}_0}^{-1} \\ &\quad \times \mathbf{1}(\mathcal{Z}_{\text{BS}_i, \text{MT}_0} > \mathcal{Z}_{\text{BS}_0, \text{MT}_0}) \\ \mathcal{I}_{\text{BS}_0 \rightarrow \text{MT}_0}^{(2\text{hop})}(\mathcal{Z}_{\text{BS}_0, \text{MT}_0}) &= \sum_{\text{BS}_j \in \Phi_{\text{BS}}^{(1,2\text{hop})}} P_{\text{BS}_j}^{(2\text{hop})} |h_{\text{BS}_j, \text{MT}_0}|^2 \mathcal{Z}_{\text{BS}_j, \text{MT}_0}^{-1} \\ &\quad \times \mathbf{1}(\mathcal{Z}_{\text{BS}_j, \text{MT}_0} > \mathcal{Z}_{\text{BS}_0, \text{MT}_0}) \end{aligned} \quad (3.4)$$

The aggregate other-cell interferences, $\mathcal{I}_{\text{BS}_0 \rightarrow \text{MT}_0}^{(1\text{hop})}(\cdot)$ and $\mathcal{I}_{\text{BS}_0 \rightarrow \text{MT}_0}^{(2\text{hop})}(\cdot)$, in (3.4) are related to the interfering BSs serving their MTs via a one- and a two-hop link, respectively.

The indicator functions in (3.4), $\mathbf{1}(\mathcal{Z}_{BS_i,MT_0} > \mathcal{Z}_{BS_0,MT_0})$ and $\mathbf{1}(\mathcal{Z}_{BS_j,MT_0} > \mathcal{Z}_{BS_0,MT_0})$ for $BS_i \in \Phi_{BS}^{(I,1hop)}$ and $BS_j \in \Phi_{BS}^{(I,2hop)}$, respectively, originate from the association criterion in (3.1). More specifically, they take into account that the power received from the serving BS is higher than that of every interfering BSs.

B. Definition of SINR: Two-Hop Link

If the typical MT, MT_0 , is served via a two-hop link, the SINR needs to be defined at both the serving RN, RN_0 , and at the probe MT, MT_0 .

The SINR at RN_0 can be formulated as follows:

$$\begin{aligned} & \text{SINR}_{BS_{R0},RN_0} \\ &= \frac{P_{BS_{R0}} |h_{BS_{R0},RN_0}|^2 \mathcal{Z}_{BS_{R0},RN_0}^{-1} \mathbf{1}(\mathcal{Z}_{BS_{R0},MT_0} > \eta_{\text{cell}} \mathcal{Z}_{RN_0,MT_0})}{\sigma_N^2 + \mathcal{I}_{BS_{R0} \rightarrow RN_0}^{(1hop)}(\mathcal{Z}_{BS_{R0},RN_0}, \mathcal{Z}_{RN_0,MT_0}) + \mathcal{I}_{BS_{R0} \rightarrow RN_0}^{(2hop)}(\mathcal{Z}_{BS_{R0},RN_0}, \mathcal{Z}_{RN_0,MT_0})} \end{aligned} \quad (3.5)$$

where we have introduced the aggregate other-cell interferences as follows:

$$\begin{aligned} & \mathcal{I}_{BS_{R0} \rightarrow RN_0}^{(1hop)}(\mathcal{Z}_{BS_{R0},RN_0}, \mathcal{Z}_{RN_0,MT_0}) \\ &= \sum_{BS_i \in \Phi_{BS}^{(I,1hop)}} P_{BS_i}^{(1hop)} |h_{BS_i,RN_0}|^2 \mathcal{Z}_{BS_i,RN_0}^{-1} \\ & \quad \times \mathbf{1}(\mathcal{Z}_{BS_i,RN_0} > \mathcal{Z}_{BS_{R0},RN_0}) \mathbf{1}(\mathcal{Z}_{BS_i,MT_0} > \eta_{\text{cell}} \mathcal{Z}_{RN_0,MT_0}) \\ & \mathcal{I}_{BS_{R0} \rightarrow RN_0}^{(2hop)}(\mathcal{Z}_{BS_{R0},RN_0}, \mathcal{Z}_{RN_0,MT_0}) \\ &= \sum_{BS_j \in \Phi_{BS}^{(I,2hop)}} P_{BS_j}^{(2hop)} |h_{BS_j,RN_0}|^2 \mathcal{Z}_{BS_j,RN_0}^{-1} \\ & \quad \times \mathbf{1}(\mathcal{Z}_{BS_j,RN_0} > \mathcal{Z}_{BS_{R0},RN_0}) \mathbf{1}(\mathcal{Z}_{BS_j,MT_0} > \eta_{\text{cell}} \mathcal{Z}_{RN_0,MT_0}) \end{aligned} \quad (3.6)$$

The aggregate other-cell interferences, $\mathcal{I}_{BS_{R0} \rightarrow RN_0}(\cdot, \cdot)$ and $\mathcal{I}_{BS_{R0} \rightarrow RN_0}^{(2hop)}(\cdot, \cdot)$, in (3.6) have the same meaning as those in (3.4). Two indicator functions, however, need to be used as a result of the association criterion in (3.1) and of the transmission protocol in (3.2). The functions $\mathbf{1}(\mathcal{Z}_{BS_i,RN_0} > \mathcal{Z}_{BS_{R0},RN_0})$ and $\mathbf{1}(\mathcal{Z}_{BS_j,RN_0} > \mathcal{Z}_{BS_{R0},RN_0})$ originate from (3.1) and take into account that the path-loss (with shadowing) of the serving BS is lower than that of every interfering BSs. The functions $\mathbf{1}(\mathcal{Z}_{BS_i,MT_0} > \eta_{\text{cell}} \mathcal{Z}_{RN_0,MT_0})$ and $\mathbf{1}(\mathcal{Z}_{BS_j,MT_0} > \eta_{\text{cell}} \mathcal{Z}_{RN_0,MT_0})$ originate from (3.2) and they take into account that, from (3.1), the conditions $\mathcal{Z}_{BS_i,MT_0} > \mathcal{Z}_{BS_0,MT_0}$ and $\mathcal{Z}_{BS_j,MT_0} > \mathcal{Z}_{BS_0,MT_0}$ hold. The

indicator function in the numerator of (3.5), $\mathbf{1}(\mathcal{Z}_{\text{BS}_{\text{R0}},\text{MT}_0} > \eta_{\text{cell}} \mathcal{Z}_{\text{RN}_0,\text{MT}_0})$, originates from (3.2) as well, since, from (3.1), the condition $\mathcal{Z}_{\text{BS}_{\text{R0}},\text{MT}_0} > \mathcal{Z}_{\text{BS}_0,\text{MT}_0}$ holds.

The SINR at MT_0 can be formulated as follows:

$$\text{SINR}_{\text{RN}_0,\text{MT}_0} = \frac{P_{\text{RN}_0} |h_{\text{RN}_0,\text{MT}_0}|^2 \mathcal{Z}_{\text{RN}_0,\text{MT}_0}^{-1}}{\sigma_N^2 + \mathcal{I}_{\text{RN}_0 \rightarrow \text{MT}_0}^{(2\text{hop})}(\mathcal{Z}_{\text{RN}_0,\text{MT}_0})} \quad (3.7)$$

where we have introduced the aggregate other-cell interference as follows:

$$\begin{aligned} & \mathcal{I}_{\text{RN}_0 \rightarrow \text{MT}_0}^{(2\text{hop})}(\mathcal{Z}_{\text{RN}_0,\text{MT}_0}) \\ = & \sum_{\substack{\text{RN}_k \in \Phi_{\text{RN}}^{(1)} \\ \text{card}\{\Phi_{\text{RN}}^{(1)}\} = \text{card}\{\Phi_{\text{BS}}^{(1,2\text{hop})}\}}} P_{\text{RN}_k} |h_{\text{RN}_k,\text{MT}_0}|^2 \mathcal{Z}_{\text{RN}_k,\text{MT}_0}^{-1} \mathbf{1}(\mathcal{Z}_{\text{RN}_k,\text{MT}_0} > \mathcal{Z}_{\text{RN}_0,\text{MT}_0}) \end{aligned} \quad (3.8)$$

The aggregate other-cell interference, $\mathcal{I}_{\text{RN}_0 \rightarrow \text{MT}_0}^{(2\text{hop})}(\cdot)$, in (3.8) is related to the interfering RNs serving their MTs via a two-hop link. The indicator function in (3.8), $\mathbf{1}(\mathcal{Z}_{\text{RN}_k,\text{MT}_0} > \mathcal{Z}_{\text{RN}_0,\text{MT}_0})$ for $\text{RN}_k \in \Phi_{\text{RN}}^{(1)}$, originates from the association criterion in (3.1). It takes into account that the power received from the serving RN is higher than that of every interfering RNs. As mentioned in *Remark 3.8*, the condition $\text{card}\{\Phi_{\text{RN}}^{(1)}\} = \text{card}\{\Phi_{\text{BS}}^{(1,2\text{hop})}\}$ originates from the relaying protocol.

Remark 3.12. As mentioned in Section 3.2.1, BSs and RNs are allowed to transmit only during the first and the second time-slot, respectively. This is the reason why there is no interference originating from the RNs in (3.3) and (3.5), as well as there is no interference originating from the BSs in (3.7). \square

Remark 3.13. The mathematical formulation of the SINRs in (3.3)-(3.8) shows that some level of spatial correlation and spatial non-homogeneity introduced by the cell association criterion in (3.1) and (3.2) is explicitly taken into account. This holds even though, based on the approximations of Section 3.2.4, it is assumed that the sets of interfering BSs and RNs are homogeneous PPPs. This originates from using the indicator functions. Also, the constraint $\text{card}\{\Phi_{\text{RN}}^{(1)}\} = \text{card}\{\Phi_{\text{BS}}^{(1,2\text{hop})}\}$ is taken into account in (3.8). \square

3.3.1 Problem Formulation

Three performance metrics are considered: i) coverage probability, ii) average rate and iii) coverage rate.

A. Coverage Probability

Let T be a reliability threshold below which transmission is not reliable anymore and communication is suspended. The coverage probability, $P_{\text{cov}}(\cdot)$, can be formulated as follows:

$$P_{\text{cov}}(T) = \mathbb{E}_{\mathcal{Z}_{\text{BS}_0, \text{MT}_0}} \left\{ P_{\text{cov}}^{(1\text{hop})}(T; \mathcal{Z}_{\text{BS}_0, \text{MT}_0}) \right\} + \mathbb{E}_{\mathcal{Z}_{\text{RN}_0, \text{MT}_0}} \left\{ P_{\text{cov}}^{(2\text{hop})}(T; \mathcal{Z}_{\text{RN}_0, \text{MT}_0}) \right\} \quad (3.9)$$

$$\begin{aligned} P_{\text{cov}}^{(1\text{hop})}(T; \mathcal{Z}_{\text{BS}_0, \text{MT}_0}) &= \Pr \{ \text{SINR}_{\text{BS}_0, \text{MT}_0} > T \mid \mathcal{Z}_{\text{BS}_0, \text{MT}_0} \} \\ &\quad \times \Pr \{ \mathcal{Z}_{\text{RN}_0, \text{MT}_0} \geq \eta_{\text{cell}}^{-1} \mathcal{Z}_{\text{BS}_0, \text{MT}_0} \mid \mathcal{Z}_{\text{BS}_0, \text{MT}_0} \} \\ P_{\text{cov}}^{(2\text{hop})}(T; \mathcal{Z}_{\text{RN}_0, \text{MT}_0}) &= \Pr \{ \text{SINR}_{\text{BS}_{\text{R}_0}, \text{RN}_0} > T \text{ and } \text{SINR}_{\text{RN}_0, \text{MT}_0} > T \mid \mathcal{Z}_{\text{RN}_0, \text{MT}_0} \} \\ &\quad \times \Pr \{ \mathcal{Z}_{\text{BS}_0, \text{MT}_0} > \eta_{\text{cell}} \mathcal{Z}_{\text{RN}_0, \text{MT}_0} \mid \mathcal{Z}_{\text{RN}_0, \text{MT}_0} \} \end{aligned} \quad (3.10)$$

where $P_{\text{cov}}^{(1\text{hop})}(\cdot; \cdot)$ and $P_{\text{cov}}^{(2\text{hop})}(\cdot; \cdot)$ are the coverage probabilities corresponding to one- and two-hop links, respectively. The conditioning upon $\mathcal{Z}_{\text{BS}_0, \text{MT}_0}$ and $\mathcal{Z}_{\text{RN}_0, \text{MT}_0}$ originates from (3.2).

B. Average Rate

The average rate, R_{average} , is defined as the expectation of the instantaneous rate, as:

$$R_{\text{average}} = \mathbb{E}_{\mathcal{Z}_{\text{BS}_0, \text{MT}_0}} \left\{ R_{\text{average}}^{(1\text{hop})}(\mathcal{Z}_{\text{BS}_0, \text{MT}_0}) \right\} + \mathbb{E}_{\mathcal{Z}_{\text{RN}_0, \text{MT}_0}} \left\{ R_{\text{average}}^{(2\text{hop})}(\mathcal{Z}_{\text{RN}_0, \text{MT}_0}) \right\} \quad (3.11)$$

$$\begin{aligned}
& R_{\text{average}}^{(1\text{hop})}(\mathcal{Z}_{\text{BS}_0, \text{MT}_0}) \\
&= \mathbb{E}_{(\cdot) \setminus \mathcal{Z}_{\text{BS}_0, \text{MT}_0}} \left\{ \text{B}_W \log_2(1 + \text{SINR}_{\text{BS}_0, \text{MT}_0}) \right. \\
&\quad \left. \times \Pr \left\{ \mathcal{Z}_{\text{RN}_0, \text{MT}_0} \geq \eta_{\text{cell}}^{-1} \mathcal{Z}_{\text{BS}_0, \text{MT}_0} \mid \mathcal{Z}_{\text{BS}_0, \text{MT}_0} \right\} \right\} \\
& R_{\text{average}}^{(2\text{hop})}(\mathcal{Z}_{\text{RN}_0, \text{MT}_0}) \\
&\stackrel{(a)}{=} \mathbb{E}_{(\cdot) \setminus \mathcal{Z}_{\text{RN}_0, \text{MT}_0}} \left\{ \frac{\text{B}_W}{2} \min \left\{ \log_2(1 + \text{SINR}_{\text{BS}_{\text{R}_0}, \text{RN}_0}), \log_2(1 + \text{SINR}_{\text{RN}_0, \text{MT}_0}) \right\} \right. \\
&\quad \left. \times \Pr \left\{ \mathcal{Z}_{\text{BS}_0, \text{MT}_0} > \eta_{\text{cell}} \mathcal{Z}_{\text{RN}_0, \text{MT}_0} \mid \mathcal{Z}_{\text{RN}_0, \text{MT}_0} \right\} \right\} \\
&\stackrel{(b)}{=} \mathbb{E}_{(\cdot) \setminus \mathcal{Z}_{\text{RN}_0, \text{MT}_0}} \left\{ \frac{\text{B}_W}{2} \log_2(1 + \min \left\{ \text{SINR}_{\text{BS}_{\text{R}_0}, \text{RN}_0}, \text{SINR}_{\text{RN}_0, \text{MT}_0} \right\}) \right. \\
&\quad \left. \times \Pr \left\{ \mathcal{Z}_{\text{BS}_0, \text{MT}_0} > \eta_{\text{cell}} \mathcal{Z}_{\text{RN}_0, \text{MT}_0} \mid \mathcal{Z}_{\text{RN}_0, \text{MT}_0} \right\} \right\}
\end{aligned} \tag{3.12}$$

where notation and definitions similar to the coverage probability are used. In particular, (a) follows from the rate of DF relaying [45, Eq. (15)] and (b) holds because $\log_2(\cdot)$ is a monotonically increasing function.

C. Coverage Rate

The coverage rate is defined as the probability that the rate is greater than a minimum value that needs to be guaranteed for data transmission. Let R_0 denote such a minimum rate requirement. By taking into account the equality (b) in (3.12), the coverage rate can be formulated, similar to (3.9), as follows:

$$\begin{aligned}
R_{\text{cov}}(R_0) &= \mathbb{E}_{\mathcal{Z}_{\text{BS}_0, \text{MT}_0}} \left\{ P_{\text{cov}}^{(1\text{hop})} \left(T^{(1\text{hop})}; \mathcal{Z}_{\text{BS}_0, \text{MT}_0} \right) \right\} \\
&\quad + \mathbb{E}_{\mathcal{Z}_{\text{RN}_0, \text{MT}_0}} \left\{ P_{\text{cov}}^{(2\text{hop})} \left(T^{(2\text{hop})}; \mathcal{Z}_{\text{RN}_0, \text{MT}_0} \right) \right\}
\end{aligned} \tag{3.13}$$

where $T^{(1\text{hop})} = 2^{R_0/\text{B}_W} - 1$, $T^{(2\text{hop})} = 2^{2R_0/\text{B}_W} - 1$, and $P_{\text{cov}}^{(1\text{hop})}(\cdot; \cdot)$, $P_{\text{cov}}^{(2\text{hop})}(\cdot; \cdot)$ are defined in (3.10).

It is apparent from (3.13) that the coverage rate can be obtained by using the same framework as that of the coverage probability, by appropriately scaling the thresholds. For this reason, it is only briefly considered in Section 3.4. Several numerical examples are, however, illustrated in Section 3.5.

Remark 3.14. Average and coverage rate in (3.11) and (3.13) are defined by taking into account the transmission bandwidth of a single RB, *i.e.*, B_W . They provide, thus, an estimate of the throughput for a typical RB. \square

Remark 3.15. The definition of coverage and average rate in (3.12) and (3.13), respectively, takes into account that new information packets are delivered to the typical MT either via one- or two-hop links. In the two-hop case, in particular, the rate is multiplied by a $1/2$ factor that accounts for the fact that two time-slots for transmission are needed. If $\mathcal{B}_{BS} = \infty$, then $\eta_{\text{cell}} = \infty$ and $P_{\text{cov}}^{(2\text{hop})}(\mathbb{T}; \mathcal{Z}_{\text{RN}_0, \text{MT}_0}) = 0$, $R_{\text{average}}^{(2\text{hop})}(\mathcal{Z}_{\text{RN}_0, \text{MT}_0}) = 0$. This implies that all the MTs are served via a one-hop link and, as expected, the system model reduces to a cellular network without RNs. If $\mathcal{B}_{BS} = 0$, then $\eta_{\text{cell}} = 0$ and $P_{\text{cov}}^{(1\text{hop})}(\mathbb{T}; \mathcal{Z}_{\text{RN}_0, \text{MT}_0}) = 0$, $R_{\text{average}}^{(1\text{hop})}(\mathcal{Z}_{\text{RN}_0, \text{MT}_0}) = 0$. This implies that all the MTs are served via a two-hop link. In both cases, the definition of coverage and average rate accounts for the number of time-slots *effectively* used, *i.e.*, one and two, respectively. This holds even though the transmission protocol under analysis foresees that the BSs and the RNs are not allowed to transmit in the second and in the first time-slot, respectively. If $\mathcal{B}_{BS} = \infty$, for example, only one (not two) time-slot appears in the computation of the rate. If $\mathcal{B}_{BS} \neq \infty$ and $\mathcal{B}_{BS} \neq 0$, some MTs are served via a one-hop link and the others via a two-hop link with some probability (see Section 3.3.2), which is explicitly reflected in the definition in (3.12) and (3.13). As a result, mathematical analysis and comparison of different cellular network setups, *e.g.*, with and without using the RNs, are fair in terms of degrees of freedom effectively used. \square

Remark 3.16. Coverage probability, coverage rate and average rate provide different information on the achievable performance of cellular and relay-aided cellular networks. Coverage probability and coverage rate correspond to the cumulative distribution function of the SINR and of the rate, respectively. They provide, as a consequence, information on the distribution of two different random variables and may serve different purposes. For example, guaranteeing a good coverage probability instead of a high rate may be relevant for cell-edge MTs. The opposite may be important for cell-center MTs. In addition, coverage probability and coverage rate may be used to compute the so-called 5th, 50th (median) and 90th percentile used in standards working groups for quantifying the performance of cell-edge and cell-center MTs [75]. While the coverage rate provides the entire distribution of the rate, the average rate provides the expectation of the rate that is achievable by a MT that is randomly distributed in a generic cell. \square

3.3.2 Useful Lemmas

From Section 3.2.4 and Section 3.3.1, three enabling results are needed for computing the coverage probability in (3.9), the average rate in (3.11), and the coverage rate in (3.13).

- The distribution of the ratio of path-loss and shadowing of the intended links (X_0, Y_0) for $X_0 \in \{\text{BS}_0, \text{BS}_{R0}, \text{RN}_0\}$ and $Y_0 \in \{\text{RN}_0, \text{MT}_0\}$, *i.e.*, the probability density function and the cumulative distribution function of $\mathcal{Z}_{X_0, Y_0} = l(r_{X_0, Y_0})/S_{X_0, Y_0}$, *i.e.*, $f_{\mathcal{Z}_{X_0, Y_0}}(\cdot)$ and $F_{\mathcal{Z}_{X_0, Y_0}}(\cdot)$. These random variables, in fact, appear in the definitions of the SINRs in (3.3)-(3.8).
- The conditional probabilities that MT_0 is served via a one-hop and a two-hop link, as follows:

$$\begin{aligned}\chi_{1\text{hop}}(\mathcal{Z}_{\text{BS}_0, \text{MT}_0}) &= \Pr\{\mathcal{Z}_{\text{RN}_0, \text{MT}_0} \geq \eta_{\text{cell}}^{-1} \mathcal{Z}_{\text{BS}_0, \text{MT}_0} \mid \mathcal{Z}_{\text{BS}_0, \text{MT}_0}\} \\ \chi_{2\text{hop}}(\mathcal{Z}_{\text{RN}_0, \text{MT}_0}) &= \Pr\{\mathcal{Z}_{\text{BS}_0, \text{MT}_0} > \eta_{\text{cell}} \mathcal{Z}_{\text{RN}_0, \text{MT}_0} \mid \mathcal{Z}_{\text{RN}_0, \text{MT}_0}\}\end{aligned}\quad (3.14)$$

They appear, in fact, in (3.9) and (3.11).

- The probabilities that MT_0 is served via a one- and a two-hop link, *i.e.*, $\chi_{1\text{hop}}$ and $\chi_{2\text{hop}}$. From Section 3.2.4, in fact, they are needed to compute the densities of the PPPs of interfering BSs and RNs.

These three enabling results are provided in *Lemma 3.1*, *Lemma 3.2* and *Lemma 3.3* available in Appendix 3.A.

3.4 System-Level Performance Evaluation

In this section, we provide tractable mathematical frameworks to the computation of coverage probability/rate and average rate. Despite the homogeneous PPP-based approximations for system-level performance evaluation introduced in Section 3.2.4, the computation of (3.9) and (3.11) is still mathematically intractable. This is mainly due to the presence of two indicator functions in the mathematical formulation of the SINR in (3.5) and (3.6). In order to obtain a tractable, yet accurate and insightful, mathematical formulation of coverage probability/rate and average rate, we capitalize on an

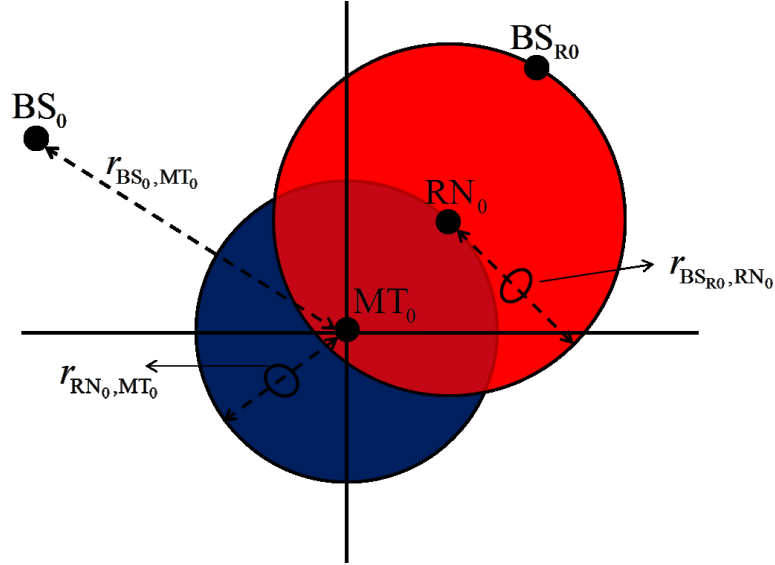


FIGURE 3.3: Rationale of *Approximation 3.5*. For ease of illustration, no shadowing is considered, as well as $\eta_{\text{cell}} = 2$ and $K_T = 1/2$. The figure illustrates typical locations for BS_0 , $\text{BS}_{\text{R}0}$, RN_0 under the assumption that MT_0 is served via a two-hop transmission and, thus, RN_0 is closer to MT_0 than to any other BSs.

approximated expression of the SINR in (3.5) and (3.6), which, in Section 3.5, is shown to be sufficiently accurate for typical system setups.

Approximation 3.5. Let $\text{SINR}_{\text{BS}_{\text{R}0}, \text{RN}_0}$ in (3.5) and (3.6). The following approximation is proposed:

$$\text{SINR}_{\text{BS}_{\text{R}0}, \text{RN}_0} \approx \frac{P_{\text{BS}_{\text{R}0}} |h_{\text{BS}_{\text{R}0}, \text{RN}_0}|^2 \mathcal{Z}_{\text{BS}_{\text{R}0}, \text{RN}_0}^{-1}}{\sigma_N^2 + \mathcal{I}_{\text{BS}_{\text{R}0} \rightarrow \text{RN}_0}^{(1\text{hop})}(\mathcal{Z}_{\text{BS}_{\text{R}0}, \text{RN}_0}) + \mathcal{I}_{\text{BS}_{\text{R}0} \rightarrow \text{RN}_0}^{(2\text{hop})}(\mathcal{Z}_{\text{BS}_{\text{R}0}, \text{RN}_0})} \quad (3.15)$$

$$\begin{aligned} \mathcal{I}_{\text{BS}_{\text{R}0} \rightarrow \text{RN}_0}^{(1\text{hop})}(\mathcal{Z}_{\text{BS}_{\text{R}0}, \text{RN}_0}) &\approx \sum_{\text{BS}_i \in \Phi_{\text{BS}}^{(1,1\text{hop})}} P_{\text{BS}_i}^{(1\text{hop})} |h_{\text{BS}_i, \text{RN}_0}|^2 \mathcal{Z}_{\text{BS}_i, \text{RN}_0}^{-1} \\ &\quad \times \mathbf{1}(\mathcal{Z}_{\text{BS}_i, \text{RN}_0} > \mathcal{Z}_{\text{BS}_{\text{R}0}, \text{RN}_0}) \end{aligned} \quad (3.16)$$

$$\begin{aligned} \mathcal{I}_{\text{BS}_{\text{R}0} \rightarrow \text{RN}_0}^{(2\text{hop})}(\mathcal{Z}_{\text{BS}_{\text{R}0}, \text{RN}_0}) &\approx \sum_{\text{BS}_j \in \Phi_{\text{BS}}^{(1,2\text{hop})}} P_{\text{BS}_j}^{(2\text{hop})} |h_{\text{BS}_j, \text{RN}_0}|^2 \mathcal{Z}_{\text{BS}_j, \text{RN}_0}^{-1} \\ &\quad \times \mathbf{1}(\mathcal{Z}_{\text{BS}_j, \text{RN}_0} > \mathcal{Z}_{\text{BS}_{\text{R}0}, \text{RN}_0}) \end{aligned}$$

which originates by neglecting the spatial constraints $\mathbf{1}(\mathcal{Z}_{\text{BS}_{\text{R}0}, \text{MT}_0} > \eta_{\text{cell}} \mathcal{Z}_{\text{RN}_0, \text{MT}_0})$, $\mathbf{1}(\mathcal{Z}_{\text{BS}_i, \text{MT}_0} > \eta_{\text{cell}} \mathcal{Z}_{\text{RN}_0, \text{MT}_0})$ and $\mathbf{1}(\mathcal{Z}_{\text{BS}_j, \text{MT}_0} > \eta_{\text{cell}} \mathcal{Z}_{\text{RN}_0, \text{MT}_0})$. \square

Remark 3.17. The approximated expression of the SINR in (3.15) is independent of $\mathcal{Z}_{\text{RN}_0, \text{MT}_0}$. \square

Rationale of Approximation 3.5: The rationale of *Approximation 3.5* can be understood by direct inspection of Fig. 3.3. For ease of illustration, Fig. 3.3 is obtained by

assuming $\eta_{\text{cell}} = 2$, *i.e.*, no bias and $K_T = 1/2$, as well as in the absence of shadowing. It illustrates typical locations of BS_0 , BS_{R0} and RN_0 . Without loss of generality, MT_0 is located at the origin. The indicator functions $\mathbf{1}(\mathcal{Z}_{\text{BS}_i, \text{MT}_0} > \eta_{\text{cell}} \mathcal{Z}_{\text{RN}_0, \text{MT}_0})$ and $\mathbf{1}(\mathcal{Z}_{\text{BS}_j, \text{MT}_0} > \eta_{\text{cell}} \mathcal{Z}_{\text{RN}_0, \text{MT}_0})$ in (3.6) enforce the interfering BSs to lie outside the disc having center where MT_0 is and of radius equal to $r_{\text{RN}_0, \text{MT}_0}$. The indicator functions $\mathbf{1}(\mathcal{Z}_{\text{BS}_i, \text{RN}_0} > \mathcal{Z}_{\text{BS}_{\text{R0}}, \text{RN}_0})$ and $\mathbf{1}(\mathcal{Z}_{\text{BS}_j, \text{RN}_0} > \mathcal{Z}_{\text{BS}_{\text{R0}}, \text{RN}_0})$ in (3.6) enforce the interfering BSs to lie outside the disc having center where RN_0 is and of radius equal to $r_{\text{BS}_{\text{R0}}, \text{RN}_0}$. As a result, the interfering BSs can lie only in the “white” area. This geometric region of the plane is difficult to be taken into account for system-level performance evaluation. As far as the indicator function $\mathbf{1}(\mathcal{Z}_{\text{BS}_{\text{R0}}, \text{MT}_0} > \eta_{\text{cell}} \mathcal{Z}_{\text{RN}_0, \text{MT}_0})$ is concerned, similar comments hold for the locations of the serving BS BS_{R0} . The rationale behind *Approximation 3.5* is to let the interfering BSs lie in the whole bi-dimensional plane with the exception of the disc having center where RN_0 is and of radius equal to $r_{\text{BS}_{\text{R0}}, \text{RN}_0}$. This geometric region is, in fact, more mathematically tractable. \square

Accuracy of Approximation 3.5: By direct inspection of Fig. 3.3, the accuracy of *Approximation 3.5* is expected to increase as $r_{\text{RN}_0, \text{MT}_0}$ gets smaller. This condition is likely to occur as the density of the RNs increases. In this case, in fact, the distance between RN_0 and MT_0 is expected to be relatively small. The accuracy of *Approximation 3.5*, however, is expected to be good also if the density of the RNs is small compared to that of the BSs. In this case, in fact, MT_0 is likely to be served via a one-hop link and the end-to-end performance is expected to be mainly determined by $\text{SINR}_{\text{BS}_0, \text{MT}_0}$ in (3.3), which is not affected by *Approximation 3.5*. In summary, the accuracy of *Approximation 3.5* is expected to get better if the density of the RNs is either much bigger or much smaller than that of the BSs. For comparable values of the densities, some inaccuracies may emerge. In Section 3.5, however, they are shown to be acceptable for typical setups and, more importantly, they are shown not to alter the inherent performance trends of relay-aided cellular networks. \square

3.4.1 Coverage Probability

In this section, we provide tractable mathematical frameworks to the computation of the coverage probability in (3.9). General and special system setups leading to closed-form mathematical formulations are presented.

Proposition 3.1. *Let the system model in Section 3.2 and Approximations 3.1-3.5. Let the SINRs in (3.3)-(3.8), and the association probabilities $\chi_{1\text{hop}}$ and $\chi_{2\text{hop}}$ in Lemma 3.3. Let the saturated and light traffic load scenarios, where $\lambda_{\text{BS}}^{(1)} = \lambda_{\text{BS}}$ and $\lambda_{\text{BS}}^{(1)} = \lambda_{\text{MT}}/\text{N}_{\text{RB}}$, respectively. Let $\lambda_{\text{BS}}^{(1,1\text{hop})} = \chi_{1\text{hop}}\lambda_{\text{BS}}^{(1)}$, $\lambda_{\text{BS}}^{(1,2\text{hop})} = \chi_{2\text{hop}}\lambda_{\text{BS}}^{(1)}$, $\lambda_{\text{RN}}^{(1)} = \chi_{2\text{hop}}\lambda_{\text{BS}}^{(1)}$ and $\text{card}\{\Phi_{\text{RN}}^{(1)}\} = \text{card}\{\Phi_{\text{BS}}^{(1,2\text{hop})}\}$. Let $P_{\text{BS}_0} = P_T$, $P_{\text{BS}_{\text{R}_0}} = K_T P_T$, $P_{\text{RN}_0} = (1 - K_T) P_T$ and $\eta_{\text{cell}} = (\mathcal{B}_{\text{BS}} P_T)/(\mathcal{B}_{\text{RN}} (1 - K_T) P_T)$. The coverage probability defined in (3.9) can be formulated as follows:*

$$P_{\text{cov}}(\mathbb{T}) \approx \mathcal{J}_{\text{BS,MT}}(\mathbb{T}) + \mathcal{J}_{\text{BS,RN}}(\mathbb{T}) \mathcal{J}_{\text{RN,MT}}(\mathbb{T}) \quad (3.17)$$

$$\begin{aligned} \mathcal{J}_{\text{BS,MT}}(\mathbb{T}) &= \pi \lambda_{\text{BS}} \Upsilon_{\text{BS,MT}} \\ &\times \int_0^{+\infty} \exp\left(-\frac{\sigma_N^2 \kappa_0 \mathbb{T}}{P_{\text{BS}_0} \Omega_{\text{BS,MT}}} y^{\frac{\beta_{\text{BS,MT}}}{2}}\right) \exp\left(-\frac{\pi \lambda_{\text{RN}} \Upsilon_{\text{RN,MT}} y^{\frac{\beta_{\text{BS,MT}}}{\beta_{\text{RN,MT}}}}}{\frac{2/\beta_{\text{RN,MT}}}{\eta_{\text{cell}}}}\right) \\ &\times \exp(-\Theta_{\text{BS,MT}}(\mathbb{T}) y) dy \\ \mathcal{J}_{\text{BS,RN}}(\mathbb{T}) &= \pi \lambda_{\text{BS}} \Upsilon_{\text{BS,RN}} \int_0^{+\infty} \exp\left(-\frac{\sigma_N^2 \kappa_0 \mathbb{T}}{P_{\text{BS}_{\text{R}_0}} \Omega_{\text{BS,RN}}} y^{\frac{\beta_{\text{BS,RN}}}{2}}\right) \\ &\times \exp(-\Theta_{\text{BS,RN}}(\mathbb{T}) y) dy \end{aligned} \quad (3.18)$$

$$\begin{aligned} \mathcal{J}_{\text{RN,MT}}(\mathbb{T}) &= \pi \lambda_{\text{RN}} \Upsilon_{\text{RN,MT}} \\ &\times \int_0^{+\infty} \exp\left(-\frac{\sigma_N^2 \kappa_0 \mathbb{T}}{P_{\text{RN}_0} \Omega_{\text{RN,MT}}} y^{\frac{\beta_{\text{RN,MT}}}{2}}\right) \exp\left(-\frac{\pi \lambda_{\text{BS}} \Upsilon_{\text{BS,MT}} y^{\frac{\beta_{\text{RN,MT}}}{\beta_{\text{BS,MT}}}}}{\frac{-2/\beta_{\text{BS,MT}}}{\eta_{\text{cell}}}}\right) \\ &\times \exp(-\Theta_{\text{RN,MT}}(\mathbb{T}) y) dy \end{aligned}$$

where $\Upsilon_{X,Y}$ is defined in (3.32) and the following functions have been introduced:

$$\begin{aligned} \Theta_{\text{BS,MT}}(x) &= \pi \lambda_{\text{BS}} \Upsilon_{\text{BS,MT}} - \pi \lambda_{\text{BS}}^{(1,1\text{hop})} \Upsilon_{\text{BS,MT}} \Psi_{\text{BS,MT}}(-x) \\ &\quad - \pi \lambda_{\text{BS}}^{(1,2\text{hop})} \Upsilon_{\text{BS,MT}} \Psi_{\text{BS,MT}}(-K_T x) \\ \Theta_{\text{BS,RN}}(x) &= \pi \lambda_{\text{BS}} \Upsilon_{\text{BS,RN}} - \pi \lambda_{\text{BS}}^{(1,1\text{hop})} \Upsilon_{\text{BS,RN}} \Psi_{\text{BS,RN}}(-x/K_T) \\ &\quad - \pi \lambda_{\text{BS}}^{(1,2\text{hop})} \Upsilon_{\text{BS,RN}} \Psi_{\text{BS,RN}}(-x) \\ \Theta_{\text{RN,MT}}(x) &= \pi \lambda_{\text{RN}} \Upsilon_{\text{RN,MT}} - \pi \lambda_{\text{BS}}^{(1,2\text{hop})} \Upsilon_{\text{RN,MT}} \Psi_{\text{RN,MT}}(-x) \\ \Psi_{\text{BS,MT}}(x) &= 1 - {}_2F_1(1, -2/\beta_{\text{BS,MT}}; 1 - 2/\beta_{\text{BS,MT}}; x) \\ \Psi_{\text{BS,RN}}(x) &= 1 - {}_2F_1(1, -2/\beta_{\text{BS,RN}}; 1 - 2/\beta_{\text{BS,RN}}; x) \\ \Psi_{\text{RN,MT}}(x) &= 1 - {}_2F_1(1, -2/\beta_{\text{RN,MT}}; 1 - 2/\beta_{\text{RN,MT}}; x) \end{aligned} \quad (3.19)$$

Proof: See Appendix 3.B. □

Remark 3.18. From the mathematical standpoint, the proof in Appendix 3.B is different from state-of-the-art papers on PPP-based modeling of cellular networks, *e.g.*, [10]. In particular: i) some steps of the mathematical derivation are possible only with the aid of *Approximations 3.1-3.4*, ii) *Approximation 3.5* has not been proposed elsewhere, and iii) the constraint $\text{card} \left\{ \Phi_{\text{BS}}^{(1,2\text{hop})} \right\} = \text{card} \left\{ \Phi_{\text{RN}}^{(1)} \right\}$ is a unique characteristic of the relaying protocol, making the mathematical steps that lead to the final result different from typical derivations. \square

Remark 3.19. As mentioned in Section 3.3.1, the coverage rate is a special case of the coverage probability. From (3.13) and *Proposition 3.1*, in particular, it can be formulated as follows:

$$R_{\text{cov}}(R_0) \approx \mathcal{J}_{\text{BS,MT}} \left(T^{(1\text{hop})} \right) + \mathcal{J}_{\text{BS,RN}} \left(T^{(2\text{hop})} \right) \mathcal{J}_{\text{RN,MT}} \left(T^{(2\text{hop})} \right) \quad (3.20)$$

where $T^{(1\text{hop})} = 2^{R_0/B_W} - 1$, $T^{(2\text{hop})} = 2^{2R_0/B_W} - 1$ and $\mathcal{J}_{\text{BS,MT}}(\cdot)$, $\mathcal{J}_{\text{BS,RN}}(\cdot)$, $\mathcal{J}_{\text{RN,MT}}(\cdot)$ are defined in (3.18). In the remainder of the present chapter, due to space limitations, special case studies for the coverage rate are not considered, since they are similar to those of the coverage probability. \square

Corollary 3.1. *Let the same assumptions as in Proposition 3.1. Let $\sigma_N^2 \rightarrow 0$, i.e., the system model is interference-limited. The coverage probability can be formulated as in (3.17) by replacing $\mathcal{J}_{\text{BS,MT}}(T) \rightarrow \mathcal{J}_{\text{BS,MT}}^{(\sigma_N^2 \rightarrow 0)}(T)$, $\mathcal{J}_{\text{BS,RN}}(T) \rightarrow \mathcal{J}_{\text{BS,RN}}^{(\sigma_N^2 \rightarrow 0)}(T)$ and $\mathcal{J}_{\text{RN,MT}}(T) \rightarrow \mathcal{J}_{\text{RN,MT}}^{(\sigma_N^2 \rightarrow 0)}(T)$ in (3.18), where:*

$$\begin{aligned} \mathcal{J}_{\text{BS,MT}}^{(\sigma_N^2 \rightarrow 0)}(T) &= \pi \lambda_{\text{BS}} \Upsilon_{\text{BS,MT}} \\ &\quad \times \int_0^{+\infty} \exp \left(- \frac{\pi \lambda_{\text{RN}} \Upsilon_{\text{RN,MT}}}{\eta_{\text{cell}}^{2/\beta_{\text{RN,MT}}}} y^{\frac{\beta_{\text{BS,MT}}}{\beta_{\text{RN,MT}}}} \right) \exp(-\Theta_{\text{BS,MT}}(T) y) dy \\ \mathcal{J}_{\text{BS,RN}}^{(\sigma_N^2 \rightarrow 0)}(T) &= \pi \lambda_{\text{BS}} \Upsilon_{\text{BS,RN}} \int_0^{+\infty} \exp(-\Theta_{\text{BS,RN}}(T) y) dy \\ &= \pi \lambda_{\text{BS}} \Upsilon_{\text{BS,RN}} / \Theta_{\text{BS,RN}}(T) \\ \mathcal{J}_{\text{RN,MT}}^{(\sigma_N^2 \rightarrow 0)}(T) &= \pi \lambda_{\text{RN}} \Upsilon_{\text{RN,MT}} \\ &\quad \times \int_0^{+\infty} \exp \left(- \frac{\pi \lambda_{\text{BS}} \Upsilon_{\text{BS,MT}}}{\eta_{\text{cell}}^{-2/\beta_{\text{BS,MT}}}} y^{\frac{\beta_{\text{RN,MT}}}{\beta_{\text{BS,MT}}}} \right) \exp(-\Theta_{\text{RN,MT}}(T) y) dy \end{aligned} \quad (3.21)$$

Proof: It follows from (3.18), by letting $\sigma_N^2 \rightarrow 0$ and by computing notable integrals. \square

Remark 3.20. If $\beta_{\text{BS,MT}}/\beta_{\text{RN,MT}}$ can be written as the ratio of two positive integers, the integrals in (3.21) can be formulated in closed-form in terms of the Meijer G-function with the aid of the Mellin-Barnes integration theorem [3, Eq. (2.24.1.1)]. Also, the integrals in (3.21) have simplified closed-form expressions for several special values of the ratio $\beta_{\text{BS,MT}}/\beta_{\text{RN,MT}}$. A simple case study occurs if $\beta_{\text{BS,MT}}/\beta_{\text{RN,MT}} = 1$, as follows:

$$\begin{aligned}\mathcal{J}_{\text{BS,MT}}^{(\sigma_N^2 \rightarrow 0)}(\mathbb{T}) &= (\lambda_{\text{BS}}/\lambda_{\text{RN}}) (\Upsilon_{\text{BS,MT}}/\Upsilon_{\text{RN,MT}}) \left(\eta_{\text{cell}}^{2/\beta_{\text{RN,MT}}} / \Theta_{\text{BS,MT}}(\mathbb{T}) \right) \\ \mathcal{J}_{\text{RN,MT}}^{(\sigma_N^2 \rightarrow 0)}(\mathbb{T}) &= (\lambda_{\text{RN}}/\lambda_{\text{BS}}) (\Upsilon_{\text{RN,MT}}/\Upsilon_{\text{BS,MT}}) \left(\eta_{\text{cell}}^{-2/\beta_{\text{BS,MT}}} / \Theta_{\text{RN,MT}}(\mathbb{T}) \right)\end{aligned}\quad (3.22)$$

Due to space limitations, other special cases are not reported in the present report. Similar closed-form expressions can be obtained for other similar integrals presented in the sequel. \square

Corollary 3.2. *Let the same assumptions as in Proposition 3.1. Let $\lambda_{\text{BS}}^{(1)} \rightarrow 0$, i.e., the system model is noise-limited. The coverage probability can be formulated as in (3.17) and (3.18), by replacing the functions $\Theta_{\text{BS,MT}}(x) \rightarrow \Theta_{\text{BS,MT}}^{(\lambda_{\text{BS}}^{(1)} \rightarrow 0)} = \pi \lambda_{\text{BS}} \Upsilon_{\text{BS,MT}}$, $\Theta_{\text{BS,RN}}(x) \rightarrow \Theta_{\text{BS,RN}}^{(\lambda_{\text{BS}}^{(1)} \rightarrow 0)} = \pi \lambda_{\text{BS}} \Upsilon_{\text{BS,RN}}$ and $\Theta_{\text{RN,MT}}(x) \rightarrow \Theta_{\text{RN,MT}}^{(\lambda_{\text{BS}}^{(1)} \rightarrow 0)} = \pi \lambda_{\text{RN}} \Upsilon_{\text{RN,MT}}$ in (3.19).*

Proof: It follows by letting $\lambda_{\text{BS}}^{(1)} \rightarrow 0$ in (3.19), which implies $\lambda_{\text{BS}}^{(\text{I,1hop})} \rightarrow 0$ and $\lambda_{\text{BS}}^{(\text{I,2hop})} \rightarrow 0$. \square

Corollary 3.3. *Let the same assumptions as in Proposition 3.1. Let $\mathcal{B}_{\text{BS}} \rightarrow +\infty$, i.e., all the MTs are served, almost surely, via a one-hop link. The coverage probability can be formulated as $\text{P}_{\text{cov}}(\mathbb{T}) \rightarrow \text{P}_{\text{cov}}^{(\mathcal{B}_{\text{BS}} \rightarrow +\infty)}(\mathbb{T}) \approx \mathcal{J}_{\text{BS,MT}}^{(\mathcal{B}_{\text{BS}} \rightarrow +\infty)}(\mathbb{T})$, where $\mathcal{J}_{\text{BS,MT}}^{(\mathcal{B}_{\text{BS}} \rightarrow +\infty)}(\cdot)$ is defined as follows:*

$$\begin{aligned}\mathcal{J}_{\text{BS,MT}}^{(\mathcal{B}_{\text{BS}} \rightarrow +\infty)}(\mathbb{T}) &= \pi \lambda_{\text{BS}} \Upsilon_{\text{BS,MT}} \\ &\quad \times \int_0^{+\infty} \exp\left(-\frac{\sigma_N^2 \kappa_0 \mathbb{T}}{P_{\text{BS}_0} \Omega_{\text{BS,MT}}} y^{\frac{\beta_{\text{BS,MT}}}{2}}\right) \exp\left(-\Theta_{\text{BS,MT}}^{(\mathcal{B}_{\text{BS}} \rightarrow +\infty)}(\mathbb{T}) y\right) dy\end{aligned}\quad (3.23)$$

where the following definitions hold for saturated and light load models, respectively:

$$\begin{aligned}\Theta_{\text{BS,MT}}^{(\mathcal{B}_{\text{BS}} \rightarrow +\infty)}(x) &= \pi \lambda_{\text{BS}} \Upsilon_{\text{BS,MT}} {}_2F_1(1, -2/\beta_{\text{BS,MT}}; 1 - 2/\beta_{\text{BS,MT}}; -x) \\ \Theta_{\text{BS,MT}}^{(\mathcal{B}_{\text{BS}} \rightarrow +\infty)}(x) &= \pi \lambda_{\text{BS}} \Upsilon_{\text{BS,MT}} - \pi (\lambda_{\text{MT}}/\text{N}_{\text{RB}}) \Upsilon_{\text{BS,MT}} \\ &\quad \times (1 - {}_2F_1(1, -2/\beta_{\text{BS,MT}}; 1 - 2/\beta_{\text{BS,MT}}; -x))\end{aligned}\quad (3.24)$$

Proof: If $\mathcal{B}_{\text{BS}} \rightarrow +\infty$, then $\eta_{\text{cell}} \rightarrow +\infty$, $\chi_{1\text{hop}} \rightarrow 1$ and $\chi_{2\text{hop}} \rightarrow 0$. This implies $\lambda_{\text{BS}}^{(I,1\text{hop})} \rightarrow \lambda_{\text{BS}}^{(I)}$, $\lambda_{\text{BS}}^{(I,2\text{hop})} \rightarrow 0$, $\exp\left(-\tau\eta_{\text{cell}}^{-2/\beta_{\text{RN,MT}}}\right) \rightarrow 1$ and $\exp\left(-\tau\eta_{\text{cell}}^{2/\beta_{\text{RN,MT}}}\right) \rightarrow 0$ for $\tau > 0$. The proof follows by noting that $\mathcal{J}_{\text{BS,MT}}(\mathbb{T}) \rightarrow \mathcal{J}_{\text{BS,MT}}^{(\mathcal{B}_{\text{BS}} \rightarrow +\infty)}(\mathbb{T})$ and $\mathcal{J}_{\text{RN,MT}}(\mathbb{T}) \rightarrow 0$. \square

Remark 3.21. The coverage probability in (3.23) can be obtained also by letting $\lambda_{\text{RN}} \rightarrow 0$, i.e., there are no RNs in the network and the system model reduces to a simple cellular network. This immediately follows from (3.18), since $\mathcal{J}_{\text{RN,MT}}(\mathbb{T}) \rightarrow 0$ if $\lambda_{\text{RN}} \rightarrow 0$, as well as $\chi_{1\text{hop}} \rightarrow 1$ and $\chi_{2\text{hop}} \rightarrow 0$. In the saturated traffic load scenario, the coverage probability in (3.23) coincides with previous mathematical frameworks reported in [76]. In the light traffic load scenario, on the other hand, it generalizes [76]. In the interference-limited regime, i.e., $\sigma_N^2 \rightarrow 0$, the coverage probability in (3.23) can be further simplified as follows:

$$\begin{aligned} \mathcal{J}_{\text{BS,MT}}^{(\mathcal{B}_{\text{BS}} \rightarrow +\infty, \sigma_N^2 \rightarrow 0)}(\mathbb{T}) &= \pi \lambda_{\text{BS}} \Upsilon_{\text{BS,MT}} \int_0^{+\infty} \exp\left(-\Theta_{\text{BS,MT}}^{(\mathcal{B}_{\text{BS}} \rightarrow +\infty)}(\mathbb{T}) y\right) dy \\ &= \pi \lambda_{\text{BS}} \Upsilon_{\text{BS,MT}} / \Theta_{\text{BS,MT}}^{(\mathcal{B}_{\text{BS}} \rightarrow +\infty)}(\mathbb{T}) \end{aligned} \quad (3.25)$$

Equation (3.25) shows that the coverage probability is independent of the density of BSs, λ_{BS} , only for the saturated load model. This finding was reported in [10], [22]. In the light load model, the coverage probability depends on λ_{BS} , λ_{MT} , N_{RB} . In the presence of RNs, (3.21) shows that it depends on λ_{RN} too. \square

Corollary 3.4. *Let the same assumptions as in Proposition 3.1. Let $\mathcal{B}_{\text{BS}} \rightarrow 0$, i.e., all the MTs are served, almost surely, via a two-hop link. The coverage probability can be formulated as $P_{\text{cov}}(\mathbb{T}) \rightarrow P_{\text{cov}}^{(\mathcal{B}_{\text{BS}} \rightarrow 0)}(\mathbb{T}) \approx \mathcal{J}_{\text{BS,RN}}^{(\mathcal{B}_{\text{BS}} \rightarrow 0)}(\mathbb{T}) \mathcal{J}_{\text{RN,MT}}^{(\mathcal{B}_{\text{BS}} \rightarrow 0)}(\mathbb{T})$, where $\mathcal{J}_{\text{BS,RN}}^{(\mathcal{B}_{\text{BS}} \rightarrow 0)}(\cdot)$ and $\mathcal{J}_{\text{RN,MT}}^{(\mathcal{B}_{\text{BS}} \rightarrow 0)}(\cdot)$ are defined as follows:*

$$\begin{aligned} \mathcal{J}_{\text{BS,RN}}^{(\mathcal{B}_{\text{BS}} \rightarrow 0)}(\mathbb{T}) &= \pi \lambda_{\text{BS}} \Upsilon_{\text{BS,RN}} \\ &\quad \times \int_0^{+\infty} \exp\left(-\frac{\sigma_N^2 \kappa_0 \mathbb{T}}{P_{\text{BSR}_0} \Omega_{\text{BS,RN}}} y^{\frac{\beta_{\text{BS,RN}}}{2}}\right) \exp\left(-\Theta_{\text{BS,RN}}^{(\mathcal{B}_{\text{BS}} \rightarrow 0)}(\mathbb{T}) y\right) dy \end{aligned} \quad (3.26)$$

$$\begin{aligned} \mathcal{J}_{\text{RN,MT}}^{(\mathcal{B}_{\text{BS}} \rightarrow 0)}(\mathbb{T}) &= \pi \lambda_{\text{RN}} \Upsilon_{\text{RN,MT}} \\ &\quad \times \int_0^{+\infty} \exp\left(-\frac{\sigma_N^2 \kappa_0 \mathbb{T}}{P_{\text{RN}_0} \Omega_{\text{RN,MT}}} y^{\frac{\beta_{\text{RN,MT}}}{2}}\right) \exp\left(-\Theta_{\text{RN,MT}}^{(\mathcal{B}_{\text{BS}} \rightarrow 0)}(\mathbb{T}) y\right) dy \end{aligned}$$

$$\begin{aligned} \Theta_{\text{BS,RN}}^{(\mathcal{B}_{\text{BS}} \rightarrow 0)}(x) &= \pi \lambda_{\text{BS}} \Upsilon_{\text{BS,RN}} - \pi \lambda_{\text{BS}}^{(I)} \Upsilon_{\text{BS,RN}} \Psi_{\text{BS,RN}}(-x) \\ \Theta_{\text{RN,MT}}^{(\mathcal{B}_{\text{BS}} \rightarrow 0)}(x) &= \pi \lambda_{\text{RN}} \Upsilon_{\text{RN,MT}} - \pi \lambda_{\text{BS}}^{(I)} \Upsilon_{\text{RN,MT}} \Psi_{\text{RN,MT}}(-x) \end{aligned} \quad (3.27)$$

as well as $\lambda_{\text{BS}}^{(I)} = \lambda_{\text{BS}}$ and $\lambda_{\text{BS}}^{(I)} = \lambda_{\text{MT}}/N_{\text{RB}}$ for saturated and light load models, respectively.

Proof: If $\mathcal{B}_{\text{BS}} \rightarrow 0$, then $\eta_{\text{cell}} \rightarrow 0$, $\chi_{1\text{hop}} \rightarrow 0$ and $\chi_{2\text{hop}} \rightarrow 1$. This implies $\lambda_{\text{BS}}^{(I,1\text{hop})} \rightarrow 0$, $\lambda_{\text{BS}}^{(I,2\text{hop})} \rightarrow \lambda_{\text{BS}}^{(I)}$, $\exp\left(-\tau\eta_{\text{cell}}^{-2/\beta_{\text{RN,MT}}}\right) \rightarrow 0$ and $\exp\left(-\tau\eta_{\text{cell}}^{2/\beta_{\text{RN,MT}}}\right) \rightarrow 1$ for $\tau > 0$. The proof follows since $\mathcal{J}_{\text{BS,MT}}(\mathbb{T}) \rightarrow 0$, $\mathcal{J}_{\text{BS,RN}}(\mathbb{T}) \rightarrow \mathcal{J}_{\text{BS,RN}}^{(\mathcal{B}_{\text{BS}} \rightarrow 0)}(\mathbb{T})$ and $\mathcal{J}_{\text{RN,MT}}(\mathbb{T}) \rightarrow \mathcal{J}_{\text{RN,MT}}^{(\mathcal{B}_{\text{BS}} \rightarrow 0)}(\mathbb{T})$. \square

Remark 3.22. In the interference-limited regime, i.e., $\sigma_N^2 \rightarrow 0$, (3.26) can be simplified as in (3.25). \square

Corollary 3.5. *Let the same assumptions as in Proposition 3.1. Let $\mathcal{B}_{\text{BS}}/\mathcal{B}_{\text{RN}} = 1$, i.e., no bias is applied for cell association. The following results hold:*

- *If $\beta_{\text{BS,MT}}/\beta_{\text{RN,MT}} \ll 1$, the coverage probability can be formulated as in Corollary 3.3.*
- *If $\beta_{\text{BS,MT}}/\beta_{\text{RN,MT}} \gg 1$, the coverage probability can be formulated as in Corollary 3.4.*
- *If $\beta_{\text{BS,MT}}/\beta_{\text{RN,MT}} = 1$, the coverage probability can be formulated as in Proposition 3.1, by setting $\eta_{\text{cell}} = 1/(1 - K_T)$ and $\beta_{\text{BS,MT}} = \beta_{\text{RN,MT}} = \beta_{\text{MT}}$.*

Proof: If $\mathcal{B}_{\text{BS}}/\mathcal{B}_{\text{RN}} = 1$ and $\beta_{\text{BS,MT}}/\beta_{\text{RN,MT}} \ll 1$, then $\chi_{1\text{hop}} \rightarrow 1$ and $\chi_{2\text{hop}} \rightarrow 0$. If $\mathcal{B}_{\text{BS}}/\mathcal{B}_{\text{RN}} = 1$ and $\beta_{\text{BS,MT}}/\beta_{\text{RN,MT}} \gg 1$, then $\chi_{1\text{hop}} \rightarrow 0$ and $\chi_{2\text{hop}} \rightarrow 1$. As a consequence, the proof follows by using the same line of thought as the proofs of Corollary 3.3 and Corollary 3.4. \square

3.4.2 Average Rate

In this section, we provide a tractable mathematical framework to the computation of the average rate in (3.11). Only the general case is presented, since special cases can be readily obtained from Section 3.4.1.

Proposition 3.2. *Let the same assumptions as in Proposition 3.1. Let $\mathcal{J}_{\text{BS,MT}}(\cdot)$, $\mathcal{J}_{\text{BS,RN}}(\cdot)$ and $\mathcal{J}_{\text{RN,MT}}(\cdot)$ defined in (3.18). The average rate defined in (3.11) can be*

formulated as follows:

$$\begin{aligned} R_{\text{average}} &= \frac{B_W}{\ln(2)} \int_0^{+\infty} \mathcal{J}_{\text{BS,MT}}(z) \frac{dz}{z+1} \\ &+ \frac{1}{2} \frac{B_W}{\ln(2)} \int_0^{+\infty} \mathcal{J}_{\text{BS,RN}}(z) \mathcal{J}_{\text{RN,MT}}(z) \frac{dz}{z+1} \end{aligned} \quad (3.28)$$

Proof: Let δ be a positive constant and Δ be a non-negative random variable. The following holds:

$$\begin{aligned} \mathbb{E}_\Delta \{\delta \log_2(1 + \Delta)\} &= \int_0^{+\infty} \Pr\{\delta \log_2(1 + \Delta) \geq x\} dx \\ &= (\delta/\ln(2)) \int_0^{+\infty} F_\Delta(z)/(z+1) dz \end{aligned} \quad (3.29)$$

where $F_\Delta(\cdot)$ is the complementary cumulative distribution function of Δ . By applying these equalities to (3.12), the proof follows using the same steps as those used for the proof of Proposition 3.1 in Appendix 3.A. \square

Remark 3.23. In the most general case formulated in (3.28) and (3.18), a two-fold integral needs to be computed for obtaining the average rate. The framework reduces to the computation of a single integral for several special cases analyzed in Section 3.4.1, *i.e.*, if the coverage probability is available in closed-form. The 1/2 factor that multiplies the second addend in (3.28) originates from the two-hop DF-based relaying protocol. \square

3.4.3 Performance Trends, Design Insight and System-Level Optimization

In this section, we discuss relevant performance trends that can be inferred from the mathematical frameworks introduced in Section 3.4.1. For brevity, coverage/average rate are not explicitly discussed in this section. Relevant comments, however, are provided once showing the numerical results in Section 3.5. For ease of presentation, the frameworks considered in this section are summarized in Table 3.2. Table 3.2, in particular, provides results for noise- and interference-limited operating regimes, since they are more conveniently formulated for understanding the inherent performance trends of the system model under analysis.

TABLE 3.2: Summary of mathematical frameworks in the presence/absence of RNs and for noise-limited ($\lambda_{\text{BS}}^{(1)} \rightarrow 0$) and interference-limited ($\sigma_N^2 \rightarrow 0$) operating regimes. Notation: $\Upsilon_{X,Y}$ is defined in (3.32), $\lambda_{\text{BS}}^{(1)} = \lambda_{\text{BS}}$ and $\lambda_{\text{BS}}^{(1)} = \lambda_{\text{MT}}/N_{\text{RB}}$ for saturated and light traffic load models, respectively, $P_{\text{BS}_0} = P_T$, $P_{\text{BS}_{\text{R}_0}} = K_T P_T$ and $P_{\text{RN}_0} = (1 - K_T) P_T$.

Recurrent Functions	
$\mathcal{G}_{X,Y}^{(\lambda_{\text{BS}}^{(1)} \rightarrow 0)}(\text{T}; P) \approx \pi \lambda_X \Upsilon_{X,Y} \int_0^{+\infty} \exp\left(-\frac{\sigma_N^2 \kappa_0 T}{P \Omega_{X,Y}} y^{\frac{\beta_{X,Y}}{2}}\right) \exp(-\pi \lambda_X \Upsilon_{X,Y} y) dy$ $\mathcal{G}_{X,Y}^{(\sigma_N^2 \rightarrow 0)}(\text{T}) \approx \frac{\lambda_X}{\lambda_X - \lambda_{\text{BS}}^{(1)} + \lambda_{\text{BS}}^{(1)} {}_2F_1(1, -2/\beta_{X,Y}; 1-2/\beta_{X,Y}; -\text{T})}$	
Case Study	Coverage Probability
Without Relays ($\lambda_{\text{RN}} \rightarrow 0$) OR With Relays ($\lambda_{\text{RN}} \neq 0$) and $\mathcal{B}_{\text{BS}}/\mathcal{B}_{\text{RN}} \gg 1$ ($\mathcal{B}_{\text{BS}} \rightarrow +\infty$) OR With Relays ($\lambda_{\text{RN}} \neq 0$) and $\frac{\mathcal{B}_{\text{BS}}}{\mathcal{B}_{\text{RN}}} = 1$ and $\frac{\beta_{\text{BS,MT}}}{\beta_{\text{RN,MT}}} \ll 1$	$P_{\text{cov}}^{(\lambda_{\text{BS}}^{(1)} \rightarrow 0)}(\text{T}) \approx \mathcal{G}_{\text{BS,MT}}^{(\lambda_{\text{BS}}^{(1)} \rightarrow 0)}(\text{T}; P_{\text{BS}_0})$ $P_{\text{cov}}^{(\sigma_N^2 \rightarrow 0)}(\text{T}) \approx \mathcal{G}_{\text{BS,MT}}^{(\sigma_N^2 \rightarrow 0)}(\text{T})$
With Relays ($\lambda_{\text{RN}} \neq 0$) and $\mathcal{B}_{\text{BS}}/\mathcal{B}_{\text{RN}} \ll 1$ ($\mathcal{B}_{\text{BS}} \rightarrow 0$) OR With Relays ($\lambda_{\text{RN}} \neq 0$) and $\frac{\mathcal{B}_{\text{BS}}}{\mathcal{B}_{\text{RN}}} = 1$ and $\frac{\beta_{\text{BS,MT}}}{\beta_{\text{RN,MT}}} \gg 1$	$P_{\text{cov}}^{(\lambda_{\text{BS}}^{(1)} \rightarrow 0)}(\text{T}) \approx \mathcal{G}_{\text{BS,RN}}^{(\lambda_{\text{BS}}^{(1)} \rightarrow 0)}(\text{T}; P_{\text{BS}_{\text{R}_0}}) \mathcal{G}_{\text{RN,MT}}^{(\lambda_{\text{BS}}^{(1)} \rightarrow 0)}(\text{T}; P_{\text{RN}_0})$ $P_{\text{cov}}^{(\sigma_N^2 \rightarrow 0)}(\text{T}) \approx \mathcal{G}_{\text{BS,RN}}^{(\sigma_N^2 \rightarrow 0)}(\text{T}) \mathcal{G}_{\text{RN,MT}}^{(\sigma_N^2 \rightarrow 0)}(\text{T})$

Before discussing the performance trends, we note, from Table 3.2, that the coverage probability in noise- and interference-limited operating regimes depends on the functions $\mathcal{G}_{X,Y}^{(\lambda_{\text{BS}}^{(1)} \rightarrow 0)}(\cdot; \cdot)$ and $\mathcal{G}_{X,Y}^{(\sigma_N^2 \rightarrow 0)}(\cdot)$, respectively. By direct inspection of them, the following two remarks hold.

Remark 3.24. Let $\mathcal{G}_{X,Y}^{(\lambda_{\text{BS}}^{(1)} \rightarrow 0)}(\cdot; \cdot)$ in Table 3.2. For typical operating conditions, *i.e.*, $\sigma_N^2 \kappa_0 / (P \Omega_{X,Y}) \ll 1$, which holds for medium-high Signal-to-Noise-Ratios (SNRs), and $\lambda_X \ll 1$, which holds for typical network densities, $\mathcal{G}_{X,Y}^{(\lambda_{\text{BS}}^{(1)} \rightarrow 0)}(\cdot; \cdot)$ monotonically decreases as the path-loss exponent $\beta_{X,Y}$ increases. The need to emphasize that the network has to operate under “typical operating conditions” originates from fact that, as a function of $\beta_{X,Y}$, the term $y^{\beta_{X,Y}/2}$ has a different behavior for $y \in (0, 1)$ and for $y \geq 1$. For “typical operating conditions”, the behavior of $\mathcal{G}_{X,Y}^{(\lambda_{\text{BS}}^{(1)} \rightarrow 0)}(\cdot; \cdot)$ is mainly determined

by the values of y for which $y \geq 1$, *i.e.*, $\int_0^{+\infty} (\cdot) dy \approx \int_1^{+\infty} (\cdot) dy$. This ambiguity originates from the unbounded path-loss model, which, however, is known to be accurate, from the standpoint of physics, for “typical operating conditions”. \square

Remark 3.25. Let $\mathcal{G}_{X,Y}^{(\sigma_N^2 \rightarrow 0)}(\cdot)$ in Table 3.2. It monotonically increases as the path-loss exponent $\beta_{X,Y} > 2$ increases. This originates from the fact that the function ${}_2F_1(1, -2/\beta_{X,Y}; 1 - 2/\beta_{X,Y}; -x)$ monotonically decreases, for every $x \geq 0$, as the path-loss exponent $\beta_{X,Y} > 2$ increases. \square

Let the case studies in Table 3.2. Based on *Remark 3.24* and *Remark 3.25*, we conclude that: *the coverage probability decreases in the noise-limited regime and increases in the interference-limited regime as the path-loss exponent of any of the links increases, respectively.*

This finding is similar to previously reported results for cellular networks, *i.e.*, in the absence of RNs [10], [21]. This is confirmed by direct inspection of Table 3.2 for $\lambda_{\text{RN}} \rightarrow 0$ as well. A major difference exists, however, between cellular (in the absence of RNs) and relay-aided cellular (in the presence of RNs) networks, which originates from the cell association criterion in (3.1) and (3.2), *i.e.*, the inherent two-tier nature of relay-aided cellular networks as opposed to the single-tier nature of cellular networks. Consider the following example. Let $\mathcal{B}_{\text{BS}}/\mathcal{B}_{\text{RN}} = 1$ (no bias) and $\beta_{\text{BS,MT}}/\beta_{\text{RN,MT}} \ll 1$. From Table 3.2, we conclude that the MTs are likely to be served via a one-hop link and that there is no performance difference between cellular and relay-aided cellular networks. As a result, the coverage probability decreases and increases as $\beta_{\text{BS,MT}}$ increases in the noise- and interference-limited regimes, respectively. Also, it is almost independent of $\beta_{\text{BS,RN}}$ and $\beta_{\text{RN,MT}}$. This operating condition results in nearly optimal performance in the noise-limited regime, but in highly sub-optimal performance in the interference-limited regime. The condition $\beta_{\text{BS,MT}}/\beta_{\text{RN,MT}} \ll 1$, in fact, implies that $\beta_{\text{BS,MT}}$ is much smaller compared to $\beta_{\text{RN,MT}}$. Based on (3.1) and (3.2), as a consequence, the transmission occurs through those links providing the smallest path-loss. Based on *Remark 3.24* and *Remark 3.25*, this maximizes the coverage probability in the noise-limited regime, but it minimizes the coverage probability in the interference-limited regime. In the latter case, it would be better to serve the intended MT via a two-hop link in order to enjoy less interference thanks to the larger path-loss exponent of the RN-to-MT links. This apparent ambiguity originates from the sub-optimality of the choice $\mathcal{B}_{\text{BS}}/\mathcal{B}_{\text{RN}} = 1$ and, more in particular, from the fact that the bias coefficients \mathcal{B}_{BS} and \mathcal{B}_{RN} are *interference-*

and channel-independent. In order to ensure that relay-aided cellular networks are no worse than cellular networks, \mathcal{B}_{BS} and \mathcal{B}_{RN} need to be adequately optimized as a function of the path-loss exponents. In the presence of RNs, otherwise, the coverage probability may be worse than in the absence of RNs. By using the same line of thought, similar conclusions can be drawn for coverage/average rate. Given the cost of deploying RNs, this is not desirable. On the other hand, optimizing the cell association criterion based on the *instantaneous* aggregate other-cell interference would be impractical, due to the fact that the cell association of each BS will depend on the cell association of any other BS available in the network.

To overcome this complexity and to exploit the presence of RNs in the network, we propose an *end-to-end (system-level) and interference-aware optimization* criterion for the bias coefficients \mathcal{B}_{BS} and \mathcal{B}_{RN} . The idea consists of optimizing \mathcal{B}_{BS} and \mathcal{B}_{RN} based on the system-level mathematical formulation of the coverage probability, by taking into account the cell association as well. The optimization criterion turns out to be, as a result, *end-to-end* and *interference-aware*. It is, in addition, *practically affordable*, since it does not require the knowledge of the association pattern of the whole network at any BS. Let $\mathcal{B}_{\text{RN}} = 1$ for simplicity, but without loss of generality. In mathematical terms, the optimization problem can be formulated as follows:

$$\begin{aligned} & \mathcal{B}_{\text{BS}}^{(\text{opt})} \\ &= \arg \max_{\mathcal{B}_{\text{BS}} \in (0, +\infty)} \{P_{\text{cov}}(\mathbb{T}; \mathcal{B}_{\text{BS}}) = \mathcal{J}_{\text{BS,MT}}(\mathbb{T}; \mathcal{B}_{\text{BS}}) + \mathcal{J}_{\text{BS,RN}}(\mathbb{T}; \mathcal{B}_{\text{BS}}) \mathcal{J}_{\text{RN,MT}}(\mathbb{T}; \mathcal{B}_{\text{BS}})\} \end{aligned} \quad (3.30)$$

where $\mathcal{J}_{\text{BS,MT}}(\cdot; \cdot)$, $\mathcal{J}_{\text{BS,RN}}(\cdot; \cdot)$, $\mathcal{J}_{\text{RN,MT}}(\cdot; \cdot)$ are defined in (3.18) by making explicit the dependence on \mathcal{B}_{BS} and setting $\Theta_{\text{BS,MT}}(\mathbb{T}) = \Theta_{\text{BS,MT}}(\mathbb{T}; \mathcal{B}_{\text{BS}})$, $\Theta_{\text{BS,RN}}(\mathbb{T}) = \Theta_{\text{BS,RN}}(\mathbb{T}; \mathcal{B}_{\text{BS}})$, $\Theta_{\text{RN,MT}}(\mathbb{T}) = \Theta_{\text{RN,MT}}(\mathbb{T}; \mathcal{B}_{\text{BS}})$, as well as $\lambda_{\text{BS}}^{(\text{I,1hop})} = \lambda_{\text{BS}}^{(\text{I,1hop})}(\mathcal{B}_{\text{BS}}) = \lambda_{\text{BS}}^{(\text{I})} \chi_{1\text{hop}}(\mathcal{B}_{\text{BS}})$, $\lambda_{\text{BS}}^{(\text{I,2hop})} = \lambda_{\text{BS}}^{(\text{I,2hop})}(\mathcal{B}_{\text{BS}}) = \lambda_{\text{BS}}^{(\text{I})} (1 - \chi_{1\text{hop}}(\mathcal{B}_{\text{BS}}))$, $\chi_{1\text{hop}} = \chi_{1\text{hop}}(\mathcal{B}_{\text{BS}}) = \int_0^{+\infty} \left(1 - F_{\mathcal{Z}_{\text{RN}_0, \text{MT}_0}}(\eta_{\text{cell}}^{-1}(\mathcal{B}_{\text{BS}}) \xi)\right) f_{\mathcal{Z}_{\text{BS}_0, \text{MT}_0}}(\xi) d\xi$, $\eta_{\text{cell}} = \eta_{\text{cell}}(\mathcal{B}_{\text{BS}}) = \mathcal{B}_{\text{BS}} / (1 - K_T)$, finally, $f_{\mathcal{Z}_{\text{BS}_0, \text{MT}_0}}(\cdot)$ and $F_{\mathcal{Z}_{\text{BS}_0, \text{MT}_0}}(\cdot)$ are provided in (3.31).

Similar optimization problems may be formulated for coverage rate and average rate. They are not reported in this section due to space limitations, but the related performance is illustrated in Section 3.5.

Remark 3.26. In general, the optimization problem in (3.30) cannot be solved in closed-form and it is not even possible to prove its convexity/concavity properties. This usually arises in optimization problems, either involving or not the use of stochastic geometry. A recent example related to stochastic geometry modeling of cellular networks is discussed in [77], where closed-form solutions are shown not be available for general system setups, despite the fact that simpler utility functions than coverage and rate are studied. In practice, however, the optimal solution of (3.30) can be obtained numerically with the aid of the Mathematica built-in function `FindMaximum`. Similar to [77], numerical solutions of (3.30) can be efficiently computed. They, however, typically lead to local optima. The effectiveness of such numerical approach is validated in Section 3.5 with the aid of Monte Carlo simulations. Without loss of generality, in Section 3.5, the starting point of the search is assumed to be $\mathcal{B}_{\text{BS}}^{(0)} = 1$ and a large search space, *i.e.*, $(\mathcal{B}_{\text{BS}}^{(\min)}, \mathcal{B}_{\text{BS}}^{(\max)}) = (10^{-20}, 10^{20})$, is considered. From a practical standpoint, in fact, this would be equivalent to having $(\mathcal{B}_{\text{BS}}^{(\min)}, \mathcal{B}_{\text{BS}}^{(\max)}) = (0, +\infty)$. \square

Remark 3.27. Even though no closed-form solution of (3.30) for arbitrary parameters exists, $\mathcal{B}_{\text{BS}}^{(\text{opt})}$ can be computed in closed-form for some special cases. From corollaries and remarks in Section 3.4.1, this holds:

1. If $\lambda_{\text{BS}}^{(1)} \rightarrow 0$ (noise-limited setup) and $\beta_{\text{BS,MT}}/\beta_{\text{RN,MT}} \gg 1$, then $P_{\text{cov}}(\text{T}, \mathcal{B}_{\text{BS}}) \propto \exp\left(-\mathcal{B}_{\text{BS}}^{2/\beta_{\text{BS,MT}}}\right)$. This implies $\mathcal{B}_{\text{BS}}^{(\text{opt})} \rightarrow 0$, *i.e.*, the optimal setup is when all the MTs are served via a two-hop link. Accordingly, relay-aided cellular networks are expected to outperform cellular networks.
2. If $\lambda_{\text{BS}}^{(1)} \rightarrow 0$ (noise-limited setup) and $\beta_{\text{BS,MT}}/\beta_{\text{RN,MT}} \ll 1$, then $P_{\text{cov}}(\text{T}, \mathcal{B}_{\text{BS}}) \propto \exp\left(-\mathcal{B}_{\text{BS}}^{-2/\beta_{\text{RN,MT}}}\right)$. This implies $\mathcal{B}_{\text{BS}}^{(\text{opt})} \rightarrow \infty$, *i.e.*, the optimal setup is when all the MTs are served via a one-hop link. Accordingly, relay-aided cellular networks are expected to underperform cellular networks.
3. If $\sigma_N^2 \rightarrow 0$ (interference-limited setup) and $\beta_{\text{BS,MT}}/\beta_{\text{RN,MT}} \gg 1$, $P_{\text{cov}}(\text{T}, \mathcal{B}_{\text{BS}}) \propto \exp\left(-\mathcal{B}_{\text{BS}}^{-2/\beta_{\text{RN,MT}}}\right)$. This implies $\mathcal{B}_{\text{BS}}^{(\text{opt})} \rightarrow \infty$, *i.e.*, the optimal setup is when all the MTs are served via a one-hop link. Accordingly, relay-aided cellular networks are expected to underperform cellular networks.
4. If $\sigma_N^2 \rightarrow 0$ (interference-limited setup) and $\beta_{\text{BS,MT}}/\beta_{\text{RN,MT}} \ll 1$, $P_{\text{cov}}(\text{T}, \mathcal{B}_{\text{BS}}) \propto \exp\left(-\mathcal{B}_{\text{BS}}^{2/\beta_{\text{BS,MT}}}\right)$. This implies $\mathcal{B}_{\text{BS}}^{(\text{opt})} \rightarrow 0$, *i.e.*, the optimal setup is when all the

MTs are served via a two-hop link. Accordingly, relay-aided cellular networks are expected to outperform cellular networks. \square

The closed-form optimal solution of the case studies in *Remark 3.27* highlights two important conclusions: i) prioritization provides, in general, better performance than assuming $\mathcal{B}_{\text{BS}} = \mathcal{B}_{\text{RN}} = 1$ and ii) if prioritization is not used, relay-aided cellular networks may not outperform cellular networks for some system setups. These conclusions originate from the fact that, for the analyzed case studies, the setup $\mathcal{B}_{\text{BS}} = \mathcal{B}_{\text{RN}} = 1$ does not result in the optimal solution of (3.30). In Section 3.5, it is shown that relay-aided cellular networks are never worse than cellular networks and that the coverage probability is maximized if $\mathcal{B}_{\text{BS}}^{(\text{opt})}$ in (3.30) is used, regardless of the noise- or interference-limited operating regime and regardless of the triplet $(\beta_{\text{BS,MT}}, \beta_{\text{BS,RN}}, \beta_{\text{RN,MT}})$.

Remark 3.28. The optimization problem in (3.30) is based on a utility function that provides system-level performance of relay-aided cellular networks. As a consequence, it depends only on long-term statistics and, in particular, it does not require any local (instantaneous) channel and interference knowledge. In practice, the optimization problem in (3.30) is solved by a “higher hierarchy” entity, *e.g.*, a BS controller, which broadcasts the optimal bias coefficients to all BSs and RNs in the network. With these optimal bias coefficients at hand, the cell association criterion in (3.1) and (3.2) is subsequently applied without the need of local or network-level estimates of the other-cell interference. Accordingly, the computational complexity of the proposed system-level optimization is kept at a minimum. \square

By direct inspection of Table 3.2, in addition, the following conclusions as a function of the densities of BSs, RNs, MTs and of the number of RBs can be drawn.

- In the noise-limited regime, the coverage probability monotonically increases as λ_{BS} and λ_{RN} increase. This originates because $\mathcal{G}_{X,Y}^{(\lambda_{\text{BS}}^{(1)} \rightarrow 0)}(\cdot; \cdot)$ monotonically increases with λ_X .
- In the interference-limited regime, the coverage probability depends, in general, on the triplet of densities $(\lambda_{\text{BS}}, \lambda_{\text{RN}}, \lambda_{\text{MT}})$. In the saturated traffic load case, it is independent of the densities if the MTs are likely to be served via a one-hop link.
- In the interference-limited regime, the coverage probability is independent of the shadowing. This originates from $\mathcal{G}_{X,Y}^{(\sigma_N^2 \rightarrow 0)}(\cdot)$, which is independent of $\Upsilon_{X,Y}$. This

trend holds regardless of the densities of BSs, RNs and MTs, *i.e.*, regardless of the triplet $(\lambda_{\text{BS}}, \lambda_{\text{RN}}, \lambda_{\text{MT}})$.

- In the interference-limited regime, if the density of RNs is high enough, *i.e.*, $\lambda_{\text{RN}} \rightarrow +\infty$, and the density of BSs, λ_{BS} , is finite, then $\mathbb{P}_{\text{cov}}^{(\sigma_N^2 \rightarrow 0)}(\mathbb{T}) \rightarrow \mathcal{G}_{\text{BS,RN}}^{(\sigma_N^2 \rightarrow 0)}(\mathbb{T})$. In this case, in fact, the MTs are likely to be served via a two-hop link and $\mathcal{G}_{\text{RN,MT}}^{(\sigma_N^2 \rightarrow 0)}(\mathbb{T}) \rightarrow 1$. Thus, the coverage probability mainly depends on the BS-to-RN links.
- Let the light load model. In the interference-limited regime, the coverage probability tends to one, as $\lambda_{\text{BS}} \rightarrow +\infty$, $\lambda_{\text{RN}} \rightarrow +\infty$. In this case, in fact, $\mathcal{G}_{\text{BS,MT}}^{(\sigma_N^2 \rightarrow 0)}(\mathbb{T}) \rightarrow 1$, $\mathcal{G}_{\text{BS,RN}}^{(\sigma_N^2 \rightarrow 0)}(\mathbb{T}) \rightarrow 1$, $\mathcal{G}_{\text{RN,MT}}^{(\sigma_N^2 \rightarrow 0)}(\mathbb{T}) \rightarrow 1$.
- Let the light load model. In the interference-limited regime, the coverage probability increases as N_{RB} increases. If $N_{\text{RB}} \rightarrow +\infty$, the coverage probability tends to one.

Remark 3.29. By comparing the main performance trends of relay-aided ad hoc networks in [13] and [14] with those of relay-aided cellular networks that originate from Table 3.2, different conclusions can be drawn. In [13] and [14], it is proved that the end-to-end performance is mainly determined by the path-loss exponent of the interferers and that the path-loss exponents of the probe links have no impact on the asymptotic performance. In the present report, on the other hand, it is proved that the end-to-end performance depends on the triplet of path-loss exponents $(\beta_{\text{BS,MT}}, \beta_{\text{BS,RN}}, \beta_{\text{RN,MT}})$, as well as that the optimal bias coefficients from (3.30) are needed for ensuring that relay-aided cellular networks are no worse than cellular networks for arbitrary values of the triplet $(\beta_{\text{BS,MT}}, \beta_{\text{BS,RN}}, \beta_{\text{RN,MT}})$. These different trends originate from the fact that the distances of the probe links are fixed in [13] and [14], while they are random variables in the present report and depend on the cell association criterion in (3.1) and (3.2). \square

3.5 Numerical and Simulation Results

In this section, numerical examples to verify the accuracy of the proposed frameworks and to discuss the impact of several parameters on coverage and rate of relay-aided cellular networks are illustrated. To reduce the space, only some figures are shown. Similar trends are observed, however, for the missing figures.

Simulation Setup

The simulation parameters are in agreement with the LTE-A standard. Unless otherwise stated: $P_T = 45$ dBm, $K_T = 0.5$, $\mathcal{F}_{\text{dB}} = 10$ dB, $\nu = c_0/f_c$, where c_0 is the speed of light in meter/sec and $f_c = 2$ GHz is the carrier frequency, $\mu_{X,Y} = 0$ dB, $\sigma_{X,Y} = 4$ dB, $\Omega_{X,Y} = 1$, $B_W = 180$ kHz, $N_{\text{RB}} = 50$ for light traffic load, $\lambda_{\text{BS}} = 1/(\pi R_{\text{cell}}^2)$, where $R_{\text{cell}} = 200$ m is the average radius of a cell, $\lambda_{\text{RN}} = 3\lambda_{\text{BS}}$. Other parameters are in the captions of the figures. It is worth mentioning that $B_W = 180$ kHz is the transmission bandwidth of a RB in the LTE-A standard and that the pair $B_W = 180$ kHz and $N_{\text{RB}} = 50$ corresponds to a total transmission bandwidth of 10 MHz [28, Table 6.2].

Monte Carlo Simulations

System-level simulations are performed by carefully reproducing the system model of Section 3.2. It is worth mentioning, however, that *Approximations 3.1-3.5* are not enforced in the system-level simulator and that they are used only for developing the frameworks. To ensure saturated and light traffic load conditions, the density of the MTs in a generic RB is adequately chosen. For the considered setup, we have used the following densities per RB: $\lambda_{\text{MT}}^{(\text{RB})} = 50\lambda_{\text{BS}}$ for saturated traffic load and $\lambda_{\text{MT}}^{(\text{RB})} = (1/5)\lambda_{\text{BS}}$ for light traffic load. For each available MT, the cell association criterion in (3.1) and (3.2) is applied, as well as serving BS, RN and one- or two-hop links are identified. Then, the SINRs defined in Section 3.3 are computed for all the available MTs. The performance metrics are computed accordingly, based on the definitions available in Section 3.3.1. The final result is obtained by averaging the performance metric of interest with respect to all the available MTs (*i.e.*, it is *not* computed only for the MT closest to the origin).

Validation of *Approximations 3.1-3.4*

Based on *Approximations 3.1-3.4*, the set of interfering BSs, $\Phi_{\text{BS}}^{(I)}$, the set of interfering BSs serving the MTs via a one- and a two-hop link, $\Phi_{\text{BS}}^{(I,1\text{hop})}$ and $\Phi_{\text{BS}}^{(I,2\text{hop})}$, and the set of interfering RNs, $\Phi_{\text{RN}}^{(I)}$, are assumed to be homogeneous PPPs, even though they are not. In Fig. 3.4, the accuracy of these assumptions is investigated. To

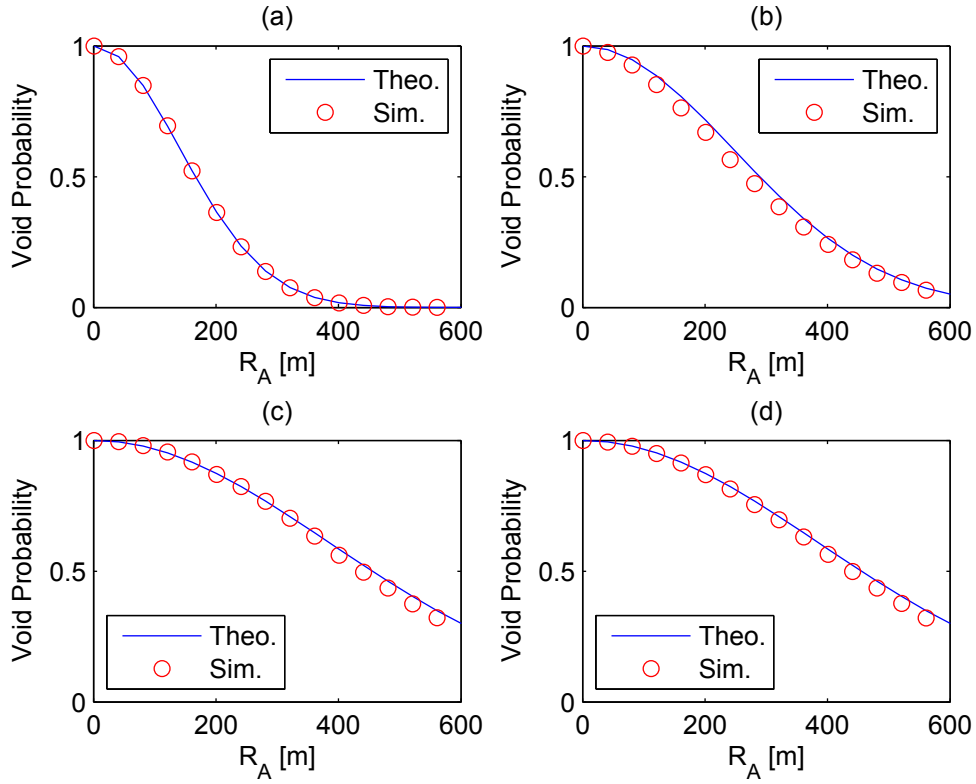


FIGURE 3.4: Void probability of $\Phi_{\text{BS}}^{(I)}$ (a), $\Phi_{\text{BS}}^{(I,1\text{hop})}$ (b), $\Phi_{\text{BS}}^{(I,2\text{hop})}$ (c), $\Phi_{\text{RN}}^{(I)}$ (d). Solid lines show the approximations and markers show Monte Carlo simulations. Setup: $\beta_{\text{BS,MT}} = \beta_{\text{BS,RN}} = \beta_{\text{RN,MT}} = 3.5$, $\mathcal{B}_{\text{BS}} = 1$. (a) and (b) refer to the saturated traffic load. (c) and (d) refer to the light traffic load.

this end, we exploit the void probability theorem of homogeneous PPPs [7, Theorem 1.1.5], which states that a point process Φ of density λ is a homogeneous PPP *if and only if*, for any region of area \mathcal{A} , the equality $\Pr\{\Phi(\mathcal{A}) = \emptyset\} = \exp(-\lambda\mathcal{A})$ holds. Assuming *Approximations 3.1-3.4* true, the following holds: $\Pr\{\Phi_{\text{BS}}^{(I,1\text{hop})}(\mathcal{A}) = \emptyset\} \approx \exp(-\lambda_{\text{BS}}^{(I,1\text{hop})}\mathcal{A})$, $\Pr\{\Phi_{\text{BS}}^{(I,2\text{hop})}(\mathcal{A}) = \emptyset\} \approx \exp(-\lambda_{\text{BS}}^{(I,2\text{hop})}\mathcal{A})$, $\Pr\{\Phi_{\text{RN}}^{(I)}(\mathcal{A}) = \emptyset\} \approx \exp(-\lambda_{\text{RN}}^{(I)}\mathcal{A})$, as well as $\Pr\{\Phi_{\text{BS}}^{(I)}(\mathcal{A}) = \emptyset\} \approx \exp(-\lambda_{\text{BS}}^{(I)}\mathcal{A})$ in the light load case and $\Pr\{\Phi_{\text{BS}}^{(I)}(\mathcal{A}) = \emptyset\} = \exp(-\lambda_{\text{BS}}^{(I)}\mathcal{A})$ in the full load case. For assessing the accuracy of *Approximations 3.1-3.4*, we compare these mathematical expressions of the void probabilities against those obtained via system-level Monte Carlo simulations, as described above. More specifically, once all the MTs are associated with their respective serving BSs and RNs, the set of active BSs and RNs for each RB are identified. Without loss of generality, we consider a region of area \mathcal{A} that is centered at the origin and of radius $R_{\mathcal{A}}$, *i.e.*, $\mathcal{A} = \pi R_{\mathcal{A}}^2$. This assumption does not bias the validation of the accuracy of *Approximations 3.1-3.4*. It just makes the simulations easier to be implemented and

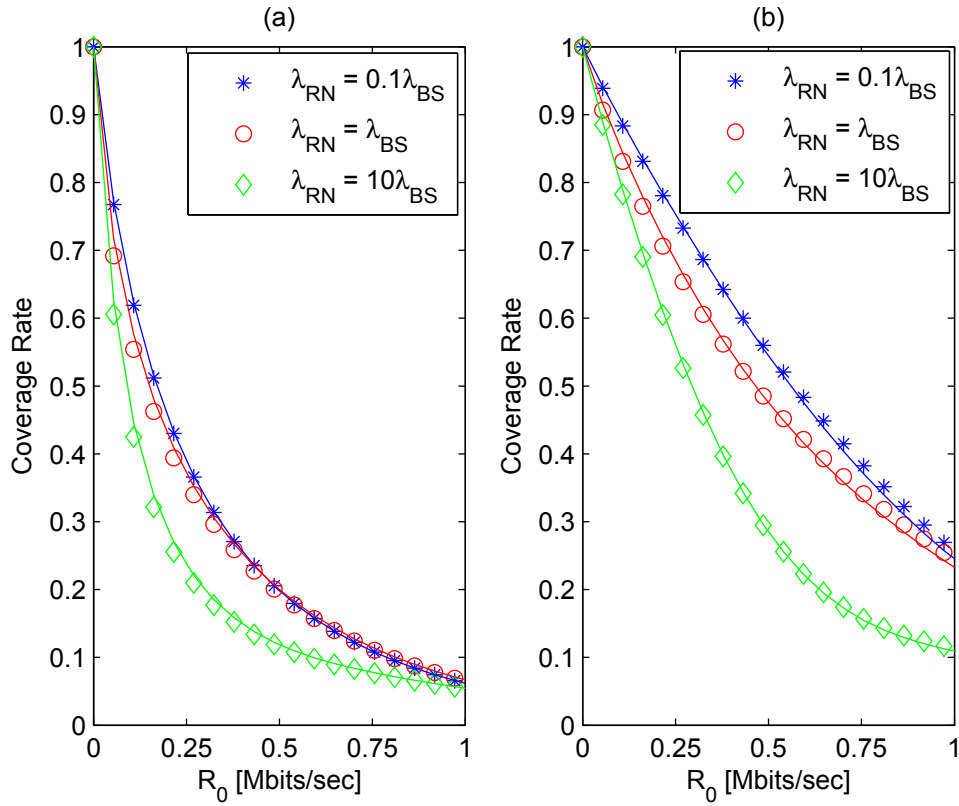


FIGURE 3.5: Coverage rate versus $\lambda_{\text{BS}}/\lambda_{\text{RN}}$. Solid lines show the frameworks and markers show Monte Carlo simulations. Setup: $\beta_{\text{BS,MT}} = \beta_{\text{BS,RN}} = \beta_{\text{RN,MT}} = 3.5$, $\mathcal{B}_{\text{BS}} = 1$. (a) and (b) refer to saturated and light traffic loads.

avoids the border effects that originate from the practical need of considering a finite simulation area. For each point process, the probability that no nodes fall in the ball of area $\mathcal{A} = \pi R_{\mathcal{A}}^2$ is computed, as a function of $R_{\mathcal{A}}$. This procedure is applied to each RB and the final empirical estimates of the void probabilities are obtained by computing the expectation with respect to the number of RBs. Theoretical (based on *Approximations 3.1-3.4*) and empirical void probabilities are illustrated in Fig. 3.4 for saturated and light traffic load models. The figure confirms that, even though, as expected, a gap exists, it is relatively small. More importantly, in addition, the shape of the void probability function is well captured by the proposed approximations. These findings substantiate the adoption of *Approximations 3.1-3.4* for system-level performance evaluation of relay-aided cellular networks.

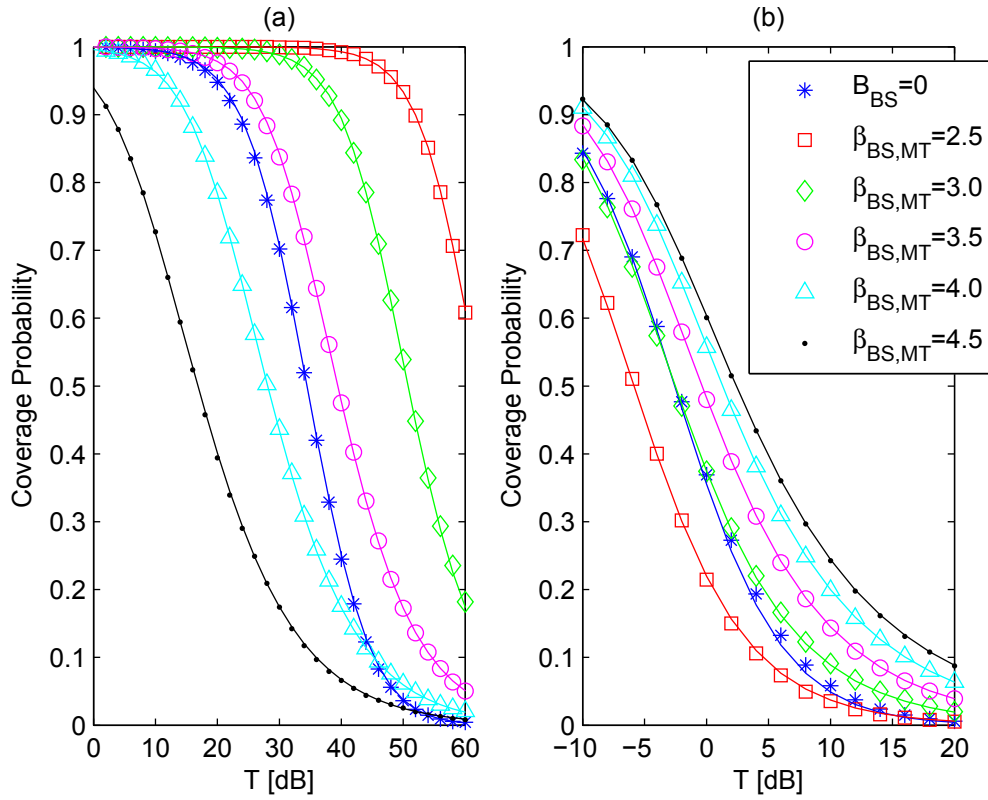


FIGURE 3.6: Coverage probability. Solid lines show the frameworks and markers show Monte Carlo simulations. (a) and (b) refer to noise-limited and saturated traffic load, respectively. Setup: $\beta_{BS,RN} = \beta_{RN,MT} = 3.5$. $\mathcal{B}_{BS} = 0$ corresponds to two-hop transmission. The other setups are for one-hop transmission, *i.e.*, $\mathcal{B}_{BS} = \infty$.

Validation of *Approximation 3.5*

In Section 3.4, it is mentioned that the accuracy of *Approximation 3.5* depends on the density of the RNs, as compared to that of the BSs. In Fig. 3.5, the accuracy of *Approximation 3.5*, as a function of the ratio $\lambda_{BS}/\lambda_{RN}$, is studied. As a case study, the coverage rate is considered. As anticipated in Section 3.4, Fig. 3.5 confirms that the accuracy of *Approximation 3.5* gets slightly better as $\lambda_{BS}/\lambda_{RN}$ either decreases or increases. We note, however, that the difference between the mathematical framework in Section 3.4 and Monte Carlo simulations is small, even for $\lambda_{BS}/\lambda_{RN} = 1$. This confirms the usefulness of *Approximation 3.5* for system-level performance evaluation of relay-aided cellular networks. All in all, Fig. 3.5 confirms that the proposed approach is accurate for arbitrary λ_{RN} .

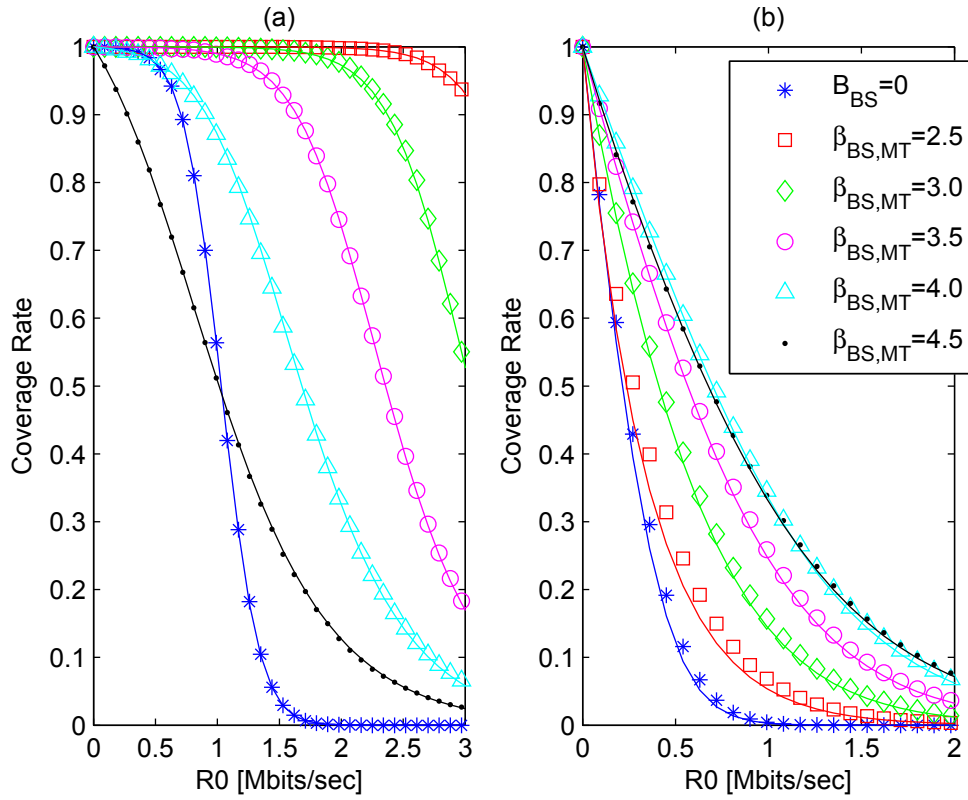


FIGURE 3.7: Coverage rate. Solid lines show the frameworks and markers show Monte Carlo simulations. (a) and (b) refer to noise-limited and light traffic load. Setup: $\beta_{BS,RN} = \beta_{RN,MT} = 3.5$. $\mathcal{B}_{BS} = 0$ corresponds to two-hop transmission. The other setups are for one-hop transmission, *i.e.*, $\mathcal{B}_{BS} = \infty$.

Coverage Probability and Rate: Framework Validation and Performance Trends

In Figs. 3.6 and 3.7, coverage probability and rate are illustrated, respectively. The objective of these figures is threefold: i) to validate the accuracy of the frameworks, ii) to highlight the differences between noise- and interference-limited relay-aided cellular networks, and iii) to highlight advantages and limitations of one- and two-hop transmission. The curves labeled $\mathcal{B}_{BS} = 0$ are obtained by forcing the relay-aided cellular network to serve all the MTs via a two-hop link. All the other curves are obtained by setting $\mathcal{B}_{BS} = \infty$, *i.e.*, by forcing the relay-aided cellular network to serve all the MTs via a one-hop link. In agreement with the conclusions drawn in Section 3.4.3, it is apparent that noise- and interference-limited networks have almost opposite performance trends. Two-hop cellular networks are not necessarily better than their one-hop counterpart, and the superiority of one- or two-hop transmission depends on the path-loss exponents. Figure 3.7, in particular, highlights that the coverage rate of two-hop transmission may

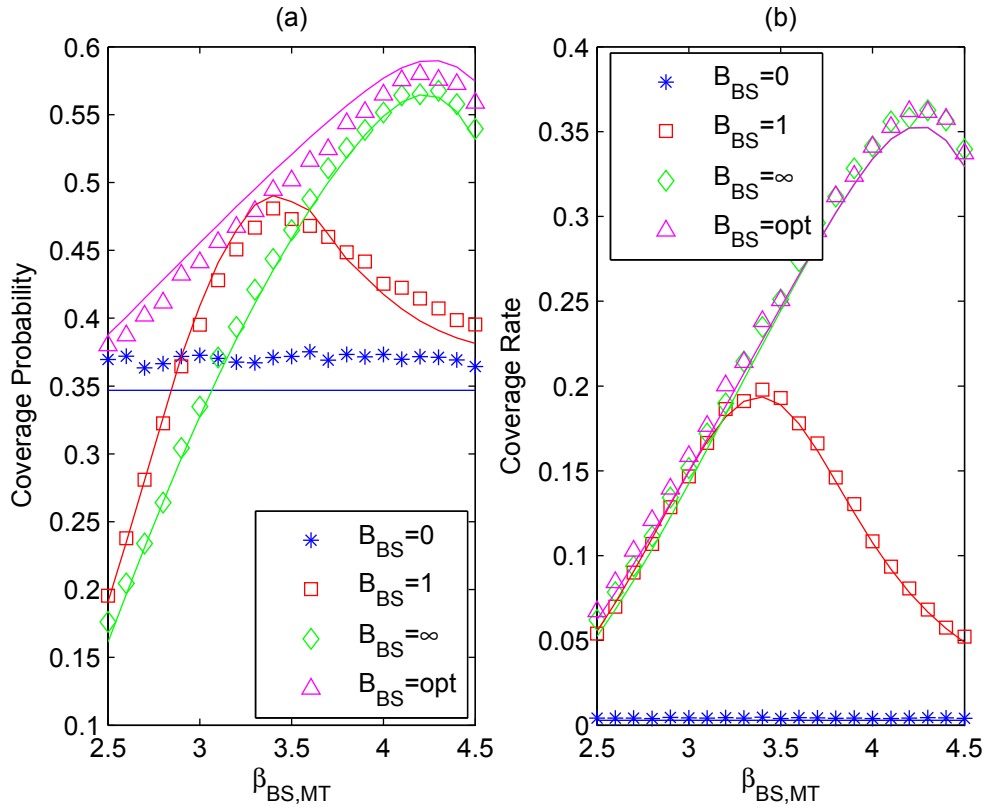


FIGURE 3.8: Coverage probability (a) and rate (b). Solid lines show the frameworks and markers show Monte Carlo simulations. Setup: $\beta_{BS,RN} = \beta_{RN,MT} = 3.5$, $T = 10$ dB in (a), $R_0 = 1$ Mbits/sec in (b), light traffic load in (a) and (b).

be better than that of one-hop transmission in the noise-limited scenario. Because of the need of two time-slots, however, this never occurs, for the considered set of parameters, in the interference-limited scenario. These trends confirm the need of the system-level optimization in (3.30), as well as the need of taking the other-cell interference into account for an accurate performance assessment and optimization of relay-aided cellular networks.

System-Level Optimization: Impact of the Path-Loss Exponents

In Figs. 3.8 and 3.9, coverage probability, coverage rate and average rate as a function of the path-loss exponents are illustrated. The objective of these figures is to assess the advantages of the system-level optimization in (3.30) and of the prioritization (end-to-end *interference-awareness*) in (3.2). To this end, four case studies are investigated: i) $\mathcal{B}_{BS} = 0$, which corresponds to a setup where all the MTs are served via a two-hop link, ii) $\mathcal{B}_{BS} = 1$, which corresponds to a setup without one- vs. two-hop prioritization, ii)

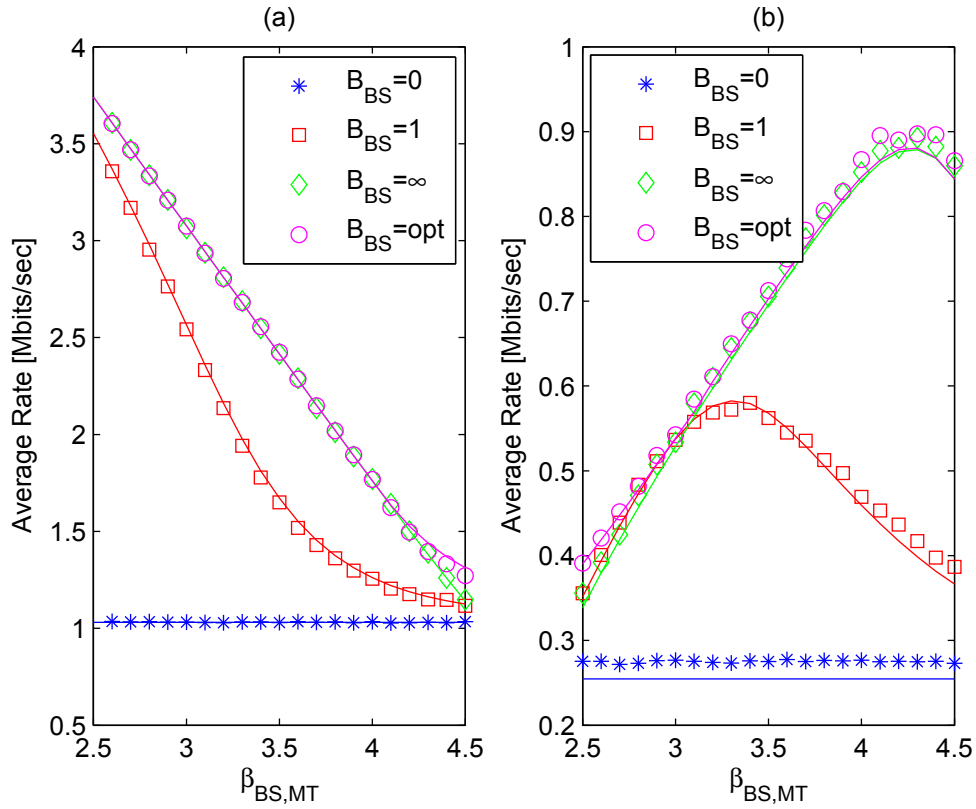


FIGURE 3.9: Average rate. Solid lines show the frameworks and markers show Monte Carlo simulations. (a) and (b) refer to noise-limited and saturated traffic load, respectively. Setup: $\beta_{BS,RN} = \beta_{RN,MT} = 3.5$.

$B_{BS} = \infty$, which boils down to a cellular network in the absence of RNs, and iv) $B_{BS} = opt$, which corresponds to the end-to-end optimal solution of (3.30). The figures confirm the need of system-level optimization and of the prioritization in (3.2) for improving the performance and for overcoming the sub-optimality of a cell association criterion that neglects the other-cell interference. It worth nothing that this holds in the noise-limited scenario as well (see Fig. 3.9 (a)), since the impact of using two-slots is not taken into account in (3.2). Again, the trends of noise- and interference-limited regimes are different. Figure 3.8 (a) confirms that the presence of RNs is more advantageous from the coverage probability standpoint. From the coverage/average rate standpoint, on the other hand, the optimal operating setup according to (3.30) is always close to that corresponding to cellular networks without using the RNs. The better coverage probability shown in Fig. 3.8 (a), however, highlights that cell-edge MTs may still benefit from half-duplex relaying based on repetition coding, if the main objective is to improve the quality of the received signal.

In general, one may find from Figure 3.6–3.9 that half-duplex relaying is not beneficial in cellular networks for many case studies when the system is interference-limited. This disappointing result can be understood as follows: the main benefit of implementing relays in cellular networks is the enhancement of the useful signals for cell-edge users to compensate the severe channel attenuation. When the network is interference-limited, this compensation on the intended signal is negated by the interference caused by the relays. Moreover, in the system model under consideration, a half-duplex relaying protocol, which requires two time-slots for transmission, is assumed and the relays are assumed to be randomly planned in the cellular networks, which are not optimal scheme in terms of the performance.

Nevertheless, the deployment of relays may still be desirable, for example, in the urban micro cellular networks where the channel model is subject to LOS or NLOS propagation as discussed in detail in Chapter 4. When the LOS/NLOS link states have been taken into account, the enhancement on the intended signal, thanks to the relays, would overtake the increase of interference since the intended links are more likely to be in LOS state than those interfering links. Another possible approach to highlight the additional potential of relaying cellular networks is by implementing the directional antennas at the relays which enhance the useful signal, and as a byproduct, reduce the other-cell interference. Instead of the interference isolation, the full-duplex relaying [78] might significantly outperforms its half-duplex counterpart as well. When full-duplex relays are considered, the transmission process is completed in one time-slot, and the interference seen by the MTs originates from both the active BSs and the active relays. In addition, the selected serving relays see the interference from the other cell BSs and relays as well. The spatial and temporal correlation between the aggregate interference at the relay nodes and at the MTs are unprecedented in half-duplex relaying cellular networks, and the validity of the proposed approximations in the chapter is questionable in the full-duplex architecture. These are interesting avenues of future work.

3.6 Conclusion

In this chapter, end-to-end coverage and rate of relay-aided cellular networks have been investigated with the aid of an abstraction model based on stochastic geometry theory. With the aid of some system-level approximations, whose accuracy has been

validated with the aid of Monte Carlo simulations, mathematically tractable expressions have been obtained, which are formulated either in integral- or in closed-form. Direct inspection of the obtained frameworks and numerical results has revealed that, in the interference-limited regime, the presence of RNs may not be always beneficial for some performance metrics and parameters setup. To overcome this limitation, a system-level and interference-aware optimization criterion of the bias coefficients used for one- or two-hop protocol selection has been proposed. The idea consists of tuning the bias coefficients in order to maximize the end-to-end coverage and rate. The accuracy of the proposed system-level modeling and the gain provided by the proposed system-level optimization have been substantiated with the aid of Monte Carlo simulations for various operating conditions. The numerical results show that, by optimizing the bias coefficients, relay-aided cellular networks are no worse than cellular networks, but in some cases the optimal biases correspond to the setup where all the MTs are served via one-hop links.

Appendix

3.A Lemma 3.1, Lemma 3.2 and Lemma 3.3

Lemma 3.1. Let $Z_{X_0, Y_0} = l(r_{X_0, Y_0})/S_{X_0, Y_0}$, where $X_0 = \arg \min_{X_i \in \Phi_X} \left\{ \frac{l(r_{X_i, Y_0})}{\varsigma S_{X_i, Y_0}} \right\}$, Φ_X is a homogeneous PPP of density λ_X , ς is a positive constant, $l(r_{X_i, Y_0}) = \kappa_0 r_{X_i, Y_0}^{\beta_{X, Y_0}}$ for $X_i \in \Phi_X$ with $\kappa_0 > 0$ and $\beta_{X, Y_0} > 2$, and S_{X_i, Y_0} for $X_i \in \Phi_X$ are i.i.d. log-normal random variables with parameters $(\mu_{X, Y_0}, \sigma_{X, Y_0}^2)$. The cumulative distribution function and the probability density function of Z_{X_0, Y_0} can be formulated as:

$$\begin{aligned}
 F_{Z_{X_0, Y_0}}(x) &= \Pr \{Z_{X_0, Y_0} \leq x\} = 1 - \exp \left(-\pi \lambda_X \kappa_0^{-2/\beta_{X, Y_0}} \Upsilon_{X, Y_0} x^{2/\beta_{X, Y_0}} \right) \\
 f_{Z_{X_0, Y_0}}(\xi) &= dF_{Z_{X_0, Y_0}}(x) / dx \Big|_{x=\xi} \\
 &= \left(2\pi \lambda_X \kappa_0^{-2/\beta_{X, Y_0}} \Upsilon_{X, Y_0} \xi^{2/\beta_{X, Y_0} - 1} / \beta_{X, Y_0} \right) \\
 &\quad \times \exp \left(-\pi \lambda_X \kappa_0^{-2/\beta_{X, Y_0}} \Upsilon_{X, Y_0} \xi^{2/\beta_{X, Y_0}} \right)
 \end{aligned} \tag{3.31}$$

where Υ_{X,Y_0} is defined as follows:

$$\Upsilon_{X,Y_0} = \exp \left(\frac{1}{10 \log_{10}(e)} \frac{2}{\beta_{X,Y_0}} \mu_{X,Y_0} + \frac{1}{2} \left(\frac{1}{10 \log_{10}(e)} \frac{2}{\beta_{X,Y_0}} \right)^2 \sigma_{X,Y_0}^2 \right) \quad (3.32)$$

Proof: It follows using a methodology similar to [76, Sec. II-A]. By definition, $\mathcal{Z}_{X_0,Y_0} = l(r_{X_0,Y_0})/S_{X_0,Y_0} = \min_{X_i \in \Phi_X} \{l(r_{X_i,Y_0})/(\varsigma S_{X_i,Y_0})\} = \min_{X_i \in \Phi_X} \{l(r_{X_i,Y_0})/S_{X_i,Y_0}\}$, since ς is a constant independent of $X_i \in \Phi_X$. Let the point process of the ratio of path-loss and shadowing be defined as $\mathcal{Z}_{Y_0} = \{l(r_{X_i,Y_0})/(S_{X_i,Y_0})\}_{X_i \in \Phi_X}$. By invoking the displacement theorem of PPPs [7, Th. 1.10], \mathcal{Z}_{Y_0} can be interpreted as a transformation of Φ_X , which is still a PPP on \mathbb{R}^+ . Its intensity measure, in particular, can be formulated, by definition, as:

$$\begin{aligned} \Lambda_{\mathcal{Z}_{Y_0}}([0, x]) &= \Pr \left\{ \frac{l(r_{X_i,Y_0})}{S_{X_i,Y_0}} \in [0, x], X_i \in \Phi_X \right\} \\ &\stackrel{(a)}{=} 2\pi \lambda_X \mathbb{E}_{S_{X_i,Y_0}} \left\{ \int_0^{\left(\frac{S_{X_i,Y_0} x}{\kappa_0}\right)^{1/\beta_{X,Y_0}}} r dr \right\} \\ &\stackrel{(b)}{=} \pi \lambda_X (x/\kappa_0)^{2/\beta_{X,Y_0}} \mathbb{E}_{S_{X_i,Y_0}} \left\{ S_{X_i,Y_0}^{2/\beta_{X,Y_0}} \right\} \\ &\stackrel{(c)}{=} \pi \lambda_X (x/\kappa_0)^{2/\beta_{X,Y_0}} \Upsilon_{X,Y_0} \end{aligned} \quad (3.33)$$

where (a) follows from the displacement theorem of PPPs, (b) follows from the computation of the integral, and (c) follows by introducing $\Upsilon_{X,Y_0} = \mathbb{E}_{S_{X_i,Y_0}} \left\{ S_{X_i,Y_0}^{2/\beta_{X,Y_0}} \right\}$, which is the fractional moment of a log-normal random variable. Υ_{X,Y_0} can be computed in closed-form from [4, Eq. (2.55)], as shown in (3.32). The cumulative distribution function of \mathcal{Z}_{X_0,Y_0} in (3.31) follows from the void probability theorem of PPPs [76, Corollary 6], i.e., $F_{\mathcal{Z}_{X_0,Y_0}}(x) = \Pr \{ \mathcal{Z}_{X_0,Y_0} \leq x \} = 1 - \exp \left(-\Lambda_{\mathcal{Z}_{Y_0}}([0, x]) \right)$. Its probability density function in (3.31) follows by computing the first derivative of the cumulative distribution function. \square

Remark 3.30. The Cumulative Distribution Functions (CDFs) and PDFs of $\mathcal{Z}_{\text{BS}_0, \text{MT}_0}$, $\mathcal{Z}_{\text{BS}_{\text{R}_0}, \text{RN}_0}$ and $\mathcal{Z}_{\text{RN}_0, \text{MT}_0}$ can be obtained from (3.31) by setting the quadruplet of parameters $(\lambda_X, \beta_{X,Y_0}, \mu_{X,Y_0}, \sigma_{X,Y_0}^2)$ as $(\lambda_{\text{BS}}, \beta_{\text{BS,MT}}, \mu_{\text{BS,MT}}, \sigma_{\text{BS,MT}}^2)$, $(\lambda_{\text{BS}}, \beta_{\text{BS,RN}}, \mu_{\text{BS,RN}}, \sigma_{\text{BS,RN}}^2)$, and $(\lambda_{\text{RN}}, \beta_{\text{RN,MT}}, \mu_{\text{RN,MT}}, \sigma_{\text{RN,MT}}^2)$, respectively. This directly follows from (3.1). \square

Lemma 3.2. Let $\chi_{1\text{hop}}(\cdot)$ and $\chi_{2\text{hop}}(\cdot)$ in (3.14), where BS_0 and RN_0 are defined in (3.1). Let $\eta_{\text{cell}} = (\mathcal{B}_{\text{BS}} P_T) / (\mathcal{B}_{\text{RN}} (1 - K_T) P_T)$. The following results hold:

$$\begin{aligned}\chi_{1\text{hop}}(\mathcal{Z}_{\text{BS}_0, \text{MT}_0}) &= 1 - F_{\mathcal{Z}_{\text{RN}_0, \text{MT}_0}}(\eta_{\text{cell}}^{-1} \mathcal{Z}_{\text{BS}_0, \text{MT}_0}) \\ \chi_{2\text{hop}}(\mathcal{Z}_{\text{RN}_0, \text{MT}_0}) &= 1 - F_{\mathcal{Z}_{\text{BS}_0, \text{MT}_0}}(\eta_{\text{cell}} \mathcal{Z}_{\text{RN}_0, \text{MT}_0})\end{aligned}\quad (3.34)$$

where $F_{\mathcal{Z}_{\text{BS}_0, \text{MT}_0}}(\cdot)$ and $F_{\mathcal{Z}_{\text{RN}_0, \text{MT}_0}}(\cdot)$ are defined in Lemma 3.1 and Remark 3.30.

Proof: By definition, it follows from Lemma 3.1. \square

Lemma 3.3. Let the cell association criterion in (3.1) and (3.2). The probabilities that MT_0 is served via a one- and a two-hop link can be formulated as follows:

$$\begin{aligned}\chi_{1\text{hop}} &= \Pr \left\{ \frac{l(r_{\text{BS}_0, \text{MT}_0})}{\mathcal{B}_{\text{BS}} P_T S_{\text{BS}_0, \text{MT}_0}} \leq \frac{l(r_{\text{RN}_0, \text{MT}_0})}{\mathcal{B}_{\text{RN}} (1 - K_T) P_T S_{\text{RN}_0, \text{MT}_0}} \right\} \\ &= \int_0^{+\infty} \left(1 - F_{\mathcal{Z}_{\text{RN}_0, \text{MT}_0}}(\eta_{\text{cell}}^{-1} \xi) \right) f_{\mathcal{Z}_{\text{BS}_0, \text{MT}_0}}(\xi) d\xi\end{aligned}\quad (3.35)$$

and $\chi_{2\text{hop}} = 1 - \chi_{1\text{hop}}$, where $F_{\mathcal{Z}_{\text{BS}_0, \text{MT}_0}}(\cdot)$, $f_{\mathcal{Z}_{\text{BS}_0, \text{MT}_0}}(\cdot)$, $F_{\mathcal{Z}_{\text{RN}_0, \text{MT}_0}}(\cdot)$ and $f_{\mathcal{Z}_{\text{RN}_0, \text{MT}_0}}(\cdot)$ are defined in Lemma 3.1 and Remark 3.30, as well as $\eta_{\text{cell}} = (\mathcal{B}_{\text{BS}} P_T) / (\mathcal{B}_{\text{RN}} (1 - K_T) P_T)$.

Proof: It follows from (3.34) of Lemma 3.2, since, by definition, $\chi_{1\text{hop}} = \mathbb{E}_{\mathcal{Z}_{\text{BS}_0, \text{MT}_0}} \{ \chi_{1\text{hop}}(\mathcal{Z}_{\text{BS}_0, \text{MT}_0}) \}$. The condition $\chi_{1\text{hop}} + \chi_{2\text{hop}} = 1$ holds by definition as well. \square

Remark 3.31. If $\beta_{\text{BS}, \text{MT}} / \beta_{\text{RN}, \text{MT}}$ can be written as the ratio of two positive integers, the integral in (3.35) can be formulated in closed-form in terms of the Meijer G-function with the aid of the Mellin-Barnes integration theorem [3, Eq. (2.24.1.1)]. Further comments are available in Remark 3.20 as well. \square

3.B Proofs of Proposition 3.1

By direct inspection of (3.9) and (3.17), Proposition 3.1 follows by proving the two following identities: $\mathbb{E}_{\mathcal{Z}_{\text{RN}_0, \text{MT}_0}} \left\{ \text{P}_{\text{cov}}^{(2\text{hop})}(\text{T}; \mathcal{Z}_{\text{RN}_0, \text{MT}_0}) \right\} \approx \mathcal{J}_{\text{BS}, \text{RN}}(\text{T}) \mathcal{J}_{\text{RN}, \text{MT}}(\text{T})$ as well as $\mathbb{E}_{\mathcal{Z}_{\text{BS}_0, \text{MT}_0}} \left\{ \text{P}_{\text{cov}}^{(1\text{hop})}(\text{T}; \mathcal{Z}_{\text{BS}_0, \text{MT}_0}) \right\} \approx \mathcal{J}_{\text{BS}, \text{MT}}(\text{T})$. The “ \approx ” signs originate from Approximations 3.1-3.5. Approximation 3.5 is not used for $\mathcal{J}_{\text{BS}, \text{MT}}(\cdot)$.

The first identity can be proved as follows. From (3.10) and Lemma 3.2, the following holds:

$$\begin{aligned} & \mathbb{E}_{\mathcal{Z}_{\text{BS}_0, \text{MT}_0}} \left\{ \mathbb{P}_{\text{cov}}^{(1\text{hop})} (\mathbf{T}; \mathcal{Z}_{\text{BS}_0, \text{MT}_0}) \right\} \\ &= \mathbb{E}_{\mathcal{Z}_{\text{BS}_0, \text{MT}_0}} \left\{ \Pr \{ \text{SINR}_{\text{BS}_0, \text{MT}_0} > \mathbf{T} \mid \mathcal{Z}_{\text{BS}_0, \text{MT}_0} \} \chi_{1\text{hop}} (\mathcal{Z}_{\text{BS}_0, \text{MT}_0}) \right\} \end{aligned} \quad (3.36)$$

The expectation $\mathbb{E}_{\mathcal{Z}_{\text{BS}_0, \text{MT}_0}} \{ \cdot \}$ corresponds to the integral with respect to y in (3.18).

The rest of the proof can be obtained from the equalities as follows:

$$\begin{aligned} & \Pr \{ \text{SINR}_{\text{BS}_0, \text{MT}_0} > \mathbf{T} \mid \mathcal{Z}_{\text{BS}_0, \text{MT}_0} \} \\ & \stackrel{(a)}{=} \Pr \left\{ |h_{\text{BS}_0, \text{MT}_0}|^2 > \frac{\mathcal{Z}_{\text{BS}_0, \text{MT}_0} \mathbf{T}}{P_{\text{BS}_0}} \left(\sigma_N^2 + \mathcal{I}_{\text{BS}_0 \rightarrow \text{MT}_0}^{(1+2)} (\mathcal{Z}_{\text{BS}_0, \text{MT}_0}) \right) \mid \mathcal{Z}_{\text{BS}_0, \text{MT}_0} \right\} \\ & \stackrel{(b)}{=} \mathbb{E}_{(\cdot) \setminus \mathcal{Z}_{\text{BS}_0, \text{MT}_0}} \left\{ \exp \left(-\frac{\mathcal{Z}_{\text{BS}_0, \text{MT}_0} \mathbf{T}}{P_{\text{BS}_0} \Omega_{\text{BS}, \text{MT}}} \left(\sigma_N^2 + \mathcal{I}_{\text{BS}_0 \rightarrow \text{MT}_0}^{(1+2)} (\mathcal{Z}_{\text{BS}_0, \text{MT}_0}) \right) \right) \right\} \\ & \stackrel{(c)}{\approx} \exp \left(-\frac{\mathcal{Z}_{\text{BS}_0, \text{MT}_0} \sigma_N^2 \mathbf{T}}{P_{\text{BS}_0} \Omega_{\text{BS}, \text{MT}}} \right) \mathbb{E}_{(\cdot) \setminus \mathcal{Z}_{\text{BS}_0, \text{MT}_0}} \left\{ \exp \left(-\frac{\mathcal{Z}_{\text{BS}_0, \text{MT}_0} \mathbf{T}}{P_{\text{BS}_0} \Omega_{\text{BS}, \text{MT}}} \mathcal{I}_{\text{BS}_0 \rightarrow \text{MT}_0}^{(1+2)} (\mathcal{Z}_{\text{BS}_0, \text{MT}_0}) \right) \right\} \end{aligned} \quad (3.37)$$

where $\mathcal{I}_{\text{BS}_0 \rightarrow \text{MT}_0}^{(1+2)} (\mathcal{Z}_{\text{BS}_0, \text{MT}_0}) = \mathcal{I}_{\text{BS}_0 \rightarrow \text{MT}_0}^{(1\text{hop})} (\mathcal{Z}_{\text{BS}_0, \text{MT}_0}) + \mathcal{I}_{\text{BS}_0 \rightarrow \text{MT}_0}^{(2\text{hop})} (\mathcal{Z}_{\text{BS}_0, \text{MT}_0})$, (a) follows from (3.3), (b) follows from the complementary cumulative distribution function of exponential random variables, *i.e.*, $\Pr \{ |h_{\text{BS}_0, \text{MT}_0}|^2 > x \} = \exp(-x/\Omega_{\text{BS}, \text{MT}})$ and (c) follows from the independence, by assumption, of $\Phi_{\text{BS}}^{(1,1\text{hop})}$ and $\Phi_{\text{BS}}^{(1,2\text{hop})}$, as stated in Approximation 3.1 and Approximation 3.3.

The expectations $\mathbb{E}_{(\cdot) \setminus \mathcal{Z}_{\text{BS}_0, \text{MT}_0}} \{ \cdot \}$ can be computed as follows:

$$\begin{aligned} & \mathbb{E}_{(\cdot) \setminus \mathcal{Z}_{\text{BS}_0, \text{MT}_0}} \left\{ \exp \left(-\frac{\mathcal{Z}_{\text{BS}_0, \text{MT}_0} \mathbf{T}}{P_{\text{BS}_0} \Omega_{\text{BS}, \text{MT}}} \mathcal{I}_{\text{BS}_0 \rightarrow \text{MT}_0}^{(1\text{hop})} (\mathcal{Z}_{\text{BS}_0, \text{MT}_0}) \right) \right\} \\ & \approx \exp \left(-\mathbb{E}_{|h_{\text{BS}_i, \text{MT}_0}|^2} \left\{ \int_{\mathcal{Z}_{\text{BS}_0, \text{MT}_0}}^{+\infty} \left(1 - \exp \left(-\frac{P_{\text{BS}_i}^{(1\text{hop})} \mathcal{Z}_{\text{BS}_0, \text{MT}_0} \mathbf{T} |h_{\text{BS}_i, \text{MT}_0}|^2}{P_{\text{BS}_0} \Omega_{\text{BS}, \text{MT}} x} \right) \right) dx \right. \right. \\ & \quad \left. \left. \times \Lambda_{\mathcal{Z}_{\text{MT}_0}}^{(1)} ([0, x]) \right\} \right) \end{aligned} \quad (3.38)$$

which is obtained by using the Probability Generating Functional (PGFL) theorem of PPPs [7, Proposition 1.2.2], where, from (3.33), the following holds:

$$\begin{aligned}\Lambda_{\mathcal{Z}_{\text{MT}_0}}([0, x]) &= \pi \lambda_{\text{BS}}^{(\text{I}, \text{1hop})} (x/\kappa_0)^{2/\beta_{\text{BS}, \text{MT}}} \Upsilon_{\text{BS}, \text{MT}_0} \\ \Lambda_{\mathcal{Z}_{\text{MT}_0}}^{(1)}([0, x]) &= d\Lambda_{\mathcal{Z}_{\text{MT}_0}}([0, x])/dx \\ &= (2/\beta_{\text{BS}, \text{MT}}) \pi \lambda_{\text{BS}}^{(\text{I}, \text{1hop})} (1/\kappa_0)^{2/\beta_{\text{BS}, \text{MT}}} x^{2/\beta_{\text{BS}, \text{MT}}-1} \Upsilon_{\text{BS}, \text{MT}_0}\end{aligned}\quad (3.39)$$

with $\Upsilon_{\text{BS}, \text{MT}_0}$ being defined in (3.32) and $P_{\text{BS}_i}^{(\text{1hop})} = P_{\text{BS}_0} = P_T$.

The other expectation can be obtained with similar steps by using the substitutions $P_{\text{BS}_i}^{(\text{1hop})} \rightarrow P_{\text{BS}_j}^{(\text{2hop})} = P_{\text{BS}_{\text{R}_0}} = K_T P_T$ and $\lambda_{\text{BS}}^{(\text{I}, \text{1hop})} \rightarrow \lambda_{\text{BS}}^{(\text{I}, \text{2hop})}$. The approximation in (3.38) originates from the PPP assumption for the interfering BSs, as stated in *Approximation 3.1* and *Approximation 3.3*.

The final expression of $\mathcal{J}_{\text{BS}, \text{MT}}(\cdot)$ follows by using the notable integrals:

$$\begin{aligned}\int_{\mathcal{X}}^{+\infty} (1 - \exp(-\mathcal{A}/x)) x^{2/\beta-1} dx &= -(\beta/2) \mathcal{X}^{2/\beta} (1 - {}_1F_1(-2/\beta; 1 - 2/\beta; -\mathcal{A}/\mathcal{X})) \\ \mathbb{E}_{|h|^2} \left\{ {}_1F_1\left(-2/\beta; 1 - 2/\beta; -\mathcal{Y}|h|^2\right) \right\} &= {}_2F_1(1, -2/\beta; 1 - 2/\beta; -\mathcal{Y}\Omega)\end{aligned}\quad (3.40)$$

where $\mathcal{A} > 0$, $\mathcal{X} > 0$, $\beta > 2$ and $|h|^2$ is an exponential random variable with mean square value Ω .

The second identity can be proved as follows. From (3.10) and *Lemma 3.2*, the following holds:

$$\begin{aligned}& \mathbb{E}_{\mathcal{Z}_{\text{RN}_0, \text{MT}_0}} \left\{ \mathbf{P}_{\text{cov}}^{(\text{2hop})}(\text{T}; \mathcal{Z}_{\text{RN}_0, \text{MT}_0}) \right\} \\ &= \mathbb{E}_{\mathcal{Z}_{\text{RN}_0, \text{MT}_0}} \left\{ \Pr \left\{ \text{SINR}_{\text{BS}_{\text{R}_0}, \text{RN}_0} > \text{T} \text{ and } \text{SINR}_{\text{RN}_0, \text{MT}_0} > \text{T} \mid \mathcal{Z}_{\text{RN}_0, \text{MT}_0} \right\} \right. \\ & \quad \left. \times \chi_{\text{2hop}}(\mathcal{Z}_{\text{RN}_0, \text{MT}_0}) \right\}\end{aligned}\quad (3.41)$$

The expectation $\mathbb{E}_{\mathcal{Z}_{\text{RN}_0, \text{MT}_0}} \{\cdot\}$ corresponds to the integral with respect to y in (3.18). In the following, thus, we focus our attention on the joint probability $\Pr \left\{ \text{SINR}_{\text{BS}_{\text{R}_0}, \text{RN}_0} > \text{T} \text{ and } \text{SINR}_{\text{RN}_0, \text{MT}_0} > \text{T} \mid \mathcal{Z}_{\text{RN}_0, \text{MT}_0} \right\}$. As for $\text{SINR}_{\text{RN}_0, \text{MT}_0}$, its definition in (3.7) is used. As for $\text{SINR}_{\text{BS}_{\text{R}_0}, \text{RN}_0}$, its approximated expression in (3.15) is used, *i.e.*, *Approximation 3.5*. Let us denote the number of interfering BSs and RNs as $\mathcal{K}_{\text{BS}}^{(\text{I}, \text{1hop})} = \text{card} \left\{ \Phi_{\text{BS}}^{(\text{I}, \text{1hop})} \right\}$,

$\mathcal{K}_{\text{BS}}^{(\text{I},2\text{hop})} = \text{card} \left\{ \Phi_{\text{BS}}^{(\text{I},2\text{hop})} \right\}$, $\mathcal{K}_{\text{BS}}^{(\text{I})} = \text{card} \left\{ \Phi_{\text{BS}}^{(\text{I})} \right\} = \mathcal{K}_{\text{BS}}^{(\text{I},1\text{hop})} + \mathcal{K}_{\text{BS}}^{(\text{I},2\text{hop})}$ and $\mathcal{K}_{\text{RN}}^{(\text{I})} = \mathcal{K}_{\text{BS}}^{(\text{I},2\text{hop})}$, where the last identity originates from the relaying protocol, as commented in *Remark 3.8*, i.e., $\text{card} \left\{ \Phi_{\text{BS}}^{(\text{I},2\text{hop})} \right\} = \text{card} \left\{ \Phi_{\text{RN}}^{(\text{I})} \right\}$. Based on the assumption of independent PPPs stated in *Approximations 3.1-3.4*, $\text{SINR}_{\text{BSR}_0, \text{RN}_0}$ and $\text{SINR}_{\text{RN}_0, \text{MT}_0}$ are independent if $\mathcal{K}_{\text{BS}}^{(\text{I},1\text{hop})}$ and $\mathcal{K}_{\text{BS}}^{(\text{I},2\text{hop})}$ are fixed and given. In other words, the following holds:

$$\begin{aligned} & \Pr \left\{ \text{SINR}_{\text{BSR}_0, \text{RN}_0} > \text{T and } \text{SINR}_{\text{RN}_0, \text{MT}_0} > \text{T} \mid \mathcal{Z}_{\text{RN}_0, \text{MT}_0}, \mathcal{K}_{\text{BS}}^{(\text{I},1\text{hop})}, \mathcal{K}_{\text{BS}}^{(\text{I},2\text{hop})} \right\} \\ & \approx \Pr \left\{ \text{SINR}_{\text{BSR}_0, \text{RN}_0} > \text{T} \mid \mathcal{K}_{\text{BS}}^{(\text{I},1\text{hop})}, \mathcal{K}_{\text{BS}}^{(\text{I},2\text{hop})} \right\} \\ & \times \Pr \left\{ \text{SINR}_{\text{RN}_0, \text{MT}_0} > \text{T} \mid \mathcal{Z}_{\text{RN}_0, \text{MT}_0}, \mathcal{K}_{\text{BS}}^{(\text{I},2\text{hop})} \right\} \end{aligned} \quad (3.42)$$

where we have taken into account that $\text{SINR}_{\text{BSR}_0, \text{RN}_0}$ is independent of $\mathcal{Z}_{\text{RN}_0, \text{MT}_0}$, as stated in *Remark 3.17*, as well as that $\text{SINR}_{\text{RN}_0, \text{MT}_0}$ is independent of $\mathcal{K}_{\text{BS}}^{(\text{I},1\text{hop})}$.

Based on the definition of $\text{SINR}_{\text{BSR}_0, \text{RN}_0}$ in (3.15), the following equalities hold:

$$\begin{aligned} & \Pr \left\{ \text{SINR}_{\text{BSR}_0, \text{RN}_0} > \text{T} \mid \mathcal{K}_{\text{BS}}^{(\text{I},1\text{hop})}, \mathcal{K}_{\text{BS}}^{(\text{I},2\text{hop})} \right\} \\ & \stackrel{(a)}{=} \Pr \left\{ |h_{\text{BSR}_0, \text{RN}_0}|^2 > \frac{\mathcal{Z}_{\text{BSR}_0, \text{RN}_0} \text{T}}{P_{\text{BSR}_0}} \right. \\ & \times \left. \left(\sigma_N^2 + \text{I}_{\text{BSR}_0 \rightarrow \text{RN}_0}^{(1\text{hop})}(\mathcal{Z}_{\text{BSR}_0, \text{RN}_0}) + \text{I}_{\text{BSR}_0 \rightarrow \text{RN}_0}^{(2\text{hop})}(\mathcal{Z}_{\text{BSR}_0, \text{RN}_0}) \right) \mid \mathcal{K}_{\text{BS}}^{(\text{I},1\text{hop})}, \mathcal{K}_{\text{BS}}^{(\text{I},2\text{hop})} \right\} \\ & \stackrel{(b)}{=} \mathbb{E}_{(\cdot) \setminus \mathcal{K}_{\text{BS}}^{(\text{I},1\text{hop})}, \mathcal{K}_{\text{BS}}^{(\text{I},2\text{hop})}} \left\{ \exp \left(- \frac{\mathcal{Z}_{\text{BSR}_0, \text{RN}_0} \text{T}}{P_{\text{BSR}_0} \Omega_{\text{BS}, \text{RN}}} (\sigma_N^2 \right. \right. \\ & \quad \left. \left. + \text{I}_{\text{BSR}_0 \rightarrow \text{RN}_0}^{(1\text{hop})}(\mathcal{Z}_{\text{BSR}_0, \text{RN}_0}; \mathcal{K}_{\text{BS}}^{(\text{I},1\text{hop})}) + \text{I}_{\text{BSR}_0 \rightarrow \text{RN}_0}^{(2\text{hop})}(\mathcal{Z}_{\text{BSR}_0, \text{RN}_0}; \mathcal{K}_{\text{BS}}^{(\text{I},2\text{hop})}) \right) \right\} \\ & \stackrel{(c)}{=} \mathbb{E}_{\mathcal{Z}_{\text{BSR}_0, \text{RN}_0}} \left\{ \exp \left(- \frac{\mathcal{Z}_{\text{BSR}_0, \text{RN}_0} \text{T}}{P_{\text{BSR}_0} \Omega_{\text{BS}, \text{RN}}} \sigma_N^2 \right) \gamma_{(\text{BS}, 1\text{hop})}(\mathcal{Z}_{\text{BSR}_0, \text{RN}_0}; \mathcal{K}_{\text{BS}}^{(\text{I},1\text{hop})}) \right. \\ & \quad \left. \times \gamma_{(\text{BS}, 2\text{hop})}(\mathcal{Z}_{\text{BSR}_0, \text{RN}_0}; \mathcal{K}_{\text{BS}}^{(\text{I},2\text{hop})}) \right\} \end{aligned} \quad (3.43)$$

where (a) and (b) follow similar to (a) and (b) in (3.37). In (b), the dependence of the aggregate interferences upon $\mathcal{K}_{\text{BS}}^{(\text{I},1\text{hop})}$ and $\mathcal{K}_{\text{BS}}^{(\text{I},2\text{hop})}$ is made explicit for clarity. In (c),

the following definitions hold:

$$\begin{aligned}
& \gamma_{(\text{BS},1\text{hop})} \left(\mathcal{Z}_{\text{BS}_{\text{R0}},\text{RN}_0}; \mathcal{K}_{\text{BS}}^{(\text{I},1\text{hop})} \right) \\
&= \mathbb{E}_{(\cdot) \setminus \mathcal{Z}_{\text{BS}_{\text{R0}},\text{RN}_0}, \mathcal{K}_{\text{BS}}^{(\text{I},1\text{hop})}} \left\{ \exp \left(- \frac{\mathcal{Z}_{\text{BS}_{\text{R0}},\text{RN}_0} \mathbb{T}}{P_{\text{BS}_{\text{R0}}} \Omega_{\text{BS},\text{RN}}} I_{\text{BS}_{\text{R0}} \rightarrow \text{RN}_0}^{(\text{I},1\text{hop})} \left(\mathcal{Z}_{\text{BS}_{\text{R0}},\text{RN}_0}; \mathcal{K}_{\text{BS}}^{(\text{I},1\text{hop})} \right) \right) \right\} \\
& \gamma_{(\text{BS},2\text{hop})} \left(\mathcal{Z}_{\text{BS}_{\text{R0}},\text{RN}_0}; \mathcal{K}_{\text{BS}}^{(\text{I},2\text{hop})} \right) \\
&= \mathbb{E}_{(\cdot) \setminus \mathcal{Z}_{\text{BS}_{\text{R0}},\text{RN}_0}, \mathcal{K}_{\text{BS}}^{(\text{I},2\text{hop})}} \left\{ \exp \left(- \frac{\mathcal{Z}_{\text{BS}_{\text{R0}},\text{RN}_0} \mathbb{T}}{P_{\text{BS}_{\text{R0}}} \Omega_{\text{BS},\text{RN}}} I_{\text{BS}_{\text{R0}} \rightarrow \text{RN}_0}^{(\text{I},2\text{hop})} \left(\mathcal{Z}_{\text{BS}_{\text{R0}},\text{RN}_0}; \mathcal{K}_{\text{BS}}^{(\text{I},2\text{hop})} \right) \right) \right\}
\end{aligned} \tag{3.44}$$

By inserting (3.16) in (3.44), the latter equation can be re-formulated as

$$\begin{aligned}
& \gamma_{(\text{BS},1\text{hop})} \left(\mathcal{Z}_{\text{BS}_{\text{R0}},\text{RN}_0}; \mathcal{K}_{\text{BS}}^{(\text{I},1\text{hop})} \right) \stackrel{(d)}{=} \gamma_{\text{BS}}^{\mathcal{K}_{\text{BS}}^{(\text{I},1\text{hop})}} \left(\mathcal{Z}_{\text{BS}_{\text{R0}},\text{RN}_0} \right) \\
& \gamma_{(\text{BS},2\text{hop})} \left(\mathcal{Z}_{\text{BS}_{\text{R0}},\text{RN}_0}; \mathcal{K}_{\text{BS}}^{(\text{I},2\text{hop})} \right) \stackrel{(d)}{=} \gamma_{\text{BS}}^{\mathcal{K}_{\text{BS}}^{(\text{I},2\text{hop})}} \left(\mathcal{Z}_{\text{BS}_{\text{R0}},\text{RN}_0} \right)
\end{aligned} \tag{3.45}$$

where:

$$\begin{aligned}
& \gamma_{(\text{BS},1\text{hop})} \left(\mathcal{Z}_{\text{BS}_{\text{R0}},\text{RN}_0} \right) \\
&= \mathbb{E}_{\text{BS}_i} \left\{ \exp \left(- \frac{\mathcal{Z}_{\text{BS}_{\text{R0}},\text{RN}_0} \mathbb{T}}{P_{\text{BS}_{\text{R0}}} \Omega_{\text{BS},\text{RN}}} P_{\text{BS}_i}^{(\text{I},1\text{hop})} |h_{\text{BS}_i,\text{RN}_0}|^2 \mathcal{Z}_{\text{BS}_i,\text{RN}_0}^{-1} \mathbf{1} \left(\mathcal{Z}_{\text{BS}_i,\text{RN}_0} > \mathcal{Z}_{\text{BS}_{\text{R0}},\text{RN}_0} \right) \right) \right\} \\
& \gamma_{(\text{BS},2\text{hop})} \left(\mathcal{Z}_{\text{BS}_{\text{R0}},\text{RN}_0} \right) \\
&= \mathbb{E}_{\text{BS}_j} \left\{ \exp \left(- \frac{\mathcal{Z}_{\text{BS}_{\text{R0}},\text{RN}_0} \mathbb{T}}{P_{\text{BS}_{\text{R0}}} \Omega_{\text{BS},\text{RN}}} P_{\text{BS}_j}^{(\text{I},2\text{hop})} |h_{\text{BS}_j,\text{RN}_0}|^2 \mathcal{Z}_{\text{BS}_j,\text{RN}_0}^{-1} \mathbf{1} \left(\mathcal{Z}_{\text{BS}_j,\text{RN}_0} > \mathcal{Z}_{\text{BS}_{\text{R0}},\text{RN}_0} \right) \right) \right\}
\end{aligned} \tag{3.46}$$

and (d) holds since the addends in (3.16) are i.i.d.. In (3.46), BS_i and BS_j denote the generic interfering BSs that belong to $\Phi_{\text{BS}}^{(\text{I},1\text{hop})}$ and $\Phi_{\text{BS}}^{(\text{I},2\text{hop})}$, respectively. In addition, $P_{\text{BS}_i}^{(\text{I},1\text{hop})} = P_{\text{BS}_0} = P_T$ and $P_{\text{BS}_j}^{(\text{I},2\text{hop})} = P_{\text{BS}_{\text{R0}}} = K_T P_T$.

Similar steps can be applied to $\Pr \left\{ \text{SINR}_{\text{RN}_0, \text{MT}_0} > T \mid \mathcal{Z}_{\text{RN}_0, \text{MT}_0}, \mathcal{K}_{\text{BS}}^{(\text{I}, 2\text{hop})} \right\}$ in (3.42).

From (3.7), we have:

$$\begin{aligned}
& \Pr \left\{ \text{SINR}_{\text{RN}_0, \text{MT}_0} > T \mid \mathcal{Z}_{\text{RN}_0, \text{MT}_0}, \mathcal{K}_{\text{BS}}^{(\text{I}, 2\text{hop})} \right\} \\
&= \exp \left(-\frac{\mathcal{Z}_{\text{RN}_0, \text{MT}_0} T}{P_{\text{RN}_0} \Omega_{\text{RN}, \text{MT}}} \sigma_N^2 \right) \gamma_{(\text{RN}, 2\text{hop})} \left(\mathcal{Z}_{\text{RN}_0, \text{MT}_0}; \mathcal{K}_{\text{BS}}^{(\text{I}, 2\text{hop})} \right) \\
& \gamma_{(\text{RN}, 2\text{hop})} \left(\mathcal{Z}_{\text{RN}_0, \text{MT}_0} \right) \\
&= \mathbb{E}_{\text{RN}_k} \left\{ \exp \left(-\frac{\mathcal{Z}_{\text{RN}_0, \text{MT}_0} T}{P_{\text{RN}_0} \Omega_{\text{RN}, \text{MT}}} P_{\text{RN}_k} |h_{\text{RN}_k, \text{MT}_0}|^2 \mathcal{Z}_{\text{RN}_k, \text{MT}_0}^{-1} \mathbf{1}(\mathcal{Z}_{\text{RN}_k, \text{MT}_0} > \mathcal{Z}_{\text{RN}_0, \text{MT}_0}) \right) \right\}
\end{aligned} \tag{3.47}$$

where $\gamma_{(\text{RN}, 2\text{hop})} \left(\mathcal{Z}_{\text{RN}_0, \text{MT}_0}; \mathcal{K}_{\text{BS}}^{(\text{I}, 2\text{hop})} \right) = \gamma_{(\text{RN}, 2\text{hop})}^{\mathcal{K}_{\text{BS}}^{(\text{I}, 2\text{hop})}} \left(\mathcal{Z}_{\text{RN}_0, \text{MT}_0} \right)$ and $P_{\text{RN}_k} = P_{\text{RN}_0} = (1 - K_T) P_T$.

To complete the proof, two steps are left: the computation of the expectations 1) of (3.42) with respect to $\mathcal{K}_{\text{BS}}^{(\text{I}, 1\text{hop})}$, $\mathcal{K}_{\text{BS}}^{(\text{I}, 2\text{hop})}$; 2) in (3.46) for $\gamma_{(\text{BS}, 1\text{hop})}(\cdot)$, $\gamma_{(\text{BS}, 2\text{hop})}(\cdot)$ and in (3.47) for $\gamma_{(\text{RN}, 2\text{hop})}(\cdot)$. Let us start with 1).

Based on *Approximation 3.5* and as illustrated in Fig. 3.3, the $\mathcal{K}_{\text{BS}}^{(\text{I})}$ interfering BSs are located outside the disc having center where RN_0 is and of radius equal to $r_{\text{BS}_{\text{R}_0}, \text{RN}_0}$, *i.e.*, outside the “red” disc in Fig. 3.3. This implies $r_{\text{BS}_i, \text{RN}_0} > r_{\text{BS}_{\text{R}_0}, \text{RN}_0}$ for $\text{BS}_i \in \Phi_{\text{BS}}^{(\text{I})}$. Let us denote this unbounded region of the plane by $\mathcal{A}(r_{\text{BS}_{\text{R}_0}, \text{RN}_0})$. Due to the properties of the PPPs [7], the following equalities hold:

$$\begin{aligned}
& \Pr \left\{ \text{card} \left\{ \Phi_{\text{BS}}^{(\text{I})} \left(\mathcal{A}(r_{\text{BS}_{\text{R}_0}, \text{RN}_0}) \right) \right\} = \mathcal{K}_{\text{BS}}^{(\text{I})} \right\} \\
&= \exp \left(-\lambda_{\text{BS}}^{(\text{I})} \mathcal{A}(r_{\text{BS}_{\text{R}_0}, \text{RN}_0}) \right) \left(\mathcal{A}^{\mathcal{K}_{\text{BS}}^{(\text{I})}}(r_{\text{BS}_{\text{R}_0}, \text{RN}_0}) / \left(\mathcal{K}_{\text{BS}}^{(\text{I})}! \right) \right) \\
& \Pr \left\{ \text{card} \left\{ \Phi_{\text{BS}}^{(\text{I}, 1\text{hop})} \left(\mathcal{A}(r_{\text{BS}_{\text{R}_0}, \text{RN}_0}) \right) \right\} = \mathcal{K}_{\text{BS}}^{(\text{I}, 1\text{hop})} \mid \mathcal{K}_{\text{BS}}^{(\text{I})} \right\} \\
&= \frac{\mathcal{K}_{\text{BS}}^{(\text{I})}!}{\mathcal{K}_{\text{BS}}^{(\text{I}, 1\text{hop})}! \left(\mathcal{K}_{\text{BS}}^{(\text{I})} - \mathcal{K}_{\text{BS}}^{(\text{I}, 1\text{hop})} \right)!} \chi_{1\text{hop}}^{\mathcal{K}_{\text{BS}}^{(\text{I}, 1\text{hop})}} (1 - \chi_{1\text{hop}})^{\mathcal{K}_{\text{BS}}^{(\text{I})} - \mathcal{K}_{\text{BS}}^{(\text{I}, 1\text{hop})}}
\end{aligned} \tag{3.48}$$

as well as $\chi_{2\text{hop}} = 1 - \chi_{1\text{hop}}$ and $\mathcal{K}_{\text{BS}}^{(\text{I}, 2\text{hop})} = \mathcal{K}_{\text{BS}}^{(\text{I})} - \mathcal{K}_{\text{BS}}^{(\text{I}, 1\text{hop})}$.

Then, the expectation of (3.42) with respect to $\mathcal{K}_{\text{BS}}^{(\text{I},1\text{hop})}$ and $\mathcal{K}_{\text{BS}}^{(\text{I},2\text{hop})}$ can be formulated as follows:

$$\begin{aligned}
& \Pr \{ \text{SINR}_{\text{BSR}_0, \text{RN}_0} > \text{T and } \text{SINR}_{\text{RN}_0, \text{MT}_0} > \text{T} | \mathcal{Z}_{\text{RN}_0, \text{MT}_0} \} \\
& \approx \mathbb{E}_{\mathcal{K}_{\text{BS}}^{(\text{I},1\text{hop})}, \mathcal{K}_{\text{BS}}^{(\text{I},2\text{hop})}} \left\{ \Pr \left\{ \text{SINR}_{\text{BSR}_0, \text{RN}_0} > \text{T} | \mathcal{K}_{\text{BS}}^{(\text{I},1\text{hop})}, \mathcal{K}_{\text{BS}}^{(\text{I},2\text{hop})} \right\} \right. \\
& \quad \left. \times \Pr \left\{ \text{SINR}_{\text{RN}_0, \text{MT}_0} > \text{T} | \mathcal{Z}_{\text{RN}_0, \text{MT}_0}, \mathcal{K}_{\text{BS}}^{(\text{I},2\text{hop})} \right\} \right\} \quad (3.49) \\
& \stackrel{(a)}{=} \exp \left(-\frac{\mathcal{Z}_{\text{RN}_0, \text{MT}_0} \text{T}}{P_{\text{RN}_0} \Omega_{\text{RN}, \text{MT}}} \sigma_N^2 \right) \\
& \quad \times \mathbb{E}_{\mathcal{Z}_{\text{BSR}_0, \text{RN}_0}} \left\{ \exp \left(-\frac{\mathcal{Z}_{\text{BSR}_0, \text{RN}_0} \text{T}}{P_{\text{BSR}_0} \Omega_{\text{BS}, \text{RN}}} \sigma_N^2 \right) \gamma(\mathcal{Z}_{\text{BSR}_0, \text{RN}_0}, \mathcal{Z}_{\text{RN}_0, \text{MT}_0}) \right\}
\end{aligned}$$

$$\begin{aligned}
& \gamma(\mathcal{Z}_{\text{BSR}_0, \text{RN}_0}, \mathcal{Z}_{\text{RN}_0, \text{MT}_0}) \\
& = \mathbb{E}_{\mathcal{K}_{\text{BS}}^{(\text{I},1\text{hop})}, \mathcal{K}_{\text{BS}}^{(\text{I},2\text{hop})}} \left\{ \gamma_{(\text{BS},1\text{hop})}^{\mathcal{K}_{\text{BS}}^{(\text{I},1\text{hop})}}(\mathcal{Z}_{\text{BSR}_0, \text{RN}_0}) \gamma_{(\text{BS},2\text{hop})}^{\mathcal{K}_{\text{BS}}^{(\text{I},2\text{hop})}}(\mathcal{Z}_{\text{BSR}_0, \text{RN}_0}) \gamma_{(\text{RN},2\text{hop})}^{\mathcal{K}_{\text{BS}}^{(\text{I},2\text{hop})}}(\mathcal{Z}_{\text{RN}_0, \text{MT}_0}) \right\} \\
& \stackrel{(b)}{=} \sum_{\mathcal{K}_{\text{BS}}^{(\text{I})}=0}^{+\infty} \Pr \left\{ \mathcal{K}_{\text{BS}}^{(\text{I})} \right\} \sum_{\mathcal{K}_{\text{BS}}^{(\text{I},1\text{hop})}=0}^{\mathcal{K}_{\text{BS}}^{(\text{I})}} \Pr \left\{ \mathcal{K}_{\text{BS}}^{(\text{I},1\text{hop})} | \mathcal{K}_{\text{BS}}^{(\text{I})} \right\} \\
& \quad \times \left[\gamma_{(\text{BS},1\text{hop})}^{\mathcal{K}_{\text{BS}}^{(\text{I},1\text{hop})}}(\gamma_{(\text{BS},2\text{hop})} \gamma_{(\text{RN},2\text{hop})})^{\mathcal{K}_{\text{BS}}^{(\text{I})} - \mathcal{K}_{\text{BS}}^{(\text{I},1\text{hop})}} \right] \\
& \stackrel{(c)}{=} \exp \left(-\chi_{1\text{hop}} \lambda_{\text{BS}}^{(\text{I})} \mathcal{A}(r_{\text{BSR}_0, \text{RN}_0}) (1 - \gamma_{(\text{BS},1\text{hop})}) \right) \\
& \quad \times \exp \left(-\chi_{2\text{hop}} \lambda_{\text{BS}}^{(\text{I})} \mathcal{A}(r_{\text{BSR}_0, \text{RN}_0}) (1 - \gamma_{(\text{BS},2\text{hop})} \gamma_{(\text{RN},2\text{hop})}) \right) \quad (3.50)
\end{aligned}$$

where the following short-hand notations $\gamma_{(\text{BS},1\text{hop})} = \gamma_{(\text{BS},1\text{hop})}(\mathcal{Z}_{\text{BSR}_0, \text{RN}_0})$, $\gamma_{(\text{BS},2\text{hop})} = \gamma_{(\text{BS},2\text{hop})}(\mathcal{Z}_{\text{BSR}_0, \text{RN}_0})$ and $\gamma_{(\text{RN},2\text{hop})} = \gamma_{(\text{RN},2\text{hop})}(\mathcal{Z}_{\text{RN}_0, \text{MT}_0})$ are used in (3.50). Also, (a) follows from (3.43) and (3.47), (b) follows from (3.48) using the short-hand notations $\Pr \left\{ \mathcal{K}_{\text{BS}}^{(\text{I})} \right\} = \Pr \left\{ \text{card} \left\{ \Phi_{\text{BS}}^{(\text{I})}(\mathcal{A}(r_{\text{BSR}_0, \text{RN}_0})) \right\} = \mathcal{K}_{\text{BS}}^{(\text{I})} \right\}$ and $\Pr \left\{ \mathcal{K}_{\text{BS}}^{(\text{I},1\text{hop})} | \mathcal{K}_{\text{BS}}^{(\text{I})} \right\} = \Pr \left\{ \text{card} \left\{ \Phi_{\text{BS}}^{(\text{I},1\text{hop})}(\mathcal{A}(r_{\text{BSR}_0, \text{RN}_0})) \right\} = \mathcal{K}_{\text{BS}}^{(\text{I},1\text{hop})} | \mathcal{K}_{\text{BS}}^{(\text{I})} \right\}$ and (c) follows applying the binomial theorem to compute the inner sum and the Taylor expansion of the exponential function to compute the outer sum.

The final step is the computation of the expectations in (3.46) and (3.47). From (3.50), more precisely, the following two terms need to be computed:

$$\begin{aligned}
\bar{\gamma}_{(\text{BS})}(\mathcal{Z}_{\text{BS}_{\text{R0}}, \text{RN}_0}) &= \mathcal{A}(r_{\text{BS}_{\text{R0}}, \text{RN}_0}) (1 - \gamma_{(\text{BS}, 1\text{hop})}(\mathcal{Z}_{\text{BS}_{\text{R0}}, \text{RN}_0})) \\
\bar{\gamma}_{(\text{BS}, \text{RN})}(\mathcal{Z}_{\text{BS}_{\text{R0}}, \text{RN}_0}, \mathcal{Z}_{\text{RN}_0, \text{MT}_0}) & \\
&= \mathcal{A}(r_{\text{BS}_{\text{R0}}, \text{RN}_0}) (1 - \gamma_{(\text{BS}, 2\text{hop})}(\mathcal{Z}_{\text{BS}_{\text{R0}}, \text{RN}_0}) \gamma_{(\text{RN}, 2\text{hop})}(\mathcal{Z}_{\text{RN}_0, \text{MT}_0})) \quad (3.51) \\
&= \mathcal{A}(r_{\text{BS}_{\text{R0}}, \text{RN}_0}) (1 - \gamma_{(\text{BS}, 2\text{hop})}(\mathcal{Z}_{\text{BS}_{\text{R0}}, \text{RN}_0})) \\
&\quad + \mathcal{A}(r_{\text{BS}_{\text{R0}}, \text{RN}_0}) \gamma_{(\text{BS}, 2\text{hop})}(\mathcal{Z}_{\text{BS}_{\text{R0}}, \text{RN}_0}) (1 - \gamma_{(\text{RN}, 2\text{hop})}(\mathcal{Z}_{\text{RN}_0, \text{MT}_0}))
\end{aligned}$$

where the last identity is more suitable for performing the computation. The steps towards this end are similar to those used for computing (3.38). Due to space limitations, we omit the details and provide only the main procedure for computing them. In particular, the following line of thought is used:

- To solve the integrals, $\mathcal{A}(r_{\text{BS}_{\text{R0}}, \text{RN}_0}) = \{r \mid r > r_{\text{BS}_{\text{R0}}, \text{RN}_0}\}$ in Fig. 3.3 is replaced by $\mathcal{A}(r_{\text{BS}_{\text{R0}}, \text{RN}_0}, r_{\text{max}}) = \{r \mid r_{\text{BS}_{\text{R0}}, \text{RN}_0} < r < r_{\text{max}}\}$. Once the integrals are solved, the limit $r_{\text{max}} \rightarrow +\infty$ is computed.
- The generic term $\mathcal{Z}_{X,Y}$ is re-written in terms of distance and shadowing, *i.e.*, $\mathcal{Z}_{X,Y} = r_{X,Y}^{\beta_{X,Y}} / S_{X,Y}$. This implies the following: $\mathcal{Z}_{X,Y} > \mathcal{Z}_{X_0,Y_0} \Rightarrow r_{X,Y} > (\mathcal{Z}_{X_0,Y_0} S_{X,Y})^{1/\beta_{X,Y}}$.
- The distances of the generic interferers, *i.e.*, $r_{\text{BS}_i, \text{RN}_0}$ and $r_{\text{BS}_i, \text{RN}_0}$ in (3.46) and $r_{\text{RN}_k, \text{RN}_0}$ in (3.47), are, by definition of PPP, uniformly distributed in the area $\mathcal{A}(r_{\text{BS}_{\text{R0}}, \text{RN}_0}, r_{\text{max}})$. Thus, their PDF is $f(r) = 1/\mathcal{A}(r_{\text{BS}_{\text{R0}}, \text{RN}_0}, r_{\text{max}})$ in the area $\mathcal{A}(r_{\text{BS}_{\text{R0}}, \text{RN}_0}, r_{\text{max}})$ and zero elsewhere.
- As for the terms $(1 - \gamma_{(\cdot)}(\cdot))$, “1–” is first moved inside the expectation. The expectations implied in (3.46) and (3.47) are computed in this order: i) first, that with respect to the distances of the interferers, ii) second, that with respect to fast-fading ((3.40) is used), iii) third the limit $r_{\text{max}} \rightarrow +\infty$ is computed, iv) fourth, that with respect to shadowing ((3.32) is used). The integrals are computed using (3.40).
- As for the computation of $\gamma_{(\text{BS}, 2\text{hop})}(\mathcal{Z}_{\text{BS}_{\text{R0}}, \text{RN}_0})$, steps ii) is performed before step i), *i.e.*, the expectation with respect to fast-fading is first computed. The resulting

integral with respect to the distances of the interferers is computed with the aid of the notable integral:

$$\begin{aligned} & \int_m^M x \left(1 + Qx^{-2b}\right) dx \\ &= \left(\frac{M^2}{2}\right) {}_2F_1\left(1, -\frac{1}{b}; 1 - \frac{1}{b}; -\frac{Q}{M^{2b}}\right) - \left(\frac{m^2}{2}\right) {}_2F_1\left(1, -\frac{1}{b}; 1 - \frac{1}{b}; -\frac{Q}{M^{2b}}\right) \end{aligned} \tag{3.52}$$

The proof follows by putting everything together and by using algebraic manipulations and simplifications.

Chapter 4

Stochastic Geometry Modeling and Analysis of Cellular Networks over Multi-State Channel Model

4.1 Introduction

Heterogeneous ultra-dense cellular networks constitute an enabling architecture for achieving the disruptive capabilities that the fifth generation (5G) of cellular networks is expected to provide [79]. Modeling, simulating, analyzing and optimizing such networks is, however, a non-trivial problem. This is due to the large number of access points that are expected to be deployed and their dissimilar characteristics, which encompass deployment density, transmit power, access technology, etc. The PPP abstraction model, due to its mathematical flexibility for modeling heterogeneous ultra-dense cellular deployments, has been extensively used in the last few years and it is gaining exponential prominence in the scientific community.

A vast majority of the researches relying on the PPP abstraction model, however, are based on some simplifying modeling assumptions. For example, the unified power-law path-loss model, where the received power (including the interference) decays as a function of r^β over a distance r , and $\beta > 2$ is referred to as the path-loss exponent, has been widely considered in the researches leveraging on stochastic geometry. Notably, this signal attenuation model, although in ubiquitous use, is quite idealized. In order to model

more realistic and general network architecture, recently, the multi-state channel model, where LOS and NLOS propagations are explicitly taken into account as suggested by 3GPP [80], has been considered in the field of wireless network modeling. For example, the authors in [81, 82] considered the signal propagation blockages from the buildings in urban areas, which are modeled with the aid of the random shape theory. In [83], the distance dependent LOS blocking probability is obtained from measured data in an outdoor local area based on the linear model. In [84] and [85], the authors considered the 3GPP suggested LOS/NLOS probabilities [80] in the performance evaluation of densely deployed cellular networks.

It has been shown by the experimental simulations in Appendix A as well as by the numerical results in Section 4.6 that the performance trends and the design guidelines obtained from the stochastic geometry analysis are quite different in the presence and in the absence of multi-state channel models. For example, the conclusion that the coverage probability of the interference-limited cellular networks is independent from the density of transmission nodes [10] by assuming the unique channel models does not hold if the multi-state channels are considered. The details are available in Section 4.6. Similar conclusions have also been implied somehow in [85]. These new behaviors and the disappointing fact that the idealized single-state channel model is unable to characterize the property of real propagation motivate the researchers to complicate their system models.

Despite the improvement in modeling, the mathematical tractability of the multi-state PPP-based abstraction model has remained elusive to date. In this chapter, we investigate the mathematical feasibility of the multi-state channel models, e.g., the random shape model [81], the linear model [83], and the 3GPP model [80], on modeling cellular networks, where LOS/NLOS channel model has been explicitly taken into account. In specific, a multi-slope channel model has been proposed to approximate the depicted multi-state models by matching the intensities of the path-loss processes. The proposed approach leverages on and generalizes the two ball approximation in [66]. Moreover, the practical antenna radiation pattern, which is usually neglected in stochastic geometry analysis, has been explicitly taken into account in our case study. The proposed approach is shown to be applicable to multi-tier heterogeneous cellular network and cell association criteria based on the smallest path-loss and the highest received power, and its accuracy has been substantiated through Monte Carlo simulations.

In addition, the PPP-abstraction model together with the multi-state channel approximation have shown to also be able to accurately approximate realistic cellular networks with the empirical LOS/NLOS conditions due to blockages of buildings. More specifically, we explicitly take realistic BS locations, building footprints, LOS/NLOS channel conditions into account, where i) the locations of the BSs are taken from a large database made available by OFCOM, the independent regulator and competition authority for the United Kingdom (UK) communications industries [9]; and ii) the footprints of the buildings are taken from a large database made available by Ordnance Survey, the Britain's mapping agency offering the most up-to-date and accurate maps of the UK [86]. Our extensive study highlights that the our abstraction model is capable of accurately predicting the performance of cellular networks in dense urban environments. To ease the presentation and to focus on the mathematical analysis in this chapter, the experimental validation of cellular network modeled by PPP-based abstraction model is presented in Appendix A of the report.

The remainder of the present chapter is organized as follows. In Section 4.2, the system model is introduced. In Section 4.3, a tractable approximation of the link state model and an approximation on the antenna radiation pattern are introduced. In Section 4.4, mathematical frameworks on the performance analysis of the PPP-abstraction model are presented. In Section 4.5, the framework is further investigated and the impact of the system parameters is studied. In Section 4.6, numerical illustrations are provided to substantiate the proposed approach with the aid of Monte Carlo simulations. Finally, Section 4.7 concludes this chapter.

4.2 System Model

4.2.1 Base Stations Modeling

In this chapter, the BSs are assumed to be distributed according to a homogeneous PPP Φ of density λ_{BS} on the bi-dimensional plane. Thanks to Slivnyak theorem, the typical MT of interest is assumed, without loss of generality, to be located at the origin of the 2D plane. We assume that all the BSs are accessible, and the MT is tagged to the BS denoted as $\text{BS}^{(0)}$ according to the association criteria described in Section 4.2.5. Similar to [10], a full frequency reuse and a saturated load scenario are assumed, which indicates

TABLE 4.1: Recurrent parameters and symbols.

Symbol	Meaning
Φ	PPP of BSs
Φ_k	PPP of BSs with links to the MT in state $k \in \{\text{LOS}, \text{NLOS}\}$
$\Lambda_k([0, x])$	intensity measure of the path-loss process of BSs with links to the MT in state k
P	transmit power of a BS
β_k	power path-loss exponent of links in state k
κ_k	path-loss constant of links in state k
$h_k^{(i)}$	the channel fading power of the BS ⁽ⁱ⁾ -to-MT link in state k
$G^{(i)}$	the antenna radiation pattern of the BS ⁽ⁱ⁾ -to-MT link for $i \in \Phi$
$L_k^{(i)}$	the path-loss of the BS ⁽ⁱ⁾ -to-MT link for $i \in \Phi_k$
$\hat{L}_k^{(i)}$	the path-loss to fading ratio of the BS ⁽ⁱ⁾ -to-MT link for $i \in \Phi_k$

that all the BSs except BS⁽⁰⁾ are interfering nodes for the intended link from BS⁽⁰⁾ to the MT. The transmit power of all the BSs is assumed to be the same, which is denoted by P .

4.2.2 Link States Modeling

In this chapter, the effects of LOS and NLOS channel propagation are explicitly taken into account in agreement with the recent research findings in [81–85, 87], as well as the 3GPP suggested system models [80]. The proposed framework encompasses a wide range of link state models which are available in the literature, including 3GPP suggested link state model for outdoor MTs in urban areas [80], random shape abstraction models based on the building shapes in metropolis [81, 82], linear model obtained from channel measurements for outdoor areas [83]. In specific, the BS-to-MT links can either be in LOS or in NLOS, and the probability of a link of length r (in meter) being in LOS or in NLOS is assumed to be independent of other links, and these probabilities for the depicted link state models are given in Table 4.2. The details of the coefficients in Table 4.2 are discussed in Section 4.6. It is assumed that the propagation state of each BS-to-MT link is independent, then, $\Phi = \Phi_{\text{LOS}} \cup \Phi_{\text{NLOS}}$, where Φ_k denotes the set of BSs with BS-to-MT links in state $k \in \{\text{LOS}, \text{NLOS}\}$.

Remark 4.1. In the present chapter, the states of the channels are assumed to be independent for the sake of mathematical tractability. The correlation between the link states, which mainly originates from the presence of same blockage obstacles for the neighboring transmission nodes, on the other hand, has been neglected. This correlation, often

TABLE 4.2: Probabilities of a link of length r being in LOS or in NLOS for link state models introduced in Section 4.2.2

	$p_{\text{LOS}}(r)$	$p_{\text{NLOS}}(r)$
3GPP model [80]	$\min\left\{\frac{18}{r}, 1\right\} \left(1 - e^{-\frac{r}{36}}\right) + e^{-\frac{r}{36}}$	$1 - p_{\text{LOS}}(r)$
Random Shape [81]	$\gamma_{\text{RS}} \exp(-\alpha_{\text{RS}} r)$	$1 - p_{\text{LOS}}(r)$
Linear model [83]	$1 - p_{\text{NLOS}}(r)$	$\min\{a_{\text{LM}} r + b_{\text{LM}}, c_{\text{LM}}\}$

manifesting itself as correlated shadowing, has been considered, for example, in [71, 88–90]. In specific, the author in [71] account for shadowing correlation by capitalizing the Owen and Steck method for the generation of equi-correlated multivariate normal distributions, which is also applicable to the system of interest in the present chapter at the cost of additional complexity. The authors in [90] highlighted the stress of taking channel correlations into account and proposed the Manhattan Poisson line process-based framework, which could be the future research interest to extend the framework in the present report. Nevertheless, as validated by the simulations in Appendix A, where the link states are determined by the empirical building blockages and the independence of link states is not assumed a priori, the simplified independence assumptions is accurate and acceptable for the considered system. \square

4.2.3 Channel Modeling

In this subsection, the channel models of the downlink BS-to-MT links are presented. The signal propagation of a generic BS-to-MT link is assumed to be subject to the path-loss as well as the Nakagami- m channel fading, which are described in detail as follows.

4.2.3.1 Path-Loss Modeling

Different path-loss models of links in LOS and in NLOS are assumed in our case study. In particular, the path-loss of a link between BS^(i) for $i \in \Phi_k$ and the MT can be formulated as follows:

$$l_k(r^{(i)}) = \kappa_k (r^{(i)})^{\beta_k} \quad (4.1)$$

where $k = \{\text{LOS}, \text{NLOS}\}$ denotes the state of the BS⁽ⁱ⁾-to-MT link, $r^{(i)}$ is the length of the link, $\kappa_k \geq 1$ and $\beta_k \geq 2$ are the path-loss constant and path-loss exponent for links in state k , respectively. In general κ_k and β_k are of different values for $k = \text{LOS}$ and $k = \text{NLOS}$.

4.2.3.2 Fast Fading

In addition to the distance dependent path-loss attenuation, each link is also subject to an independent and fast varying channel fading. In the present chapter, the Nakagami- m fading is assumed. Let $h_k^{(i)}$ denote the fading power of the BS⁽ⁱ⁾-to-MT link, where $k \in \{\text{LOS}, \text{NLOS}\}$ denotes the link state. Then, $h_k^{(i)} \sim \mathcal{G}(m_k, m_k/\Omega_k)$. The Nakagami- m fading includes Rayleigh fading ($m_k = 1$) as a special case, and it can closely approximate Nakagami- q fading and Rician fading [4], where the latter one is widely used to model propagation paths consisting of a LOS link. More specifically, the one-to-one matching of the fading figures between the m parameter of Nakagami- m distribution and the q parameter of Nakagami- q distribution, $m = \frac{(1+q^2)^2}{2(1+2q^4)}$ [4, Eq. (2.25)], allows the Nakagami- m distribution to closely approximate the Nakagami- q distribution. Similarly, the one-to-one mapping between the m parameter and the Rician K factor, $m = \frac{(1+K^2)^2}{1+2K^2}$ [4, Eq. (2.26)], allows the Nakagami- m distribution to closely approximate the Rice distribution.

4.2.4 Radiation Pattern Modeling

To enhance the received signal from the intended BS as well as to reduce the other-cell interference, directional antennas are equipped at both the BSs and the MTs, where the radiation pattern as a function of the boresight angle $\theta_S \in [-\pi, \pi)$ is denoted as $G_S(\theta_S)$, where $S \in \{\text{BS}, \text{MT}\}$. The antenna gain of a generic BS⁽ⁱ⁾-to-MT link is $G^{(i)} = G_{\text{BS}}(\theta_{\text{BS}})G_{\text{MT}}(\theta_{\text{MT}})$. Similar to [91], parameterized antenna radiation patterns are considered in the present paper such that the total radiated power (TRP) remains constant over the parameter space, i.e., $(1/2\pi) \int_{-\pi}^{\pi} G_S(\theta_S) d\theta_S = 1$ for $S \in \{\text{BS}, \text{MT}\}$.

More specifically, the following antenna models are considered in this chapter whose radiation patterns are given in Table 4.3: i) omni-directional antenna; ii) 3GPP antenna pattern [92], where $\theta_S^{(3\text{dB})}$ denotes the 3dB beamwidth in degrees, $\varphi_S^{(3\text{GPP})} = \theta_S^{(3\text{dB})} \sqrt{A_S/12}$,

TABLE 4.3: Radiation Patterns in Section 4.2.4, where $S \in \{\text{BS}, \text{MT}\}$

	$G_S(\theta_S)$
Omni-directional	1
3GPP Pattern	$g_S^{(3\text{GPP})} 10^{-6(\theta_s/\theta_S^{(3\text{dB})})^2/5} \mathbf{1}_{[0, \varphi_S^{(3\text{GPP})})}(\theta_S)$ $+ g_S^{(3\text{GPP})} 10^{-A_S/10} \mathbf{1}_{[\varphi_S^{(3\text{GPP})}, \pi)}(\theta_S)$
UWLA	$\left g_S^{(\text{UWLA})} N_S^{-1} \sin(N_S \pi \nu^{-1} \cos(\theta_S) d_S) \sin^{-1}(\pi \nu^{-1} \cos(\theta_S) d_S) \right ^2$
Sectors with transition	$g_S^{(1;\text{Sec})} \mathbf{1}_{[0, \theta_S^{(1;\text{Sec})})}(\theta) + g_S^{(2;\text{Sec})} \mathbf{1}_{[\theta_S^{(3;\text{Sec})}, \pi)}(\theta)$ $+ g_S^{(1;\text{Sec})} \left(1 - \left(\theta - \theta_S^{(1;\text{Sec})}\right) / \gamma_S\right) \mathbf{1}_{[\theta_S^{(1;\text{Sec})}, \theta_S^{(2;\text{Sec})})}(\theta)$ $+ \left(2g_S^{(2;\text{Sec})} \left(\theta - \theta_S^{(2;\text{Sec})}\right) / \gamma_S\right) \mathbf{1}_{[\theta_S^{(2;\text{Sec})}, \theta_S^{(3;\text{Sec})})}(\theta)$

$g_S^{(3\text{GPP})}$ is the TRP normalization factor; iii) uniform weighted linear array (ULWA) [93], where N_S denotes the number of arrays with uniform spacing equal to d_S , ν is the wavelength of transmitted signal, and $g_S^{(\text{UWLA})}$ is the normalization factor; iv) antenna sectors with transition width [91], where $g_S^{(1;\text{Sec})} = \left(2\pi - (2\pi - 3\gamma_S/2 - \varpi_S) g_S^{(2;\text{Sec})}\right) / \varpi_S$, $\theta_S^{(1;\text{Sec})} = (\varpi_S - \gamma_S)/2$, $\theta_S^{(2;\text{Sec})} = (\varpi_S + \gamma_S)/2$, $\theta_S^{(3;\text{Sec})} = \varpi_S/2 + \gamma_S$. The details on the chosen of the parameters are given in Section 4.6.

For ease of description, the MT and its serving BS, denoted by $\text{BS}^{(0)}$, are assumed to be capable of perfectly estimating the angles of arrival and of adjusting the antenna steering orientations accordingly without alignment errors. Therefore, the maximum achievable antenna gain is always assumed on the intended link for all the depicted radiation pattern models. The antenna arrays of all non-intended links, on the other hand, are assumed to be independently oriented with respect to each other according to a uniform distribution on $[-\pi, \pi)$ [66].

4.2.5 Cell Association Criterion

By taking into account the trade-off between performance and flexibility, two different cell association criteria, which are based on the smallest path-loss, and highest received power, respectively, are studied in this chapter. Let $l_k(r^{(i)})$ defined in Section 4.2.3 be the path-loss of the $\text{BS}^{(i)}$ -to-MT link in state k , where $k \in \{\text{LOS}, \text{NLOS}\}$. Let $h_k^{(i)}$ denote the fast fading of the $\text{BS}^{(i)}$ -to-MT link. Then, the cell association policies are as follows:

A. Smallest Path-loss Association

In this scenario, the MT is assumed to be served by the BS of the smallest path-loss to it. In other word, the path-loss of the intended link is:

$$L^{(0)} = \min \left\{ L_{\text{LOS}}^{(0)}, L_{\text{NLOS}}^{(0)} \right\} \quad (4.2)$$

where $L_k^{(0)} = \min_{i \in \Phi_k} \left\{ L_k^{(i)} = l_k(r^{(i)}) \right\}$ denotes the smallest path-loss of the links in state k for $k \in \{\text{LOS}, \text{NLOS}\}$. In practical, by assuming the position of the MT is quasi-static, the intended BS selected by the smallest path-loss association criterion is the one which provides the highest average received power to the MT since the transmit power and antenna radiation pattern of each BS are assumed to be the same, and the impact of fast fading has been averaged.

B. Highest Received Power Association

Let $\hat{L}_{\text{LOS}}^{(0)}$, $\hat{L}_{\text{NLOS}}^{(0)}$, denote the smallest path-loss-to-fading ratio of the links in LOS and NLOS, respectively, i.e., $\hat{L}_k^{(0)} = \min_{i \in \Phi_k} \left\{ \hat{L}_k^{(i)} = l_k(r^{(i)}) / h_k^{(i)} \right\}$ for $k \in \{\text{LOS}, \text{NLOS}\}$. Then, the path-loss-to-fading ratio of the intended link for this cell association is:

$$\hat{L}^{(0)} = \min \left\{ \hat{L}_{\text{LOS}}^{(0)}, \hat{L}_{\text{NLOS}}^{(0)} \right\} \quad (4.3)$$

The intended BS chosen by this cell association criterion is the one which provides the highest received power to the MT, which is optimal in performance at the cost of implementation complexity.

4.2.6 Problem Formulation

The performance of the cellular network consisting of PPP distributed BSs is evaluated from the distribution of the SINR of the received signal at the MT for the two cell association criteria. Specifically, when smallest path-loss association is assumed, the

SINR can be formulated as follows:

$$\begin{aligned} \text{SINR} &= \begin{cases} \frac{\text{PG}^{(0)} h_{\text{LOS}}^{(0)} / L_{\text{LOS}}^{(0)}}{\sigma_N^2 + i_{agg}(L_{\text{LOS}}^{(0)})} & \text{if } L^{(0)} = L_{\text{LOS}}^{(0)} \leq L_{\text{NLOS}}^{(0)} \\ \frac{\text{PG}^{(0)} h_{\text{NLOS}}^{(0)} / L_{\text{NLOS}}^{(0)}}{\sigma_N^2 + i_{agg}(L_{\text{NLOS}}^{(0)})} & \text{if } L^{(0)} = L_{\text{NLOS}}^{(0)} < L_{\text{LOS}}^{(0)} \end{cases} \\ &= \sum_k \frac{\text{PG}^{(0)} h_k^{(0)} / L^{(0)}}{\sigma_N^2 + i_{agg}(L^{(0)})} \delta(L^{(0)} - L_k^{(0)}) \end{aligned} \quad (4.4)$$

where k in \sum_k is the short hand notation of $k \in \{\text{LOS}, \text{NLOS}\}$, σ_N^2 is the power of additive white Gaussian noise, the conditional aggregate other-cell interference is $i_{agg}(L^{(0)}) = \sum_k \sum_{i \in \Phi_k} \left(\text{PG}^{(i)} h_k^{(i)} / L_k^{(i)} \right) \mathbf{1}(L_k^{(i)} > L^{(0)})$, where the indicator function originates from the cell association criterion.

When highest received power association is assumed, the SINR is

$$\text{SINR} = \frac{\text{PG}^{(0)} / \widehat{L}^{(0)}}{\sigma_N^2 + \widehat{i}_{agg}(\widehat{L}^{(0)})} \quad (4.5)$$

where the conditional interference is $\widehat{i}_{agg}(\widehat{L}^{(0)}) = \sum_k \sum_{i \in \Phi_k} \left(\text{PG}^{(i)} / \widehat{L}_k^{(i)} \right) \mathbf{1}(\widehat{L}_k^{(i)} > \widehat{L}^{(0)})$.

Based on the SINR of the received signal, the coverage probability (P_{cov}), and the average rate (R) are used to quantify the performance of the cellular network. The performance metrics are formulated as follows:

$$P_{\text{cov}}(V_T) = \Pr \{ \text{SINR} \geq V_T \} \quad (4.6)$$

$$R = \mathbb{E}_{\text{SINR}} [\text{BW} \log_2(1 + \text{SINR})] \stackrel{(a)}{=} \frac{\text{BW}}{\ln(2)} \int_0^\infty \frac{P_{\text{cov}}(t)}{t+1} dt \quad (4.7)$$

where (a) follows from [21].

By leveraging on the theoretical state models in Section 4.2.2, and by taking into account the antenna gains in Section 4.2.4, the performance metrics under consideration are not mathematically tractable due to a couple of unsolvable integrals. Numerical evaluation of these integrals are time-consuming. More details of the mathematical intractability are discussed in Appendix 4.B where the distribution of the aggregate interference is calculated. In the next section, a general tractable approximation on the link state models introduced in Section 4.2.2, which is referred to as multi-ball approximation,

and an approximation on the radiation patterns in Section 4.2.4, which is referred to as multi-lobe approximation, are proposed for mathematically evaluating (4.6)-(4.7). The proposed approximations have been proved to be applicable to all the link state models and the antenna models considered in this chapter.

4.3 Tractable Modeling on Link States and Radiation Patterns

As mentioned in Section 4.2.6, the depicted link state models in Section 4.2.2, and the radiation patterns in Section 4.2.4 are useful for system-level simulations, they are, on the other hand, not tractable for mathematical performance analysis. In this section, we introduce two approximations, which is tractable yet accurate, for incorporating all the link state models and all the radiation patterns introduced in Section 4.2 in PPP-based cellular networks.

4.3.1 Multi-ball Link State Approximation

Inspired by the two-ball approximation proposed in [66], in this paper, we approximate the state probability of links from BSs to a typical MT as a piece-wise constant function of the link length r . In particular, we split the bi-dimensional plane with PPP distributed BSs in $N + 1$ regions, which correspond to N balls centered at the typical MT with radius denoted by $D_1 < \dots < D_N$. Then, the probability of a BS-to-MT link being in state k , for $k \in \{\text{LOS}, \text{NLOS}\}$, can be formulated by

$$\begin{cases} p_k^{(\text{approx})}(r) = \sum_{n=1}^{N+1} q_k^{[D_{n-1}, D_n]} \mathbf{1}_{[D_{n-1}, D_n]}(r) \\ \sum_k q_k^{[D_{n-1}, D_n]} = 1, \text{ for } n = 1, 2, \dots, N + 1 \end{cases} \quad (4.8)$$

where $q_k^{[D_{n-1}, D_n]} \geq 0$ is the probability of the BS-to-MT link being in state k when $r \in [D_{n-1}, D_n]$, and we introduce the notation $D_0 = 0$, $D_{N+1} = +\infty$. The second equality in (4.8) corresponds to the constraint that the total probabilities of each state should be one.

Throughout this report, the approximation in (4.8) is referred to as multi-ball approximation, which is optimized from the point of view of the typical MT. It is apparent

that increase the number of balls will increase the accuracy of the approximation as well as the computational complexity in the mathematical analysis. In the next subsection, we introduce the methodology used for estimating D_n and $q_k^{[D_{n-1}, D_n]}$, for $n = 1, \dots, N$, from the link state models in Section 4.2.2.

4.3.2 Path-loss Intensity Matching

As introduced in Section 4.2.3, the path-loss of the BS-to-MT link not only depends on the distance from the BS to the MT, but also depends on the state of the link. From the displacement theorem of PPPs [7], we know that the path-losses of the BS-to-MT links can be considered as an independent and identical displacement or translation from a bi-dimensional PPP to a one-dimensional process, which is still a PPP. Inspired by this fact, the proposed methodology for matching the multi-ball approximation and other models in Section 4.2.2 are based on the intensity measure of the process of path-losses, which explicitly takes the dependence between the link length and link state into account. Moreover, the intensity is directly related to the calculation of the performance metrics in (4.6),(4.7) as described in Section 4.4.

Let Ψ denote the set of path-losses of the BS-to-MT links where the BSs belong to Φ . From the independence assumption, $\Psi = \bigcup_k \Psi_k$, where Ψ_k denotes the set of path-losses of the BSs in Φ_k . The intensity of Ψ_k for $k \in \{\text{LOS}, \text{NLOS}\}$ can be obtained from its definition [76] as follows:

$$\Lambda_k([0, x]) = 2\pi\lambda_{\text{BS}} \int_0^\infty \Pr\{l_k(r) \in [0, x]\} p_k(r) r dr \quad (4.9)$$

where $l_k(r)$ is the path-loss defined in Section 4.2.3, $p_k(r)$ is the probability of a link of distance r being in state k , which is given in Table 4.2 and in (4.8). From the independence assumption, the intensity of Ψ is $\Lambda([0, x]) = \sum_k \Lambda_k([0, x])$. From the definition in (4.9), the intensity measure $\Lambda_k([0, x])$ for the depicted link state models in Section 4.2.2 and for the multi-ball approximation are computed in Table 4.4.

TABLE 4.4: path-loss Intensity on Link State Models in Section 4.2.2

3GPP suggested path-loss model
$\Lambda_{\text{LOS}}^{(3\text{GPP})}([0, x]) = \pi \lambda_{\text{BS}} \left(\frac{x}{\kappa_{\text{LOS}}} \right)^{2/\beta_{\text{LOS}}} \overline{\mathcal{H}}(x - \kappa_{\text{LOS}} 18^{\beta_{\text{LOS}}}) + 2\pi \lambda_{\text{BS}} \mathcal{H}(x - \kappa_{\text{LOS}} 18^{\beta_{\text{LOS}}})$ $\times \left(624 - 36e^{-(x/\kappa_{\text{LOS}})^{1/\beta_{\text{LOS}}}/36} \left(18 + (x/\kappa_{\text{LOS}})^{1/\beta_{\text{LOS}}} \right) + 18(x/\kappa_{\text{LOS}})^{1/\beta_{\text{LOS}}} \right)$ $\Lambda_{\text{NLOS}}^{(3\text{GPP})}([0, x]) = \pi \lambda_{\text{BS}} \mathcal{H}(x - \kappa_{\text{NLOS}} 18^{\beta_{\text{NLOS}}})$ $\times \left(-1572 + \left(\left(\frac{x}{\kappa_{\text{NLOS}}} \right)^{\frac{1}{\beta_{\text{NLOS}}}} - 18 \right)^2 + 72e^{-\frac{1}{36} \left(\frac{x}{\kappa_{\text{NLOS}}} \right)^{\frac{1}{\beta_{\text{NLOS}}}} \left(18 + \left(\frac{x}{\kappa_{\text{NLOS}}} \right)^{\frac{1}{\beta_{\text{NLOS}}}} \right)} \right)$
Random Shape Based Link State Model
$\Lambda_{\text{LOS}}^{(\text{RS})}([0, x]) = 2\pi \lambda_{\text{BS}} \gamma_{\text{RS}}$ $\times \left(\alpha_{\text{RS}}^{-2} - \alpha_{\text{RS}}^{-2} \left(1 + \alpha_{\text{RS}} (x/\kappa_{\text{LOS}})^{1/\beta_{\text{LOS}}} \right) e^{-\alpha_{\text{RS}} (x/\kappa_{\text{LOS}})^{1/\beta_{\text{LOS}}}} \right)$ $\Lambda_{\text{NLOS}}^{(\text{RS})}([0, x]) = 2\pi \lambda_{\text{BS}}$ $\times \left(\frac{1}{2} \left(\frac{x}{\kappa_{\text{NLOS}}} \right)^{\frac{2}{\beta_{\text{NLOS}}}} - \gamma_{\text{RS}} \alpha_{\text{RS}}^{-2} + \gamma_{\text{RS}} \alpha_{\text{RS}}^{-2} \left(1 + \alpha_{\text{RS}} \left(\frac{x}{\kappa_{\text{NLOS}}} \right)^{\frac{1}{\beta_{\text{NLOS}}}} \right) e^{-\alpha_{\text{RS}} \left(\frac{x}{\kappa_{\text{NLOS}}} \right)^{\frac{1}{\beta_{\text{NLOS}}}} \right)$
Linear Model
$\Lambda_{\text{LOS}}^{(\text{Linear})}([0, x]) = 2\pi \lambda_{\text{BS}}$ $\times \left\{ \left(1/2 - b_{\text{LM}}/2 - (x/\kappa_{\text{LOS}})^{1/\beta_{\text{LOS}}} a_{\text{LM}}/3 \right) (x/\kappa_{\text{LOS}})^{2/\beta_{\text{LOS}}} \right.$ $\times \overline{\mathcal{H}} \left(x - \kappa_{\text{LOS}} ((c_{\text{LM}} - b_{\text{LM}})/a_{\text{LM}})^{\beta_{\text{LOS}}} \right)$ $+ (6a_{\text{LM}}^2)^{-1} \left((c_{\text{LM}} - b_{\text{LM}})^3 + 3a_{\text{LM}}^2 (x/\kappa_{\text{LOS}})^{2/\beta_{\text{LOS}}} (1 - c_{\text{LM}}) \right)$ $\times \left. \mathcal{H} \left(x - \kappa_{\text{LOS}} ((c_{\text{LM}} - b_{\text{LM}})/a_{\text{LM}})^{\beta_{\text{LOS}}} \right) \right\}$ $\Lambda_{\text{NLOS}}^{(\text{Linear})}([0, x]) = 2\pi \lambda_{\text{BS}}$ $\times \left\{ \left(b_{\text{LM}}/2 + (x/\kappa_{\text{NLOS}})^{1/\beta_{\text{NLOS}}} a_{\text{LM}}/3 \right) (x/\kappa_{\text{NLOS}})^{2/\beta_{\text{NLOS}}} \right.$ $\times \overline{\mathcal{H}} \left(x - \kappa_{\text{NLOS}} ((c_{\text{LM}} - b_{\text{LM}})/a_{\text{LM}})^{\beta_{\text{NLOS}}} \right)$ $+ 1/(6a_{\text{LM}}^2) \left((b_{\text{LM}} - c_{\text{LM}})^3 + 3a_{\text{LM}}^2 c_{\text{LM}} (x/\kappa_{\text{NLOS}})^{2/\beta_{\text{NLOS}}} \right)$ $\times \left. \mathcal{H} \left(x - \kappa_{\text{NLOS}} ((c_{\text{LM}} - b_{\text{LM}})/a_{\text{LM}})^{\beta_{\text{NLOS}}} \right) \right\}$
Multi-ball Link State Model
$\Lambda_{\text{LOS}}^{(\text{N-Ball})}([0, x]) = \Xi^{(\text{N-Ball})}(x, \text{LOS}), \quad \Lambda_{\text{NLOS}}^{(\text{N-Ball})}([0, x]) = \Xi^{(\text{N-Ball})}(x, \text{NLOS})$ $\Xi^{(\text{N-Ball})}(x, k) =$ $\pi \lambda_{\text{BS}} \left\{ \sum_{n=1}^N q_k^{[D_{n-1}, D_n]} \left[\overline{\mathcal{H}} \left(x - \kappa_k D_n^{\beta_k} \right) \mathcal{H} \left(x - \kappa_k D_{n-1}^{\beta_k} \right) \left((x/\kappa_k)^{2/\beta_k} - D_{n-1}^2 \right) \right. \right.$ $\left. \left. + \mathcal{H} \left(x - \kappa_k D_n^{\beta_k} \right) \left(D_n^2 - D_{n-1}^2 \right) \right] + q_k^{[D_N, \infty]} \mathcal{H} \left(x - \kappa_k D_N^{\beta_k} \right) \left((x/\kappa_k)^{2/\beta_k} - D_N^2 \right) \right\}$

From the intensities, the estimation of D_n and $q_k^{[D_{n-1}, D_n]}$ for $n = 1, \dots, N$ in (4.8) is implemented by solving the following optimization problem:

$$\arg \min_{\{D_n\}, \{q_k^{[D_{n-1}, D_n]}\}} \left\{ \left\| \log \left(\Lambda^{(\text{N-Ball})}([0, x_m]) \right) - \log \left(\Lambda^{(X)}([0, x_m]) \right) \right\|_F^2 \right\} \quad (4.10)$$

where $X \in \{3\text{GPP}, \text{RS}, \text{Linear}\}$ indicates the 3GPP model, random shape model and linear model, respectively, x_m is chosen to capture the main body of $\Lambda^{(X)}([\cdot, \cdot])$, the

logarithm in (4.10) is used to better control the accuracy of the estimation.

In practice, the optimization problem in (4.10) can be solved by using, e.g., the Matlab built-in function ‘lsqcurvefit’ with a random initial searching point whose accuracy has been verified in our simulations. The total probability constraint for two state models can be explicitly taken into account in ‘lsqcurvefit’ function by adjusting only $q_{\text{LOS}}^{[D_{n-1}, D_n]}$ while its NLOS counterpart is $1 - q_{\text{LOS}}^{[D_{n-1}, D_n]}$, and vice versa.

4.3.3 Multi-Lobe Radiation Pattern Approximation

The computation of the performance metrics in (4.6),(4.7) involves the averaging over the radiation patterns given in Table 4.3, since the perfect alignment is not assumed for the interfering links. When the 3GPP suggest antenna pattern, the UWLA antenna, and the sector radiation pattern are considered, the expectation with respect to the antenna gain of the interfering links leads to an unsolvable integral. In this subsection, we introduce a radiation pattern approximation, which is referred to as multi-lobe approximation, to facilitate the computation involving the depicted antenna models. The accuracy of the approximation is confirmed by the numerical examples shown in Section 4.6. The approximation finds its rational from the multi-ball approximation. In specific, the antenna gain of the BS or of the MT can be approximated by the following piece-wise constant function:

$$G_S^{(\text{approx})}(\theta_S) = \sum_{t_S=1}^{T_S} g_S^{(t_S)} \mathbf{1}_{[\varphi_S^{(t_S-1)}, \varphi_S^{(t_S)}]}(|\theta_S|) \quad (4.11)$$

where $S \in \{\text{BS}, \text{MT}\}$, $\theta_S \in [-\pi, \pi)$, T_S is the number of lobes of the radiation pattern, $g_S^{(t_S)}$ is the antenna gain of the t_S -th lobe, $0 < \varphi_S^{(1)} < \dots < \varphi_S^{(T_S-1)} < \pi$ corresponds to the angle of the lobe, and $\varphi_S^{(0)} = 0$, $\varphi_S^{(T_S)} = \pi$.

By direct inspection of (4.11), the probability density function (PDF) of the antenna gain of a generic interfering link from BS⁽ⁱ⁾-to-MT, i.e., $G^{(i)} = G_{\text{BS}}^{(\text{approx})}(\theta_{\text{BS}}^{(i)}) G_{\text{MT}}^{(\text{approx})}(\theta_{\text{MT}}^{(i)})$, is:

$$f_{G^{(\text{approx})}}(\vartheta) = \sum_{t_{\text{BS}}=1}^{T_{\text{BS}}} \sum_{t_{\text{MT}}=1}^{T_{\text{MT}}} \frac{\phi_{\text{BS}}^{(t_{\text{BS}})}}{2\pi} \frac{\phi_{\text{MT}}^{(t_{\text{MT}})}}{2\pi} \delta\left(\vartheta - g_{\text{BS}}^{(t_{\text{BS}})} g_{\text{MT}}^{(t_{\text{MT}})}\right) \quad (4.12)$$

where $\phi_S^{(t_S)} = 2\left(\varphi_S^{(t_S)} - \varphi_S^{(t_S-1)}\right)$ for $S \in \{\text{BS}, \text{MT}\}$.

4.3.4 Radiation Pattern Matching

The parameters $g_S^{(t_S)}$ and $\varphi_S^{(t_S)}$, for $t_S = 1, \dots, T_S$, of the multi-lobe approximation are estimated from the radiation patterns in Table 4.3 by solving a similar optimization problem as in (4.10), which is given as follows:

$$\arg \min_{\{\varphi_S^{(\cdot)}\}, \{g_S^{(\cdot)}\}} \left\{ \left\| \log_{10} \left(G_S^{(X)}(\theta_S) \right) - \log_{10} \left(G_S^{(\text{approx})}(\theta_S) \right) \right\|_F^2 \right\} \quad (4.13)$$

where the logarithm is chosen for achieving better accuracy in the sidelobe region. Since the antenna gain is usually measured in dB, $\log_{10}(\cdot)$ is used instead of $\ln(\cdot)$.

4.4 The Coverage Probability of Cellular Networks

Since the average rate defined in (4.7) is directly related to the coverage probability, in this section, we mainly focus on the calculation of the coverage probability for three association criteria introduced in Section 4.2.5. In specific, the probability density functions (PDFs) of the smallest path-loss, and of the smallest path-loss-to-fading ratio, respectively, are first presented as preliminaries. Then, the CF of the aggregate other-cell interference are introduced. The PDFs and CFs are later used to facilitate the computation of the coverage probabilities, which are presented at the end of this section.

4.4.1 Preliminaries

In this subsection, the PDFs of the smallest path-loss, and of the smallest path-loss to fading ratio are presented, which correspond to the two association criteria in Section 4.2.5.

Proposition 4.1. *Let the typical MT located at the origin. Assume the downlink BS-to-MT links follow the multi-ball link state model as depicted in Section 4.3.1. When the smallest path-loss association is considered, the PDF of the smallest path-loss, $L^{(0)}$, defined in (4.2) is as follows:*

$$f_{L^{(0)}}(x) = \sum_k \Lambda_k^{(\text{N-Ball})(1)}([0, x)) \exp \left(- \sum_{\mathcal{K}} \Lambda_{\mathcal{K}}^{(\text{N-Ball})}([0, x)) \right) \quad (4.14)$$

where $k, \mathcal{K} \in \{\text{LOS}, \text{NLOS}\}$, $\Lambda_k^{(\text{N-Ball})}([0, x])$ denotes the intensity of the path-losses whose links are in state k , and is given in Table 4.4, the first order derivative of the intensity can be formulated as follows:

$$\begin{aligned} \Lambda_k^{(\text{N-Ball})^{(1)}}([0, x]) &= \frac{d}{dx} \Lambda_k^{(\text{N-Ball})}([0, x]) \\ &= \pi \lambda_{\text{BS}} \left\{ \sum_{n=1}^{N+1} q_k^{[D_{n-1}, D_n]} \frac{2}{\beta_k} \kappa_k^{-2/\beta_k} x^{2/\beta_k - 1} \overline{\mathcal{H}}\left(x - \kappa_k D_n^{\beta_k}\right) \mathcal{H}\left(x - \kappa_k D_{n-1}^{\beta_k}\right) \right\} \end{aligned} \quad (4.15)$$

Proof: From the void probability theorem of PPPs [76, Corollary 6], the null probability of the path-loss process Ψ in $[0, x]$, where $x > 0$, is:

$$\Pr \{l(r) > x\} = \Pr \{\text{no pathloss less than } x\} = \exp(-\Lambda([0, x])) \quad (4.16)$$

Therefore, the CDF of $L^{(0)}$ is $F_{L^{(0)}}(x) = \Pr \{L^{(0)} < x\} = 1 - \exp(-\Lambda([0, x]))$ and the PDF of $L^{(0)}$ can be computed by $f_{L^{(0)}}(x) = (dF_{L^{(0)}}(x))/dx$. The PDF in (4.14) follows by computing the derivative of an exponential function. \square

Proposition 4.2. Let the typical MT located at the origin. Assume the downlink BS-to-MT links follow the multi-ball link state model as depicted in Section 4.3.1. When the highest received power association is considered, the PDF of the smallest path-loss-to-fading ratio, $\widehat{L}^{(0)}$, defined in (4.3) is as follows:

$$f_{\widehat{L}^{(0)}}(x) = \sum_k \widehat{\Lambda}_k^{(\text{N-Ball})^{(1)}}([0, x]) \exp\left(-\sum_{\mathcal{K}} \widehat{\Lambda}_{\mathcal{K}}^{(\text{N-Ball})}([0, x])\right) \quad (4.17)$$

where $k, \mathcal{K} \in \{\text{LOS}, \text{NLOS}\}$, the intensity of the path-loss-to-fading ratio of links in state k is

$$\begin{aligned} \widehat{\Lambda}_k^{(\text{N-Ball})}([0, x]) &= \pi \lambda_{\text{BS}} \left\{ \sum_{n=1}^N q_k^{[D_{n-1}, D_n]} \widetilde{\mathcal{Q}}_k\left(\frac{2}{\beta_k}, \frac{\kappa_k D_n^{\beta_k}}{x}, \frac{\kappa_k D_{n-1}^{\beta_k}}{x}\right) (x/\kappa_k)^{2/\beta_k} \right. \\ &+ \sum_{n=1}^N q_k^{[D_{n-1}, D_n]} \left(\overline{\mathcal{Q}}_k\left(0, \frac{\kappa_k D_n^{\beta_k}}{x}\right) (D_n^2 - D_{n-1}^2) - \widetilde{\mathcal{Q}}_k\left(0, \frac{\kappa_k D_n^{\beta_k}}{x}, \frac{\kappa_k D_{n-1}^{\beta_k}}{x}\right) D_{n-1}^2 \right) \\ &\left. + q_k^{[D_N, \infty]} \left(\overline{\mathcal{Q}}_k\left(\frac{2}{\beta_k}, \frac{\kappa_k D_N^{\beta_k}}{x}\right) (x/\kappa_k)^{2/\beta_k} - \overline{\mathcal{Q}}_k\left(0, \frac{\kappa_k D_N^{\beta_k}}{x}\right) D_N^2 \right) \right\} \end{aligned} \quad (4.18)$$

where

$$\mathcal{Q}_k(v, z) = \frac{1}{\Gamma(m_k)} \left(\frac{\Omega_k}{m_k}\right)^v \gamma\left(m_k + v, \frac{m_k}{\Omega_k} z\right) \quad (4.19)$$

$$\bar{\mathcal{Q}}_k(v, z) = \frac{1}{\Gamma(m_k)} \left(\frac{\Omega_k}{m_k} \right)^v \Gamma \left(m_k + v, \frac{m_k}{\Omega_k} z \right) \quad (4.20)$$

$$\tilde{\mathcal{Q}}_k(v, z_1, z_2) = \mathcal{Q}_k(v, z_1) - \mathcal{Q}_k(v, z_2) \quad (4.21)$$

and the derivative of intensity is:

$$\begin{aligned} \hat{\Lambda}_k^{(\text{N-Ball})(1)}([0, x]) &= \pi \lambda_{\text{BS}} q_k^{[D_N, \infty]} \frac{2}{\beta_k} \kappa_k^{-2/\beta_k} x^{2/\beta_k - 1} \bar{\mathcal{Q}}_k \left(\frac{2}{\beta_k}, \frac{\kappa_k D_N^{\beta_k}}{x} \right) \\ &+ \pi \lambda_{\text{BS}} \sum_{n=1}^N \frac{2}{\beta_k} q_k^{[D_{n-1}, D_n]} \kappa_k^{-2/\beta_k} x^{2/\beta_k - 1} \tilde{\mathcal{Q}}_k \left(\frac{2}{\beta_k}, \frac{\kappa_k D_n^{\beta_k}}{x}, \frac{\kappa_k D_{n-1}^{\beta_k}}{x} \right) \end{aligned} \quad (4.22)$$

Proof: From the independence assumption of the fast fading, the intensity measure of the path-loss-to-fading ratios of the links from BSs to the typical MT can be formulated by $\hat{\Lambda}([0, x]) = \sum_k \Pr \{l_k(r)/h_k \in [0, x]\} = \mathbb{E}_{h_k} \left\{ \Lambda_k^{(\text{N-Ball})}([0, h_k x]) \right\}$. The result in (4.18) is obtained by calculating the expectation with respect to the channel fading. The rest of the proof follows a same procedure as in Proposition 4.1. \square

4.4.2 Characteristic function of the aggregate interference

The computation of the coverage probability by taking into account the influence of aggregate other-cell interference leverages on the probability generating functional (PGFL) of PPPs and on the Gil-Pelaez inversion theorem for smallest path-loss association and highest received power association, respectively. In both cases, the characteristic function (CF), or the Laplace transform of the interference is involved. In the following propositions, the CFs of the interference for two different cell association criteria are provided, respectively.

Proposition 4.3. *Let the downlink BS-to-MT links follow the multi-ball link state model as depicted in Section 4.3.1, and let the cell association based on the smallest path-loss. Conditioned on the path-loss of the intended link, the aggregate other-cell interference is:*

$$i_{agg} \left(L^{(0)} \right) = \sum_k \sum_{i \in \Phi_k} \left(\text{PG}^{(i)} h_k^{(i)} / L_k^{(i)} \right) \mathbf{1} \left(L_k^{(i)} > L^{(0)} \right) \quad (4.23)$$

where $k \in \{\text{LOS}, \text{NLOS}\}$. The characteristic function of the interference in (4.23) is:

$$\text{CF}_{i_{agg}} \left(\omega, L^{(0)} \right) = \prod_k \exp \left(\sum_{t_{\text{BS}}=1}^{T_{\text{BS}}} \sum_{t_{\text{MT}}=1}^{T_{\text{MT}}} \frac{\phi_{\text{BS}}^{(t_{\text{BS}})}}{2\pi} \frac{\phi_{\text{MT}}^{(t_{\text{MT}})}}{2\pi} \mathcal{T}_k \left(\omega, L^{(0)}, g_{\text{BS}}^{(t_{\text{BS}})}, g_{\text{MT}}^{(t_{\text{MT}})} \right) \right) \quad (4.24)$$

where

$$\begin{aligned} \mathcal{T}_k(\omega, x, g) = & \pi \lambda_{\text{BS}} \sum_{n=1}^N q_k^{[D_{n-1}, D_n]} \left\{ \overline{\mathcal{H}} \left(x - \kappa_k D_{n-1}^{\beta_k} \right) D_{n-1}^2 \mathcal{F}_k \left(\omega, \kappa_k D_{n-1}^{\beta_k}, g \right) \right. \\ & + \overline{\mathcal{H}} \left(x - \kappa_k D_n^{\beta_k} \right) \mathcal{H} \left(x - \kappa_k D_{n-1}^{\beta_k} \right) (x/\kappa_k)^{2/\beta_k} \mathcal{F}_k(\omega, x, g) \\ & \left. - \overline{\mathcal{H}} \left(x - \kappa_k D_n^{\beta_k} \right) D_n^2 \mathcal{F}_k \left(\omega, \kappa_k D_n^{\beta_k}, g \right) \right\} \end{aligned} \quad (4.25)$$

$$\begin{aligned} & + \pi \lambda_{\text{BS}} q_k^{[D_N, \infty]} \left\{ \overline{\mathcal{H}} \left(x - \kappa_k D_N^{\beta_k} \right) D_N^2 \mathcal{F}_k \left(\omega, \kappa_k D_N^{\beta_k}, g \right) \right. \\ & \left. + \mathcal{H} \left(x - \kappa_k D_N^{\beta_k} \right) (x/\kappa_k)^{2/\beta_k} \mathcal{F}_k(\omega, x, g) \right\} \\ \mathcal{F}_k(\omega, x, g) = & 1 - {}_2F_1 \left(m_k, -\frac{2}{\beta_k}, 1 - \frac{2}{\beta_k}, j\omega \text{Pg}\Omega_k / (xm_k) \right) \end{aligned} \quad (4.26)$$

Proof: See Appendix 4.B. □

Proposition 4.4. *Let the downlink BS-to-MT links follow the multi-ball link state model as depicted in Section 4.3.1, and let the cell association based on the highest received power. Conditioned on the path-loss-to-fading ratio of the intended link, the aggregate other-cell interference is:*

$$\widehat{i}_{agg} \left(\widehat{L}^{(0)} \right) = \sum_k \sum_{i \in \Phi_k} \left(\text{PG}^{(i)} / \widehat{L}_k^{(i)} \right) \mathbf{1} \left(\widehat{L}_k^{(i)} > \widehat{L}^{(0)} \right) \quad (4.27)$$

The characteristic function of the interference in (4.27) is:

$$\text{CF}_{\widehat{i}_{agg}} \left(\omega, \widehat{L}^{(0)} \right) = \prod_k \exp \left(\sum_{t_{\text{BS}}=1}^{T_{\text{BS}}} \sum_{t_{\text{MT}}=1}^{T_{\text{MT}}} \frac{\phi_{\text{BS}}^{(t_{\text{BS}})}}{2\pi} \frac{\phi_{\text{MT}}^{(t_{\text{MT}})}}{2\pi} \widehat{\mathcal{T}}_k \left(\omega, \widehat{L}^{(0)}, g_{\text{BS}}^{(t_{\text{BS}})}, g_{\text{MT}}^{(t_{\text{MT}})} \right) \right) \quad (4.28)$$

where

$$\begin{aligned}
 & \widehat{\mathcal{T}}_k(\omega, x, g) \\
 &= \pi \lambda_{\text{BS}} \sum_{n=1}^N q_k^{[D_{n-1}, D_n]} \\
 & \times \left\{ \frac{1}{\Gamma(m_k)} \left(D_{n-1}^2 \gamma \left(m_k, \frac{m_k \kappa_k D_{n-1}^{\beta_k}}{\Omega_k x} \right) - D_n^2 \gamma \left(m_k, \frac{m_k \kappa_k D_n^{\beta_k}}{\Omega_k x} \right) \right) \right. \\
 & \left. + \widehat{\mathcal{F}}_k(1, x, \omega, g) \widetilde{Q}_k \left(\frac{2}{\beta_k}, \frac{\kappa_k D_n^{\beta_k}}{x}, \frac{\kappa_k D_{n-1}^{\beta_k}}{x} \right) \left(\frac{x}{\kappa_k} \right)^{2/\beta_k} + \frac{m_k}{\Omega_k} \widehat{E}_k(D_n, D_{n-1}, x, \omega, g) \right\} \\
 & + \pi \lambda_{\text{BS}} q_k^{[D_N, \infty]} \left\{ \frac{D_N^2}{\Gamma(m_k)} \gamma \left(m_k, \frac{m_k \kappa_k D_N^{\beta_k}}{\Omega_k x} \right) - D_N^2 \frac{m_k}{\Omega_k} \left(\kappa_k D_N^{\beta_k} \right)^{m_k} \right. \\
 & \left. \times E_k \left(\frac{m_k}{\Omega_k} \kappa_k D_N^{\alpha_k}, x, \omega, g \right) + \widehat{\mathcal{F}}_k(1, x, \omega, g) \overline{Q}_k \left(\frac{2}{\beta_k}, \frac{\kappa_k D_N^{\beta_k}}{x} \right) \left(\frac{x}{\kappa_k} \right)^{2/\beta_k} \right\}
 \end{aligned} \tag{4.29}$$

$$\widehat{\mathcal{F}}_k(y, x, \omega, g) = 1 - {}_1F_1 \left(-\frac{2}{\beta_k}, 1 - \frac{2}{\beta_k}, \frac{j\omega P g}{x} y \right) \tag{4.30}$$

$$\begin{aligned}
 \widehat{E}_k(D_n, D_{n-1}, x, \omega, g) &= D_n^2 \left(\kappa_k D_n^{\beta_k} \right)^{m_k} E_k \left(\frac{m_k}{\Omega_k} \kappa_k D_n^{\alpha_k}, x, \omega, g \right) \\
 & - D_{n-1}^2 \left(\kappa_k D_{n-1}^{\beta_k} \right)^{m_k} E_k \left(\frac{m_k}{\Omega_k} \kappa_k D_n^{\alpha_k}, x, \omega, g \right)
 \end{aligned} \tag{4.31}$$

$$E_k(y, x, \omega, g) = \frac{\gamma(m_k, xy)}{\Gamma(m_k)} \overline{\overline{\mathcal{F}}}_k(x, \omega, g) - \frac{y^{m_k} e^{-xy}}{x \Gamma(m_k)} B_k(y, x, \omega, g) \tag{4.32}$$

$$\overline{\overline{\mathcal{F}}}_k(x, \omega, g) = \frac{1}{x^{m_k}} {}_2F_1 \left(m_k, -\frac{2}{\beta_k}, 1 - \frac{2}{\beta_k}, \frac{j\omega P g}{x} \right) \tag{4.33}$$

$$B_k(y, x, \omega, g) \approx \frac{\widehat{\mathcal{F}}_k(m_k, x, \omega, g) - \widehat{\mathcal{F}}_k(y, 1, \omega, g)}{y - m_k/x} \tag{4.34}$$

Proof: See Appendix 4.B. □

4.4.3 Prony approximation on the CDF of Gamma distribution

Assume a random variable h_k follows a Gamma distribution, i.e., $h_k \sim \mathcal{G}(m_k, m_k/\Omega_k)$. Then, by applying the Prony approximation, the complementary cumulative distribution function (CCDF) of h_k can be closely approximated by a series of exponential functions,

which can be formulated as follows:

$$\Pr \{h_k \geq V_T\} = 1 - \frac{1}{\Gamma(m_k)} \gamma(m_k \cdot V_T m_k / \Omega_k) \approx \sum_{n_p=1}^{N_{\text{Prony}}} a_{n_p} \exp(-V_T b_{n_p} m_k / \Omega_k) \quad (4.35)$$

When $m_k = 1$, i.e., Rayleigh fading is considered, $\Pr \{h_k \geq V_T\} = \exp(-V_T / \Omega_k)$, and no approximation is assumed. The parameters a_{n_p} and b_{n_p} for $n_p = 1, 2, \dots, N_{\text{Prony}}$ in (4.35) can be obtained by solving the following optimization problem using the Matlab built-in function ‘fmincon’:

$$\arg \min_{\{a_{n_p}\}, \{b_{n_p}\}} \left\{ \left\| 1 - \frac{1}{\Gamma(m_k)} \gamma(m_k \cdot V_T m_k / \Omega_k) - \sum_{n_p=1}^{N_{\text{Prony}}} a_{n_p} \exp(-V_T b_{n_p} m_k / \Omega_k) \right\|_F^2 \right\} \quad (4.36)$$

4.4.4 Coverage Probability for Smallest path-loss Association

The SINR of the received signal at the MT when smallest path-loss association is assumed can be expressed by:

$$\text{SINR}_{\text{PL}} = \sum_k \frac{\text{PG}^{(0)} h_k^{(0)} / L_k^{(0)}}{\sigma_N^2 + i_{agg}(L_k^{(0)})} \delta(L^{(0)} - L_k^{(0)}) \quad (4.37)$$

where $k \in \{\text{LOS}, \text{NLOS}\}$. The coverage probability of the SINR in (4.37) is given in the following proposition.

Proposition 4.5. *Let the downlink BS-to-MT links follow the multi-ball link state model as depicted in Section 4.3.1, and let the the smallest path-loss cell association. The coverage probability of the SINR in (4.37) is:*

$$\text{P}_{\text{cov}}^{(\text{PL})}(V_T) = \sum_k \int_0^\infty \mathcal{J}_k(V_T, x) \Lambda_k^{(\text{N-Ball})(1)}([0, x]) \exp\left(-\sum_{\mathcal{K}} \Lambda_{\mathcal{K}}^{(\text{N-Ball})}([0, x])\right) dx \quad (4.38)$$

where $k, \mathcal{K} \in \{\text{LOS}, \text{NLOS}\}$, $\mathcal{J}_k(V_T, x)$ is the coverage probability conditioned on the path-loss of the intended link in state k , which can be formulated by

$$\mathcal{J}_k(V_T, x) \approx \sum_{n_p=1}^{N_{\text{Prony}}} a_{n_p} \exp\left(-\frac{b_{n_p} m_k V_T x \sigma_N^2}{\Omega_k \text{PG}^{(0)}}\right) \text{CF}_{i_{agg}}\left(j \frac{b_{n_p} m_k V_T x}{\Omega_k \text{PG}^{(0)}}, x\right) \quad (4.39)$$

where $\text{CF}_{i_{agg}}(\cdot, \cdot)$ is the CF defined in (4.24).

Proof: From the total probability theorem, the coverage probability of the system can be formulated by:

$$P_{\text{cov}}^{(\text{PL})}(\mathbf{V}_T) = \sum_k \mathbb{E}_{L_k^{(0)}} \left[\mathcal{J}_k(\mathbf{V}_T, L_k^{(0)}) \Pr \left\{ L^{(0)} = L_k^{(0)} \right\} \right] \quad (4.40)$$

where the probability that the intended link is in state k can be calculated by:

$$\Pr \left\{ L^{(0)} = L_k^{(0)} \right\} \stackrel{(a)}{=} \prod_{\bar{k}} \Pr \left\{ L_{\bar{k}}^{(0)} > L_k^{(0)} \right\} \stackrel{(b)}{=} \prod_{\bar{k}} \exp \left(-\Lambda_{\bar{k}}^{(\text{N-Ball})} \left([0, L_k^{(0)}] \right) \right) \quad (4.41)$$

where $\bar{k} \in \{\text{LOS}, \text{NLOS}\}$ and $\bar{k} \neq k$; (a) follows from the independence assumption; (b) is obtained from the void probability of the path-loss process. The conditional coverage probability can be calculated by

$$\begin{aligned} \mathcal{J}_k(\mathbf{V}_T, x) &= \Pr \left\{ h_k^{(0)} \geq V_T L_k^{(0)} (\sigma_N^2 + i_{\text{agg}}(x)) \left(\text{PG}^{(0)} \right)^{-1} \right\} \\ &\stackrel{(c)}{\approx} \sum_{n_p=1}^{N_{\text{Prony}}} a_{n_p} \mathbb{E}_{i_{\text{agg}}(\cdot)} \left[\exp \left(-b_{n_p} m_k V_T L_k^{(0)} (\sigma_N^2 + i_{\text{agg}}(x)) \left(\text{PG}^{(0)} \Omega_k \right)^{-1} \right) \right] \end{aligned} \quad (4.42)$$

where (c) follows from the Prony approximation of the CCDF of Nakagami- m random variable introduced in Section 4.4.3. The rest of the proof follows by calculating the expectation in (4.42) with the aid of the conditional CF given in Proposition 4.3, and the expectation in (4.40) with the aid of the PDF of $L_k^{(0)}$, i.e., $f_{L_k^{(0)}}(x) = \Lambda_k^{(\text{N-Ball})(1)}([0, x]) \exp \left(-\Lambda_k^{(\text{N-Ball})}([0, x]) \right)$. This concludes the proof. \square

4.4.5 Coverage Probability for Highest Received Power Association

The SINR of the received signal at the MT when the highest received power association is assumed can be expressed by:

$$\text{SINR}_{\text{HP}} = \frac{\text{PG}^{(0)} / \widehat{L}^{(0)}}{\sigma_N^2 + \widehat{i}_{\text{agg}}(\widehat{L}^{(0)})} \quad (4.43)$$

The coverage probability of the SINR in (4.43) is given in the following proposition.

Proposition 4.6. *Let the downlink BS-to-MT links follow the multi-ball link state model as depicted in Section 4.3.1, and let the highest received power cell association. The*

coverage probability of the SINR in (4.43) is:

$$P_{\text{cov}}^{(\text{HP})}(\mathbf{V}_T) = \int_0^\infty \hat{\mathcal{J}}(\mathbf{V}_T, x) f_{\hat{L}^{(0)}}(x) dx \quad (4.44)$$

where $f_{\hat{L}^{(0)}}(x)$ is given in (4.17), $\hat{\mathcal{J}}(\mathbf{V}_T, x)$ is the coverage probability conditioned on the path-loss-to-fading ratio of the intended link, which is formulated by

$$\hat{\mathcal{J}}(\mathbf{V}_T, x) = \frac{1}{2} - \frac{1}{\pi} \int_0^\infty \frac{1}{\omega} \text{Im} \left\{ \exp \left(-j\omega \frac{\text{PG}^{(0)}}{x\mathbf{V}_T} \right) \exp(j\omega\sigma_N^2) \text{CF}_{i_{agg}}(\omega, x) \right\} d\omega \quad (4.45)$$

where $\text{CF}_{i_{agg}}(\omega, x)$ is the CF of interference defined in (4.28).

Proof: Conditioned on the smallest path-loss-to-fading ratio, the CCDF of the SINR in (4.43) can be expressed as the CDF of the interference, i.e.,

$$\Pr \left\{ \text{SINR}_{\text{HP}}(\hat{L}^{(0)}) \geq \mathbf{V}_T \right\} = \Pr \left\{ i_{agg}(\hat{L}^{(0)}) \leq \text{PG}^{(0)} / (\mathbf{V}_T \hat{L}^{(0)}) - \sigma_N^2 \right\} \quad (4.46)$$

Then, (4.45) can be derived from (4.46) by applying the Gil-Pelaez inversion theorem [94]. The coverage probability in (4.44) is obtained by calculating the expectation $\mathbb{E}_{\hat{L}_0} \left[\hat{\mathcal{J}}(\mathbf{V}_T, \hat{L}_0) \right]$ with the aid of the PDF of $\hat{L}^{(0)}$ defined in (4.17). \square

4.4.6 Fast Fourier Transform Based Efficient Computation

It is worthy to mention that the numerical evaluation of the coverage probability consisting of a two-fold integral and invoking the Gil-Pelaez inversion theorem is not efficient in the state-of-the-art computational software, e.g., in Mathematica 10. To address the computational problem, and to improve the stability of the proposed algorithm, a fast computation technique is introduced in this section, which can be used to efficiently evaluate the integral involving Gil-Pelaez inversion theorem.

Lemma 4.1. Let $\text{CF}_X(\omega)$ denote the CF of the random variable X . By invoking the Gil-Pelaez inversion theorem [94], the CDF of X can be expressed as:

$$\Pr \{X \leq T\} = \frac{1}{2} - \frac{1}{\pi} \int_0^\infty \frac{1}{\omega} \text{Im} \{ e^{-j\omega T} \text{CF}_X(\omega) \} d\omega \quad (4.47)$$

Let $\bar{f}(\omega_n) = (\text{CF}_X(\omega_n)/\omega_n) \mathcal{H}(\omega_n)$, where $\omega_n = -(\mathcal{N}\beta)/2 + \beta n$ for $n = 0, \dots, \mathcal{N} - 1$; \mathcal{N} is a real positive integer which is power of 2; β denotes the sampling interval of the

input function $\bar{f}(\omega)$. Then, if the sampling frequency constraint $1/\beta > T/\pi$ is satisfied, (4.47) can be approximated by:

$$\Pr \{X \leq T\} \approx \frac{1}{2} - \frac{1}{\pi} \text{Im} \left\{ (-1)^k \beta \mathbf{F}_{(-1)^n \bar{f}(\omega_n)} [k] \right\} \quad (4.48)$$

where $k = \lceil TN\beta/(2\pi) \rceil + N/2$.

Proof: It is noticeable that the output of the integral in (4.47) is equivalent to the imaginary part of the continuous Fourier transform (CFT) of $\bar{f}(\omega_n)$. Then, the rest of the proof follows [95, Eq. 5-10] where the continuous Fourier transform is numerically evaluated using fast Fourier transform (FFT). Finally, the sampling frequency constraint should be satisfied such that $k < N$. \square

Lemma 4.1 is directly applicable to the evaluation of Proposition 4.6. More specifically, by assuming the system is interference limited, i.e., $\sigma_N^2 \rightarrow 0$, $P_{\text{cov}}^{(\text{HP})}(\mathbf{V}_T)$ in (4.44) can be evaluated by

$$\begin{aligned} P_{\text{cov}}^{(\text{HP})}(\mathbf{V}_T) &\stackrel{(a)}{=} \frac{1}{2} - \frac{1}{\pi} \text{Im} \left\{ \int_0^\infty \int_0^\infty \frac{1}{\omega} \exp \left(-j\omega \frac{PG^{(0)}}{xV_T} \right) \text{CF}_{\hat{i}_{agg}}(\omega, x) f_{\hat{L}^{(0)}}(x) d\omega dx \right\} \\ &\stackrel{(b)}{=} \frac{1}{2} - \frac{1}{\pi} \text{Im} \left\{ \int_0^\infty \exp \left(-j \frac{2\pi u}{N\beta} y \right) \bar{g}(y) dy \right\} \\ &\approx \frac{1}{2} - \frac{1}{\pi} \text{Im} \left\{ (-1)^k \beta \mathbf{F}_{(-1)^n \bar{g}(y_n)} [k] \right\} \end{aligned} \quad (4.49)$$

where (a) follows by inserting (4.45) into (4.44), (b) is obtained through the change of variable $y = G^{(0)}P\omega N\beta/(2\pi uxV_T)$, and by introducing $\bar{g}(y)$ defined as follows,

$$\bar{g}(y) = (1/y) \int_0^\infty \text{CF}_{\hat{i}_{agg}} \left(2\pi uxV_T y / (G^{(0)}PN\beta), x \right) f_{\hat{L}^{(0)}}(x) dx \quad (4.50)$$

where $u < N/2$ is a positive integer, and $k = u + N/2$ in the intended k -th output of the FFT. It is noticeable that the approximation introduced by the round operation in (4.48) is avoided thanks to the change of variable. In practice, the FFT in (4.49) can be efficiently computed using the Mathematica built-in function ‘Fourier’ with setup ‘FourierParameters $\rightarrow \{1, -1\}$ ’, and $u = 1$ is chosen to reduce the aliasing.

4.4.7 Generalization

The proposed analytical framework leveraging on the multi-ball link state approximation investigates the performance of single-tier cellular networks. The extension to multi-tier cellular networks is straightforward. In this subsection, the coverage probability of multi-tier cellular networks, where the cell association is based on the biased smallest path-loss, is presented.

Consider a multi-tier cellular network consisting of \mathcal{P} tiers of BSs which are characterized by different transmit power P_p for $p = 1, 2, \dots, \mathcal{P}$ as well as different directivity gains $g_{\text{BS},p}^{(t_p)}$ for $t_p = 1, 2, \dots, T_{\text{BS},p}$. The BSs of each tier are distributed according to independent homogeneous PPPs of density $\lambda_{\text{BS}}^{(p)}$ for $p = 1, 2, \dots, \mathcal{P}$. Moreover, independent multi-ball link state models are assumed for BSs in each tier. In specific, the probability of a BS-to-MT link of length r , where the BS belongs to tier p , can be formulated as follows:

$$\begin{cases} p_{k,p}(r) = \sum_{n=1}^{N_p+1} q_{k,p}^{[D_{n-1}^{(p)}, D_n^{(p)}]} \mathbf{1}_{[D_{n-1}^{(p)}, D_n^{(p)}]}(r) \\ \sum_k q_{k,p}^{[D_{n-1}^{(p)}, D_n^{(p)}]} = 1, \quad n = 1, 2, \dots, N_p + 1 \end{cases} \quad (4.51)$$

The MT is assumed to be associated to a BS in tier p , for $p = 1, 2, \dots, \mathcal{P}$, if

$$\bar{B}_p / l_p^{(0)}(r) > \bar{B}_{\bar{p}} / l_{\bar{p}}^{(0)}(r) \quad (4.52)$$

where $\bar{p} = 1, 2, \dots, \mathcal{P}$ and $\bar{p} \neq p$, $l_p^{(0)}(r) = \min \{ l_{\text{LOS},p}^{(0)}(r), l_{\text{NLOS},p}^{(0)}(r) \}$ denotes the smallest path-loss of the links with BSs belonging to tier p , $\bar{B}_p = B_p P_p G_p^{(0)}$, B_p is the biasing factor, $G_p^{(0)}$ denotes the antenna gain of the intended link of tier p .

The SINR of the received signal in this case study is as follows:

$$\begin{aligned} \text{SINR}^{(\text{Multi})} &= \sum_{p=1}^{\mathcal{P}} \sum_k \frac{P_p G^{(0)} h_{k,p}^{(0)} / l_{k,p}^{(0)}(r)}{\sigma_{\text{N}}^2 + \sum_{\bar{p}=1}^{\mathcal{P}} \sum_{\bar{k}} \sum_{i \in \Phi_{\bar{k},\bar{p}}} [P G^{(i)} h_{\bar{k},\bar{p}}^{(i)} / l_{\bar{k},\bar{p}}^{(i)}(r)] \mathbf{1}_{(l_{\bar{k},\bar{p}}^{(i)}(r) > \bar{B}_{\bar{p}} \bar{B}_p^{-1} l_{k,p}^{(0)}(r))}} \\ &\times \delta \left(\bar{\bar{L}}^{(0)} - l_{k,p}^{(0)}(r) / \bar{B}_p \right) \end{aligned} \quad (4.53)$$

where $\bar{\bar{L}}^{(0)} = \min \{ l_{\text{LOS},1}^{(0)}(r) / \bar{B}_1, l_{\text{NLOS},1}^{(0)}(r) / \bar{B}_1, \dots, l_{\text{LOS},\mathcal{P}}^{(0)}(r) / \bar{B}_{\mathcal{P}}, l_{\text{NLOS},\mathcal{P}}^{(0)}(r) / \bar{B}_{\mathcal{P}} \}$.

Proposition 4.7. *Let the SINR of the multi-tier cellular network in (4.53), the coverage probability can be formulated as follows:*

$$\begin{aligned} P_{\text{cov}}^{(\text{Multi})}(\mathbf{V}_T) &= \sum_{p=1}^{\mathcal{P}} \sum_k \int_0^\infty \mathcal{J}_{k,p}^{(\text{Multi})}(\mathbf{V}_T, x) \Lambda_{k,p}^{(\text{N-Ball})(1)}([0, x]) \\ &\quad \times \exp\left(-\sum_{\hat{p}=1}^{\mathcal{P}} \sum_{\hat{k}} \Lambda_{\hat{k},\hat{p}}^{(\text{N-Ball})}\left(\left[0, \frac{\overline{B}_{\hat{p}}}{B_p} x\right]\right)\right) dx \end{aligned} \quad (4.54)$$

where $\mathcal{J}_{k,p}^{(\text{Multi})}(\mathbf{V}_T, x)$ denotes the coverage probability conditioned on the path-loss of the intended link from tier p and in state k , which can be formulated by

$$\begin{aligned} &\mathcal{J}_{k,p}^{(\text{Multi})}(\mathbf{V}_T, x) \\ &\approx \sum_{n_{k,p}=1}^{N_{\text{Prony}}^{(k,p)}} a_{n_{k,p}} \exp\left(-\frac{b_{n_{k,p}} m_{k,p} \mathbf{V}_T \sigma_N^2}{\Omega_{k,p} P_p G_p^{(0)}} x\right) \text{CF}_{i_{agg}}^{(\text{Multi})}\left(j \frac{b_{n_{k,p}} m_{k,p} \mathbf{V}_T x}{\Omega_{k,p} P_p G_p^{(0)}}, x\right) \end{aligned} \quad (4.55)$$

The intensity measure $\Lambda_{k,p}^{(\text{N-Ball})}([0, x])$ and its derivative $\Lambda_{k,p}^{(\text{N-Ball})(1)}([0, x])$ are of the same form as their counterparts in Proposition 4.1 by replacing λ_{BS} with $\lambda_{\text{BS}}^{(p)}$, D_n with $D_n^{(p)}$ for $n = 1, 2, \dots, N_p$, $q_k^{[D_{n-1}, D_n]}$ with $q_k^{[D_{n-1}^{(p)}, D_n^{(p)}]}$, κ_k with $\kappa_{k,p}$, and β_k with $\beta_{k,p}$. And the CF of the interference in the heterogeneous cellular network is

$$\begin{aligned} &\text{CF}_{i_{agg}}^{(\text{Multi})}(\omega, x) \\ &= \prod_{\bar{p}=1}^{\mathcal{P}} \prod_k \exp\left(\sum_{t_{\text{BS},\bar{p}}=1}^{T_{\text{BS},\bar{p}}} \sum_{t_{\text{MT},\bar{p}}=1}^{T_{\text{MT},\bar{p}}} \frac{\phi_{\text{BS}}^{(t_{\text{BS}})}}{2\pi} \frac{\phi_{\text{MT}}^{(t_{\text{MT}})}}{2\pi} \mathcal{T}_{\bar{k},\bar{p}}\left(\omega, \frac{\overline{B}_{\bar{p}}}{B_p} x, g_{\text{BS},\bar{p}}^{(t_{\text{BS},\bar{p}})}, g_{\text{MT},\bar{p}}^{(t_{\text{MT},\bar{p}})}\right)\right) \end{aligned} \quad (4.56)$$

$\mathcal{T}_{\bar{k},\bar{p}}(\cdot, \cdot, \cdot)$ is of the same form as its counterpart in Proposition 4.3 by replacing the subscript k with $\{\bar{k}, \bar{p}\}$. \square

4.5 Performance Trends and Design Insights

In this section, the fundamental performance trends of the cellular network relying on the emerging multi-ball link state models are studied, which shed light on the engineering design and system-level optimization. Due to the space limitation and to ease the presentation, the trends are derived based on the single-tier cellular network by considering the smallest path-loss association. Similar conclusions can be drawn by analyzing other case study at the cost of more complicated algebraic manipulations.

a) *The impact of antenna radiation pattern*

From the direct inspection of (4.39) and of the distributions of the antenna patterns in Table 4.3, the following trends can be derived: 1) the antenna gain of the intended link in the absence of alignment errors $G^{(0)} > 1$ are capable of enhancing the useful signal, which is equivalent to reducing the threshold of the coverage by noticing the term $V_T/G^{(0)}$ in (4.39); 2) the impact of the antenna gains of the interfering links $G^{(i)} \leq G^{(0)}$ can be studied by focusing our attention on the CF of interference in (4.39), specifically, on the term $V_T G^{(i)}/G^{(0)}$ before computing the expectation with respect to $G^{(i)}$. It is obvious that $G^{(i)}/G^{(0)} < 1$, so the antenna gains of the interfering links are capable of increasing the performance of the system.

b) *The impact of BS density λ_{BS}*

The analysis follows the same line of thought as [96] where two scenarios are studied: 1) $\kappa_{NLOS} D_1^{\beta_{NLOS}} > \kappa_{LOS} D_1^{\beta_{LOS}} \gg L^{(0)}$ which corresponds to a dense deployment of BSs, i.e., large λ_{BS} ; 2) $L^{(0)} \gg \kappa_{NLOS} D_N^{\beta_{NLOS}} > \kappa_{LOS} D_N^{\beta_{LOS}}$ which corresponds to a sparse deployment of BSs, i.e., small λ_{BS} . To ease the presentation, Rayleigh fading with $\Omega_{LOS} = \Omega_{NLOS} = 1$, omni-directional antennas at the BSs and the MT are assumed for all the links. Then, the coverage probability for sparse and dense cellular networks, respectively, are as follows:

$$P_{cov}^{(sparse)}(V_T) \stackrel{(a)}{=} \int_0^\infty \left[\frac{2\pi}{\beta_{NLOS}} q_{NLOS}^{[D_N, \infty]} \kappa_{NLOS}^{-2/\beta_{NLOS}} x^{2/\beta_{NLOS}-1} \exp\left(-\frac{V_T x \sigma_N^2}{\lambda_{BS}^{\beta_{NLOS}/2} P \xi^{(0)}}\right) - \pi q_{NLOS}^{[D_N, \infty]} \left(\frac{x}{\kappa_{NLOS}}\right)^{\frac{2}{\beta_{NLOS}}} {}_2F_1\left(1, -\frac{2}{\beta_{NLOS}}, 1 - \frac{2}{\beta_{NLOS}}, -V_T\right) \right] dx \quad (4.57)$$

$$P_{cov}^{(dense)}(V_T) \stackrel{(b)}{=} \int_0^\infty \Theta(V_T, y) \frac{2\pi}{\beta_{LOS}} \kappa_{LOS}^{-2/\beta_{LOS}} y^{2/\beta_{LOS}-1} q_{LOS}^{[0, D_1]} dy \quad (4.58)$$

$$\begin{aligned} \Theta(V_T, y) = & \exp\left(-\sum_k \pi \lambda_{BS}^{1-\beta_{LOS}/\beta_k} q_k^{[0, D_1]} \left(\frac{y}{\kappa_k}\right)^{2/\beta_k} {}_2F_1\left(1, -\frac{2}{\beta_k}, 1 - \frac{2}{\beta_k}, -V_T\right)\right) \\ & + \pi \sum_k \sum_{n=1}^N \left(q_k^{[D_{n-1}, D_n]} - q_k^{[D_n, D_{n+1}]}\right) \lambda_{BS} D_n^2 {}_2F_1\left(1, -\frac{2}{\beta_k}, 1 - \frac{2}{\beta_k}, -\frac{V_T y}{\kappa_k \lambda_{BS}^{\beta_{LOS}/2} D_n^{\beta_k}}\right) \end{aligned} \quad (4.59)$$

where (a) is obtained by noticing that $q_{\text{LOS}}^{[D_{\text{N}}, \infty]} \approx 0$ for practical setups, and in the sparse deployed network, the BSs are distributed outside the ball with largest radius; and (b) holds by taking into account that, in general $q_{\text{LOS}}^{[0, D_1]} \gg q_{\text{NLOS}}^{[0, D_1]}$, $\beta_{\text{NLOS}} \gg \beta_{\text{LOS}}$, and by neglecting the impact of noise since the dense deployed network is interference-limited.

From (4.57), it is observed that the coverage probability monotonically increases as λ_{BS} increases in sparse cellular network. From (4.58) and (4.59), we notice that the first addend inside the exponential function in (4.59) monotonically decreases as λ_{BS} increases. The impact of density in the second addend can be drawn by focusing on the terms $\lambda_{\text{BS}} D_n^2$ and $\lambda_{\text{BS}}^{\beta_{\text{LOS}}/2} D_n^{\beta_k}$. From them, we realize that increasing λ_{BS} is equivalent to increasing the radius of the first ball D_1 of the link state model while keeping the LOS/NLOS probabilities constant. Since $q_{\text{LOS}}^{[0, D_1]} \gg q_{\text{NLOS}}^{[0, D_1]} \approx 0$ for typical system setups, this implies that more links are in LOS as λ_{BS} increases, which degrades the coverage probability [96]. In conclusion, the coverage probability monotonically increases as λ_{BS} increases in sparse network while it monotonically decreases as λ_{BS} increases in dense network. This implies that at least one optimal density exists which maximizes the coverage probability.

4.6 Numerical and Simulation Results

In this section, the some numerical examples are illustrated to validate the accuracy of the proposed multi-ball state approximation and to show the performance trend of cellular networks with LOS/NLOS links compared to those with the single state model. Unless otherwise stated, the following simulation setup, which is in agreement with the LTE-A standard, is assumed. The transmit power of the BSs is $P = 30$ dBm; the noise power is $\sigma_N^2 = -174 + 10 \log_{10}(\text{B}_W) + \mathcal{F}_{\text{dB}}$, where $\text{B}_W = 20$ MHz is the transmission bandwidth and $\mathcal{F}_{\text{dB}} = 10$ dB is the noise figure; $\kappa_{\text{LOS}} = \kappa_{\text{NLOS}} = (4\pi/\nu)^2$ is the free space path-loss at a distance of 1 meter from the transmitter, where $\nu = c/f_c$ is the signal wavelength, $c \approx 3 \times 10^8$ meters/sec is the speed of light, and $f_c = 2.1$ GHz is the signal frequency; the path-loss exponents of LOS and NLOS links are $\beta_{\text{LOS}} = 2.5$ and $\beta_{\text{NLOS}} = 3.5$; the fast-fading envelope of the LOS links follows a Nakagami- m distribution with parameters $m = 2$ and $\Omega_{\text{LOS}} = 1$; the fast-fading envelope of the NLOS links follows a Rayleigh distribution with parameter $\Omega_{\text{NLOS}} = 1$. The network density, λ_{BS} , is expressed in terms of the average cell radius, i.e., $R_{\text{cell}} = \sqrt{1/(\pi\lambda)}$,

TABLE 4.5: Three-ball approximations of state models in Section 4.2.2 obtained as the solution of (4.10).

	D_1	D_2	D_3	$q_{\text{LOS}}^{[0,D_1]}$	$q_{\text{LOS}}^{[D_1,D_2]}$	$q_{\text{LOS}}^{[D_2,D_3]}$	$q_{\text{LOS}}^{[D_3,\infty]}$
3GPP model	47.7989	215.9387	1874.442	0.9446	0.2142	0.0243	0.0021
Random Shape	5.2414	20.2029	60.4573	0.9941	0.6166	0.1851	0
Linear model	8.7212	31.2749	70.5092	0.8979	0.7673	0.5211	0.2

TABLE 4.6: Four-lobe approximations of antenna radiation patterns in Section 4.2.4 obtained as the solution of (4.13).

	$\varphi^{(1)}$	$\varphi^{(2)}$	$\varphi^{(3)}$	$g^{(1)}$	$g^{(2)}$	$g^{(3)}$	$g^{(4)}$
3GPP Pattern	16.152°	32.304°	48.455 °	7.783	2.673	0.312	0.047
UWLA	6.44°	14.46°	176.78°	9.903	1.975	0.390	11.521
Sectors	30°	40°	45°	4.946	2.469	0.025	0.05

and $R_{\text{cell}}=63.1771$ meters unless otherwise stated. This is the setup for an ultra dense cellular network which agrees with the empirical BSs deployment from the combination of O2 and Vodafone in London, see A.2.1.

Furthermore, when the random shape based link state model is considered, $\gamma_{\text{RS}} = 1$, $\alpha_{\text{RS}} = 0.046$ for the Manhattan region as used by [81]. When the linear model is considered, $a_{\text{LM}} = 0.0078$, $b_{\text{LM}} = 0.1$, and $c_{\text{LM}} = 0.8$ for the outdoor local area with foliage [83]. For the 3GPP suggested pathloss model, no specific parameters need to be defined. For simplicity, we assume that the antenna structure at the BSs and the MT are the same. When the 3GPP suggested antenna model is assumed, a 6 sector scenario [92] is assumed where $\theta^{(3\text{dB})} = 35^\circ$, $A = 23$, $\varphi^{(3\text{GPP})} = 48.46^\circ$, $g^{(3\text{GPP})} = 9.33$. When UWLA patterns are assumed, $d = v/2$, and 8 antennas are assumed, $g^{(\text{UWLA})} = 12.1631$. When sector pattern with transition width are considered, $g^{(2;\text{Sec})} = 0.05$, $\varpi = 70^\circ$, $\gamma = 10^\circ$, which corresponds to a 3 sectors scenario. In the present chapter, we use the 3-ball state model and 4-lobe antenna patterns to approximate the state models in Section 4.2.2 and antenna pattern models in Section 4.2.4, respectively, which provides a good matching accuracy while still keeping the computational complexity at a low level. The parameters of the state approximation and pattern approximation are provided in Table 4.5 and 4.6, respectively.

The Monte Carlo simulations results are obtained by considering the actual link state models introduced in Section 4.2.2 as well as the actual antenna radiation patterns in

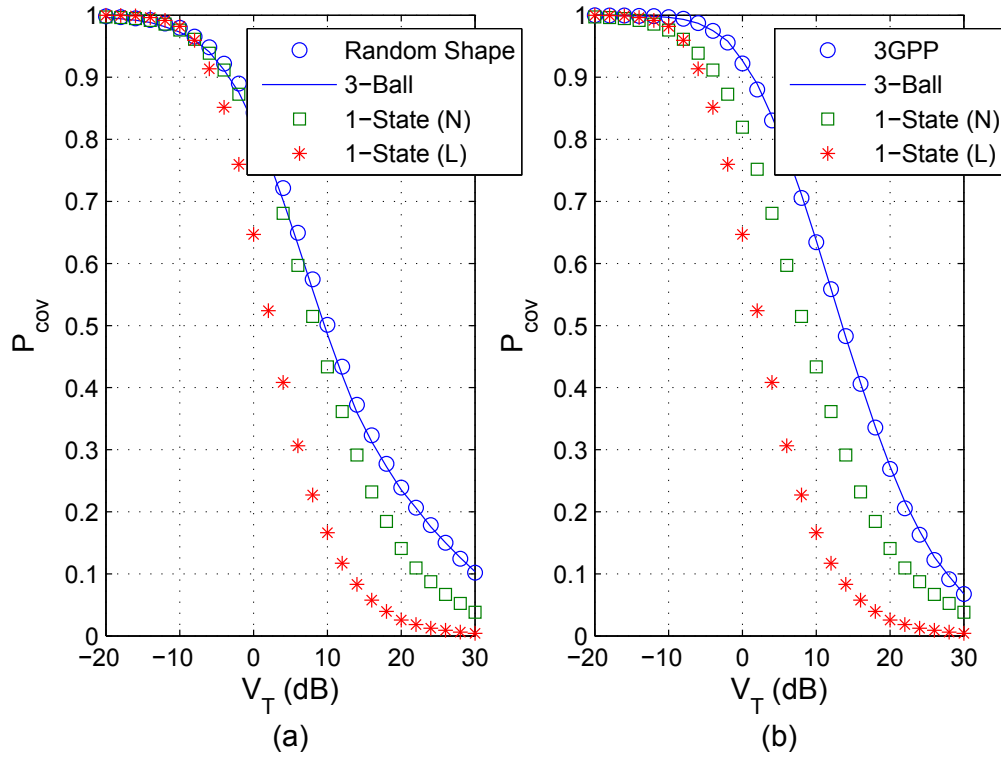


FIGURE 4.1: Coverage probability of smallest pathloss association by assuming sectored antennas unless otherwise stated. 1) "Random Shape": the LOS/NLOS link states follows the random shape model. 2) "3GPP": link states follows 3GPP model. 3) "3-Ball": link states follow corresponding 3-ball approximations and 4-lobe radiation pattern approximation is considered. 4) "1-State (N)" all links are in NLOS. 5) "1-State (L)" all links are in LOS.

Section 4.2.4. The multi-ball approximation and the multi-lobe approximation are not enforced in the simulator, they are, on the other hand, considered for the analytical performance analysis, e.g., using *Proposition 4.5*, *4.6*.

Selected numerical results are illustrated in Figs. 4.1–4.4. In general, a good agreement between mathematical framework and simulators is observed. More specifically, in Fig. 4.1, the suitability of the proposed multi-ball approximation and multi-lobe approximation for studying random shape link state models, 3GPP link state model and sectored antenna patterns in cellular networks are investigated. Besides the LOS/NLOS link state models, Fig. 4.1 also provides the coverage probability when LOS and NLOS links are not differentiated (typical approach used in the literature), and a single-state link model is assumed. In this case, all links are assumed to be either in LOS or in NLOS. The figures show that neglecting LOS and NLOS links results in significantly different performance estimates, which are usually lower bounds for the coverage probability

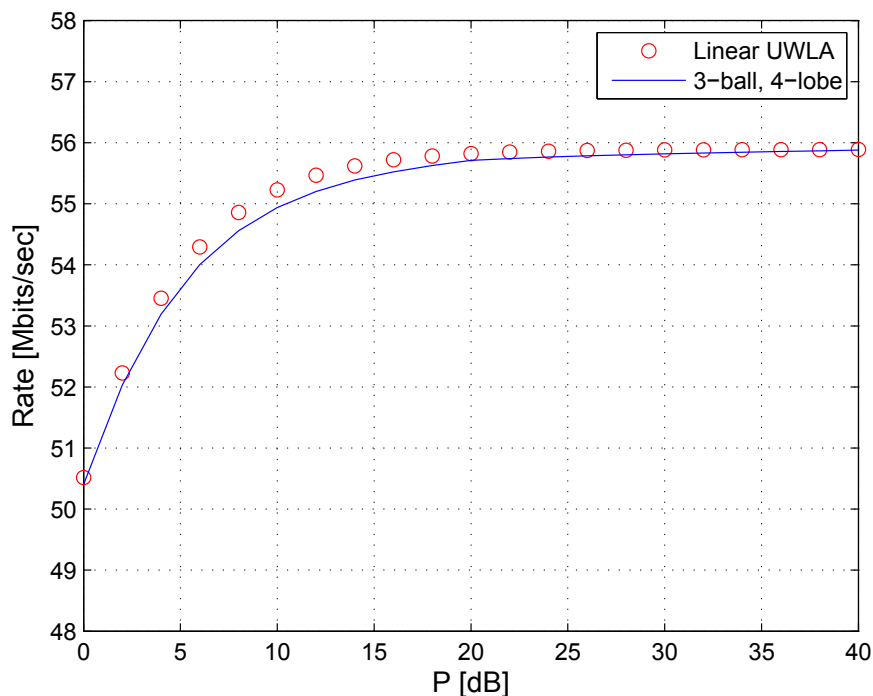


FIGURE 4.2: Average rate of smallest pathloss association. Markers show the Monte Carlo simulation results with link states following the linear model, and UWLA patterns are assumed. Solid line shows the 3-ball model with 4-lobe antennas.

by assuming LOS/NLOS states. This confirms the compelling need of using adequate path-loss and link state models for an accurate prediction of the performance of cellular networks. The higher numerical complexity of the resulting mathematical frameworks, which originates from the distance-dependent link state model, is, as a result, justified.

In Fig. 4.2, the average rate with respect to the transmit power of BSs is shown. The numerical results confirms the accuracy of the multi-ball model on approximating the linear model, and the accuracy of the multi-lobe model on approximating the UWLA patterns. Furthermore, it shows that when the transmit power is larger than 20dB, increasing the transmit power will not results in a gain in the performance, since the system is interference limited, and any increase in P on the intended link is counterbalanced with the increase of interference.

In Fig. 4.3, the coverage probability of cellular networks using highest received power association is shown. The mathematical framework in *Proposition 4.6* is evaluated with the aid of the fast computation technique in *Lemma 4.1*. Notably, increasing the number of the sampling points on the input signal for FFT will improve the accuracy of the

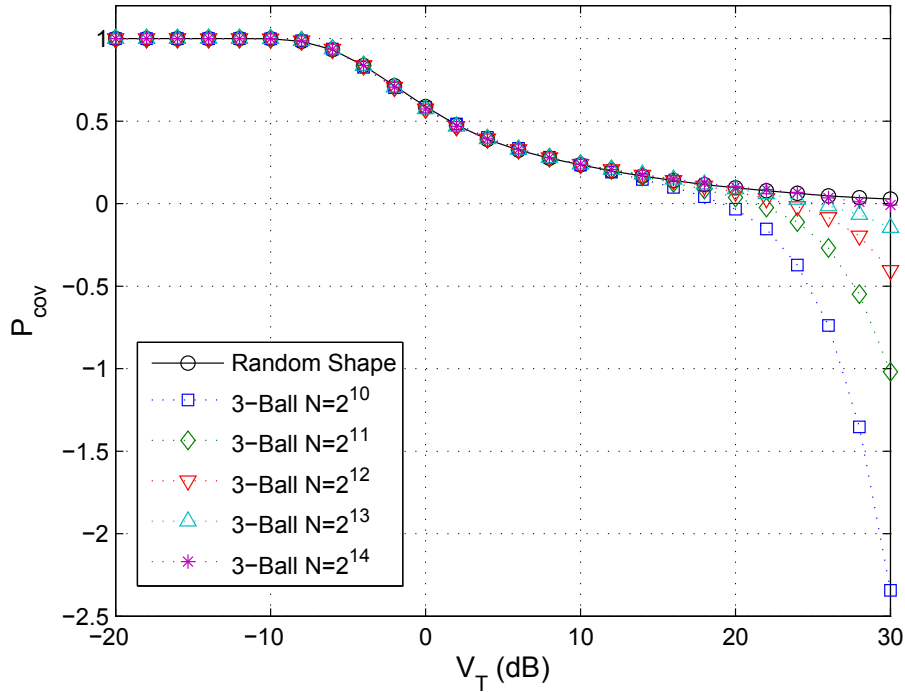


FIGURE 4.3: Coverage probability of highest received power association. Omni-directional antenna is assumed. The fast computation technique in *Lemma 4.1* is used by considering $\mathcal{N} = 2^{10}, 2^{11}, 2^{12}, 2^{13}, 2^{14}$ sampling points.

framework at the expense of increasing computational complexity. In general, the single-fold integral and the FFT can be efficiently evaluated in the commercial computational software, e.g., in *Mathematical 10*.

Finally, in Fig. 4.4, the impact of the density of BSs deployments is illustrated. The figure confirms, according to Section 4.5, that an optimal deployment density exists, as well as that the performance trend depends on the adequate link state model. In general, the optimal BSs densities, for different link state models, are different.

4.7 Conclusion

In this chapter, a new mathematical framework for computing the coverage probability and average rate cellular networks has been proposed by taking into account of the effect of LOS/NLOS propagation and the antenna gain. A multi-ball approximation for modeling the link state probabilities has been introduced, which is mathematically tractable and is shown to be able to accurately estimate other link state models available in the literature. The proposed approach is applicable to different cell association criteria

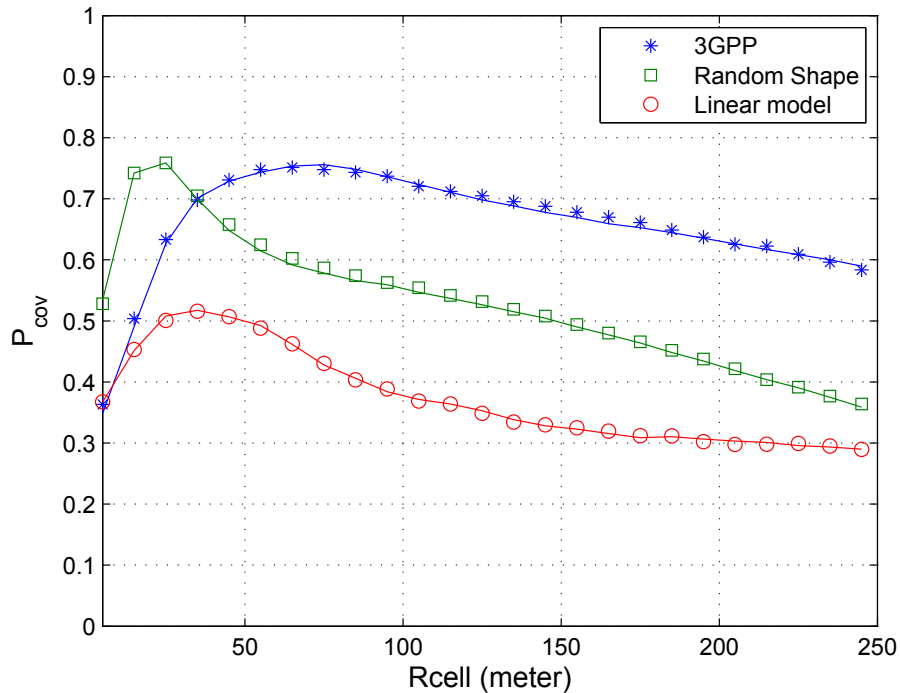


FIGURE 4.4: Coverage probability vs. BSs density, smallest pathloss association is assumed. $V_T = 10\text{dB}$. Markers show the Monte Carlo simulation results, where 1) "3GPP": link states follow 3GPP model. 2) "Random Shape": link states follow random shape model. 3) "3-Ball": link states follow linear model. 3GPP antenna gain patterns are assumed at both BSs and MTs. Solid line shows the 3-ball approximation with 4-lobe antenna pattern.

and multi-tier heterogeneous networks. And a FFT based fast computation technique is proposed to facilitate the computation involving the Gil-Pelaez inversion. It is shown from the framework that an optimal BS density exists when the LOS/NLOS attenuation is considered.

Appendix

4.A Useful Notable integrals

Notable Integral 1: Let \mathcal{A} be a real positive number, \mathcal{B} be a complex number with $\text{Re}\{\mathcal{B}\} \leq 0$, and $\beta > 2$ be a real number, the following identity holds [26]:

$$\int_{\mathcal{A}}^{\infty} (\exp(\mathcal{B}/t) - 1)t^{2/\beta-1} dt = (\beta/2) \mathcal{A}^{2/\beta} (1 - {}_1F_1(-2/\beta; 1 - 2/\beta; \mathcal{B}/\mathcal{A})) \quad (4.60)$$

Notable Integral 2: Let $m > 0$, $\Omega > 0$ be two real positive numbers, \mathcal{B} be a complex number with $\text{Re}\{\mathcal{B}\} < \text{Re}\{m/\Omega\}$, the following identity holds [4]:

$$\int_0^\infty \frac{m^m t^{m-1}}{\Omega^m \Gamma(m)} e^{\mathcal{B}t} e^{-mt/\Omega} dt = \frac{m^m}{\Omega^m} (m/\Omega - \mathcal{B})^{-m} \quad (4.61)$$

Notable Integral 3: Let $m > 0$, $\Omega > 0$ be two real positive numbers, \mathcal{B} be a complex number with $\text{Re}\{\mathcal{B}\} < \text{Re}\{m/\Omega\}$, the following identity holds [41, Eq. 8.350.1]:

$$\int_0^X \frac{m^m t^{m-1}}{\Omega^m \Gamma(m)} e^{\mathcal{B}t} e^{-mkt/\Omega} dt = \left(1 - \mathcal{B} \frac{\Omega}{m}\right)^{-m} \gamma\left(m, x \left(\frac{m}{\Omega} - \mathcal{B}\right)\right) / \Gamma(m) \quad (4.62)$$

Notable Integral 4: Let $m > 0$, $\Omega > 0$ be two real positive numbers, \mathcal{B} be a complex number with $\text{Re}\{\mathcal{B}\} < \text{Re}\{m/\Omega\}$, the following identity holds [41, Eq. 7.522.9]:

$$\int_0^\infty {}_1F_1\left(-\frac{2}{\beta}, 1 - \frac{2}{\beta}, \mathcal{B}t\right) \frac{m^m t^{m-1}}{\Omega^m \Gamma(m)} e^{-\frac{m}{\Omega}t} dt = {}_2F_1\left(m, -\frac{2}{\beta}, 1 - \frac{2}{\beta}, \mathcal{B} \frac{\Omega}{m}\right) \quad (4.63)$$

Notable Integral 5: Let m, X be real positive numbers, and z be a large real positive number. Let $f(t)$ be a holomorphic function in a domain that contains the nonnegative reals. The following approximation holds [97, Eq. 2.15]:

$$\int_0^X t^{m-1} e^{-zt} f(t) dt \approx \frac{\gamma(m, zX)}{\Gamma(m)} \int_0^\infty t^{m-1} e^{-zt} f(t) dt - \frac{X^m e^{-Xz}}{z} \frac{f(X) - f(m/z)}{X - m/z} \quad (4.64)$$

4.B Proof of Propositions in Section 4.4.2

1) *The proof of Proposition 4.3:*

The CF of $i_{agg}(\cdot)$ in (4.23) is computed from its definition as follows:

$$\begin{aligned} \text{CF}_{i_{agg}}(\omega, L^{(0)}) &\stackrel{(a)}{=} \prod_k \mathbb{E}_{(\cdot) \setminus L^{(0)}} \left[\exp \left(j\omega \sum_{i \in \Phi_k} \left(\text{PG}^{(i)} h_k^{(i)} / L_k^{(i)} \right) \mathbf{1} \left(L_k^{(i)} > L^{(0)} \right) \right) \right] \\ &\stackrel{(b)}{=} \prod_k \exp \left(\mathbb{E}_{(\cdot) \setminus L^{(0)}} \left[\int_0^\infty \left(\exp \left(j\omega \text{PG}^{(i)} h_k^{(i)} / x \right) - 1 \right) d\Lambda_k^{(\text{N-Ball})} \left([L^{(0)}, x) \right) \right] \right) \\ &\stackrel{(c)}{=} \prod_k \exp \left(\mathbb{E}_{(\cdot) \setminus L^{(0)}} \left[\int_{L^{(0)}}^\infty \left(\exp \left(j\omega \text{PG}^{(i)} h_k^{(i)} / x \right) - 1 \right) \Lambda_k^{(\text{N-Ball})(1)}([0, x)) dx \right] \right) \end{aligned} \quad (4.65)$$

where (a) is by the independence assumption; (b) is obtained from the PGFL of PPP [7]; (c) follows from the fact that $\frac{d}{dx} \Lambda_k^{(\cdot)}([L^{(0)}, x]) = \frac{d}{dx} [\Lambda_k^{(\cdot)}([0, x]) - \Lambda_k^{(\cdot)}([0, L^{(0)}])] = \Lambda_k^{(\cdot)(1)}([0, x])$. The expectation in (4.65) is computed with respect to $G^{(i)}$ and $h_k^{(i)}$. By inserting (4.15) into (4.65), the integral in (4.65) can be solved with the aid of the notable integral in (4.60). In addition, it should be point out that the integral in (4.65) is unsolvable, to the best of the author's knowledge, if other intensity measures in Table 4.4 are considered. After some mathematical simplifications, we have:

$$\begin{aligned}
 & \text{CF}_{i_{agg}}(\omega, L^{(0)}) \\
 &= \prod_k \exp \left\{ \pi \lambda_{\text{BS}} \sum_{n=1}^N q_k^{[D_{n-1}, D_n]} \left[\overline{\mathcal{H}}(L^{(0)} - \kappa_k D_{n-1}^{\beta_k}) D_{n-1}^2 \mathbb{E} \left[\widehat{\mathcal{F}}_k(\omega, \kappa_k D_{n-1}^{\beta_k}, G^{(i)}, h_k^{(i)}) \right] \right. \right. \\
 &+ \overline{\mathcal{H}}(L^{(0)} - \kappa_k D_n^{\beta_k}) \mathcal{H}(L^{(0)} - \kappa_k D_{n-1}^{\beta_k}) \left(\frac{L^{(0)}}{\kappa_k} \right)^{2/\beta_k} \mathbb{E} \left[\widehat{\mathcal{F}}_k(\omega, L^{(0)}, G^{(i)}, h_k^{(i)}) \right] \\
 &- \left. \left. \overline{\mathcal{H}}(L^{(0)} - \kappa_k D_n^{\beta_k}) D_n^2 \mathbb{E} \left[\widehat{\mathcal{F}}_k(\omega, \kappa_k D_n^{\beta_k}, G^{(i)}, h_k^{(i)}) \right] \right] \right. \\
 &+ \pi \lambda_{\text{BS}} q_k^{[D_N, \infty]} \left[\overline{\mathcal{H}}(L^{(0)} - \kappa_k D_N^{\beta_k}) D_N^2 \mathbb{E} \left[\widehat{\mathcal{F}}_k(\omega, \kappa_k D_N^{\beta_k}, G^{(i)}, h_k^{(i)}) \right] \right. \\
 &+ \left. \left. \mathcal{H}(L^{(0)} - \kappa_k D_N^{\beta_k}) \left(\frac{L^{(0)}}{\kappa_k} \right)^{2/\beta_k} \mathbb{E} \left[\widehat{\mathcal{F}}_k(\omega, L^{(0)}, G^{(i)}, h_k^{(i)}) \right] \right] \right\}
 \end{aligned} \tag{4.66}$$

where $\widehat{\mathcal{F}}_k(\cdot, \cdot, \cdot, \cdot)$ is defined in (4.30).

The rest of the proof follows by the computation of the expectations in (4.66) with respect to the channel fading and the antenna gain, respectively. In specific, the expectations on $\widehat{\mathcal{F}}_k(\cdot, \cdot, \cdot, \cdot)$ is computed through the following procedure: 1) the expectation with respect to the Nakagami- m fading is first computed with the aid of the notable integral in (4.63); 2) the expectations with respect to $G^{(i)}$ are computed by using the PDF in (4.12)

2) The proof of Proposition 4.4:

Following the same procedure as the proof of *Proposition 4.3*, the conditional CF of the interference in (4.27) can be formulated by

$$\begin{aligned}
 & \text{CF}_{\widehat{i}_{agg}} \left(\omega, \widehat{L}^{(0)} \right) \\
 &= \prod_k \exp \left(\mathbb{E}_{G^{(i)}} \left[\int_{\widehat{L}^{(0)}}^{\infty} \left(\exp \left(j\omega P G^{(i)} / x \right) - 1 \right) \widehat{\Lambda}_k^{(\text{N-Ball})(1)} ([0, x)) dx \right] \right) \\
 &\stackrel{(a)}{=} \prod_k \exp \left(\mathbb{E}_{G^{(i)}, h_k^{(i)}} \left[\int_{\widehat{L}^{(0)}}^{\infty} \left(\exp \left(j\omega P G^{(i)} / x \right) - 1 \right) h_k^{(i)} \Lambda_k^{(\text{N-Ball})(1)} \left([0, h_k^{(i)} x) \right) dx \right] \right)
 \end{aligned} \tag{4.67}$$

where (a) is obtained by swapping the order of expectations/integrals in order to ease the computation. By inserting (4.15) into (4.67), the integral in (4.67) can be solved with the aid of the notable integral in (4.60). After some mathematical simplifications, we have

$$\begin{aligned}
 & \text{CF}_{\widehat{i}_{agg}} \left(\omega, \widehat{L}^{(0)} \right) \\
 &= \prod_k \exp \left\{ \pi \lambda_{\text{BS}} \sum_{n=1}^N q_k^{[D_{n-1}, D_n]} \mathbb{E} \left[\overline{\mathcal{H}} \left(\widehat{L}^{(0)} - \frac{\kappa_k D_{n-1}^{\beta_k}}{h_k^{(i)}} \right) D_{n-1}^2 \widehat{\mathcal{F}}_k \left(\omega, \kappa_k D_{n-1}^{\beta_k}, G^{(i)}, h_k^{(i)} \right) \right. \right. \\
 &+ \overline{\mathcal{H}} \left(\widehat{L}^{(0)} - \frac{\kappa_k D_n^{\beta_k}}{h_k^{(i)}} \right) \mathcal{H} \left(\widehat{L}^{(0)} - \frac{\kappa_k D_{n-1}^{\beta_k}}{h_k^{(i)}} \right) \left(\frac{h_k^{(i)} \widehat{L}^{(0)}}{\kappa_k} \right)^{2/\beta_k} \widehat{\mathcal{F}}_k \left(\omega, \widehat{L}^{(0)}, G^{(i)}, 1 \right) \\
 &- \left. \overline{\mathcal{H}} \left(\widehat{L}^{(0)} - \kappa_k D_n^{\beta_k} / h_k^{(i)} \right) D_n^2 \widehat{\mathcal{F}}_k \left(\omega, \kappa_k D_n^{\beta_k}, G^{(i)}, h_k^{(i)} \right) \right] \\
 &+ \pi \lambda_{\text{BS}} q_k^{[D_N, \infty]} \mathbb{E} \left[\overline{\mathcal{H}} \left(\widehat{L}^{(0)} - \kappa_k D_N^{\beta_k} / h_k^{(i)} \right) D_N^2 \widehat{\mathcal{F}}_k \left(\omega, \kappa_k D_N^{\beta_k}, G^{(i)}, h_k^{(i)} \right) \right. \\
 &+ \left. \left. \mathcal{H} \left(\widehat{L}^{(0)} - \kappa_k D_N^{\beta_k} / h_k^{(i)} \right) \left(h_k^{(i)} \widehat{L}^{(0)} / \kappa_k \right)^{2/\beta_k} \widehat{\mathcal{F}}_k \left(\omega, \widehat{L}^{(0)}, G^{(i)}, 1 \right) \right] \right\}
 \end{aligned} \tag{4.68}$$

The rest of the proof follows by the computation of the expectations in (4.68) through the following procedure: 1) the change of variables $y_{n-1} = h_k^{(i)} / (\kappa_k D_n^{\beta_k})$, for $n = 1, 2, \dots, N$, are applied in each addend inside the exponential function when computing the expectations with respect to the Nakagami-m fading; 2) the truncated integrals over y_{n-1} are then calculated with the aid of the approximation in (4.64); 3) the expectation with respect to $G^{(i)}$ is computed by the PDF given in (4.12).

Chapter 5

Conclusion and Future Work

5.1 Summary

In this dissertation, the network interference modeling and performance analysis of cellular networks (in the presence of relays) has been proposed relying on the PPP-based abstraction model. Compared to prior works on stochastic geometry modeling and analysis, the mathematical flexibilities of the PPP model on the average symbol error probability evaluation, on the modeling of relays-aided cooperation networks, and on the modeling of LOS/NLOS channel propagation have been investigated in this dissertation. The specific contributions of each chapter are as follows:

In Chapter 2, the distribution of the aggregate other-cell interference is characterized in a variety of MIMO cellular networks where the BSs are distributed according to a homogeneous PPP, and an equivalent-in-distribution based approach has been proposed, in which the interference is expressed by a generalized compound Gaussian representation, to reuse the common methodology developed for AWGN channels to evaluate the ASEP. The framework is applicable to a large number of MIMO arrangements, including receive-diversity, spatial-multiplexing, orthogonal space-time block coding, zero-forcing reception and zero-forcing precoding. The proposed approach leads to exact two-fold integral expressions for the error probability for arbitrary b -dimensional modulations in the presence of other-cell interference and additive noise. When the system is interference limited, the mathematical framework simplifies to a single integral expression.

The performance trends with respect to the MIMO setups can be observed from an asymptotic analysis of the error probability.

In Chapter 3, a tractable mathematical framework to the analysis and optimization of two-hop relay-aided cellular networks is introduced. The proposed approach leverages stochastic geometry for system-level analysis, by modeling the locations of base stations, relay nodes and mobile terminals as points of homogeneous PPPs. A flexible cell association and relay-aided transmission protocol based on the best biased average received power are considered. Computationally tractable integrals and closed-form expressions for coverage and rate are provided, and the inherent performance trends of relay-aided cellular networks are identified. It is shown, notably, that coverage and rate highly depend on the path-loss exponents of one- and two-hop links. In the interference-limited regime, in particular, it is shown that, if the system is not adequately designed, the presence of relay nodes may provide negligible performance gains. By capitalizing on the proposed mathematical framework, a system-level and interference-aware optimization criterion of the bias coefficients is proposed.

In Chapter 4, by relying on the PPP abstraction modeling for the locations of the BSs and by considering the effect of LOS/NLOS propagation, a tractable mathematical framework for evaluating the coverage probability and average rate of cellular networks has been proposed with the aid of a multi-ball approximation modeling of the link state models. The proposed mathematical framework is applicable to cell association criteria based on the smallest path-loss and on the highest received power. It also accounts for practical antenna radiation patterns, and for multi-tier cellular network deployments. A fast computation technique has been proposed to speed up the evaluation of the mathematical framework involving the Gil-Pelaez inversion. It is shown that an optimal density of cellular network deployment exists when the LOS and NLOS propagation are explicitly taken into account.

5.2 Future work

In this section, several possible future research avenues are enumerated to extend the research in this dissertation.

- Cellular networks modeling based on non-PPP point processes

The assumption of a homogeneous PPP abstraction modeling has been widely adopted by the research community due to its mathematical tractability. It is, in fact, a pure random deployment and is more tractable than other point processes in the literature [59]. It also corresponds to a worst case scenario for estimating the performance of real network deployment as it completely neglects the dependence of the BSs deployment. Recently, special efforts have been made by the academia towards modeling the base stations as non-PPP point processes. For example, the determinantal point process, including the Ginibre Point Process, has been used to model the network deployment with repulsion in [98], [99]. The Poisson cluster process has been used by the authors in [100] and in [101] to model nodes that are clustered around highly populated areas. A few analytically tractable performance metrics have been derived based on these non-PPP processes with the idealized single state channel model. To this end, it is interesting to extend the research in this dissertation to the non-PPP processes.

- Channel modeling with more realistic path-loss function

In Chapter 4, the idealized single-state channel modeling has been generalized to take into account the LOS and NLOS channel propagation. It is shown that the performance trend of the PPP modeled two-state cellular networks is quite different from its single-state counterpart. Nevertheless, the two-state model is still a simplified assumption, although suggested by 3GPP for system level simulation, as the path-loss exponent generally decreases when the link length increases in practice. It is interesting to compare the performance trend of the practical distance dependent path-loss model with the two-state simplification, and to investigate the mathematical tractability of practical models.

- Relay-aided millimeter wave cellular networks

As discussed in Chapter 3, the relay nodes in interference-limited dense cellular networks may provide negligible performance gains if the relays are not carefully deployed. The relays, on the other hand, may have significant impact on the cellular networks operating on millimeter wave frequency band. In spite of common belief, recently conducted channel measurements have shown the suitability of the millimeter wave frequency for cellular communications [102]. However, the cell radius for millimeter wave transmission is limited to 100-200 meters [102], and it is shown in recent performance analysis of

millimeter wave cellular networks that the system is noise limited for typical setups [66]. Moreover, a link between the outdoor cellular BS and an indoor user cannot be established on millimeter wave band due to the blockage of walls. To this end, it is interesting to investigate the performance of the relay deployments in millimeter wave cellular networks, which might be an enabling technology for 5G.

Appendix A

Simulation and Experimental Validation of the PPP Abstraction with Multi-State Channel Model

A.1 Introduction

Throughout this report, the BSs in cellular networks are always modeled according to a homogeneous PPP, where the locations of the BSs are not assumed to be regularly deployed, but they are assumed to be randomly distributed according to a PPP. This approach, due to its mathematical flexibility for modeling heterogeneous ultra-dense cellular deployments, has been extensively used in the last few years and it is gaining exponential prominence in the scientific community.

Despite that, the experimental validation of the PPP-based abstraction for modeling cellular networks has remained elusive to date. This is especially true for modeling macro cellular BSs, whose deployment is, usually, not totally random. A few researchers have tried to justify the PPP-based model by using empirical data for the locations of the BSs, e.g., [10], [59], [11]. These studies have confirmed the potential accuracy and the usefulness of the PPP-based model. They, however, are based on a small set of data and on simplifying modeling assumptions. Notably, they do not account for the footprints of

TABLE A.1: BS statistics from OFCOM - The city of London ($\mathcal{A} = 4 \text{ km}^2$).

	O2+Vod.	O2	Vod.
Number of BSs	319	183	136
Number of rooftop BSs	95	62	33
Number of outdoor BSs	224	121	103
Average cell radius (m)	63.1771	83.4122	96.7577

the buildings and rely on simplified channel models, where LOS and NLOS propagation conditions that originate from the presence of buildings are neglected. This is mostly due to the inherent difficulties in obtaining accurate data related to the locations of the BSs and of the buildings in urban areas [81].

In this Appendix, we investigate the accuracy of the PPP-based abstraction for modeling cellular networks with the aid of experimental data. We explicitly take realistic BS locations, building footprints and LOS/NLOS channel conditions into account. More specifically: i) the locations of the BSs are taken from a large database made available by OFCOM, the independent regulator and competition authority for the United Kingdom (UK) communications industries [9]; and ii) the footprints of the buildings are taken from a large database made available by Ordnance Survey, the Britain’s mapping agency offering the most up-to-date and accurate maps of the UK [86]. Our extensive study highlights that the empirical link state model can be accurately approximated through the multi-ball approximation proposed in Chapter 4, and the PPP-based model is capable of accurately predicting the performance of cellular networks in dense urban environments.

A.2 System Model

A.2.1 Base Stations Modeling

In order to test the accuracy of the PPP-based model for the locations of the BSs, we use experimental data from an actual deployment of BSs that correspond to the city of London in UK from OFCOM [9]. More specifically, we consider the BSs of two telecommunication operators: O2 and Vodafone. The empirical data is summarized in Tables A.1. The following terminology and notation are used: i) “rooftop BSs” is referred to the BSs that lay inside a geographical region (polygon) where a building is

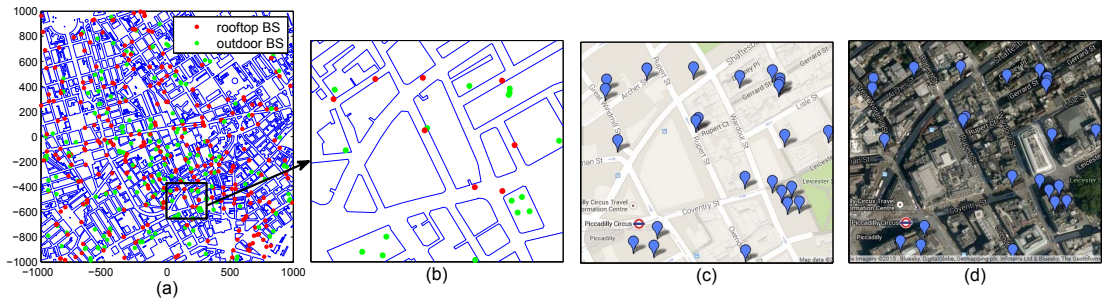


FIGURE A.1: London case study. Dense urban environment, where the 55.9% of the area is occupied by buildings. Horizontal and vertical axis provide distances expressed in meters. (a) Entire region under analysis. (b) Magnification of a smaller region. (c) Google map view of (b). (d) Satellite view of (b).

located; ii) “outdoor BSs” is referred to the BSs that lay in a geographical region where no buildings are located. Information about the locations of the buildings is provided in Section A.2.2; and iii) \mathcal{A} denotes the area of the geographical region under analysis. From the number of BSs (\mathcal{N}) and \mathcal{A} , the density of BSs is obtained as $\lambda_{\text{BS}} = \mathcal{N}/\mathcal{A}$. Accordingly, the average cell radius shown in the tables is computed as $R_c = \sqrt{1/(\pi\lambda_{\text{BS}})}$ [66].

To study the impact of network densification and the potential gains of sharing the BSs between telecommunication operators, two scenarios are investigated. In the first scenario, the BSs of O2 and Vodafone operate at different frequencies, thus they do not interfere with each other. This is equivalent to having just one telecommunication operator in the region of interest. Hence, only the BSs of one telecommunication operator are accessible to the typical MT. In the second scenario, O2 and Vodafone share the BSs and they operate at the same frequency. So, a denser deployment of BSs is available in the region of interest and the BSs of both telecommunication operators are accessible to the typical MT. Furthermore, full frequency reuse for the BSs of the same telecommunication operator and a saturated load traffic model are assumed. This implies that, with the exception of the serving BS, all the accessible BSs at a given frequency act as interferers for the probe MT.

As far as the PPP-based model for the locations of the BSs is concerned, we assume that the number of BSs is a Poisson random variable with the same density as the empirical data, and the locations of the BSs are assumed to be uniformly distributed in the same region \mathcal{A} .

A.2.2 Buildings Modeling

To take realistic blockages into account, i.e., LOS and NLOS propagation conditions due to the locations and the shapes of buildings (see also Section A.2.3), we use experimental data corresponding to the actual deployments of buildings in London where the data is obtained from OS [86]. In particular, the same geographical regions as those of the locations of the BSs in Section A.2.1 are considered. To make sure that the data obtained from the two independent websites of OFCOM and OS can be merged together, we have verified their consistency with the aid of Google maps for the same areas. Figures A.1 provide a graphical representation of the geographical areas under analysis, by merging the data from OFCOM and OS. As far as the buildings are concerned, their elevation is not considered, since this data is not available in the database. Therefore, the analysis of its impact is postponed to a future research study.

A.2.3 Blockages Modeling

The presence of buildings in dense urban environments constitute an inherent source of blockages, which results in LOS and NLOS links. Modeling LOS and NLOS propagation conditions constitute an important requirement for assessing the physical layer performance of transmission schemes within the 3GPP [80]. In this chapter, we are interested in the performance evaluation of outdoor MTs, and in what follows, the blockage models for a generic BS-to-outdoor-MT link are introduced.

A.2.3.1 Empirical-Based Model

Based on the locations of the BSs and on the locations and the shapes of the buildings described in Sections A.2.1 and A.2.2, respectively, LOS and NLOS propagation conditions can be empirically taken into account. In this chapter, the empirical LOS and NLOS links are identified as follows. Let a generic “outdoor BS” and a generic outdoor MT in the region of interest. The related link is in LOS if no building is intersected by connecting the BS and the MT with a straight line. Otherwise, the link is in NLOS. Let a generic “rooftop BS”, the BS-to-MT links are assumed to be in NLOS. This is a simplifying assumption used in other literature as well [103], which seems acceptable if no information on the elevation of the buildings is available.

A.2.3.2 Multi-Ball Approximation

Due to the presence of blockages (i.e., buildings), a generic BS-to-MT link may be either in LOS or in NLOS with a probability that depends on the BS-to-MT distance, the locations of the BSs, as well as the locations and the shapes of the buildings. This dependence on the distance and on the network topology makes the simulation and the analysis of cellular networks based on the PPP-based model less tractable and more time-consuming. In this chapter, we compare the empirical-based model against the multi-ball approximation proposed in Chapter 4. The proposed approximation is optimized from the point of view of the typical MT and, thus, the spatial deployments of the BSs and of the buildings are explicitly taken into account. This makes it suitable for system-level performance evaluation and optimization. The parameters of the multi-ball approximation can be obtained through the intensity matching, which is described in Section A.3. Further details of the multi-ball approximation are not presented in this chapter again. The readers can refer to Chapter 4.

A.2.3.3 1-State Model

In stochastic geometry modeling, LOS and NLOS propagation conditions are often neglected and all links are assumed to be either in LOS or NLOS. This case study is considered in this test as well, in order to better understand the differences between 1-state and 2-state blockage models.

A.2.4 Channel Modeling

In addition to modeling blockages, we consider a practical channel model. In particular, path-loss, shadowing and fast-fading are considered. Let a generic BS denoted by BS_i and a generic outdoor MT denoted by MT_t .

As for the path-loss, we consider a bounded model $l_k(r^{(i,t)}) = \kappa_k (\max\{r_0, r^{(i,t)}\})^{\beta_k}$, where $r^{(i,t)}$ denotes the BS-to-MT distance, $k = \text{LOS}$ or $k = \text{NLOS}$ if the BS-to-MT link is in LOS or in NLOS, κ_k denotes the free-space path-loss, β_k denotes the path-loss exponent, and r_0 is a positive constant that avoids the singularity of the path-loss model for $r^{(i,t)} \rightarrow 0$.

As for the shadowing, we consider that it is distributed according to log-normal random variable with mean and standard deviation (in dB) equal to μ_k and to σ_k , respectively. In this chapter, shadowing is denoted by $X_k^{(i,t)}$.

As for the fast-fading, we consider that the envelope of the links in LOS and in NLOS is distributed according to a Nakagami- m (with $m \geq 0.5$) and a Rayleigh random variable with mean power Ω , respectively. In this chapter, the envelope of the fast-fading is denoted by $h_k^{(i,t)}$. Fast-fading and shadowing are assumed to be independently distributed.

Thus, the received power at MT_t can be formulated as:

$$P_R = \frac{P h_k^{(i,t)} X_k^{(i,t)}}{\kappa_k (\max \{r_0, r^{(i,k)}\})^{\beta_k}} \quad (\text{A.1})$$

where P is the transmit power of BS_i .

A.2.5 Cell Association Modeling

The typical (probe) MT is assumed to be served by any accessible BS that provides the highest average received power to it. Thus, path-loss and shadowing are both taken into account for cell association. Fast-fading, on the other hand, is averaged out and neglected. This is, in fact, the typical operating condition based on 3GPP specifications [80].

Let MT_t be the typical MT and the probe link be identified by the subscript “0”. Let $C_k^{(0,t)}$ be defined as follows:

$$C_k^{(0,t)} = \min_{i \in \Phi_{\text{BS}}^{(k)}} \left\{ C_k^{(i,t)} = \frac{\kappa_k (\max \{r_0, r^{(i,t)}\})^{\beta_k}}{X_k^{(i,t)}} \right\} \quad (\text{A.2})$$

where $\Phi_{\text{BS}}^{(k)}$ is the PPP of the BSs in state k , and $1/C_k^{(0,t)}$ is the highest average received power at MT_k from any accessible BS whose BS-to- MT_k link is in LOS if $k = \text{LOS}$ or in NLOS if $k = \text{NLOS}$. From (A.2), the serving BS of MT_t is that corresponding to the inverse average received power defined as $C^{(0,t)} = \min \{C_{\text{LOS}}^{(0,t)}, C_{\text{NLOS}}^{(0,t)}\}$, since it provides the best link.

TABLE A.2: 3-ball approximation of empirical blockage models obtained as the solution of (4.10).

D_1 (meters)	D_2 (meters)	D_3 (meters)	$q_{\text{LOS}}^{[0,D_1]}$	$q_{\text{LOS}}^{[D_1,D_2]}$	$q_{\text{LOS}}^{[D_2,D_3]}$	$q_{\text{LOS}}^{[D_3,\infty]}$
15.1335	56.5978	195.7149	0.7948	0.3818	0.0939	0

A.2.6 Problem Statement

Let BS_0 be the serving BS of MT_t . Based on (A.1) and (A.2), the signal-to-interference-plus-noise-ratio (SINR) at the typical MT, MT_t , can be formulated as follows:

$$\text{SINR} = \frac{Ph_k^{(0,t)}/C_k^{(0,t)}}{\sigma_N^2 + \sum_{\bar{k} \in \{\text{LOS}, \text{NLOS}\}} \sum_{i \in \Phi_{\text{BS}}^{(\bar{k})} \setminus \text{BS}_0} \mathcal{I}_{\bar{k},k}^{(i,t)}}} \quad (\text{A.3})$$

where $\mathcal{I}_{\bar{k},k}^{(i,t)} = (Ph_{\bar{k}}^{(i,t)}/C_{\bar{k}}^{(i,t)})\mathbf{1}(C_{\bar{k}}^{(i,t)} > C_k^{(0,t)})$ denotes the generic interfering term, $k \in \{\text{LOS}, \text{NLOS}\}$ refers to the LOS/NLOS state of the BS_0 -to- MT_t link, σ_N^2 denotes the noise power.

In this chapter, the performance metric for quantifying the accuracy of the PPP-based model is the CCDF of the SINR, since it provides complete information on its distribution. In addition, it corresponds to the coverage probability of a typical MT as a function of the link reliability threshold. Let T be this threshold, it can be formulated as follows:

$$P_{\text{cov}}(T) = \Pr\{\text{SINR} > T\} \quad (\text{A.4})$$

A.3 Numerical Results: Experimental Validation

In this section, we illustrate several numerical examples in order to validate the accuracy of the PPP-based abstraction for modeling cellular networks, as well as to confirm the tightness of the proposed multi-ball approximation for simplifying the simulation and for enabling the mathematical modeling of cellular networks.

Simulation Setup Unless otherwise stated, the following simulation setup, which is in agreement with the long term evolution advanced (LTE-A) standard, is assumed. The transmit power of the BSs is $P = 30$ dBm; the noise power is $\sigma_N^2 = -174 +$

$10 \log_{10} (B_W) + \mathcal{F}_{\text{dB}}$, where $B_W=20$ MHz is the transmission bandwidth and $\mathcal{F}_{\text{dB}} = 10$ dB is the noise figure; $\kappa_{\text{LOS}} = \kappa_{\text{NLOS}} = (4\pi/\nu)^2$ is the free space path-loss at a distance of 1 meter from the transmitter, where $\nu = c/f_c$ is the signal wavelength, $c \approx 3 \times 10^8$ meters/sec is the speed of light, and $f_c=2.1$ GHz is the signal frequency; $r_0 = 1$ meter; the path-loss exponents of LOS and NLOS links are $\beta_{\text{LOS}} = 2.5$ and $\beta_{\text{NLOS}} = 3.5$; the mean and standard deviation of the shadowing are $\mu_{\text{LOS}} = \mu_{\text{NLOS}} = 0$ dB, $\sigma_{\text{LOS}} = 5.8$ dB, and $\sigma_{\text{NLOS}} = 8.7$ dB; the fast-fading envelope of the LOS links follows a Nakagami- m distribution with parameters $m = 2$ and $\Omega_{\text{LOS}} = 1$; the fast-fading envelope of the NLOS links follows a Rayleigh distribution with parameter $\Omega_{\text{NLOS}} = 1$. Used notation: “O2” means that only the BSs from O2 are accessible; “Vodafone” means that only the BSs from Vodafone are accessible; and “O2+Vodafone” means that all BSs from O2 and Vodafone are accessible.

Multi-Ball Approximation of the Blockages In this section, we study the accuracy of the proposed multi-ball approximation for modeling spatial blockages, under the assumption that the BSs are distributed according to a PPP. The solution of the intensity matching by solving the optimization in (4.10) is summarized in Table A.2 by assuming $N = 3$, which provides a good matching accuracy while still keeping the computational complexity at a low level. The intensity measure of the empirical-based model of the blockages is obtained by using the following procedure based on the actual locations and shapes of the buildings obtained from the OS database.

Step 1: The geographical region illustrated in Figs. A.1 for London is considered. As discussed in Section A.2.2, this data is obtained from OS. The BSs are generated according to a PPP of density λ_{BS} , which is chosen according to the data in Table A.1. Outdoor and rooftop BSs are identified.

Step 2: In the same areas, the MTs are generated according to another PPP of density $\lambda_{\text{MT}} = 10\lambda_{\text{BS}}$. This choice of λ_{MT} guarantees saturated traffic conditions, i.e., all the BSs have at least one MT to serve based on the cell association in Section A.2.5. Among all the MTs, one MT among those that do not lay in a building (outdoor MTs) is randomly chosen as the typical MT.

Step 3: Let the probe (typical) MT, its distance r and link state (LOS or NLOS) with respect to any accessible BSs are computed according to Section A.2.3.1.

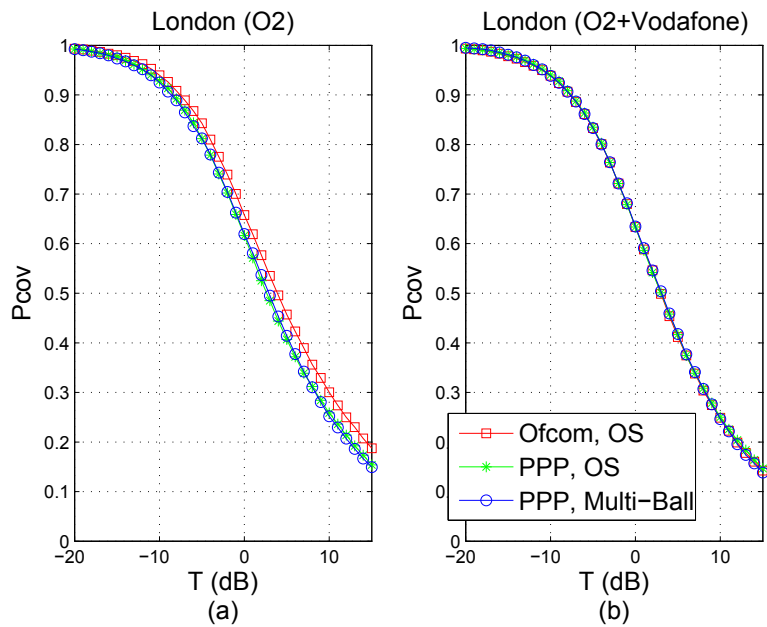


FIGURE A.2: Coverage probability in three case studies: 1) “OFCOM, OS”: the BSs are obtained from the OFCOM database and the buildings from the OS database. 2) “PPP, OS”: the BSs are distributed according to a PPP and the buildings are obtained from the OS database. 3) “PPP, Multi-Ball”: the BSs are distributed according to a PPP and the multi-ball approximation in Table A.2 is used.

Step 4: Step 2 and Step 3 are repeated several thousands of times in order to get sufficient statistical data. From this data, two vectors are obtained: a vector containing the distances whose links are in LOS and a vector containing the distances whose links are in NLOS.

Step 5: From the vectors computed in Step 4, $p_{\text{LOS}}(r)$ and $p_{\text{NLOS}}(r)$ are estimated by using, e.g., the `hist` function of Matlab. To this end, a resolution step equal to $\Delta r = 1$ meter and $M = 2000$ discrete distances are considered. Thus, the LOS and NLOS probabilities are available for the set of distances r_m for $m = 1, 2, \dots, M$, where $\Delta r = r_m - r_{m-1} = 1$ meter. The corresponding LOS and NLOS probabilities are $p_{\text{LOS}}(r_m)$ and $p_{\text{NLOS}}(r_m)$ for $m = 1, 2, \dots, M$.

Step 6: Finally the intensity measure of the path-losses is computed by the following discrete (empirical) approximation of (4.9) (for $k = \{\text{LOS}, \text{NLOS}\}$):

$$\Lambda_k^{(\text{em})}([0, x]) \approx 2\pi\lambda_{\text{BS}}\Delta r \sum_{m=1}^M \Pr\left\{\kappa_k(\max\{r_0, r_m\})^{\beta_k} \leq x\right\} p_k(r_m) r_m \quad (\text{A.5})$$

PPP-Based Modeling of the BSs In Figs. A.2, we study the accuracy of the PPP-based abstraction for modeling cellular networks, by either considering or not the multi-ball approximation for modeling blockages. As discussed in Sections A.2.1 and A.2.2, the empirical coverage probability is obtained by using the locations of the BSs and the footprints of the buildings from the OFCOM and OS databases, respectively. The following procedure for computing the empirical coverage probability is used.

Step 1: The geographical region illustrated in Figs. A.1 for London is considered. As discussed in Section A.2.2, this data is obtained from OS. Two case studies for the locations of the BSs are considered. 1) The BSs are distributed according to their actual locations obtained from OFCOM (Figs. A.1, Tables A.1). 2) The BSs are distributed according to a PPP whose density is the same as that of Tables A.1. In both cases, outdoor and rooftop BSs are identified.

Step 2: In the same areas, the MTs are generated according to another PPP of density $\lambda_{\text{MT}} = 10\lambda_{\text{BS}}$. This choice of λ_{MT} guarantees saturated traffic conditions, i.e., all the BSs have at least one MT to serve based on the cell association in Section A.2.5. Among all the MTs, one MT among those that do not lay in a building (outdoor MTs) is randomly chosen as the typical MT.

Step 3: Let the probe (typical) MT, its distance r and link state (LOS or NLOS) with respect to any accessible BSs are computed according to Section A.2.3.1.

Step 4: For each link between the probe MT and the accessible BSs, path-loss, shadowing and fast-fading gains are generated according to Section A.2.4.

Step 5: Let the probe MT and the accessible BSs, its serving BS is identified by using (A.2) in Section A.2.5.

Step 6: The SINR and its associated coverage probability are computed by using (A.3) and (A.4), respectively.

Step 7: Steps 1-6 are repeated 10^6 times in order to get sufficient statistical data. The final coverage probability is computed as the empirical mean of the obtained 10^6 realizations for each target reliability threshold.

If the 1-state model in Section A.2.3.3 is considered, the same procedure is used. The only difference is that all the links are assumed to be, a priori, either in LOS or NLOS.

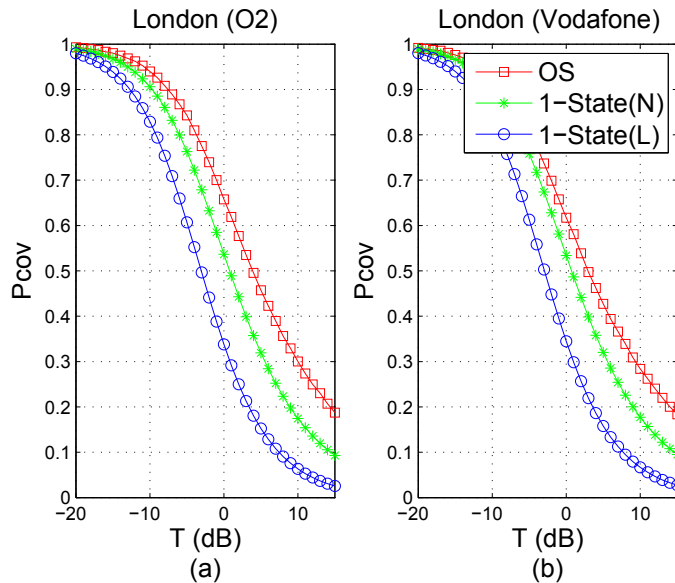


FIGURE A.3: Coverage probability: impact of blockages. Three case studies are analyzed: 1) “OS”: the buildings are obtained from the OS database. 2) “1-State (N)”: all links are in NLOS. 3) “1-State (L)”: all links are in LOS.

All in all, Figs. A.2 confirm the accuracy of the PP-based abstraction model, and the tightness of the proposed multi-ball and multi-lobe approximations in practical scenarios.

Achievable Performance: Impact of Blockages In Fig. A.3, we study the impact of the blockage model on the coverage probability. This figure highlights the importance of accurately modeling blockages. More specifically, the widespread used 1-state model provides different results from the more accurate and realistic LOS/NLOS blockage model, which accounts for the locations of buildings. Figure A.3 points out that the coverage probability may be better than that predicted by using the 1-state model, since the links in LOS result in good probe links while the links in NLOS result in less interference. The proposed multi-ball approximation turns out to be a useful tool for taking LOS/NLOS propagation conditions into account at an affordable complexity, eventually leading to the mathematical analysis and optimization of cellular networks.

A.4 Conclusion

With the aid of experimental data for the actual locations of BSs and for the actual locations and shapes of buildings, we have studied the accuracy of the PPP-based abstraction

for modeling cellular networks. This study has highlighted that the PPP-based model is sufficiently accurate for modeling dense urban environments of major metropolitan areas. We have observed that accurate models for the blockages is needed for obtaining reliable estimates of the coverage probability of cellular networks. Finally, we have validated the accuracy of flexible multi-ball approximation for incorporating realistic blockage into the PPP-based abstraction of cellular networks. Based on these findings, the PPP-based model seems to be sufficiently accurate and tractable for enabling the mathematical analysis and optimization of emerging ultra-dense cellular networks, which use advanced wireless access transmission schemes.

Bibliography

- [1] M. Abramowitz and I. A. Stegun, *Handbook of Mathematical Functions with Formulas, Graphs, and Mathematical Tables*. Dover Publications, June 1964.
- [2] A. Erdelyi, W. Magnus, F. Oberhettinger, and F. G. Tricomi, *Higher Transcendental Functions – Vol I*. McGraw-Hill, Inc., 1953.
- [3] A. P. Prudnikov, Y. A. Brychkov, and O. I. Marichev, *Integrals and Series - Vol. 3: More Special Functions*. CRC, 1990.
- [4] M. K. Simon and M.-S. Alouini, *Digital Communication over Fading Channels, 2st ed.* John Wiley & Sons, Inc., 2005.
- [5] A. T. James, “Distributions of matrix variates and latent roots derived from normal samples,” *The Annals of Mathematical Statistics*, vol. 35, pp. 475–501, June 1964.
- [6] D. H. Ring and W. R. Young, “The hexagonal cells concept.” [Online]. Available: <http://www.privateline.com/archive/Ringcellreport1947.pdf>, Dec 1947.
- [7] F. Baccelli and B. Blaszczyszyn, *Stochastic Geometry and Wireless Networks, Part I: Theory*. Now Publishers, Sep. 2009.
- [8] M. Haenggi, *Stochastic Geometry for Wireless Networks*. Cambridge University Press, 2013.
- [9] OFCOM, “Sitefinder database.” [Online]. Available: <http://stakeholders.ofcom.org.uk/sitefinder/sitefinder-dataset/>.
- [10] J. G. Andrews, F. Baccelli, and R. K. Ganti, “A tractable approach to coverage and rate in cellular networks,” *IEEE Trans. Commun.*, vol. 59, pp. 3122–3134, Nov. 2011.

-
- [11] C.-H. Lee, C.-Y. Shihet, and Y.-S. Chen, “Stochastic geometry based models for modeling cellular networks in urban areas,” *Springer Wireless Netw.*, p. 10, Oct. 2012.
- [12] G. Anjin and M. Haenggi, “Asymptotic deployment gain: A simple approach to characterize the sinr distribution in general cellular networks,” *IEEE Trans. Commun.*, vol. 63, pp. 962–976, Mar. 2015.
- [13] M. D. Renzo and W. Lu, “End-to-end error probability and diversity analysis of af-based dual-hop cooperative relaying in a poisson field of interferers at the destination,” *Wireless Communications, IEEE Transactions on*, vol. 14, pp. 15–32, Jan 2015.
- [14] M. D. Renzo and W. Lu, “On the diversity order of selection combining dual-branch dual-hop af relaying in a poisson field of interferers at the destination,” *Vehicular Technology, IEEE Transactions on*, vol. 64, pp. 1620–1628, April 2015.
- [15] M. D. Renzo and W. Lu, “The equivalent-in-distribution (eid)-based approach: On the analysis of cellular networks using stochastic geometry,” *Communications Letters, IEEE*, vol. 18, pp. 761–764, May 2014.
- [16] W. Lu and M. D. Renzo, “Performance evaluation of relay-aided cellular networks by using stochastic geometry,” in *Computer Aided Modeling and Design of Communication Links and Networks (CAMAD), 2014 IEEE 19th International Workshop on*, pp. 265–269, Dec 2014.
- [17] W. Lu and M. D. Renzo, “Interference-aware dual-hop cooperative relaying in a poisson field of interferers,” in *Global Communications Conference (GLOBECOM), 2014 IEEE*, pp. 4143–4149, Dec 2014.
- [18] W. Lu and M. D. Renzo, “Performance analysis of spatial modulation mimo in a poisson field of interferers,” in *Computing, Networking and Communications (ICNC), 2014 International Conference on*, pp. 662–668, Feb 2014.
- [19] M. Z. Win, P. C. Pinto, and L. A. Shepp, “A mathematical theory of network interference and its applications,” *Proc. of the IEEE*, vol. 97, pp. 205–230, Feb. 2009.

- [20] M. D. Renzo, C. Merola, A. Guidotti, F. Santucci, and G. E. Corazza, "Error performance of multi-antenna receivers in a poisson field of interferers: A stochastic geometry approach," *IEEE Trans. Commun.*, vol. 61, pp. 2025–2047, May 2013.
- [21] M. D. Renzo, A. Guidotti, and G. E. Corazza, "Average rate of downlink heterogeneous cellular networks over generalized fading channels - a stochastic geometry approach," *IEEE Trans. Commun.*, vol. 61, pp. 3050–3071, July 2013.
- [22] H. S. Dhillon, R. K. Ganti, F. Baccelli, and J. G. Andrews, "Modeling and analysis of k-tier downlink heterogeneous cellular networks," *IEEE J. Sel. Areas Commun.*, vol. 30, pp. 550–560, Apr. 2012.
- [23] H.-S. Jo, Y. J. Sang, P. Xia, and J. G. Andrews, "Heterogeneous cellular networks with flexible cell association: A comprehensive downlink sinr analysis," *IEEE Trans. Wireless Commun.*, vol. 11, pp. 3484–3495, Oct. 2012.
- [24] H. ElSawy, E. Hossain, and M. Haenggi, "Stochastic geometry for modeling, analysis, and design of multi-tier and cognitive cellular wireless networks: A survey," *IEEE Commun. Surveys and Tutorials.*, vol. 15, pp. 996–1019, 3rd quarter 2013.
- [25] M. D. Renzo and P. Guan, "A mathematical framework to the computation of the error probability of downlink mimo cellular networks by using stochastic geometry," *IEEE Trans. Commun.*, vol. 62, pp. 2860–2879, Aug. 2014.
- [26] M. D. Renzo and P. Guan, "Stochastic geometry modeling of coverage and rate of cellular networks using the gil-pelaez inversion theorem," *IEEE Commun. Lett.*, vol. 18, pp. 1575–1578, Sep. 2014.
- [27] H. S. Dhillon, M. Kountouris, and J. G. Andrews, "Downlink mimo hetnets: Modeling, ordering results and performance analysis," *IEEE Trans. Wireless Commun.*, vol. 12, pp. 5208–5222, Oct. 2013.
- [28] A. Ghosh, J. Zhang, J. G. Andrews, and R. Muhamed, *Fundamentals of LTE*. Prentice-Hall, Sep. 2010.
- [29] G. Geraci, H. S. Dhillon, J. G. Andrews, J. Yuan, and I. B. Collin, "Physical layer security in downlink multi-antenna cellular networks," *IEEE Trans. Wireless Commun.*, vol. 62, pp. 2006–2012, June 2014.

- [30] C. Li, J. Zhang, and K. B. Letaief, "Throughput and energy efficiency analysis of small cell networks with multi-antenna base stations," *IEEE Trans. Wireless Commun.*, vol. 13, pp. 2505–2017, May 2014.
- [31] M. Zorzi and S. Pupolin, "Slotted aloha for high-capacity voice cellular communications," *IEEE Trans. Veh. Technol.*, vol. 43, pp. 1011–1021, Nov. 1994.
- [32] D. K. McGraw and J. F. Wagner, "Elliptically symmetric distributions," *IEEE Trans. Inform. Theory*, vol. IT-14, pp. 110–120, Jan. 1968.
- [33] H. Huang, C. P. Papadias, and C. Venkatesan, *MIMO Communication for Cellular Networks*. Springer, Nov. 2011.
- [34] V. Tarokh, H. Jafarkhani, and A. R. Calderbank, "Space-time block codes from orthogonal designs," *IEEE Trans. Inform. Theory*, vol. 45, pp. 1456–1467, July 1999.
- [35] D. A. Gore, R. W. H. Jr., and A. J. Paulraj, "Transmit selection in spatial multiplexing systems," *IEEE Commun. Lett.*, vol. 6, pp. 491–493, Nov 1999.
- [36] R. J. Muirhead, *Aspects of Multivariate Statistical Theory*. New York: Wiley, 1982.
- [37] W. Lu, M. D. Renzo, and A. Busson, "Stochastic geometry modeling and analysis of the error probability of two-tier cellular networks," in *IEEE European Conf. Networks and Commun.*, pp. 1–6, June 2014.
- [38] M. D. Renzo, F. Graziosi, and F. Santucci, "Further results on the approximation of log-normal power sum via pearson type iv distribution: A general formula for log-moments computation," *IEEE Trans. Commun.*, vol. 57, pp. 893–898, Apr. 2009.
- [39] M. D. Renzo, F. Graziosi, and F. Santucci, "A unified framework for performance analysis of csi-assisted cooperative communications over fading channels," *IEEE Trans. Commun.*, vol. 57, pp. 2551–2557, Sep. 2009.
- [40] "The wolfram functions site." [Online] Available: <http://functions.wolfram.com/HypergeometricFunctions/Hypergeometric1F1/03/01/04/01/0004/>.

- [41] I. S. Gradshteyn and I. M. Ryzhik, *Tables of Integrals, Series and Products*, 7th ed. San Diego, CA: Academic, 2007.
- [42] A. Winkelbauer, "Moments and absolute moments of the normal distribution." [Online] Available: <http://arxiv.org/pdf/1209.4340.pdf>.
- [43] IEEE 802.16 Relay Task Group, "Multi-hop relay system evaluation methodology." IEEE 802.16j-6/013r3, Feb. 2007.
- [44] S. W. Peters, A. Y. Panah, K. T. Truong, and R. W. H. Jr., "Relay architectures for 3gpp lte-advanced," *EURASIP J. Wireless Commun. and Networking*, vol. 2009, July 2009.
- [45] J. N. Laneman, D. N. C. Tse, and G. W. Wornell, "Cooperative diversity in wireless networks: Efficient protocols and outage behavior," *IEEE Trans. Inform. Theory.*, vol. 50, pp. 3062–3080, Dec. 2004.
- [46] M. O. Hasna and M.-S. Alouini, "End-to-end performance of transmission systems with relays over rayleigh-fading channels," *IEEE Trans. Wireless Commun.*, vol. 2, pp. 1126–1131, Nov. 2003.
- [47] G. K. Karagiannidis, T. A. Tsiftsis, and R. K. Mallik, "Bounds for multihop relayed communications in nakagami- m fading," *IEEE Trans. Commun.*, vol. 54, pp. 18–22, Jan. 2006.
- [48] S. Ikki and M. H. Ahmed, "Performance analysis of cooperative diversity wireless networks over nakagami- m fading channel," *IEEE Commun. Lett.*, vol. 11, pp. 334–336, Apr. 2007.
- [49] N. C. Beaulieu and S. S. Soliman, "Exact analysis of multihop amplify-and-forward relaying systems over general fading links," *IEEE Trans. Commun.*, vol. 60, pp. 2123–2134, Aug. 2012.
- [50] H. A. Suraweera, H. K. Garg, and A. Nallanathan, "Performance analysis of two hop amplify-and-forward systems with interference at the relay," *IEEE Commun. Lett.*, vol. 14, pp. 692–694, Aug. 2010.
- [51] F. Al-Qahtani, T. Duong, C. Zhong, K. Qaraqe, and H. Alnuweiri, "Performance analysis of dual-hop af systems with interference in nakagami- m fading channels," *IEEE Sig. Proc. Lett.*, vol. 18, pp. 454–457, Aug. 2011.

- [52] S. S. Ikki and S. Aissa, "Multihop wireless relaying systems in the presence of cochannel interferences: Performance analysis and design optimization," *IEEE Trans. Veh. Tech.*, vol. 61, pp. 566–573, Feb. 2012.
- [53] H. A. Suraweera, D. S. Michalopoulos, and C. Yuen, "Performance analysis of fixed gain relay systems with a single interferer in nakagami- m fading channels," *IEEE Trans. Veh. Tech.*, vol. 61, pp. 1457–1463, Mar. 2012.
- [54] M. A. Mohammadi, H. A. Suraweera, and X. Zhou, "Outage probability of wireless ad hoc networks with cooperative relaying," in *IEEE Global Commun. Conf.*, pp. 4632–4638, Dec 2012.
- [55] C. Zhong, H. A. Suraweera, A. Huang, Z. Zhang, and C. Yuen, "Outage probability of dual-hop multiple antenna af relaying systems with interference," *IEEE Trans. Commun.*, vol. 61, pp. 108–119, Jan. 2013.
- [56] A. H. Forghani, S. S. Ikki, and S. Aissa, "On the performance and power optimization of multihop multibranch relaying networks with cochannel interferers," *IEEE Trans. Veh. Tech.*, vol. 62, pp. 3437–3443, July 2013.
- [57] G. Zhu, C. Zhong, H. A. Suraweera, Z. Zhang, and C. Yuen, "Ergodic capacity comparison of different relay precoding schemes in dual-hop af systems with cochannel interference," *IEEE Trans. Commun.*, vol. 62, pp. 2314–2328, July 2014.
- [58] V. A. Aalo, K. P. Peppas, G. Efthymoglou, M. Alwakeel, and S. Alwakeel, "Serial amplify-and-forward relay transmission systems in nakagami- m fading channels with a poisson interference field," *IEEE Trans. Veh. Tech.*, vol. 63, pp. 2183–2196, June 2014.
- [59] A. Guo and M. Haenggi, "Spatial stochastic models and metrics for the structure of base stations in cellular networks," *IEEE Trans. Wireless Commun.*, vol. 12, pp. 5800–5821, Nov. 2013.
- [60] W. Lu and M. D. Renzo, "Stochastic geometry modeling of cellular networks: Analysis, simulation and experimental validation." to appear. [Online]. Available: <http://arxiv.org/pdf/1506.03857.pdf>.
- [61] M. D. Renzo and W. Lu, "Stochastic geometry modeling and performance evaluation of mimo cellular networks using the equivalent-in-distribution (eid)-based

- approach,” *Communications, IEEE Transactions on*, vol. 63, pp. 977–996, March 2015.
- [62] S. Singh, H. S. Dhillon, and J. G. Andrews, “Offloading in heterogeneous networks: Modeling, analysis, and design insights,” *IEEE Trans. Wireless Commun.*, vol. 12, pp. 2484–2497, May 2013.
- [63] H. ElSawy and E. Hossain, “On stochastic geometry modeling of cellular uplink transmission with truncated channel inversion power control,” *IEEE Trans. Wireless Commun.*, vol. 13, pp. 4454–4469, Aug. 2014.
- [64] S. Singh, X. Zhang, and J. G. Andrews, “Joint rate and sinr coverage analysis for decoupled uplink-downlink biased cell associations in hetnets.” to appear. [Online]. Available: <http://arxiv.org/pdf/1412.1898v1.pdf>.
- [65] T. Bai and R. W. H. Jr., “Coverage and rate analysis for millimeter wave cellular networks,” *IEEE Trans. Wireless Commun.*, vol. 14, pp. 1100–1114, Feb. 2015.
- [66] M. D. Renzo, “Stochastic geometry modeling and analysis of multi-tier millimeter wave cellular networks,” *IEEE Trans. Wireless Commun.*, vol. 14, pp. 5038–5057, Sept. 2015.
- [67] J. G. Andrews, R. K. Ganti, M. Haenggi, N. Jindal, and S. Weber, “A primer on spatial modeling and analysis in wireless networks,” *IEEE Commun. Mag.*, vol. 48, pp. 156–163, Nov. 2010.
- [68] I. Krikidis, “Simultaneous information and energy transfer in large-scale networks with/without relaying,” *IEEE Trans. Commun.*, vol. 62, pp. 900–912, Mar. 2014.
- [69] J. B. Andersen, T. S. Rappaport, and S. Yoshida, “Propagation measurements and models for wireless communications channels,” *IEEE Commun. Mag.*, vol. 33, pp. 42–49, Jan. 1995.
- [70] G. L. Stuber, *Principles of Mobile Communication, 3rd ed.* Springer, 2012.
- [71] M. Di Renzo, “A stochastic geometry approach to the rate of downlink cellular networks over correlated log-normal shadowing,” in *Vehicular Technology Conference (VTC Fall), 2013 IEEE 78th*, pp. 1–5, Sept 2013.

- [72] V. M. Nguyen and F. Baccelli, “A stochastic geometry model for the best signal quality in a wireless network,” in *IEEE Workshop on Spatial Stochastic Models for Wireless Networks*, pp. 465–471, June 2010.
- [73] S. M. Yu and S.-L. Kim, “Downlink capacity and base station density in cellular networks,” in *IEEE Workshop on Spatial Stochastic Models for Wireless Networks*, pp. 1–7, May 2013.
- [74] J.-S. Ferenc and Z. Neda, “On the size distribution of poisson voronoi cells,” *Physica A: Statistical Mechanics and its Applications*, vol. 385, pp. 518–526, Nov. 2007.
- [75] F. Boccardi, J. G. Andrews, H. Elshaer, M. Dohler, S. Parkvall, P. Popovski, and S. Singh, “Why to decouple the uplink and downlink in cellular networks and how to do it.” submitted. [Online]. Available: <http://arxiv.org/ftp/arxiv/papers/1503/1503.06746.pdf>.
- [76] B. Blaszczyzyn, M. K. Karray, and H. P. Keeler, “Using poisson processes to model lattice cellular networks,” in *IEEE Int. Conf. Computer Commun.*, pp. 773–781, Apr. 2013.
- [77] Y. Lin, W. Bao, W. Yu, and B. Liang, “Optimizing user association and spectrum allocation in hetnets: A utility perspective,” *IEEE J. Sel. Areas Commun.*, vol. 33, pp. 1025–1039, June 2015.
- [78] G. Liu, F. Yu, H. Ji, V. Leung, and X. Li, “In-band full-duplex relaying: A survey, research issues and challenges,” *Communications Surveys Tutorials, IEEE*, vol. 17, pp. 500–524, Secondquarter 2015.
- [79] 5G-PPP, “5g vision - the 5g infrastructure public private partnership: The next generation of communication networks and services.” [Online]. Available: <http://5g-ppp.eu/wp-content/uploads/2015/02/5G-Vision-Brochure-v1.pdf>.
- [80] 3GPP - Technical Specification Group Radio Access Network, “Evolved universal terrestrial radio access (e-utra). further advancements for eutra physical layer aspects (release 9).” 3GPP TR 36.814 V9.0.0 (2010-03), Mar. 2010.
- [81] T. Bai, R. Vaze, and R. W. Heath, “Analysis of blockage effects on urban cellular networks,” *IEEE Trans. Wireless Commun.*, vol. 13, pp. 5070–5083, Sep. 2014.

- [82] S. Singh, M. N. Kulkarni, A. Ghosh, and J. G. Andrews, "Tractable model for rate in self-backhauled millimeter wave cellular networks," *IEEE J. Sel. Areas Commun.*, vol. 33, pp. 2196–2211, Oct. 2015.
- [83] T. A. Thomas and F. W. Vook, "System level modeling and performance of an outdoor mmwave local area access system," in *IEEE Personal, Indoor, and Mobile Radio Communication (PIMRC)*, pp. 108–112, Sep. 2014.
- [84] C. Galiotto, I. Gomez-Miguel, N. Marchetti, and L. Doyle, "Effect of los/nlos propagation on area spectral efficiency and energy efficiency of small cells," in *IEEE Global Commun. Conf.*, pp. 3471–3476, Dec. 2014.
- [85] M. Ding, P. Wang, D. Lopez-Perez, G. Mao, and Z. Lin, "Performance impact of los and nlos transmissions in small cell networks." Available online: arXiv:1503.04251v1.
- [86] Ordnance Survey and Britain's mapping agency, "Os open data." [Online]. Available: <https://www.ordnancesurvey.co.uk/opendatadownload/products.html>.
- [87] C. Galiotto, N. Pratas, N. Marchetti, and L. Doyle, "A stochastic geometry framework for los/nlos propagation in dense small cell networks." Available online: arXiv:1412.5065v2.
- [88] S. Szyszkowicz, H. Yanikomeroglu, and J. Thompson, "On the feasibility of wireless shadowing correlation models," *Vehicular Technology, IEEE Transactions on*, vol. 59, pp. 4222–4236, Nov 2010.
- [89] B. Blaszczyzyn and M. Karray, "Quality of service in wireless cellular networks subject to log-normal shadowing," *Communications, IEEE Transactions on*, vol. 61, pp. 781–791, February 2013.
- [90] F. Baccelli and X. Zhang, "A correlated shadowing model for urban wireless networks," in *Computer Communications (INFOCOM), 2015 IEEE Conference on*, pp. 801–809, April 2015.
- [91] J. Wildman, P. H. J. Nardelli, M. Latva-aho, and S. Weber, "On the joint impact of beamwidth and orientation error on throughput in wireless directional poisson networks," *IEEE Trans. Wireless Commun.*, vol. 13, pp. 7072–7085, June 2014.

- [92] 3GPP - Technical Specification Group Radio Access Network, "Spatial channel model for multiple input multiple output (mimo) simulations (release 9)." 3GPP TR 25.996 V9.0.0 (2009-12), Dec. 2009.
- [93] Harry L. Van Trees, *Optimum Array Processing, Part IV of Detection, Estimation, and Modulation Theory*. John Wiley & Sons, 2002.
- [94] J. Gil-Pelaez, "Note on the inversion theorem," *Biometrika*, vol. 38, pp. 481–482, Dec. 1951.
- [95] D. H. Bailey and P. N. Swarztrauber, "A fast method for the numerical evaluation of continuous fourier and laplace transform," *SIAM Journal on Scientific Computing*, vol. 15, pp. 1105–1110, Sep. 1994.
- [96] W. Lu and M. D. Renzo, "System-level analysis/optimization of cellular networks with simultaneous wireless information and power transfer: Stochastic geometry modeling." submitted.
- [97] N. M. Temme, "Incomplete laplace integrals: Uniform asymptotic expansion with application to the incomplete beta function," *SIAM Journal on Mathematical Analysis*, vol. 18, pp. 1638–1663, Nov. 1987.
- [98] N. Deng, W. Zhou, and M. Haenggi, "The ginibre point process as a model for wireless networks with repulsion," *IEEE Trans. Wireless Commun.*, vol. 14, pp. 107–121, Jan. 2015.
- [99] L. Yingzhe, F. Baccelli, H. Dhillon, and J. Andrews, "Statistical modeling and probabilistic analysis of cellular networks with determinantal point processes," *IEEE Trans. Commun.*, vol. 63, pp. 3405–3422, Sep. 2015.
- [100] N. Deng, W. Zhou, and M. Haenggi, "Heterogeneous cellular network models with dependence," *IEEE J. Sel. Areas Commun.*, vol. 33, pp. 2167–2181, Oct. 2015.
- [101] Y. J. Chun, M. O. Hasna, and A. Ghayeb, "Modeling heterogeneous cellular networks interference using poisson cluster processes," *IEEE J. Sel. Areas Commun.*, vol. 33, pp. 2182–2195, Oct. 2015.
- [102] T. S. Rappaport, S. Sun, R. Mayzus, H. Zhao, Y. Azar, K. Wang, G. N. Wong, J. K. Schultz, M. Samimi, and F. Gutierrez, "Millimeter wave mobile communications for 5g cellular: It will work!," *IEEE Access*, vol. 1, pp. 335–349, May 2013.

-
- [103] M. N. Kulkarni, S. Singh, and J. G. Andrews, "Coverage and rate trends in dense urban mmwave cellular networks," in *IEEE Global Commun. Conf.*, pp. 3809–3814, Dec. 2014.

Titre : Nouveaux Résultats sur la Modélisation des Réseaux Cellulaires basée sur la Géométrie Stochastique: Analyse des Performances et Validation Expérimentale

Mots clés : réseaux cellulaire, relais, géométrie stochastique

Résumé : Récemment, il a été proposé un nouveau paradigme de modélisation des réseaux sans fil qui s'appuie sur les processus ponctuels de Poisson (PPP), et de manière générale sur la géométrie stochastique. L'analyse, au travers de ces outils mathématiques, présente une complexité indépendante de la taille du réseau, et permet d'estimer avec précision des quantités pratiques liées aux performances des réseaux cellulaires. Cette thèse a porté sur la faisabilité mathématique de l'approche fondée sur les PPP en proposant de nouvelles méthodes mathématiques d'approximations justes incorporant des modèles de propagation du canal radio.

Dans un premier temps, un nouveau cadre mathématique, considéré comme une approche Equivalent-in-Distribution (EiD), a été proposée pour le calcul exact de la probabilité d'erreur

dans les réseaux cellulaires.

Dans un deuxième temps, nous étudions les performances des réseaux cellulaires en présence de relais, où trois processus ponctuels de Poisson modélisent respectivement les nœuds relais, les stations de base, et les terminaux mobiles. Pour ce modèle, nous avons considéré des critères souples d'association.

Enfin, nous considérons la modélisation des réseaux cellulaires au travers d'un PPP et d'un modèle unifié d'atténuation de signal généralisée qui prend en compte deux types de liaisons physiques: line-of-sight (LOS) et non-line-of-sight (NLOS). Un modèle de complexité réduite décrivant les propriétés de la liaison radio a aussi été proposée et permet de prendre en compte dans nos calculs un grand nombre de modèle radio proposés dans la littérature.

Title : New Results on Stochastic Geometry Modeling of Cellular Networks: Modeling, Analysis and Experimental Validation

Keywords : cellular networks, relays, stochastic geometry

Abstract : Recently, a new network paradigm by modeling the wireless nodes as a Poisson Point Process (PPP), leveraging on the mathematical tools of stochastic geometry for tractable mathematical analysis, has been proposed with the capability of fairly accurately estimating the performance of practical cellular networks. This dissertation investigated the mathematical tractability of the PPP-based approach by proposing new mathematical methodologies, fair approximations incorporating practical channel propagation models.

First, a new mathematical framework, which is referred to as an Equivalent-in-Distribution (EiD)-based approach, has been proposed for computing exact error probability of cellular networks based on random spatial networks.

Second, the performance of relay-aided cooperative cellular networks, where the relay nodes, the base stations, and the mobile terminals are modeled according to three independent PPPs, has been analyzed by assuming flexible cell association criteria.

Third, the PPP modeling of cellular networks with unified signal attenuation model is generalized by taking into account the effect of line-of-sight (LOS) and non-line-of-sight (NLOS) channel propagation. A tractable yet accurate link state model has been proposed to estimate other models available in the literature.

